ol. 101 No. 1 October 1, 1978 ISSN 0003-2670

ANALYTICA CHIMICA ACTA

International journal devoted to all branches of analytical chemistry

ELSEVIER SCIENTIFIC PUBLISHING COMPANY

ANALYTICA CHIMICA ACTA

International journal devoted to all branches of analytical chemistry
Revue internationale consacrée à tous les domaines de la chimie analytique
Internationale Zeitschrift für alle Gebiete der analytischen Chemie

PUBLICATION SCHEDULE FOR 1978 (incorporating the section on Computer Techniques and Optimization).

	J	F	M	A	M	J	J	A	S	O	N	D
Analytica Chimica Acta	96/1	96/2	97/1	97/2	98/1	98/2	99/1	99/2	100	101/1	101/2	102
Section on Computer Techniques and Optimization			103/1			103/2			103/3			103/4

Scope. *Analytica Chimica Acta* publishes original papers, short communications, and reviews dealing with every aspect of modern chemical analysis, both fundamental and applied. The section on *Computer Techniques and Optimization* is devoted to new developments in chemical analysis by the application of computer techniques and by interdisciplinary approaches, including statistics, systems theory and operation research. The section deals with the following topics: Computerized acquisition, processing and evaluation of data. Computerized methods for the interpretation of analytical data including chemometrics, cluster analysis, and pattern recognition. Storage and retrieval systems. Optimization procedures and their application. Automated analysis for industrial processes and quality control. Organizational problems.

Submission of Papers. Manuscripts (three copies) should be submitted to:
for *Analytica Chimica Acta:* Dr. A. M. G. Macdonald, Department of Chemistry, The University, P.O. Box 363; Birmingham B15 2TT, England;
for the section on *Computer Techniques and Optimization:* Dr. J. T. Clerc, Laboratorium für Organische Chemie, Swiss Federal Institute of Technology, Universitätstrasse 16, CH-8092 Zürich, Switzerland.

Information for Authors. Papers in English, French and German are published. There are no page charges. Manuscripts should conform in layout and style to the papers published in this Volume. Authors should consult Vol. 93, p. 379 for detailed information. Reprints of this information are available from the Editors or from: Elsevier Editorial Services Ltd., Mayfield House, 256 Banbury Road, Oxford OX2 7DE (Great Britain).

Reprints. Fifty reprints will be supplied free of charge. Additional reprints (minimum 100) can be ordered. An order form containing price quotations will be sent to the authors together with the proofs of their article.

Advertisements. Advertisement rates are available from the publisher.

Subscriptions. Subscriptions should be sent to: Elsevier Scientific Publishing Company, P.O. Box 211, 1000 AE Amsterdam, The Netherlands. The section on *Computer Techniques and Optimization* can be subscribed to separately.

Publication. *Analytica Chimica Acta* (including the section on *Computer Techniques and Optimization*) appears in 8 volumes in 1978. The subscription for 1978 (Vols. 96–103) is Dfl. 1000.00 plus Dfl. 120.00 (postage) (Total approx. U.S. $486.96). The subscription for the *Computer Techniques and Optimization* section only (Vol. 103) is Dfl. 125 plus Dfl. 15.00 (postage) (Total approx. U.S. $60.87). Journals are sent automatically by air mail to the U.S.A. and Canada at no extra cost and to Japan, Australia and New Zealand for a small additional postal charge. All earlier volumes (Vols. 1–95) except Vols. 23 and 28 are available at Dfl. 144.00 (U.S. $63.00), plus Dfl. 10.00 (U.S. $4.35) postage and handling, per volume.

Claims for issues not received should be made within three months of publication of the issue, otherwise they cannot be honoured free of charge.

Customers in the U.S.A. and Canada who wish to obtain additional bibliographic information on this and other Elsevier journals should contact our Journal Information Center, 52, Vanderbilt Avenue, New York, NY 10017. Tel: (212) 867-9040.

ANALYTICA CHIMICA ACTA
VOL. 101 (1978)

ANALYTICA CHIMICA ACTA

International journal devoted to all branches of analytical chemistry

ELSEVIER SCIENTIFIC PUBLISHING COMPANY

Anal. Chim. Acta, Vol. 101 (1978)

Printed in The Netherlands

Analytica Chimica Acta, 101 (1978) 1—8

THE ROTATING DISC ELECTRODE IN FLOWING SYSTEMS
Part 2. A Flow system for automated anodic stripping voltammetry of discrete samples†

J. WANG and M. ARIEL*
Dept. of Chemistry, Technion, I.I.T., Haifa (Israel)
(Received 30th March 1978)

SUMMARY

The construction and characterization of a flow-through system for automatic a.s.v. analysis of discrete samples, based on the Autoanalyzer principle, is discussed. The flow-through cell is equipped with a rotated disc electrode (a thin mercury film deposited on a glassy carbon substrate) as detector. Carry-over effects in the system are examined and the procedure is adjusted to minimize their influence. The system allows the simultaneous determination of trace metals (lead, cadmium and copper) at the ppb level, at a rate of 10 samples per hour, with relatively inexpensive equipment.

Polarography and voltammetry have become accepted methods of detection in the automated analysis of discrete samples based on the AutoAnalyzer principle [1]. As early as 1967, Lento [2] suggested the use of DME-equipped flow cells for automated systems; several other studies [3—5] have been devoted to determinations based on polarographic flow systems. Lund and Opheim [6, 7] have discussed in depth the construction and characteristics of such a system. Concentrations down to ppm levels have been determined by various workers.

Current interest in heavy metal contaminants has resulted in an ever-increasing demand for their determination in a variety of matrices. Quite often, for example, in many clinical analyses or in monitoring the quality of water sources, the rapid determination of heavy metals at the ppb level is required in a large number of essentially similar samples. In such cases, automated systems based on the Autoanalyzer principle can prove economical in both time and manpower per sample. Anodic stripping voltammetry (a.s.v.) is a very useful method for determining traces of heavy metals in complex samples [7] and is suitable for the simultaneous determination of several heavy-metal ions at concentrations down to the sub-ppm level. A.s.v. has been adapted lately for use in flow systems, and in particular for the monitoring of heavy metals in natural waters [9—12]. These monitoring devices include new a.s.v. flow cells, in which the sample solution flows past

†This paper was presented in part at the Euroanalysis III Conference, Dublin, held in August 1978.

a stationary tubular [9, 10] or disc [11] working electrode, or past a rotated disc electrode [12]. The rotated disc electrode permits low solution flow rates, i.e. low sample volumes, to be used without sacrificing sensitivity.

The present paper reports the adaptation of the flow-through cell with the rotated disc electrode for the simultaneous determination of lead, copper and cadmium at the ppb level, in an automated system which is based on the Autoanalyzer principle of sequential sampling and washing, with a gas segment between two adjacent solutions.

EXPERIMENTAL

Apparatus

The components of the automated system with the flow-through cell (detail A) are shown in Fig. 1. The pyrex glass cell consists of a horizontal tube (7 mm i.d., 90 mm long) through which the solution flows, joined by a vertical tube (13 mm i.d., junction ca. 15 mm from inlet) serving for the introduction of the rotated working electrode. The construction of the electrode, the synchronous motor employed for its rotation and the connection

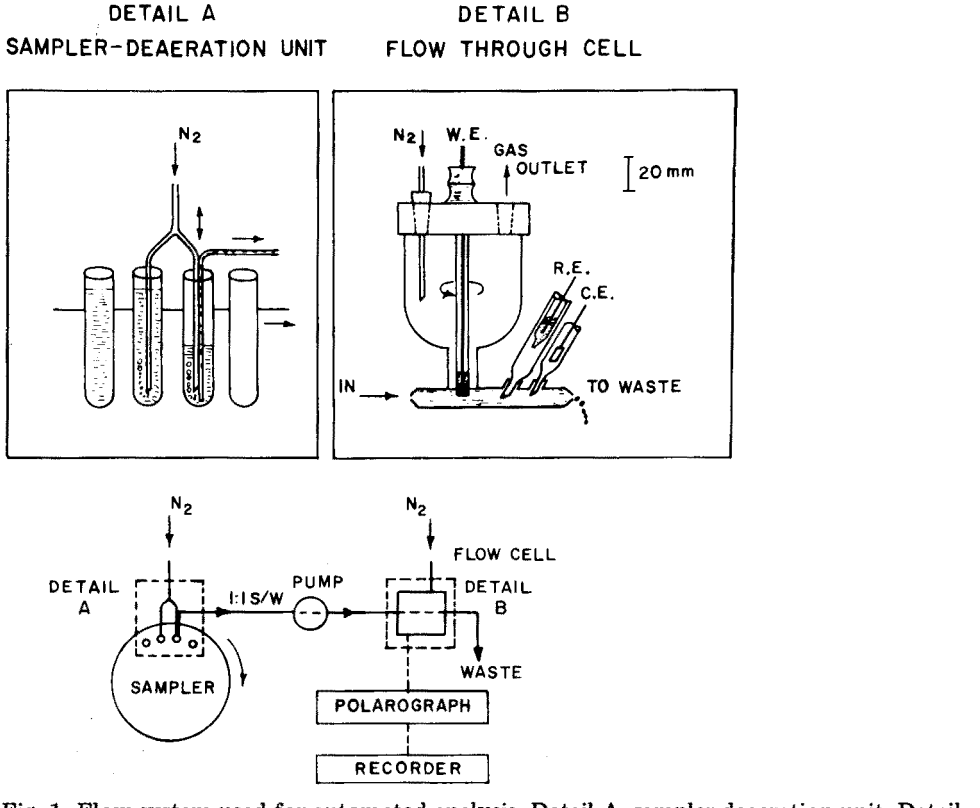

Fig. 1. Flow system used for automated analysis. Detail A, sampler-deaeration unit. Detail B, flow cell.

between the two have been described [11, 12]. The working electrode dips about 2 mm below the solution surface, so that the disc is ca. 5 mm above the "floor" of the horizontal tube. The vertical tube widens towards the top to accept a Teflon cell cover, which in addition to the working electrode also holds a thin Teflon tube for passage of nitrogen over the solution surface and a small escape tube. Glass joints placed 15 and 30 mm downstream from the working electrode (on the horizontal flow tube) allow the introduction of the salt bridges leading to the reference and the counter electrodes; an Ag/AgCl, saturated KCl electrode with a salt bridge filled with the sample solution is the reference electrode against which all potentials are reported; a platinum foil dipped in the sample stream serves as counter electrode.

The gas segmentation, which separates successive samples, escapes by the vertical tube of the working electrode compartment. The spatial coincidence of debubbler and working electrode in this cell design optimizes conditions: sample mixing in the detector is minimized and response time is shortened. The solution leaving the cell is discarded to waste; at the flow rates employed (3—8 ml min^{-1}) its level near the working electrode remains constant (7 mm, the i.d. of the detector); no changes in solution level in the vertical tube were observed on rotating the electrode or during debubbling.

The flow cell with rotated electrode described earlier and adapted for the continuous monitoring of metals in natural waters [12] is less efficient when applied to discrete samples: the vertical flow direction causes increased mixing between successive samples.

The sampler consists of a tray holding 40 test tubes (19 mm i.d., 150 mm long), with a 20-ml sample in each, and a sampler deaeration unit (Fig. 1). Nitrogen is bubbled simultaneously into two adjacent solutions [6], through an inverted pyrex glass U-tube (2.5 mm i.d., 3.5 mm o.d.) whose branches are spaced to fit the distance between the centres of two adjacent test tubes; their ends taper so that the diameter of the nitrogen outlet is 1 mm. The simultaneous deaeration of two solutions (that being sampled and the subsequent one) instead of three [6] suffices, because the relatively long sampling period ensures complete deaeration of the second sample. Sampling is effected through a tube (3.5 mm i.d., 4.5 mm o.d., 160 mm long) clamped alongside the leading branch of the deaeration U-tube, with its open end near the bottom of the sample test tube and its top bent at 90° to connect, via a piece of tygon tubing, with the pump head. A variable-speed Masterflex pump (Cole Palmer No. 7545 equipped with a No. 7015 head) serves to pass sample solutions and gas segments to the flow cell. Solution flow rate is controlled with a solid-state Masterflex controller. The dead volume of the system, consisting of the solution volume in the sampling tube, the tygon tubing leading to the pump head and that leading to the inlet of the flow cell (up to the working electrode) is 4.2 ml. A PAR 174 polarograph and a 3077 Yokogawa X-Y recorder served for recording current—voltage curves.

Reagents and solutions

Suprapur (Merck) HNO_3 and HCl and triple-distilled water were employed for the preparation of the various solutions and for cleaning the test tubes and flow system after each series of measurements. Stock solutions (10^{-3} M), prepared as described earlier [11], were stored in polyethylene bottles. Suprapur KCl, KNO_3, acetic acid and ammonia solutions served as supporting electrolytes.

Manifold procedure

The first test tube on the tray contains the mercury plating solution (1 ml of a 3.6×10^{-3} M Hg^{2+} stock solution added to 19 ml of triple-distilled water, giving a final Hg^{2+} concentration of 1.8×10^{-4} M); this is followed by alternating sample and wash test tubes, the latter containing triple-distilled water and a suitable supporting electrolyte. The rear positions on the tray hold the standard calibration solution test tubes, also alternated with wash tubes.

The branches of the sampler-deaeration unit dip into the first two tubes, with nitrogen bubbling simultaneously through both. The first step consists of plating the fixed mercury film which then serves as the working electrode for the series of determinations consisting of the complete set of sample tubes on the tray. Mercury(II) solution is pumped into the cell, at a rate of 5.0 ml min^{-1}, with the working electrode held at +0.5 V, without rotation. As soon as the solution reaches the cell, the deposition potential for mercury (—1.0 V) is imposed on the electrode and rotation is started at 2675 rpm. Film deposition continues for 2 min; both electrode rotation and solution flow are then stopped and the potential is switched to 0.0 V, to dissolve any metals which may have co-deposited with the mercury.

The sampler-deaeration unit is now advanced one notch, as described below, to start pumping the first sample and deaerate both the sample and wash solutions simultaneously. The solutions are pumped into the cell at a rate of 5 ml min^{-1} according to the following schedule: the time required for the solution to reach the detector (dead time, 50 s) plus that passing until steady state has been attained in the detector (response time, 1 min; see below) plus the deposition period. This is followed by stopped flow and rotation of the working electrode for a 10-s rest period and during the stripping step. Pumping is then resumed during the transfer step of the sampler-deaeration unit to the next pair of test tubes, now consisting of a wash solution tube followed by a sample tube. During the probe transfer step, a gas segment is aspirated through the unit, thus separating the two adjacent solutions. To prevent the introduction of oxygen into the system, the probe is raised in two stages. First, the probe is raised by ca. 5 cm for 10 s, with renewed pumping to clear the clamped sampling and deaeration tubes of residual sample solutions (with their ends still within the tube head space) while the second deaeration tube remains dipped in the adjacent solution, thus ensuring continuous sparging. The gas segment aspirated through the sampling tube is therefore composed of nitrogen escaping

from the clamped deaeration tube and held in the tube head space. After 10 s, the probe is raised completely to clear both tubes, the sampler tray is advanced one notch and the probe is lowered again for renewed pumping and deaeration. Pumping of the wash solution starts; this stage, designed in the Autoanalyzer process to clear the system of carry-over effects, is also exploited here to redissolve any residual metals from the mercury film. The working electrode is held throughout the 3-min wash cycle at 0.0 V and rotated for the first 30 s; this procedure ensures efficient film and cell clean-up. The anodic stripping voltammogram of the wash solution is recorded only once in each series of determinations, to obtain blank values, on the wash test tube occupying either the leading or final position of the tray, and the procedure employed is the same as that described for a sample tube. At the end of each series, the mercury film is dissolved by switching the potential of the working electrode to +0.5 V. The aspirating rate for samples at the ppb level is 20 tubes h^{-1}, with a 1:1 ratio between the sample and wash solutions, thus allowing the determination of 10 samples/hour.

RESULTS AND DISCUSSION

Carry-over studies

Flow systems of the type described here are characterized by the interaction of two adjacent solutions, resulting mainly from the presence of a thin solution film on the tubing walls in the region occupied by the gas segment and from partial mixing of the two solutions in the detector during debubbling [13]. In systems consisting of alternate sample and wash solutions, the concentrations in the detector increase and decrease between the two steady states corresponding to unadulterated sample and wash solutions. The time elapsing between the arrival of a sample in the detector and the attainment of a steady state is the response time.

The response time of the system was determined by initiating deposition (i.e. imposing the deposition potential on the working electrode and starting rotation) after varying time intervals had elapsed from the moment the sample solution reached the detector, and then recording the corresponding current peaks. Experiments were carried out with a 2.0×10^{-7} M Pb^{2+} solution in 0.05 M KCl, with deposition starting 0—90 s after the solution had reached the detector. Table 1 shows that, under the given conditions, steady-state peak currents were obtained after a 60-s waiting period. This response time was employed in all further experiments, although under standardized conditions if the calibration solutions and procedures are identical to those applied for samples, the deposition step can be initiated before the attainment of steady state. Any change in one or more of the parameters affecting the carry-over of two solutions (solution flow rate, tube diameter, solution viscosity, etc. [13]) requires a renewed determination of the response time.

TABLE 1

Measurement of the response time

Deposition delay[a] (s)	i_p[b] (μA)	Signal ratio i_p/i_p (steady state)
0	0.69	0.54
15	0.94	0.73
30	1.12	0.87
45	1.21	0.94
60	1.28	1.00
75	1.28	1.00
90	1.28	1.00

[a]Time elapsed between arrival of sample solution in detector and initiation of deposition. [b]Mean of 3 separate measurements of 2×10^{-7} M Pb^{2+} in 0.05 M KCl; solution flow rate, 5.0 ml min^{-1}; deposition for 1 min at —0.9 V; scan rate, 50 mV s^{-1}.

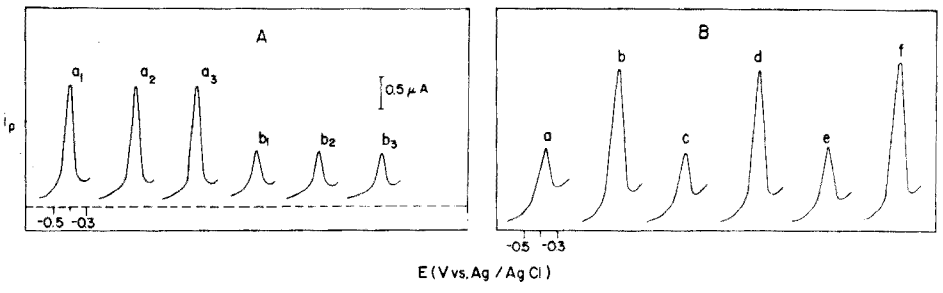

Fig. 2. Continuous flow data for Pb^{2+} determinations. (A) Triplicate analyses of 2.3×10^{-7} M followed by 0.9×10^{-7} M solutions. 0.05 M KNO_3 solution; deposition period and potential, 1 min at —1.0 V; scan rate, 50 mV s^{-1}; solution flow rate: 5.0 ml min^{-1}. (B) Carry-over between samples: (a) (c) (e) 0.65×10^{-7} M Pb^{2+}; (b) (d) (f) 1.7×10^{-7} M Pb^{2+}; 0.04 M HOAc—0.04 M NH_4OAc solution; scan rate, 100 mV s^{-1}; other conditions as in (A).

The degree of carry-over, i.e. the influence of the concentration of one solution on the result obtained for the subsequent solution, may be tested by using a correlation proposed by Broughton et al. [14]: three samples with a relatively high concentration C_a are followed by three samples with low concentration C_b (all alternated with wash solutions). The series C_{a_1}, C_{a_2}, C_{a_3}, C_{b_1}, C_{b_2}, C_{b_3} results in peak currents i_{a_1}, i_{a_2}, i_{a_3}, i_{b_1}, i_{b_2}, i_{b_3}. The total carry-over between C_{a_3} and C_{b_1} is given by

$$K = (i_{b_1} - i_{b_3})/(i_{a_3} - i_{b_3}) \quad (1)$$

Results of such a test run with lead(II) solutions are shown in Fig. 2 (A). The stripping peak currents (μA) obtained were:

$i_{a_1} = 0.165$; $i_{a_2} = 0.164$; $i_{a_3} = 0.165$; $i_{b_1} = 0.064$; $i_{b_2} = 0.063$; $i_{b_3} = 0.063$;

the value computed for K (0.01) shows carry-over effects to be negligible in this system.

Figure 2(B) further illustrates the performance of the system. Tests were also made with sequential determinations of 2×10^{-7} M Pb^{2+} and 1.8×10^{-7} M Cd^{2+} solutions, with deposition at −1.1 V from 0.1 M KNO_3. The carry-over found between successive determinations did not differ significantly from the blank values.

Quantitative evaluation, stability and precision

Quantification is effected with the aid of standard solutions placed in the rear positions of the sample tray; the standards are put through the analytical procedure under conditions identical to those used for samples. The response of the system to standard solutions in the range 3—22 ppb, with 1-min deposition periods, is shown in Fig. 3. The linear correlation found for copper(II) and cadmium(II) concentration and peak height again showed carry-over effects to be negligible. Whenever the simultaneous determination of several metal ions is required, the standard solutions in the calibration test tubes contain the appropriate mixtures of metal ions.

The stability of the thin mercury film, deposited on the working electrode at the beginning of each series of determinations, has an important bearing on the utility of the method [10—12]. The performance of the system was tested during an unbroken 2-h period of operation for sequential determinations (20 test tubes containing 1.0×10^{-7} M Pb^{2+} and 1.1×10^{-7} M Cd^{2+} in 0.04 M acetate buffer solution alternating with an appropriate wash solution); the relative standard deviations over the complete series of measurements were 4% and 6% for the Pb^{2+} and Cd^{2+} stripping current peaks, respectively.

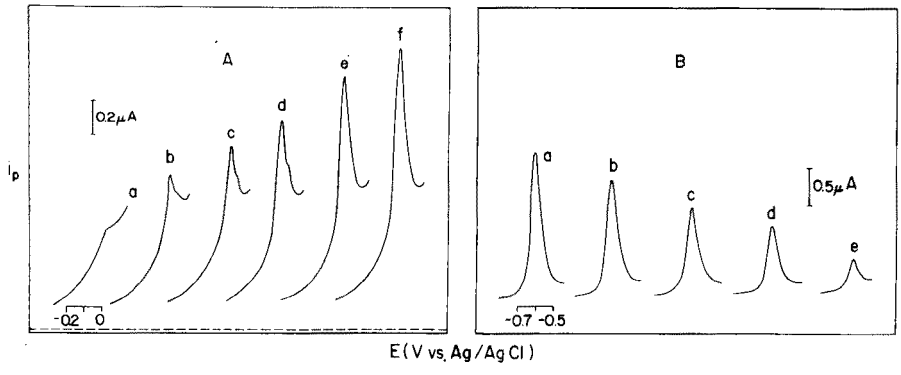

Fig. 3. Calibration with standards placed on the sample tray. (A) Cu^{2+} calibration with sequential samples of ascending concentration (3—15 ppb) in 0.016 M HOAc/0.016 M NH_4OAc solution; deposition period and potential, 1 min at −1.0 V; scan rate, 50 mV s^{-1}; solution flow rate, 5.0 ml min^{-1}. (B) Cd^{2+} calibration with sequential samples of descending concentration (22—4 ppb) in 0.1 M KCl solution; deposition period and potential, 1 min at −1.1 V; scan rate, 100 mV s^{-1}; solution flow rate, 5.0 ml min^{-1}.

The limit of detection of the method equals that of batch a.s.v. (sub-ppb). The wash solutions (solutions of the appropriate supporting electrolytes in triple-distilled water) sometimes contain trace concentrations (0.1—1 ppb) of some of the metal ions to be determined in a concentration range similar to that in the samples. Under these circumstances, the wash solutions are better dispensed with. Sampling rates for these samples with low concentrations remain satisfactory: the factors which prolong the duration of each determination—longer deposition times of 2—4 min and longer response times — are offset by the time saved by the elimination of the wash step. Further improvement of the sampling rate may be effected by: (1) employing sensitive and rapid pulse methods during the stripping step [15, 16]; (2) initiating the deposition step before 100% steady state has been achieved in the detector; and (3) decreasing the dead volume of the system. Work is continuing in those directions and the system is also being adapted for the simultaneous determination of higher concentrations (0.1—1 ppm) of metals.

The technique is easily adapted for the automated a.s.v. analysis of a variety of discrete samples. The characteristic procedure parameters — deposition time, flow rate, response time, etc. — must be adjusted to suit the requirements of each particular case (sample solution viscosity, available sample volume, concentration level, etc.). The preliminary stages of sample preparation, frequently dictated by the nature of the sample, usually lend themselves easily to automation with the components available for Auto-analyzers, so that a fully mechanized procedure can be evolved.

REFERENCES

1 L. T. Skeggs, Am. J. Clin. Pathol., 28 (1957) 311.
2 H. G. Lento, Automation in Analytical Chemistry, Technicon Symposia, 1966, Vol. I, Mediad, White Plains, N.Y., 1967, p. 598.
3 B. Fleet, S. Win and T. S. West, Automation in Analytical Chemistry, Technicon Symposia, 1967, Vol. II, Mediad, White Plains, N.Y., 1968, p. 355.
4 A. Cinci and S. Silvestri, Farmaco Ed. Prat., 27 (1972) 28.
5 L. F. Cullen, M. F. Brindle and G. J. Papariello, J. Pharm. Sci., 62 (1973) 1708.
6 W. Lund and L. N. Opheim, Anal. Chim. Acta, 79 (1975) 35.
7 W. Lund and L. N. Opheim, Anal. Chim. Acta, 82 (1976) 24.
8 T. R. Copeland and R. K. Skogerboe, Anal. Chem., 46 (1974) 1257 A.
9 W. R. Seitz, R. Jones, L. N. Klatt and W. D. Mason, Anal. Chem., 45 (1973) 840.
10 S. H. Lieberman and A. Zirino, Anal. Chem., 46 (1974) 20.
11 J. Wang and M. Ariel, J. Electroanal. Chem., 83 (1977) 217.
12 J. Wang and M. Ariel, Anal. Chim. Acta, 99 (1978) 89.
13 L. Snyder, J. Levine, R. Stoy and A. Conetta, Anal. Chem., 48 (1976) 942 A.
14 P. M. G. Broughton, M. A. Buttolp, A. H. Gowenlock, D. W. Neill and R. G. Skentebery, J. Clin. Path., 22 (1969) 278.
15 J. H. Christie, J. H. Turner and R. A. Osteryoung, Anal. Chem., 49 (1977) 1899.
16 J. H. Christie and R. A. Osteryoung, Anal. Chem., 48 (1976) 869.

Analytica Chimica Acta, 101 (1978) 9—16

SOLVENT EXTRACTION IN CONTINUOUS FLOW INJECTION ANALYSIS
Determination of Molybdenum in Plant Material

H. BERGAMIN F°*, J. X. MEDEIROS, B. F. REIS and E. A. G. ZAGATTO

Centro de Energia Nuclear na Agricultura (CENA), C.P. 13.400 Piracicaba, São Paulo (Brazil)

(Received 20th February 1978)

SUMMARY

A method is proposed for solvent extraction in continuous flow injection analysis. Optimal tube lengths, pumping rates, extraction efficiency, sample volumes, etc. are discussed. The thiocyanate method for the determination of molybdenum in plant material is used to demonstrate the feasibility of the method. A phase-separation chamber and a proportional injector are described. The proposed method can be used to determine molybdenum in plant ash solutions down to 0.05 ppm with good reproducibility and accuracy, at a rate of about 30 samples per hour.

In the last three years, a novel technique of semi-automated analysis has been developed, with many applications in agricultural, environmental, hydrological and clinical chemistry. This technique of flow-injection analysis, first introduced by Růžička and Hansen [1], is based on injection of an aqueous sample into a continuous stream of reagent with subsequent spectrophotometric [1—6, 8, 9, 14—16], potentiometric [3, 7, 9—11, 17] or turbidimetric [13, 16] measurement. Single or sequential reagent addition [1—17], sample splitting [4—6], controlled dilution [6], dialysis [6] and titration [9] are the main analytical operations related to the development of this technique.

Solvent extraction is very often required in analytical chemistry. Liquid—liquid extraction has been semi-automated by several workers [18—20], most of whom used air-segmented flow systems. The advantages and difficulties of automated solvent extraction, with some analytical applications, have been discussed in a comprehensive review [21]. The feasibility of solvent extraction in a flow-injection system generally characterized by a high degree of sample dispersion is demonstrated in this paper. The phase separation chamber described can be used for solvents both heavier and lighter than water, and the proportional injector is designed to allow large sample volumes to be introduced smoothly into the system.

The geometry of the phase-separation chamber, pumping rates, coil lengths, reagent concentrations, salting-out effect and sample volumes were investigated for the determination of molybdenum by the thiocyanate

method [22, 23]. Some analytical characteristics of the proposed method applied to plant material are presented.

Preliminary considerations

To perform solvent extraction in a flow-injection system, a flow diagram similar to that presented in Fig. 1 is employed. The sample (S) is injected into a carrier stream (C), and the other reagents are added by confluence. The reactions of interference masking and colour development start at point A and take place mainly in the reaction coil (C_R). The extraction starts at point B, where the solvent stream meets the carrier stream, and proceeds in the following extraction coil (C_E). If a salting-out effect is necessary for the improvement of extraction conditions, two extraction coils (each 210 cm long) can be used, and a final stream of concentrated electrolyte solution can be placed to join the carrier stream halfway between the two coils. The extraction coil is connected to the phase-separation chamber. One of the streams from this chamber goes to measurement and contains only the organic phase. The pressure must be slightly smaller than that of the solvent flow, to avoid the presence of the discarded phase in the flow-cell.

In order to achieve sensitivity at a reasonable sampling rate, several criteria must be met. First, the dispersion of the samples in the system must be as small as possible. Introduction of large sample volumes is necessary to minimize the effect of the large volume of some parts of the system (mainly the flow-through cuvette). The connections between injection port and point A (Fig. 1), and between the separation chamber and the cuvette must be kept as short as possible. The merging flow rates must be small, compared to the carrier flow. The total volume of the system must be minimal, i.e., all coils, the separation chamber and the flow-cell must be as small as possible. The coil lengths depend on the kinetics of the chemical processes involved and must be defined experimentally; the size of the phase-separation chamber depends on the characteristics of the organic and aqueous phases, the flow rate, the phase ratio, etc. Secondly, the organic-to-aqueous phase ratio must be as low as possible. This ratio is defined here as the ratio

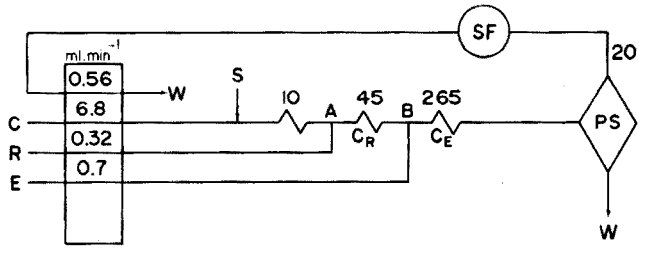

Fig. 1. Flow diagram finally used. C, R and E are the carrier, reagent and extraction streams, respectively. C_R and C_E are the reaction and extraction coils. PS is the phase separation chamber, SF the spectrophotometer, S the injector, and W waste. The numbers near the coils indicate coil lengths, in cm. For details, see text.

between solvent flow rate and carrier flow rate at point B (Fig. 1), and cannot be changed at will. If the ratio is too low, the sampling rate suffers a sharp decrease, and phase separation becomes more difficult. Thirdly, all reactions should be completed as fully as possible; gènerally, however, a compromise is necessary between reaction completion, sampling rate and sample dispersion. The only reactions that must be completely quantitative are the masking reactions for interferences.

EXPERIMENTAL

Instrumentation

The manifold finally used is shown in Fig. 1. The samples were injected with the device shown in Fig. 2. This injector, made from perspex, permits the smooth introduction into the system of sample volumes in the range of 0.1—20 ml, with a reproducibility better than 1% and a carryover less than 0.1%. This injector operates as follows: the samples are aspirated into the sample loop (between points *a* and *a'* in Fig. 2A) by means of the peristaltic pump, when the injector is in its sample aspiration position; the sample volume is defined exactly by the sample loop, the excess of sample being discarded. During the sampling cycle, the carrier stream passes through the loop between *b* and *b'*. In the sample introduction position (Fig. 2B), the sample loop is placed in the carrier line, and the measured volume is introduced into the stream.

The manifold was made of polyethylene tubing (0.85 mm i.d.). The coils connectors, supports, etc., have already been described [2]. The phase-separation chamber (Fig. 3), with an inner volume of 0.11 cm^3, was also made from perspex.

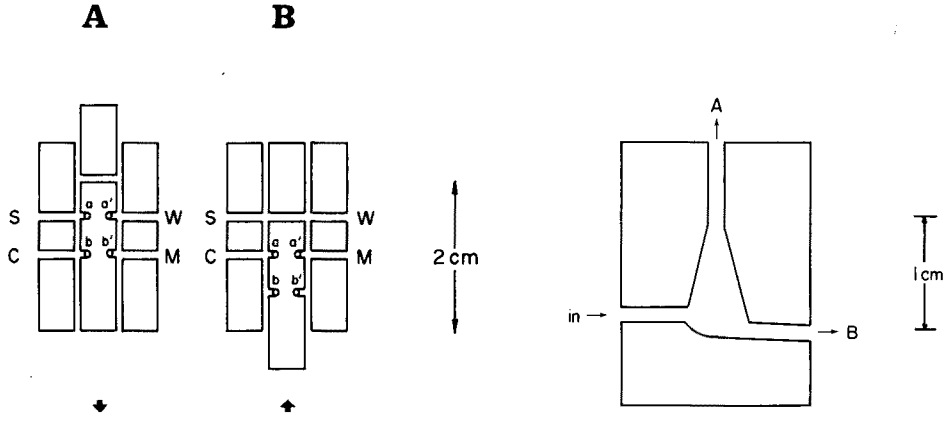

Fig. 2. Schematic diagram of the proportional injector in the sampling position (A) and in the sample introduction position (B). See text for details.

Fig. 3. The phase-separation chamber. When the solvent is lighter than water, the spectrophotometer is connected to A and B is the outlet to waste.

A Technicon AA II peristaltic pump was used with tygon tubing. The Beckman Model 25 spectrophotometer was connected to a Beckman Model 24 25ACC recorder, and was equipped with a Hellma flow-through cuvette (Type 178, light path 10 mm, volume 0.080 ml). The dual-beam mode was used, with distilled water as blank. The wavelength was set at 470 nm.

Reagents and standards

All chemicals were of analytical-reagent grade; the isoamyl alcohol was further purified by distillation. Deionized water was used.

The carrier solution consisted of 3 M HCl containing 25 ppm iron(III) (from $FeCl_3 \cdot 6H_2O$). The colour-forming reagent was 3 M HCl containing (unless otherwise stated) 10% (w/v) $SnCl_2 \cdot 2H_2O$ and 10% (w/v) KSCN, prepared freshly each day.

The standards contained the same concentrations of iron(III) and HCl as the carrier solution. They were made by appropriate dilutions of a stock solution containing 150 mg MoO_3 per l (100 ppm Mo) prepared as described earlier [23].

RESULTS AND DISCUSSION

Initial flow design

Preliminary tests showed that the limiting factor for the sampling rate, with the available flow-through cell and tubing, was the flow rate through the cuvette. A sampling rate of about 30 samples per hour could be achieved when a 0.5 ml min^{-1} flow was employed. The solvent flow rate was fixed at the slightly higher value of 0.7 ml min^{-1}, and the other flow rates were chosen to furnish a reasonable initial phase ratio (see below).

To establish the best length of the reaction coil, given that all iron(III) must be reduced by the tin(II) chloride before extraction with isoamyl alcohol [24, 25], the carrier stream was replaced by a 100-ppm iron(III) solution at 3.9 ml min^{-1}, and the point where the colour of iron(III) thiocyanate faded, was noted. This point lay about 30 cm from point A (Fig. 1); for security, a 45-cm coil was used, and, under these conditions, photometric signals were not detected. These preliminary tests also confirmed that masking reactions can be made fully quantitative in flow-injection systems. The other quantities in Fig. 1 were selected according to the general considerations noted above.

Salting-out effect

This effect was studied with the flow diagram shown in Fig. 1 modified by using two extraction coils, each 210 cm long, with the flow of salting-out agent (at 0.32 ml min^{-1}) joining the carrier stream at the midpoint between the coils. For these tests, the carrier flow-rate was 3.9 ml min^{-1} and 1.2-ml portions of a 4-ppm Mo standard were injected. Water and saturated solutions of sodium fluoride or potassium aluminium sulphate were used as the

salting-out streams. The corresponding recorded peak heights indicated that the salt concentration increased the signal only slightly (ca. 5%). Therefore, this procedure was not employed for the determination of molybdenum, because the incorporation of an additional stream would cause greater sample dilution, and would make the system more complex. This procedure could, of course, be used for other systems involving more difficult extractions.

Reagent concentration

The optimal concentration of potassium thiocyanate in the reagent stream was established experimentally; the system used was the same as that shown in Fig. 1 except that the extraction coil (C_E) was increased to 420 cm; the carrier flow-rate was 3.9 ml min^{-1}. Injections of 1.1 ml of a 1-ppm Mo standard were made, and the potassium thiocyanate concentration was varied between 2.5 and 40%. As the sensitivity was confirmed to be nearly independent of the thiocyanate concentration, a concentration of 10% was used. This solution also contained 10% tin(II) chloride, as this concentration was enough to reduce 100 ppm iron(III).

Phase ratio

The final system shown in Fig. 1 was established from tests in which a carrier flow-rate of 3.9 ml min^{-1} was used with a 420-cm extraction coil. The samples were 8.75 ml of a 2-ppm Mo standard, and the solvent flow rate was varied from 0.42 to 2.5 ml min^{-1}. It was necessary to decrease the flow rate through the flow-cell to 0.32 ml min^{-1}, when the solvent flow was 0.42 ml min^{-1}.

The sensitivity improved when the solvent flow was low (Fig. 4), with consequent lowering of the organic to aqueous phase ratio. This caused, however, a sharp decrease in the sampling rate, because it was necessary to diminish the flow rate through the flow-cell, which is the limiting factor in sampling rate. Another way of lowering the phase ratio, without lowering the sampling rate, would be to increase the carrier flow, but the sensitivity would decrease because of insufficient extraction time (Fig. 5).

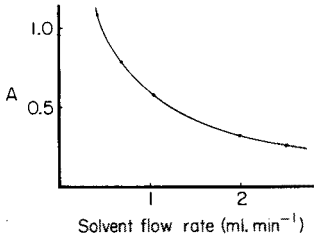

Fig. 4. Influence of the solvent flow rate on the sensitivity of the method. For details, see text.

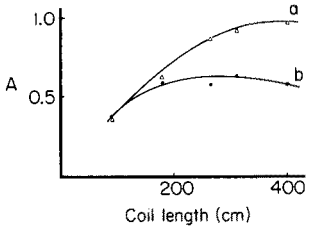

Fig. 5. Influence of the length of the extraction coil in the extraction procedure. Curve *a* corresponds to an infinite sample volume and curve *b*, to an 8.75-ml sample. For details, see text.

Extraction procedure

To establish the optimal length of the extraction coil, the system shown in Fig. 1 was employed, with lengths varying from 90 to 420 cm. The 2-ppm Mo standard used was either injected into the system (8.75 ml) or made to replace the carrier stream (infinite volume). The extraction was nearly complete (Fig. 5) when a 420-cm coil was used. In this case, however, the sample dispersion would be very large, even with large sample volumes (Fig. 5). A 260-cm coil was therefore chosen, because it was then possible to attain about 90% of the maximum possible extraction, with a reasonable degree of sample dispersion.

Sample volume

Sample volumes varying from 1.1 to 8.75 ml of a 2-ppm Mo standard were injected into the manifold shown in Fig. 1. The sensitivity more than doubled as the sample volume was increased over this range, largely because sample dispersion was minimized. In this situation, the original idea of a small sample volume injected into a reagent stream [1] must be modified. When sensitivity is critical and large dead volumes are present in the system, the samples must be introduced into an inert carrier stream [16], with further addition of concentrated reagents via small merging flows. A low degree of sample dispersion and better conditions of mixing are then attained. The injection of larger sample volumes was made possible by using the new proportional injector and the confluence configuration. It must be emphasized that in the proposed method the sample volume has little influence on sampling rate.

Analytical characteristics

The proposed method utilizes the flow-diagram shown in Fig. 1, with a 260-cm extraction coil and injected volumes of 2.25 ml. An organic to aqueous phase ratio of about 1:10 is used, and molybdenum levels down to about 0.1 ppm can be measured with good reproducibility (see Fig. 6) at a typical sampling rate of about 30 samples per hour. The stability of the system is very good. When infinite sample volumes were utilized, the fluctuation corresponding to an absorbance of 0.9 A was only ±0.002 A at the plateau achieved, over a period of 2 h.

Table 1 indicates that the method shows adequate recoveries when applied to plant extracts.

To check the feasibility of using the flow-injection solvent extraction method with solvents heavier than water, a variation of this method employing a 1:1 isoamyl alcohol—carbon tetrachloride mixture [23] was used. The pumping tubes were replaced by Solvaflex tubing, and the separation chamber by a glass chamber. Similar results were obtained, with a decrease in sampling rate because of the higher viscosity of the extracting mixture. Unfortunately, phase separation was not feasible when a phase ratio smaller than 1:6 was used.

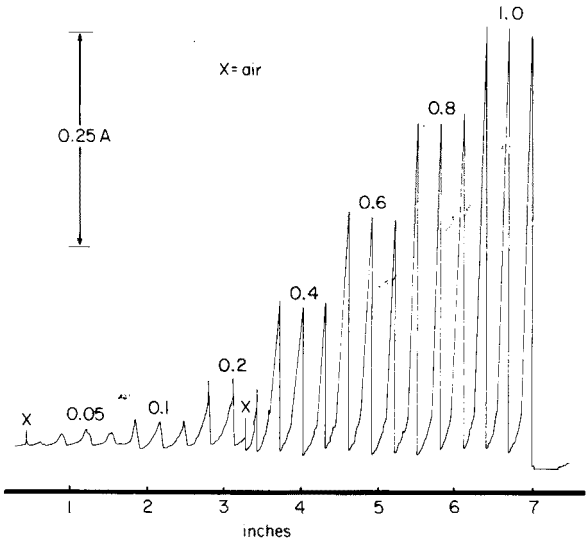

Fig. 6. Calibration graph for the proposed method. The numbers near the peaks represent ppm Mo. Paper speed, 4 min per in. For details, see text.

TABLE 1

Determination of molybdenum in plant extracts

Sample number	Foliar material	Mo in extract (ppm)	Recovery[a] (%)
1	*Saccharum spp*	0.040	101.0
2	*Saccharum spp*	0.025	101.5
3	*Phaseolus vulgaris L.*	0.100	107.8
4	*Phaseolus vulgaris L.*	0.475	92.0
5	*Heleanthus annus L.*	0.030	107.9
6	*Heleanthus annus L.*	0.050	107.5
7	*Brachiaria spp*	0.025	96.4

[a]After addition of 3.64 μg Mo to 10 ml of sample.

The proposed method could be improved by using a flow-cell with a smaller volume. A smaller solvent flow and consequently a better phase ratio would then be possible without losing sampling rate. Studies on this point are now being made.

Peter B. Vose and Francisco José Krug are thanked for their assistance in preparing this manuscript.

REFERENCES

1 J. Růžička and E. H. Hansen, Anal. Chim. Acta, 78 (1975) 145.
2 J. Růžička and J. W. B. Stewart, Anal. Chim. Acta, 79 (1975) 79.
3 J. W. B. Stewart, J. Růžička, H. Bergamin F° and E. A. G. Zagatto, Anal. Chim. Acta, 81 (1976) 371.
4 J. Růžička, J. W. B. Stewart and E. A. G. Zagatto, Anal. Chim. Acta, 81 (1976) 387.
5 J. W. B. Stewart and J. Růžička, Anal. Chim. Acta, 82 (1976) 137.
6 J. Růžička and E. H. Hansen, Anal. Chim. Acta, 87 (1976) 353.
7 J. Růžička, E. H. Hansen and E. A. G. Zagatto, Anal. Chim. Acta, 88 (1977) 1.
8 E. H. Hansen, J. Růžička and B. Rietz, Anal. Chim. Acta, 89 (1977) 241.
9 J. Růžička, E. H. Hansen and H. Mosbaek, Anal. Chim. Acta, 92 (1977) 219.
10 E. H. Hansen, A. K. Ghose and J. Růžička, Analyst, 102 (1977) 705.
11 E. H. Hansen, F. J. Krug, A. K. Ghose and J. Růžička, Analyst, 102 (1977) 714.
12 J. Růžička, E. H. Hansen, H. Mosbaek and F. J. Krug, Anal. Chem., 49 (1977) 1858.
13 F. J. Krug, H. Bergamin F°, E. A. G. Zagatto and S. S. Jørgensen, Analyst, 102 (1977) 503.
14 D. Betteridge and J. Růžička, Talanta, 23 (1976) 409.
15 S. S. Jørgensen, H. Bergamin F°, E. A. G. Zagatto, F. J. Krug and S. R. B. Bringel, CENA, BC-047 (1977).
16 H. Bergamin F°, B. F. Reis and E. A. G. Zagatto, Anal. Chim. Acta, 97 (1978) 427.
17 H. Bergamin F°, F. J. Krug, E. A. G. Zagatto, H. Fonseca, M. Graner, J. N. Nogueira, and A. V. K. O. Annicchino, CENA-BC 049 (1977).
18 W. S. Sebborn, Analyst, 94 (1969) 324.
19 H. J. Hinckers, W. Theisen and S. Goenechea, Mikrochim. Acta, (1972) 24.
20 J. M. Carter and G. Nickless, Analyst, 95 (1970) 148.
21 J. T. van Gemert, Talanta, 20 (1973) 1045.
22 C. E. Crouthamel and C. E. Johnson, Anal. Chem., 26 (1954) 1284.
23 C. M. Johnson and T. H. Arkley, Anal. Chem., 26 (1954) 572.
24 J. O. Hibbits and R. T. Williams, Anal. Chim. Acta, 26 (1962) 363.
25 O. C. Bataglia, Thesis, ESALQ-USP, Piracicaba, S.P., Brazil, 1972.

Analytica Chimica Acta, 101 (1978) 17—23

MERGING ZONES IN FLOW INJECTION ANALYSIS
Part 1. Double Proportional Injector and Reagent Consumption

H. BERGAMIN F°*, E. A. G. ZAGATTO, F. J. KRUG and B. F. REIS

Centro de Energia Nuclear na Agricultura (CENA), C.P. 13400 Piracicaba, S. Paulo (Brazil)

(Received 21st March 1978)

SUMMARY

A double proportional injector is described, and an improvement of the continuous flow-injection method is discussed. Sample and reagent are both injected into an inert carrier stream; the reagent is consumed only in the presence of the sample, and can otherwise be recovered continuously. The main characteristics of the flow injection system, e.g. high sampling rate and good accuracy, precision and sensitivity, are maintained. The proposed system is compared with other flow-injection systems suggested earlier. The determination of phosphate in plant material by the molybdenum blue flow-injection method was chosen to demonstrate the feasibility of the system; the consumption of ascorbic acid is only 9% of that in the original method.

In 1975, Růžička and Hansen [1] introduced the concept of flow injection analysis, which is based on injection of an aqueous sample into a continuously moving carrier stream of reagent without air segmentation. Further development [2—5] showed that many desirable analytical characteristics such as high sampling rate and good accuracy, reproducibility and sensitivity, can be achieved with low sample and reagent consumption despite the simplicity of design and low cost. This technique, however, could not be recommended for spectrophotometric or turbidimetric analysis of very dilute samples, when the difference in colour or refractive index between sample and reagent is very pronounced.

Recently, Bergamin et al. [6] extended the concept of flow injection analysis to solve this problem. The sample was introduced into an inert carrier stream, with the addition of the necessary reagents in higher concentrations via slow merging streams. With this confluence configuration and a single proportional injector [7] which can introduce large sample volumes, it was possible to enhance the sensitivity of the flow-injection method in systems characterized by large dead volumes. In all these cases, however, the reagent was consumed during the entire analytical time, as normally happens in all continuous flow analyzers.

This paper describes an improvement of the flow-injection system in which both sample and reagent are introduced into inert carrier streams, with synchronized merging and interaction. The reagent is thus consumed

during only part of the time, and a constant ratio of sample and reagent amounts is always attained. To do this, it is necessary to utilize a double proportional injector, which is an improvement of the single proportional injector design [7].

To illustrate the feasibility of the proposed method, the determination of phosphate in plant extracts by the molybdenum blue flow-injection method [2, 8] was chosen.

EXPERIMENTAL

Instrumentation

Sample and reagent were introduced into the system by means of the injector depicted in Fig. 1. This injector, made from perspex, can be used as a single proportional injector, in the straight or confluence configurations [6] and also as a double proportional injector. It permits the smooth introduction into the system of sample and reagent volumes in the range 0.01—20 ml, with a reproducibility better than 1% and a carryover of less than 0.1% [7]. The injector is operated as follows. In the loading position (Fig. 1A), the sample (S) is aspirated to fill the sample loop (L_S), which exactly defines the sample volume; the excess of sample goes to waste (W). Simultaneously, the reagent (R) is pumped to fill the reagent loop (L_R); its excess, slightly diluted by the reagent carrier stream (C_R), is accumulated in the reagent recovery vessel (D). In this position, the sample and reagent carrier streams (C_S and C_R) are pumped to merge at point A, then going to the manifold (M).

In the injection position (Fig. 1B), the selected volumes of sample and reagent are pushed by the carrier streams, merging at point A simultaneously, and then going to the manifold. The sample aspiration tube aspirates water

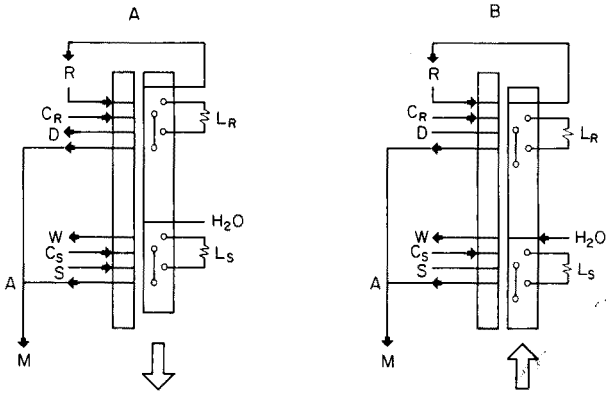

Fig. 1. Schematic presentation of the double proportional injector in the loading (A) and injection (B) positions. S and R are sample and reagent; L_S and L_R are the sample and reagent loops; C_S and C_R are the sample and reagent carrier streams; D is the reagent outflow to a recovery vessel; W is the waste; A is the confluence point placed 5 cm from the injection ports; M represents the manifold. For details see text.

and the pumped reagent is directed back to the reagent reservoir. The sample section corresponds to a single proportional injector.

The peristaltic pump, manifold, spectrophotometer and accessories have already been described [6]. A Hitachi Perkin-Elmer model 139 spectrophotometer furnished with a Hellma type 178 flow-through cuvette and connected to a Beckman model 1005 10-in. recorder was used for phosphate determination.

Preliminary tests

The manifolds represented by the flow diagrams in Fig. 2 were chosen to study some characteristics of the original flow-injection system (A), the symmetrical confluence system (B) and the proposed system (C). In all cases, the injected volumes were 0.13 ml, the carrier stream was phosphate buffer of pH 7.0, the flow rates were 2.0 ml min^{-1}, and the reaction coil length was 40 cm. A methyl orange solution (0.002% w/v in 0.01 M KH_2PO_4—0.01 M K_2HPO_4) was used to simulate the sample or reagent, and the signal was measured at 460 nm.

To diminish the sample dilution at point A, an asymmetrical model system similar to that shown in Fig. 2C was used, with the following parameters: sample carrier stream, 4.0 ml min^{-1}; reagent carrier stream, 1.0 ml min^{-1}; injected sample, 0.32 ml of 0.002% methyl orange solution; injected reagent, 0.08 ml of 0.008% methyl orange solution; sample and reagent carrier streams, phosphate buffer; reaction coil length, 40 cm.

Determinations of phosphate

Phosphate determinations in plant material were done with the proposed and the original flow-injection systems. The flow diagrams were similar to those depicted in Fig. 2A and 2C, with the following parameters:

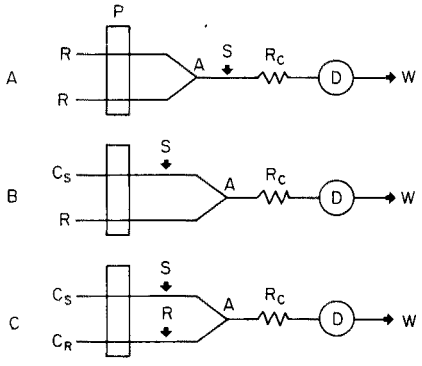

Fig. 2. Flow-diagrams of the original flow-injection system (A), the symmetrical confluence system (B), and the proposed system (C). The sample (S) is injected either into the reagent (R) or into the sample carrier stream (C_S). The reagent (R) is pumped either by the peristaltic pump (P) or injected into the reagent carrier stream (C_R). A is the confluence point, R_C is the reaction coil, D is the flow-through detector and W denotes waste.

(a) Original flow injection system. Molybdate stream, 3.9 ml min^{-1}. Ascorbic acid stream, 3.9 ml min^{-1}. Injected sample volume, 0.15 ml.

(b) Proposed flow-injection system. Sample carrier stream (molybdate solution), 3.9 ml min^{-1}. Ascorbic acid carrier stream (water), 3.9 ml min^{-1}. Sample and reagent injected volumes, 0.15 ml.

In all cases, the rate of sample aspiration and reagent pumping was 2.0 ml min^{-1}, the reaction coil length was 125 cm and absorbances were measured at 660 nm.

Reagents and standards

All chemicals were of analytical grade and distilled water was used for all solutions.

The reagents for the phosphate determinations were 1% (w/v) ascorbic acid solution and 0.6% (w/v) ammonium heptamolybdate solution in 0.4 M nitric acid.

Standard solutions were prepared to contain 0, 10, 20, 30, 40, 50 and 60 ppm P (as phosphate) in 0.4 M perchloric acid.

Samples

The extracts were obtained after nitric—perchloric acid digestion [4] of foliar material from *Sorghum* spp.

RESULTS AND DISCUSSION

The original flow-injection system (Fig. 2A) permits a slightly higher sampling rate than the other systems, mainly because the flow rate through the sample loop is higher in this configuration. In the ideal case, this system should be also the most sensitive one, because there are no confluence points. However, it cannot be employed when the difference in colour or refractive index between sample and reagent is pronounced, because a sharp negative or positive peak appears [6]. Figure 3A shows that dilution of the reagent by the sample is most pronounced when the reagent is most required, i.e. when the sample is at its maximum. This causes a loss in sensitivity when the measured signal depends on the reagent concentration. When the chemical reaction is slow, another consideration arises: a somewhat longer time is necessary for the reagent to reach the centre of the sample zone [1]. Therefore, for a given sample dispersion, the time available for the development of the reaction is shorter in this system, compared with the two other systems investigated.

The confluence system (Fig. 2B) was first developed to solve the negative peak problem [6]. The mixing conditions between sample and reagent are better, the reagent shows no concentration gradient at the sample zone (Fig. 3B) and the chemical reaction starts at point A (Fig. 2B) where the reagent also reaches the centre of the sample zone. It must be emphasized that this system gives higher sensitivity than the original one, despite the

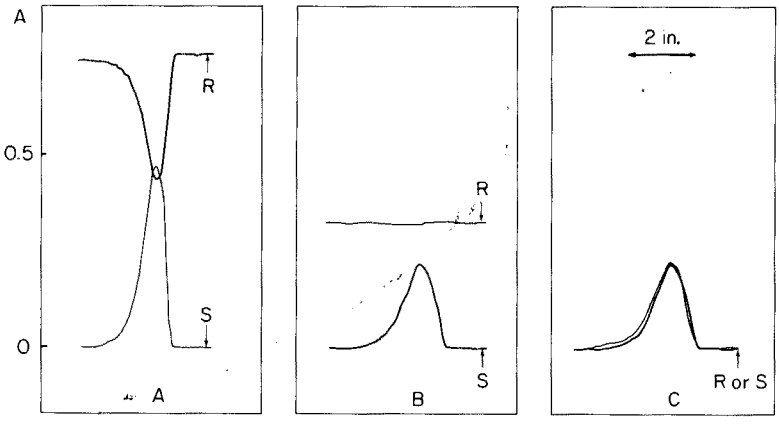

Fig. 3. Record peak profiles obtained with methyl orange indicator for simulation of sample (S) and reagent (R), in the original (A), symmetrical confluence (B), and proposed (C) systems. Paper speed, 5 in. per min. For details, see text.

sample dilution that occurs at point A. In the symmetrical system depicted in Fig. 2B, the dilution factor at point A is 50%, causing an attenuation in the sample signal. This attenuation can be minimized by changing the merging flow rates, with a consequent increase in sensitivity. It should be stressed that the confluence configuration permits the introduction of large sample volumes into the system, which is sometimes necessary [7].

In the proposed system, the reagent is injected simultaneously with the sample, and perfect synchronization of sample and reagent zones can be attained, as shown in Fig. 3C. It is also clear from Fig. 3 that the reagent consumption, which is proportional to the area under the reagent signal, is much lower with the proposed system. This system has similar characteristics to that shown in Fig. 2B, but as the reagent undergoes dispersion in the line, the latter system sometimes gives less sensitivity. The confluence system may be regarded as a particular design of the proposed system, with an infinite reagent volume.

Figure 4 is related to the asymmetrical proposed system, where the sample dilution factor at point A (Fig. 2) is diminished, to achieve greater sensitivity. This figure shows that good synchronization can be attained even with the asymmetrical configuration, and that the typical reproducibility of flow-injection systems is maintained. It is important to note that when this system was used with a sampling rate of ca. 200 samples per h, the concentration of the methyl orange in the reagent deposit was more than 90% of the initial concentration, and the volume of reagent that was returned was about 40% of the total pumped reagent. To re-utilize the reagent recovered, its concentration can be restored if the volume of diluent added is known. This amount can be calculated by multiplying the number of samples analyzed by the volume of the reagent loop.

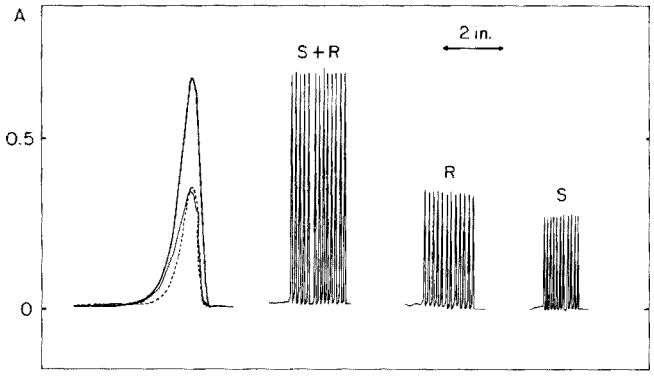

Fig. 4. Recorded peaks obtained with methyl orange indicator in the asymmetrical confluence system. From right to left, the first sequence of peaks corresponds to the sample (S) injected several times, the second sequence to the reagent (R), and the third sequence to sample plus reagent (S + R) injected simultaneously. The peak profiles on the left indicate the good synchronization of the merging zones of sample and reagent. Paper speed, 5 in. per min and 0.2 in. per min, corresponding to the high and low speeds, respectively.

TABLE 1

Results obtained for phosphate in *Sorghum* spp. by the original and proposed flow-injection methods. The data, referred to the extracts, were obtained with 5 repetitions.

Sample	Original method		Proposed method	
	Phosphate (ppm)	R.s.d. (%)	Phosphate (ppm)	R.s.d. (%)
1	47.3	0.34	44.4	0.86
2	42.4	0.58	41.8	0.14
3	41.6	1.21	41.0	0.41
4	15.0	0.90	13.6	0.36
5	51.0	0.60	53.6	0.53
6	16.4	0.59	15.0	0.52
7	55.0	0.59	58.6	0.77
8	47.3	0.34	51.0	0.20
9	10.2	1.47	8.5	1.21
10	42.4	1.25	42.4	0.66
Av.		0.787		0.566
Ascorbic acid consumption (ml/sample)	1.67		0.15	

The feasibility of this system in real analysis was demonstrated by comparing the results of determinations of phosphate in plant material obtained with the original flow-injection design [2, 8], and the proposed method. The results presented in Table 1 indicate that both systems give the same

reproducibility and accuracy. After routine measurements of several hundred samples, it was noticed that the consumption of ascorbic acid by the proposed method was only 9% of the consumption when the original system was used.

The next paper of this series will deal with the consumption of lanthanum in the determination of calcium in plant material by continuous flow-injection atomic absorption analysis.

Partial support of this project by DANIDA (Project 104DAN8/241) is greatly appreciated. The authors thank Dr. J. Růžička and Dr. E. H. Hansen for advice, and P. B. Vose for assistance in preparing the manuscript.

REFERENCES

1 J. Růžička and E. H. Hansen, Anal. Chim. Acta, 78 (1975) 145.
2 J. Růžička and J. W. B. Stewart, Anal. Chim. Acta, 79 (1975) 79.
3 J. W. B. Stewart, J. Růžička, H. Bergamin F°. and E. A. G. Zagatto, Anal. Chim. Acta, 81 (1976) 371.
4 F. J. Krug, H. Bergamin F°. , E. A. G. Zagatto and S. S. Jørgensen, Analyst, 102 (1977) 503.
5 J. Růžička, E. H. Hansen and E. A. G. Zagatto, Anal. Chim. Acta, 88 (1977) 1.
6 H. Bergamin F°., B. F. Reis and E. A. G. Zagatto, Anal. Chim. Acta, 97 (1978) 427.
7 H. Bergamin F°., J. X. Medeiros, B. F. Reis and E. A. G. Zagatto, Anal. Chim. Acta, 101 (1978) 9.
8 J. Růžička, E. H. Hansen, H. Mosbaek and F. J. Krug, Anal. Chem., 49 (1977) 1858.

Analytica Chimica Acta, 101 (1978) 25—31

THE RAPID DETERMINATION OF TOTAL CARBON AND SULFUR IN GEOLOGICAL MATERIALS BY COMBUSTION AND INFRARED ABSORPTION PHOTOMETRY

S. TERASHIMA

Geological Survey of Japan, Hisamoto 135, Kawasaki 213 (Japan)

(Received 27th February 1978)

SUMMARY

A method, based on infrared absorption following combustion in a high-frequency induction furnace is described for the simultaneous determination of total carbon and sulfur in geological samples. Suitable accelerators, the effects of chemical composition and coexisting elements, and the elimination of interference from water are discussed. The limit of detection is 20 ppm for carbon and 5 ppm for sulfur; the relative standard deviations are 6% or less for 100—1000 μg of carbon or sulfur. The method has been applied satisfactorily to standard rocks, NBS minerals, and geological exploration reference samples. The analysis time is less than 1 min.

Combustion methods are very popular for the determination of total carbon [1—3] or sulfur [1, 3—7] in geological samples, but more than five minutes are necessary for each run for carbon or sulfur, and the procedures are generally complicated.

Recently, simultaneous determinations of carbon and sulfur were achieved by combining combustion in a high-frequency induction furnace with infrared absorption photometry. The method provides highly sensitive and rapid results, and has been applied to analyses of iron and steel [8]. No application, however, has been made to geological materials. In this study the selection of accelerators, effect of coexisting elements, and elimination of water interference were examined so that the method could be applied to a variety of geological materials. The preparation of calibration standards is also discussed.

EXPERIMENTAL

Apparatus

A Kokusai Electric I.R.-Matic "C-S" VK-111 AS analyzer with automatic balance and printer were used. The instrument is a simultaneous carbon—sulfur automatic analyzer based on combustion with a high-frequency induction furnace followed by Luft-type non-dispersive infrared detectors. It consists of linearizers, integrators, blank adjusters, single-point calibrating

adjusters and weight compensators. The results are given by digital read-out or print-out after combustion.

A ceramic crucible (ca. 5 ml; Kokusai Electric I.R. Type) was used with oxygen as the combustion and carrier gas, and nitrogen as purge gas.

Reagents

Calcium carbonate (Johnson Matthey Chemicals Ltd.), crystalline sulfur (99.9999%) and silicon dioxide were used as calibration standards. Silicon dioxide was freed from carbon and sulfur by igniting at 1200°C.

Iron powder and tungsten chips (Kokusai Electric Co.) were used as accelerators.

Study of accelerators and blanks

Recently, Ohnuma et al. [8] reported that a tungsten accelerator was better than copper or tin for the determination of carbon and sulfur in iron and steel samples. Geological samples yielded imperfect combustion with tungsten alone and a combination of iron and tungsten was adopted. Two scoops of each of iron powder (ca. 1.2 g) and tungsten chips (ca. 2.6 g) were used for the 0.5-g samples to ensure complete combustion; one scoop of each was used for samples less than 0.2 g.

Several authors have recommended that the sample and accelerators [2, 3, 5—7] should be mixed. In this study, however, mixing led to longer analysis times and lower recoveries of carbon and sulfur.

Average blank values of 25 μg of carbon and 9 μg of sulfur were detected after combustion with two scoops of both accelerators. These values were decreased to 20 μg and 6 μg, respectively, when the crucible was used after igniting it at 1200°C for 3 h. This small improvement in accuracy was ignored in the general procedure except when the levels of carbon and sulfur being determined were below 100 ppm, in which case careful control of the amounts of accelerator used is necessary as the carbon blank value becomes significant.

Effect of coexisting elements

Carbon and sulfur are present in various chemical forms in geological materials. The effects of different compositions were examined with synthetic samples (Table 1).

The interference of various substances was examined for silicon dioxide powder (100 mg) containing carbon (0.1 mg) and sulfur (0.1 mg). No interference was observed from 200 mg of aluminium, chromium, iron, manganese, magnesium, titanium and zinc oxides. Sulfur recovery from compounds with low melting points was low (Table 2) and carbon recovery was increased by sodium peroxide and potassium nitrate.

Elimination of water interference

Generally, the recovery is slightly less than 100% in the determination of sulfur by a combustion method [9]. Sulfur losses are most noticeable in

TABLE 1

Effect of chemical composition in the determination of 1000 ppm of carbon or sulfur in synthetic silicon dioxide samples

Element	Added as	Found[a] (ppm)	Element	Added as	Found[a] (ppm)
C	Calcium carbonate	999 ± 11	S	Chalcopyrite	989 ± 13
C	Graphite	994 ± 10	S	Barium sulfate	994 ± 10
S	Crystalline sulfur	1000 ± 8	S	Sodium sulfate	998 ± 10
S	Pyrite	1001 ± 8			

[a]Average (n = 5) ± standard deviation.

TABLE 2

Effect of added substances on the determination of 0.1 mg of carbon and 0.1 mg of sulfur

Substance	M.p. (°C)	Added (mg)	Relative error[a] (%)	
			C	S
CuO	1026	100	−2	−8
Na_2O_2	460 (dec.)	50	+456	−13
NaCl	800	100	0	−53
KNO_3	334	100	+13	−30
$K_2Cr_2O_7$	398	100	0	−48

[a]Average (n = 2).

samples containing a high percentage of water, which is deposited on the walls of the delivery tubes or the surface of the dust filter and absorbs some sulfur dioxide [3, 6].

This difficulty was overcome by placing an additional tube, filled with magnesium perchlorate (12 g), between the dust filter and original drying tube, and by combusting smaller samples. The results for samples which contain more than 4% of water are shown in Table 3.

Calibration curves

The calibration standards for carbon and sulfur were prepared from known amounts of calcium carbonate, crystalline sulfur and silicon dioxide; samples were ground and mixed in an agate mortar.

Nearly linear calibration curves were obtained for 200—10000 ppm of carbon and 200—2000 ppm of sulfur with 0.5-g samples. For amounts less than 200 ppm, the curves were slightly curved, giving high results for carbon and low results for sulfur; several calibration standards were used for low carbon and sulfur analyses. When 0.1-g samples were used, the calibration was nearly linear for 200—50000 ppm of carbon and 200—5000 ppm of sulfur.

TABLE 3

Relation between amounts of sample and dehydrating agents in the determination of sulfur in selected sediments

Sample	Taken (g)	Found[a] S (ppm)		NBS values (ppm)
		$Mg(ClO_4)_2$ (12 g + 8 g)[b]	$Mg(ClO_4)_2$ (8 g)[c]	
GXR-1[d]	0.2	2436	2380	
GXR-1	0.5	2200	2123	
NBS-97[d]	0.1	158	125	168
NBS-97	0.2	143	85	
NBS-98[d]	0.1	250	190	280
NBS-98	0.2	210	145	
NBS-98a[d]	0.1	1300	1190	
NBS-98a	0.2	1254	955	

[a]Average (n = 3). [b]After modification. [c]Originally. [d]Water contents: GXR-1, 4.4%; NBS-98, >5%; NBS-97, 98a, >9%.

Recommended procedure

Place magnesium perchlorate (12 g and 8 g, respectively) in the drying tubes. Pass oxygen (2.5 l min^{-1}, 1.5 kg cm^{-2}) and nitrogen (0.4 l min^{-1}, 0.6 kg cm^{-2}) through the apparatus. Adjust the blank corrector for carbon and sulfur according to the amounts of the accelerators used.

Weigh the powdered sample (0.1 g for 0.05—5% carbon, 0.05—1% sulfur or >4% water, and 0.5 g for 0—0.05% carbon and sulfur) into a crucible and level the top of the sample powder. Cover the surface with iron powder (ca. 0.6 g for 0.1-g samples, 1.2 g for 0.5-g samples) and add tungsten chips (ca. 1.3 g for 0.1-g samples, 2.6 g for 0.5-g samples). Place the crucible on the pedestal of the furnace. Introduce the crucible into the non-preheated combustion tube by raising the locking mechanism handle. Combust for 35—60 s during which time the tube reaches about 1800°C.

RESULTS AND DISCUSSION

Study of precision

The precision and recovery for carbon and sulfur in rocks were examined. Known amounts of calcium carbonate and crystalline sulfur were added to rock samples (JG-1 granodiorite and JB-1 basalt). The results are given in Table 4. The relative standard deviations are 6% or less for 100-1000 μg of carbon and sulfur. The recovery is 96—103% for carbon and 97—102% for sulfur.

Analysis of geological samples

Results for carbon and sulfur in a variety of standard reference samples are given in Table 5. The values for carbon by Abbey [10] and Flanagan [11]

TABLE 4

Precision and recovery in the determination of carbon and sulfur

Samples	Taken (g)	C and S added (μg)	Carbon			Sulfur		
			Found[a] (μg)	s_r (%)	Recovery (%)	Found[a] (μg)	s_r (%)	Recovery (%)
JG-1	0.5	0	109	6	—	5.5	24	—
JG-1	0.5	50	160	4	102	55	6	99
JG-1	0.5	100	212	4	103	102	6	97
JG-1	0.2	500	548	2	101	514	2	102
JB-1	0.5	0	236	5	—	6.8	26	—
JB-1	0.2	500	574	2	96	506	2	101
JB-1	0.2	1000	1086	1	99	999	2	100

[a]Average (n = 5).

TABLE 5

Analytical results for carbon and sulfur in standard silicates

Samples	Carbon (ppm)			Sulfur (ppm)		
	This study[a]	Abbey [10][b]	Flanagan [11][b]	This study[a]	Abbey [10]	Terashima [12]
G-2	246	218	218	93	< 100?	64
GSP-1	336	328	410	348	400	200
AGV-1	48	27	164	14	100?	46
PCC-1	543	437	328	20	100?	20
DTS-1	314	164	218	8	< 100	11
BCR-1	67	82?	82	412	400?	398
MRG-1	3012	2757	—	640	600	544
SY-1	1290	—	1010	203	—	—
SY-2	1430	1256?	—	128	100	112
SY-3	1202	1092	—	533	500	346
NIM-D	1150	1147?	1092	68	200?	66
NIM-G	144	273?	273	100	100?	68
NIM-L	432	491?	546	537	600	510
NIM-N	222	300?	273	50	100?	45
NIM-P	283	273?	273	109	200?	110
NIM-S	132	218?	273	23	200?	35
JG-1	219	218?	246	11	—	14
JB-1	472	491?	519	14	—	59

[a]Average (n = 4—5). [b]Values calculated from carbon dioxide.

were re-calculated from the carbon dioxide values; the present carbon values for PCC-1 and DTS-1 are significantly higher than those obtained previously. The differences may arise from the presence of non-carbonate carbon in the samples. For sulfur, the agreement is poor for several samples. The

present results are generally higher than the x.r.f. values [12] for samples containing more than 200 ppm of sulfur; this may result from the use of different calibration standards.

The results for limestone, feldspar, clay and phosphate (National Bureau of Standards) and soils, sediments and copper ore (Association of Exploration Geochemists of Geochemical Exploration Reference) are listed in Table 6. High carbon (>5%) and sulfur (>1%) contents were determined after diluting the reference sample with silicon dioxide. The agreement for carbon between the present study and others is generally good.

The results for sulfur are in accord with or slightly lower than the values for all samples except the NBS-1a limestone. The NBS certificate value (2660 ppm) was obtained from eleven determinations by a gravimetric method. Three values of more than 3000 ppm were included in the NBS results. Others have added new data, as listed in Table 7. Most workers reported a content of 2700 ppm, but the results of Searle [7] and this study are over 3000 ppm. This limestone sample should therefore be cross-checked further by different methods and laboratories; the selection of accelerator may be important (Table 7).

The analysis time depends on the carbon or sulfur contents. In general, 40 s for carbon and 45 s for sulfur are required in the determination of 0.05% levels with 0.5-g samples. For 0.1-g samples, 5% of carbon and 1% of sulfur can be determined in less than 60 s.

TABLE 6

Analytical results for carbon and sulfur in NBS minerals and Geochemical Exploration Reference samples (GXR)

Samples	Carbon (%)		Sulfur (ppm)	
	This study[a]	Others[b]	This study[a]	Others[b]
NBS-1a Limestone, argillaceous	9.73	9.76	3073	2660
NBS-88a Limestone, dolomitic	12.83	12.72	4	—
NBS-70a Feldspar, potash	0.005	—	3	—
NBS-99a Feldspar, soda	0.03	—	19	—
NBS-97 Clay, flint	0.32	—	158	168
NBS-97a Clay, flint	0.06	—	308	—
NBS-98 Clay, plastic	0.40	—	250	280
NBS-98a Clay, plastic	0.81	—	1300	—
NBS-120a Phosphate	1.04	0.87	2900	—
GXR-1 Jasperoid	0.17	—	2436	2600
GXR-2 Soil	2.64	2.68[c]	315	300
GXR-3 Hot spring deposit	1.33	1.34[c]	2420	2500
GXR-4 Porphyry copper ore	0.06	—	17600	17150
GXR-5 Soil	1.65	—	278	300
GXR-6 Soil	0.18	0.19[c]	131	200

[a]Average (n = 3—5). [b]Certificate values by NBS. GXR samples data from Allcott and Lakin [13]. [c]S. Nagata (Geol. Surv. Jpn.); obtained by CHN analyzer.

TABLE 7

Comparison of furnace types and accelerators used in determination of sulfur in NBS-1a limestone

Sulfur content (ppm)		Furnace	Accelerators	References
Mean	Range			
2660	1880—3096			Certificate value (1931)
2700	2600—2800	Resistance[a]	Fe + Sn	[4]
2725	2700, 2750	Resistance[b]	V_2O_5	[5]
3060	3060 ± 233	Induction	$Fe+MoO_3+CrO_3$	[7]
2700		Resistance[c]	Sn	[6]
2700		Induction	Fe	[6]
2775	2750, 2800	Induction	Fe	[3]
3073	3000—3120	Induction	Fe + W	This study

[a]1310—1320°C. [b]950°C. [c]1450°C.

Conclusion

The sensitivity of the method is 0.5 μg of carbon and sulfur; the limit of detection for 0.5-g samples is 20 ppm for carbon and 5 ppm for sulfur, at the 2 σ confidence level. The method has been applied satisfactorily to a variety of geological materials. The analysis time for two elements in one sample is less than one minute.

The author is grateful to Dr. S. Abbey for supplying useful papers, and to Dr. N. Tono, Dr. A. Ando and Dr. S. Ishihara for helpful suggestions.

REFERENCES

1 A. E. Foscolos and R. R. Barefoot, Geol. Surv. Can. Paper, 70-11 (1970).
2 J. G. Sen Gupta, Anal. Chim. Acta, 51 (1970) 437.
3 J. L. Bouvier, J. G. Sen Gupta and S. Abbey, Geol. Surv. Can. Paper, 72-31 (1972).
4 M. E. Coller and R. K. Leininger, Anal. Chem., 27 (1955) 949.
5 J. G. Sen Gupta, Anal. Chem., 35 (1963) 1971.
6 J. G. Sen Gupta, Anal. Chim. Acta, 49 (1970) 519.
7 P. L. Searle, Analyst, 93 (1968) 540.
8 A. Ohnuma, S. Ihara and E. Oguchi, Gakushin, Open-file Report (Jpn.), 19—9847 (1975).
9 J. W. Fulton and R. E. Fryxell, Anal. Chem., 31 (1959) 401.
10 S. Abbey, Geol. Surv. Can. Paper, 77-34 (1977).
11 F. J. Flanagan, Geochim. Cosmochim. Acta, 37 (1973) 1189.
12 S. Terashima, Bull. Geol. Surv. Jpn., 27 (1976) 185.
13 G. H. Allcott and H. W. Lakin, U.S. Geol. Surv. Open-file Report, 1974, p. 33.

Analytica Chimica Acta, 101 (1978) 33—43

SEMI-AUTOMATED DETERMINATION OF ANTIMONY IN ROCKS

C. Y. CHAN*

Ontario Geological Survey, Ministry of Natural Resources, 77 Grenville Street, Toronto, Ontario (Canada)

P. N. VIJAN

Laboratory Services Branch, Ministry of the Environment, 880 Bay Street, Toronto, Ontario (Canada)

(Received 23rd February 1978)

SUMMARY

A simple, rapid and accurate method for the determination of total antimony in rock samples is described. An automated hydride generation procedure is used to generate stibine gas from solutions of rock samples prepared by digestion with a mixture of hydrofluoric and sulfuric acids. The evolved hydride is carried to a heated quartz tube by an argon stream and the atomic absorption of antimony recorded. The method is practically free from interferences. As little as 0.08 μg Sb g^{-1} can be determined; the average r.s.d. over the range 0.16—4.5 μg g^{-1} is 6.5%. Close agreement is obtained between results obtained on 14 U.S. Geological survey rocks by this method and those reported by neutron activation analysis.

Rocks generally contain 0.1—5 ppm of antimony. Igneous rocks contain a few tenths of a ppm; sedimentary and maphic rocks, shales, etc. contain higher concentrations. The accurate determination of such low concentrations is laborious and time-consuming. All recently reported results on new and old USGS rock standards that are considered reliable have been obtained by instrumental neutron activation analysis (i.n.a.a.) [1]. However, the method requires very complex and costly equipment, and is slow. Of the several spectrophotometric methods described in the literature, that based on the reaction of rhodamine B with antimony(V) in hydrochloric acid [2] has been considered appropriate, but even this is not sensitive enough, is tedious and requires >1 g of sample and large quantities of reagents. The same difficulties are inherent in the method [3] based on the volatilization of antimony triiodide followed by TOPO—MIBK extraction. Graphite-furnace atomic absorption spectrometry [4] has the required sensitivity, but suffers from matrix interferences, poor precision and possible volatility losses during the ashing step.

There is a need for a method of determining antimony in rocks which is specific, sensitive, precise, accurate, rugged, involves very few procedural steps, requires equipment and staff within the budget of an average laboratory

and has rapid turn-around time on a batch of samples. Earlier experience with a semi-automated hydride generation—atomic absorption technique indicated that such a method for the determination of antimony in rocks would meet these criteria.

Vijan et al. [5—9] have published methods for determinations of arsenic, selenium, lead and tin in environmental samples by automated generation of volatile hydrides of these elements, followed by their atomization in a heated quartz tube and measurement of their atomic absorption signals. These methods have become very popular; many papers have been published on the subject, and discussed in the above references. Inhat and Miller [10] have reviewed the different hydride generation systems and atomization techniques.

Pierce and Brown [4] have demonstrated the superiority of automated hydride generation combined with heated quartz tube atomization over manual methods and graphite furnace atomization methods. Fiorino et al. [11] determined antimony in food samples, but their absorption signals were transient as opposed to the steady-state signals given by the continuous automated generation of stibine. They point to the high cost of equipment required for the latter technique. However, a reconditioned multi-channel peristaltic pump costs only about the same as a commercial hydride generation kit, and the advantages outweigh the increased cost. The use of an automated sampler is not necessary and can be dispensed with by hand feeding the sample solutions.

EXPERIMENTAL

Reagents

Hydrofluoric acid (Baker 49.3%), hydrochloric acid (ACS 37—38%) and sulfuric acid (ACS 95.5—96.5%) were used. All other chemicals used were ACS analytical-reagent grade.

Digestion mixture. Mix 1 part of hydrofluoric acid, 1 part of sulfuric acid and 1 part of distilled water. Store in a polyethylene bottle.

Borohydride solution. Dissolve 3.0 g of sodium borohydride (Fisher Scientific) and 0.3 g of sodium hydroxide in 300 ml of distilled water. Use fresh. It may be stored in a refrigerator for a few days.

Stock standard antimony solution. (1000 ppm; Harleco, as $SbCl_3$). Prepare working standard solutions (5—30 ng Sb ml^{-1}) by serial dilution of the stock standard with a mixture of 10% sulfuric and 20% hydrochloric acids.

Potassium iodide solutions. Dissolve 10 g of potassium iodide and 0.1 g of sodium hydroxide (2 pellets) in 100 ml of distilled water.

Apparatus

An atomic absorption spectrometer capable of giving a stable signal at the Sb 217.6-nm line is required. A Techtron Model AA5 equipped with

HTV R106 photomultiplier tube and a 1—10-mV variable range strip chart recorder was used. The sampler and proportioning pump were reconditioned Technicon modules. The quartz cell, 10 cm long and 0.6 cm i.d., with a 17-cm long inlet tube (4 mm o.d.) fused onto it at the centre, was wound with a 22-gauge asbestos-coated chromel A heating wire (Sargent Welch, Cat. No. 585126). It was further insulated with a layer of asbestos tape and a layer of asbestos cord. The temperature of this furnace was controlled with a variable transformer. The argon flow was regulated by a calibrated flow-meter. A 4-place Sartorius analytical balance was used for weighing the samples. The flow system is shown in Fig. 1 and the optimal instrumental parameters are as follows: wavelength, 217.6 nm; lamp current, 10 mA; slit width, 100 μm; flow rate (argon), 300 ml min^{-1}; instrument damping, D (maximum); recorder span, 2 mV full-scale; recorder speed, 0.25 cm min^{-1}; atomizer temperature, 850 ± 10°C; sample time, 1 min; wash time, 2 min.

Sample and standards preparation

The rock sample (100.0 mg) is weighed on a piece of weighing paper and transferred to a 50-ml Teflon beaker (Chempure). A blank and 5, 10, 15 and 20 ng ml^{-1} antimony standards are included in a set of samples by adding 0.0, 0.05, 0.1, 0.15 and 0.20 ml of a 1.5 μg ml^{-1} standard solution of antimony to 5 Teflon beakers by means of a 0.2-ml class A graduated pipette with 0.001-ml subdivisions. Digestion mixture (5 ml) is dispensed into each beaker. The beakers are heated gently on a hot plate for 30 min and fumed at medium heat. Any dark, insoluble matter, if present, is oxidized by careful

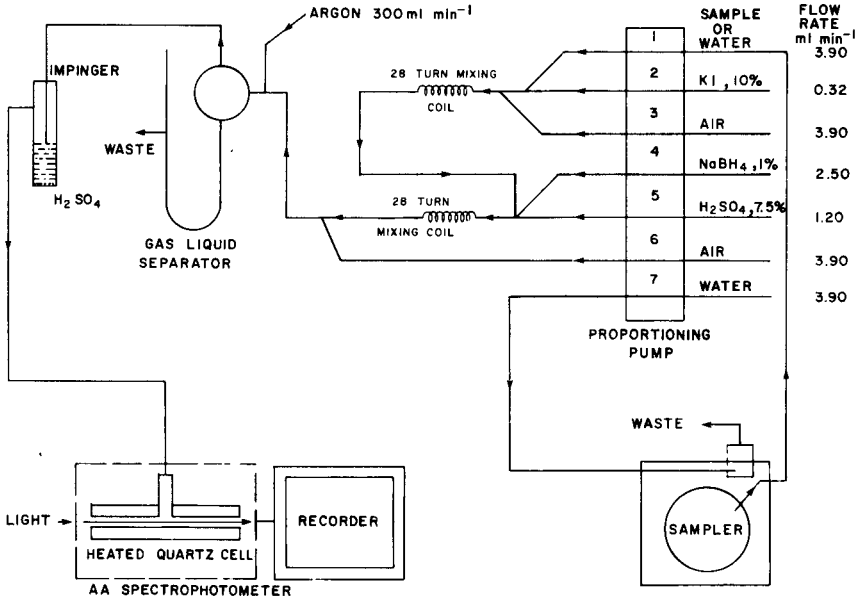

Fig. 1. Autoanalyzer—a.a.s. flow system for determination of antimony.

addition of a few drops of concentrated nitric acid. The contents are allowed to fume moderately for 10—15 min. Excessive fuming and formation of a dry crust should be avoided. The contents are allowed to cool to room temperature and 5 ml of distilled water are added to each beaker. The contents are heated close to the boiling point and cooled again to room temperature. Hydrochloric acid (1 + 1, 6 ml) is added to each beaker and the contents are quantitatively transferred to 18 × 150-mm culture tubes calibrated for 15 ml. The volumes are made to 15 ml with distilled water and the contents mixed. A well digested sample should yield a clear solution. Alternatively, undigested standards prepared in a mixed acid solution (10% H_2SO_4—20% HCl) may be used since digested and undigested standards yield comparable signals.

Determination of antimony

The instrumental parameters listed above are established and the equipment allowed to warm up for 20—30 min. The quartz tube furnace is fastened securely to the top of the burner head and aligned with the light beam to allow maximum light from the hollow-cathode lamp to reach the detector. The quartz cell is heated to the required temperature. The manifold tubes are inserted into the appropriate reagent bottles and the proportioning pump is started. The argon gas is turned on immediately and its flow adjusted at 300 ml min^{-1}. The performance of the system is checked by feeding a 10 ng ml^{-1} standard solution of antimony. The sample, standard and reagent blank solutions are transferred to the sample cups held in the sampling tray. Every 10th cup is filled with a 10 ng ml^{-1} standard solution to monitor instrumental drift. The sampler is started and the absorption signals recorded. The heights of the standard peaks are measured and a calibration graph is drawn. The concentrations of antimony in the sample solutions are read from this graph using their respective peak heights. For a sample weight of 100 mg and volume of 15 ml, μg Sb g^{-1} = ppb Sb in sample solution × 0.15.

RESULTS AND DISCUSSION

Interferences

Under the experimental conditions of this method, the elements most likely to interfere are those whose ions react with sodium borohydride in strongly acidic media either to form volatile hydrides or to precipitate as the metals. The interference may result from the alteration of the rate of reaction or co-precipitation of the analyte or both. The elements which form volatile hydrides are those of periodic groups IVA, VA and VIA, and those which precipitate as metals are some of those in groups IB, IIB and VIII. Fortunately, the concentrations of these elements are very low in the common rock-forming minerals except for silica, which is volatilized during the digestion process.

TABLE 1

Concentrations of foreign elements found to have no interfering effect on analysis for 10 ng Sb ml^{-1}

Element	Concn. ($\mu g\ ml^{-1}$)	Equiv. content in rock (%)[a]	Element	Tolerance limit ($\mu g\ ml^{-1}$)	Equiv. content in rock (ppm)[a]
Ca	4000	60	Cu	20	3000
Mg	4000	60	Ni	10	1500
K	4000	60	Co	40	6000
Na	4000	60	Bi	10	1500
Al	4000	60	As	5	750
Fe	4000	60	Se	20	3000
Zn	200	3	Sn	20	3000
Pb	200	3	Te	1	150
Ti	200	3			
Cd	200	3			

[a]Based on 0.1 g of sample in 15 ml of solution.

Table 1 shows that the method is free of interference from large concentrations of the major constituents of rocks such as aluminum, iron, calcium, magnesium, sodium, potassium and titanium. The maximum concentrations of these elements in the prepared solutions of standard rocks, as calculated from previously reported analytical results will be 800, 620, 533, 805, 660, 387 and 100 $\mu g\ ml^{-1}$, so there should be no interferences from these elements. The accuracy of the results obtained (Table 2) supports this finding.

The stock arsenic and tellurium solutions used in the interference study contained traces of antimony as an impurity. A 3 $\mu g\ ml^{-1}$ tellurium solution produced an antimony signal equivalent to 3 ng Sb ml^{-1}. Progressively smaller peaks were obtained for 2 and 1 $\mu g\ ml^{-1}$ tellurium solutions. The possibility of molecular absorption was excluded by the use of non-absorbing 217.0-nm line which produced no signals. A similar antimony signal was observed for 10 μg As ml^{-1} solutions. Also a 15% depression of the 10 ppb antimony signal is caused by 10 μg As ml^{-1} or 3 μg Te ml^{-1} solutions, such concentrations corresponding to 1500 μg As g^{-1} and 300 μg Te g^{-1} in a rock sample. Occurrence of arsenic and tellurium at these concentrations in natural rocks is highly unlikely.

Common anions such as chloride, nitrate, perchlorate and phosphate do not interfere. Sulfite and sulfide ions interfere by producing a non-specific absorption peak from hydrogen sulfide. Sulfites rarely occur in rocks, but pyrites and pyrrhotite do so more frequently. However, under the conditions of sample digestion, both sulfites and sulfides are destroyed and do not pose any problem.

TABLE 2

Results for antimony in standard rocks in comparison with reported values by neutron activation[a]

Standard rock		This study			I.n.a.a.[b]		
		($\mu g\ g^{-1}$)	n	s_r	($\mu g\ g^{-1}$)	n	s_r
USGS	AGV-1[c]	4.37	9	5.1	4.17	6	3.4
	BCR-1	0.59	10	3.8	0.49	6	23.6
	G-1	0.30	10	19.6	0.31	5	25.8
	GSP-1	3.21	9	4.6	3.22	6	9.1
	PCC-1	1.34	10	5.7	1.36	6	14.8
	DTS-1	0.46	10	7.7	0.46	4	6.2
	BHVO-1[c]	0.17	7	11.5	0.16	6	24.4
	MAG-1	0.82	10	8.9	0.88	6	12.2
	QLO-1	1.99	10	2.6	2.03	6	21.3
	RGM-1	1.26	9	4.3	1.30	6	7.5
	SCo-1	2.49	9	3.65	2.51	6	4.0
	SDC-1	0.54	10	3.6	0.53	6	19.5
	SGR-1	3.74	9	5.4	3.70	6	2.9
	STM-1	1.65	8	4.8	1.67	6	3.5
Canadian	SY-2	0.31	6	9.3			
	SY-3	0.37	6	9.0			
	MRG-1	0.39	6	4.2			
	MRB-1	0.18	6	3.85			
		Average s_r =		6.5			

[a]The results given are the mean values ($\bar{x}$), the number of determinations (n) and the relative standard deviation (s_r).
[b]Values obtained from ref. [1], page 68 (Schwarz and Rowe) except for G-1, PCC-1 and DTS-1, which were taken from p. 162.
[c]Analysed singly with each set of replicates to assess between run precision.

Effect of acid concentration

The acid concentration of the sample solution has an important effect on the degree of interference. With the potassium iodide line eliminated (Fig. 1), when the concentration of sulfuric acid in the sample was reduced from 10% to 1% (v/v) less than 1 $\mu g\ ml^{-1}$ of copper, selenium and tin began to show significant depression of the 10-ppb antimony signal. Sets of 20 ng Sb ml^{-1} standards, prepared in hydrochloric, nitric, perchloric and sulfuric acids of incremental concentrations between 0.1% and 30.0% (v/v) were processed twice in the analysis system (Fig. 1), once with potassium iodide reagent and a second time with distilled water pumping through channel 2. The results of this study are depicted in Fig. 2. The maximum absorbance of 20 ng Sb ml^{-1} is 0.09 in the absence of potassium iodide as against 0.180 in its presence. This is an effect of the oxidation state of antimony and is explained later.

It is also evident from curve A that potassium iodide is ineffective as a reducing agent in a medium less than 2% acid. Its full potential is realised at

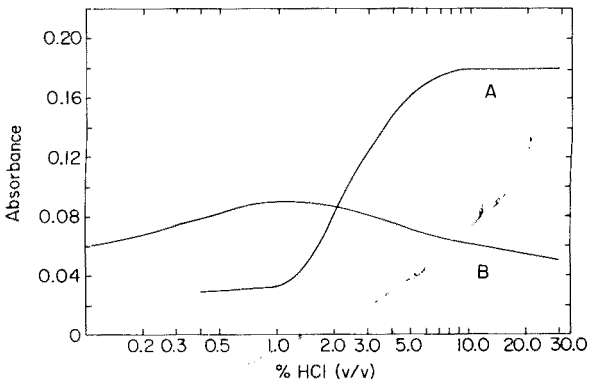

Fig. 2. Effect of acid concentration on the absorbance signal of antimony (20 ng Sb ml^{-1}). A, in the presence of KI; B, in the absence of KI.

acid concentrations greater than 7%. The other acids investigated behaved similarly, as did mixtures of acids.

Sulfuric acid is considered very suitable for solubilizing antimony in most chemical forms. That lower boiling nitric, hydrochloric and hydrofluoric acids are easily expelled on heating to fumes of sulfur trioxide, is a desirable property which allows close control of the final concentration of acids in the prepared sample solutions. The use of nitric acid may be necessary if the samples contain organic matter. Antimony halides are reported [12] to be volatile under certain conditions of digestion and the use of hydrochloric acid should be avoided during the digestion phase. However, no losses of antimony were discovered when up to 1 ml of hydrochloric acid was deliberately added to the samples and standards prior to digestion. Addition of hydrochloric acid to the cold digestate is considered necessary. Consistently more precise results were obtained in its presence than in its absence. It appears to speed up the dissolution of the sample as well as to provide a desirable medium for reduction of Sb(V) to Sb(III) by potassium iodide.

Effect of oxidation state of antimony

Test solutions of antimony(V) were prepared by oxidizing a standard antimony(III) solution with 0.1 N potassium permanganate solution or from a 100-ppm stock solution prepared from antimony pentoxide.

In the absence of potassium iodide, a 20 ng ml^{-1} solution of antimony(III) produced a signal six times higher than that of antimony(V). When potassium iodide was present, antimony in either oxidation state produced signals of equal magnitude. The potassium iodide, therefore, functions primarily as a reductant for antimony(V) to antimony(III).

All standard antimony solutions prepared in 10% hydrochloric or sulfuric acids or their mixtures were found to be stable, except that some conversion of antimony(III) to antimony(V) occurs on storage. This was indicated by

the lower than expected absorption peak heights obtained in the absence of potassium iodide. Lower acidities appear to favour this conversion. However, this should be of no concern because potassium iodide (10% w/v solution) is an essential component of the analysis system. It quantitatively converts antimony(V) to antimony(III) before it is determined, and it also increases the tolerance of the method towards selenium by reducing it to the element. These findings are in agreement with Fiorini et al. [11]. Potassium iodide solutions (5—10% w/v) equivalent to 0.2—0.4% in the final mixed stream were adequate; a 10% solution was used to allow for the reduction of other species such as iron(III), as well. Other reducing agents such as chromium(II) [13] and sodium sulfite were investigated without success.

Precision, accuracy, sensitivity and detection limit

Table 2 shows the results obtained for the U.S. Geological Survey and Canadian standard rock samples. Mean "ppm Sb" values represent the average of replicate analyses run as a single batch. Therefore, the r.s.d. values reported represent within-run precision. Standard rocks AGV-1 and BHVO-1 were run singly with each batch of replicates to provide data for between-run precision at the higher and lower ends of the range of antimony concentrations in 18 rocks. Sample SY-2, SY-3 and MRG-1 are certified reference materials supplied by the Geological Survey of Canada (G.S.C.). The values for antimony shown in the report [14] issued by G.S.C. are uncertain, and for this reason no recommended values were assigned. Sample MRB-1 is an in-house rhyolite rock standard.

The between-run and within-run precisions of the method are similar. The values indicate the overall precision of the method including errors of weighing and use of home-made calibrated test tubes. The r.s.d. of the determinative step was found to be 1.8% for 10 replicate measurements made on 20 ng Sb ml^{-1} solutions under optimum experimental conditions. Table 2 shows that the accuracy of the results in relation to the i.n.a.a. values is satisfactory. The results reported by Katz and Grossman by the same technique (ref. 1, pp. 52—3) are significantly higher for BHVO-1, G-1 and QLO-1, but lower for PCC-1, SDC-1 and SGR-1.

The detection limit of the method is 0.26 ng Sb ml^{-1} or 0.04 μg Sb g^{-1} on the basis of a 100-mg sample. Ten recorder tracings obtained on a composite of prepared solutions of BHVO-1 (average peak height for 1.13 ng Sb ml^{-1}) were used to calculate the detection limit, defined as the concentration which is twice the standard deviation of the measurements taken near 1 ng Sb ml^{-1}.

The sensitivity and the linearity are illustrated in Fig. 3, together with some recorder tracings for actual sample solutions. The calibration graph was linear up to 50 ng Sb ml^{-1} under optimum conditions of instrument performance. The sensitivity (ng Sb ml^{-1} corresponding to an absorbance of 0.0044) calculated from Fig. 3 is 0.44. Reagent blanks rarely gave any visible peaks. When they did, a maximum peak height of 1.5 divisions of the chart paper was obtained.

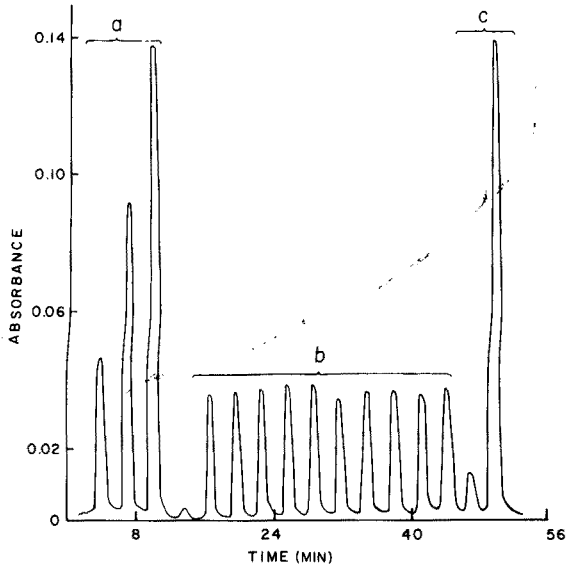

Fig. 3. Signal peaks for: (a) digested antimony standard solutions (5, 10 and 15 ng ml^{-1}); (b) reagent blank and 10 replicates of SDC-1; (c) BHVO-1 and AGV-1.

TABLE 3

Recovery of antimony added as $SbCl_3$ to typical rock samples

Rock sample	Antimony (μg)			Recovery (%)
0.1 g	Added	Found	Recovered	
Andesite 1	0	0.189[a]	—	—
	0.150	0.339	0.150	100.0
	0.150	0.337	0.148	98.6
Andesite 2	0	0.075[a]	—	
	0.450	0.531	0.456	101.3
	0.450	0.525	0.450	100.0
Andesite 2	0	0.075[a]	—	
	0.750	0.840	0.765	102.0
	0.750	0.817	0.742	98.9
				Mean, 100.1%

[a]Average of two results.

Table 3 shows the recovery data obtained by additions of the analyte to two in-house standard rock samples. The amounts of antimony added correspond to 1.5, 4.5 and 7.5 μg g^{-1} in a rock sample. A mean recovery of 100.1% was obtained.

General comments and suggestions

The analytical system described is very rugged. It has given continuous service without breakdown of any component for more than a year except for occasional change of fouled-up tubing. The baseline is so stable that low instrument damping may be used though, obviously, the use of a different instrument may change the baseline characteristics as well as the linear range of the calibration curve. However, the use of organic solvents or detergents poisons the system and must be avoided. Accumulation of heavy metals in reagent lines causes a drastic decrease in sensitivity. Pumping 1% (v/v) hydrogen peroxide, distilled water, 4% (w/v) ammoniacal EDTA, distilled water, in that sequence, through the reagent lines usually cleans the manifold tubes and restores the sensitivity. If this treatment fails, the tubes should be replaced. It is important to disengage the roller head of the peristaltic pump and unstretch the manifold tubes at the end of the analysis. The concentrated sulfuric acid in the impinger drier requires replacement when the liquid level reaches to within 2—3 mm of the tip of the inlet tube.

It is important to turn on the carrier gas stream before or soon after the peristaltic pump is started. Failure to do so may foul up the flow-meter and may also cause a minor flashback in the impinger because of backfiring of hydrogen. The temperature of the quartz tube may be varied within ±10°C without significant effect on sensitivity but, for precise results, temperature fluctuations should be avoided. The damper in the exhaust over the burner head assembly should be barely open to allow the poisonous gases to escape without causing a draft in the area of the atomizer. The effect of the flow rate of carrier gas on the antimony signal is large, and an accurate regulation of the gas flow is necessary for good precision. The use of nitrogen as a sweep gas causes 30—40% loss in sensitivity as compared with argon.

The use of an automatic sampler is not mandatory. The sample solutions can be fed to the sample channel manually and held there until the recorder pen begins to rise. The choice of 15 ml as the final volume of the prepared solution provides sufficient quantity for duplicate measurements. Any other convenient volume may be used if so desired.

The system can also measure arsenic with a sensitivity and detection limit comparable with those for antimony, in the same prepared solutions of rocks, provided that no losses occur during digestion. A few measurements of arsenic showed that indiscriminate losses of this element do occur and a modification in the sample preparation procedure will be necessary.

The authors gratefully acknowledge the technical assistance and helpful suggestions provided by M. W. A. Baig.

REFERENCES

1 F. J. Flanagan, U.S. Geological Survey Professional Paper 840.
2 E. B. Sandell, Colorimetric Determination of Traces of Metals, Vol. III, 3rd edn., Interscience Publishers Inc., New York, 1959, pp. 258—265.
3 E. P. Welsch and T. T. Chao, Anal. Chim. Acta, 76 (1975) 65.
4 F. D. Pierce and H. R. Brown, Anal. Chem., 49 (1977) 1417.
5 P. N. Vijan and G. R. Wood, At. Absorpt. Newsl., 13 (1974) 595.
6 P. N. Vijan and G. R. Wood, Talanta, 23 (1976) 89.
7 P. N. Vijan and G. R. Wood, Analyst, 101 (1976) 966.
8 P. N. Vijan, A. C. Rayner, D. Sturgis and G. R. Wood, Anal. Chim. Acta, 82 (1976) 329.
9 P. N. Vijan and C. Y. Chan, Anal. Chem., 48 (1976) 1788.
10 M. Inhat and H. J. Miller, J. Ass. Offic. Anal. Chem., 60 (1977) 813.
11 J. A. Fiorino, J. W. Jones and S. G. Capar, Anal. Chem., 48 (1977) 120.
12 W. F. Hillebrand and G. E. F. Lundell, Applied Inorganic Analysis, 2nd edn., J. Wiley, New York, 1955, p. 273.
13 Akira Miyazaki, Akira Kimura and Yoshimi Umezaki, Anal. Chim. Acta, 90 (1977) 119.
14 S. Abbey, A. H. Gillieson and G. Perrault, A Report on the Collaborative Analysis of Three Canadian Rock Samples (SY-2, SY-3 and MRG-1) for use as Certified Reference Materials, 1975, Geological Survey of Canada, Ottawa.

Analytica Chimica Acta, 101 (1978) 45—62

A GROUP SEPARATION SCHEME FOR RADIOCHEMICAL NEUTRON ACTIVATION ANALYSIS FOR 24 TRACE ELEMENTS IN ROCKS AND MINERALS

T. SMET[§], J. HERTOGEN*, R. GIJBELS** and J. HOSTE

Instituut voor Nucleaire Wetenschappen, Rijksuniversiteit Gent, Proeftuinstraat 86, B 9000 Gent (Belgium)

(Received 13th April 1978)

SUMMARY

A group separation scheme has been developed for radiochemical neutron activation analysis for Ca, Cu, Zn, Ga, Rb, Sr, Zr, Sb, Cs, Ba, La, Nd, Sm, Eu, Gd, Tb, Ho, Tm, Yb, Lu, Hf, Ta, W and Th in a wide variety of silicate rocks and minerals, especially ultrabasic rocks and mafic minerals. The samples are decomposed in a hydrofluoric acid—nitric acid mixture in a PTFE-lined bomb. The soluble fluorides (Cu, Zn, Ga, Rb, Zr, Sb, Cs, Hf, Ta, W and Pa) are separated into three groups of elements by sequential elution from a cation-exchange resin. The insoluble fluorides (Ca, Rb, Sr, Cs, Ba and REE) are dissolved and purified from interfering iron and scandium activities by extraction with tri-n-butyl phosphate. If necessary, the four main groups can be purified further from interfering activities such as ^{59}Fe, ^{51}Cr and ^{60}Co. The accuracy and reproducibility of the procedure were tested by repeated analysis of U.S. Geological Survey standard granite G-2, andesite AGV-1 and dunite DTS-1.

Neutron activation analysis (n.a.a.) is an established analytical technique in geochemistry owing to its high sensitivity and accuracy for the determination of many trace elements. The introduction of high-resolution Ge(Li) detectors paved the way for the now widely used instrumental neutron activation analysis (i.n.a.a.) [1]. It is a convenient multi-element technique, allowing the determination of about 23 elements in a variety of silicate rocks and minerals. Data processing in i.n.a.a. lends itself readily to automation, and has greatly benefited from the recent developments in the field of small computers.

Nevertheless, i.n.a.a. has its limitations, for the sensitivity depends on the ratio of the photopeaks of the element of interest to the Compton background activity of matrix elements (Na and Fe) and/or trace elements with high neutron activation cross-sections, such as Sc, Cr and Co. The precise determination of less sensitive trace elements such as Rb, Sr, Zr, Sb, Cs and Ba, is therefore limited to rather favourable cases. Multi-element i.n.a.a.

[§] Research Associate of the "Interuniversitair Instituut voor Kernwetenschappen".
*Research Associate of the "Nationaal Fonds voor Wetenschappelijk Onderzoek".
**Present address: Universitaire Instelling Antwerpen, Department of Chemistry, Universiteitsplein 1, B 2610 Wilrijk, Belgium.

of minerals can be applied successfully only to minerals which are poor in Sc, Cr, Fe and Co, such as feldspars and apatites. Therefore an instrumental determination of the so-called large-ion lithophilic trace elements in mafic minerals and ultrabasic rocks is very difficult, if not impossible. In such samples, these elements often have to be determined at very low concentration levels in the presence of relatively high Sc, Cr, Fe and Co concentrations.

The large-ion lithophilic elements can, however, be determined after chemical group separations, aimed at the removal of interfering activities. In this approach, the time-consuming chemical separations are limited as much as possible, by taking full advantage of the possibilities of present-day high-resolution γ-ray spectrometry. Such group separation schemes have been described by various workers [2—6].

The group separation scheme presented here was developed primarily for the determination of trace elements of proven geochemical interest in ultrabasic rocks and nodules and in pyroxene, amphibole or olivine phenocrysts. The samples are decomposed in a mixture of hydrofluoric acid—nitric acid in a high-pressure bomb, with subsequent separation of the REE and alkaline earths as insoluble fluorides. The soluble fluorides are separated by a cation-exchange procedure. The quantitative separation of the REE as a group very early in the separation scheme, with negligible risks of losses or internal fractionation in the course of the procedure, is one of the great advantages of the method. Basically, four chemical groups are obtained which can be further purified from interfering activities if necessary. Manpower requirements are far from excessive; the procedure was designed so that it can be carried out by one analyst.

In ultrabasic rocks, 18 trace elements were determined: Ca, Cu, Zn, Ga, Rb, Sb, Cs, Ba, La, Ce, Nd, Sm, Eu, Ho, Tm, Yb, Lu, Hf, Ta. The scheme can also be applied to more common basaltic and evolved rock samples. In conjunction with i.n.a.a., Ca, Cu, Zn, Ga, Sr, Zr, Sb and W can then be determined, while analysis for other elements (Rb, Cs, Ba) becomes more precise. No provisions were made in the procedure for determinations of Na, Sc, Cr, Fe, Co and U. With the exception of uranium, these elements can readily be determined via i.n.a.a., either on a separate sample aliquot or on the same sample aliquot used for the chemical procedure.

Outline of the radiochemical procedure

The radiochemical separation scheme is summarized in Fig. 1. After irradiation, the samples are decomposed in a polytetrafluoroethylene (PTFE)-lined high-pressure bomb [7, 8] in a mixture of hydrofluoric acid and nitric acid. The bomb has a useful volume of ca. 100 ml and is similar to that described by Bernas [9]. Hydrofluoric acid is evaporated and the residue taken up in 0.1 M HF. Ca, Sr, Ba and REE precipitate quantitatively as fluorides and are removed by centrifugation. The supernate contains the major fraction of Cu, Zn, Ga, Zr, Sb, Hf, Ta, W and Pa. The elements Na, K, Sc, Cr, Co, Rb and Cs are distributed over both phases.

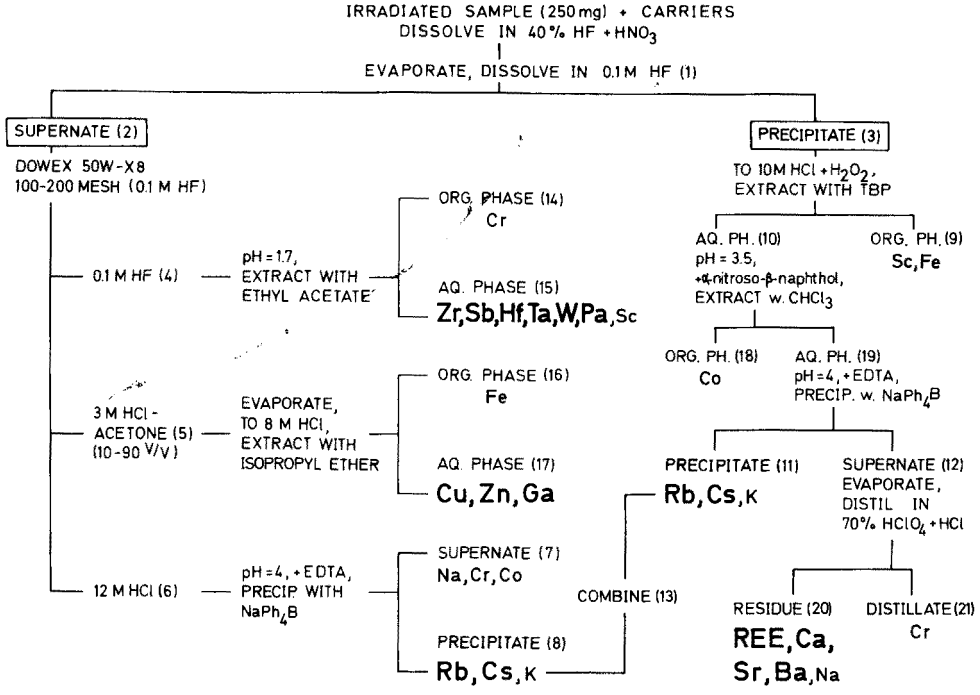

Fig. 1. Radiochemical group separation scheme. Elements determined in the fraction are printed in bold face. Interfering elements are printed in ordinary type. Fraction numbers are given in parentheses for easy reference to the text.

The supernate is loaded onto a cation-exchange column in 0.1 M HF. Sc, Zr, Sb, Hf, Ta, W, Pa and part of the Cr are eluted with 0.1 M HF [10]; chromium is extracted as perchromic acid in ethyl acetate [11, 12]. Cu, Zn, Ga and Fe are eluted with 10:90 (v/v) 3 M hydrochloric acid—acetone [13]. Iron(III), but not Fe(II), can be eliminated from an 8 M HCl solution by solvent extraction in isopropyl ether [14]. However, gallium is also extracted under these conditions [15], and a double extraction is required to prevent gallium from ending up in the iron fraction. Finally, Na, K, Cr, Co, Rb, and Cs are eluted with 12 M HCl. K, Rb and Cs are isolated by precipitation with tetraphenylboron; ethylenediaminetetraacetic acid is added as hold-back reagent for Cr and Co.

The initial fluoride precipitate is dissolved in 10 M hydrochloric acid. Sc and Fe are selectively extracted from this solution with 100% tri-n-butyl phosphate [16], and cobalt is extracted as Co—1-nitroso-2-naphthol into chloroform [17]. The elements K, Rb and Cs are again isolated with tetraphenylboron, in the presence of ethylenediaminetetraacetic acid, to inhibit co-precipitation of heavy REE. The two tetraphenylborate precipitates are combined. Finally, the supernate is purified from interfering chromium

activity by distilling CrO_2Cl_2 from boiling perchloric acid in the presence of hydrochloric acid [18].

In analyses of samples where the ^{51}Cr activity does not present a problem in fractions 4 and 12, these purification steps can be omitted. The same holds for ^{59}Fe and ^{60}Co in fractions 5 and 10. The abridged procedure (Fig. 2) can be applied to the analysis of feldspar minerals and of the common basaltic and evolved rock types.

Ca, Sr, Ba and REE are quantitatively recovered; the radiochemical yields for the other elements are determined by re-activation.

EXPERIMENTAL

Standards

Comparative rock standards were preferred to synthetic multi-element group monitors. The preparation of such monitors, in which the activity ratios of the different elements mimic those observed in actual samples, is cumbersome and undeniably prone to systematic errors. Of course, the use of standard rocks also has disadvantages, e.g. spectral interferences and masking of less intense γ-rays. The precision of the determination of certain elements depends on the precision with which these elements can be measured in the standard. However, this is much less of a problem in a radiochemical group separation scheme than it is in i.n.a.a., because the standard rock is processed in the same way as the samples.

The trace element abundances in several widely distributed primary rock standards such as U.S. Geological Survey BCR-1, AGV-1 and G-2, are now quite accurately known. These rocks can therefore serve as suitable monitors

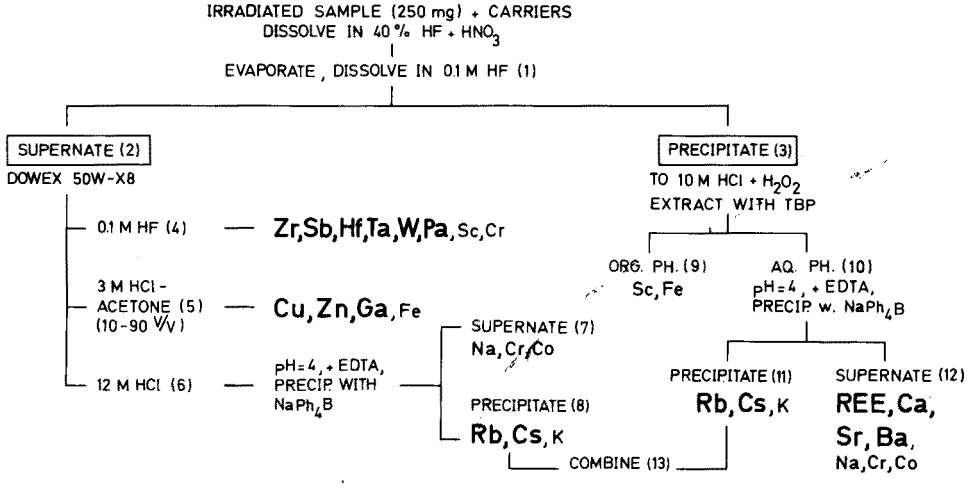

Fig. 2. Abridged separation procedure. Bold type, small type and numbers in parentheses have the same meanings as in Fig. 1.

for the standardization of secondary in-house standard rocks. Besides BCR-1 and AGV-1, two in-house standards were used: FU-130 and FU-128 (an alkali basalt and a hawaiite, sampled by De Paepe [19] on Fuerteventura, Canary Islands). Both were standardized partly by i.n.a.a. [20] and partly by r.n.a.a. [21].

Irradiations

The samples were ground in an agate mortar to a particle size of 50—100 μm, and were irradiated without further treatment.

Irradiation vials were prepared as follows: quartz ampoules were cleaned in hot aqua regia, rinsed with water and dried; polyethylene vials were cleaned with aqueous 3% H_2O_2 solution, rinsed with water and acetone, and dried.

Samples with low abundances of the trace elements of interest were irradiated in the BR-2 reactor at Mol, Belgium. Depending on the available sample weights, 50 to a maximum of 250-mg samples of finely powdered rock or mineral were sealed in quartz vials (4-mm outside diameter, 0.5-mm wall thickness). Samples and 100 mg of a standard rock were irradiated together for 4—6 days in a thermal neutron flux of ca. 10^{13} n cm^{-2} s^{-1}. Tiny steel wires (0.2-mm diameter) were attached around the quartz ampoules, at half sample height, to monitor the lateral and vertical flux gradients inside the irradiation can.

The other samples were irradiated in the 250-kW Thetis reactor of the authors' Institute, in a thermal neutron flux of ca. 1.5×10^{12} n cm^{-2} s^{-1} for two periods of 7.5 h at 5-day intervals. Samples weighing 200—2500 mg were packed in polyethylene vials. Iron discs were used to monitor the flux gradients.

Carrier solutions

Mixed stock solutions of the following carrier elements were prepared. The concentrations (in mg ml^{-1}) of the respective *element* are noted in parentheses; these concentrations are at least 100 times higher than the highest sample concentration.

1. La_2O_3 (10), Sm_2O_3 (1) and Yb_2O_3 (1), dissolved in 14 M HNO_3;
2. HfO_2 (0.85), Ta_2O_5 (0.1), H_2WO_4 (0.04) and Zr (10), dissolved in 40% HF with a few drops of fuming HNO_3;
3. Cu (20), Ga (20) and ZnO (120), dissolved in 6 M HNO_3;
4. Sb_2O_3 (0.8), dissolved in 6 M NH_4OH, with some tartaric acid added;
5. $Sr(NO_3)_2$ (1), dissolved in water;
6. RbCl (110), CsCl (22), dissolved in water.

Before transfer of the irradiated samples, 1 ml each of solutions 1, 2 and 5, and 100 μl each of solutions 3, 4 and 6 were pipetted into the PTFE vessel, and evaporated to dryness under an i.r. lamp.

Counting equipment and counting scheme

Counting was done with two coaxial Ge(Li) detectors with active volumes

of 53 cm^3 and 78 cm^3, and with two extra-high-resolution low-energy photon detectors (LEPD). The first LEPD [22] was a planar Ge(Li) detector with an active diameter of 10 mm, a sensitive depth of 5 mm, and an energy resolution of 460 eV at 100 keV. The second LEPD was a hyperpure germanium detector with an active diameter of 10 mm, a sensitive depth of 7 mm and a resolution of 450 eV at 100 keV; a boron ion-implanted layer functioned as the upper surface electrode, eliminating interfering x-ray peaks from metallic contact layers.

In comparison with i.n.a.a., a group separation procedure requires more measuring time, because each sample is separated into several fractions. Table 1 lists the counting scheme for the different fractions, together with

TABLE 1

Measuring scheme for the various fractions of the group separation system

Fraction[a]	Waiting time (days)	Detector[b]	Nuclides measured[c]
4, 15: 0.1 M HF	2—3	A	^{97}Zr (743.2), ^{122}Sb (564.0; 692.5), ^{124}Sb (602.7; 1691.0), ^{182}Ta (1189.0), ^{187}W (685.7), ^{233}Pa (300.2; 311.9)
	28	A	^{95}Zr (724.2; 756.9), ^{124}Sb (602.7; 1691.0), ^{181}Hf (133.0; 482.0), ^{182}Ta (222.1; 1189.0; 1221.1; 1231.0), ^{233}Pa (300.2; 311.9)
5, 17: HCl—acetone	2—3	A	^{64}Cu (511.0), ^{65}Zn (1115.5), ^{69m}Zn (438.7), ^{72}Ga (630.1; 834.1; 894.3)
13: Rb, Cs	7	A	^{86}Rb (1076.0), ^{134}Cs (569.3; 604.7; 795.8)
12, 20: Ca, Sr, Ba, REE	7	A	^{47}Ca (1296.9), ^{131}Ba (496.3), ^{140}La (328.7; 487.0; 815.8; 1596.2), ^{141}Ce (145.4), ^{153}Sm (103.2), ^{152}Eu (344.2), ^{160}Tb (298.6), ^{175}Yb (282.6; 396.1), ^{177}Lu (208.4)
		B	^{147}Nd (91.0), ^{153}Sm (69.7; 103.2), ^{152}Eu (121.8), ^{160}Tb (86.8), ^{166}Ho (80.6), ^{169}Yb (63.5), ^{177}Lu (208.4)
	14	A	cf. REE fraction after 1 week, A + ^{85}Sr (514.0), ^{131}Ba (373.2), ^{147}Nd (531.0), ^{152}Eu (244.5; 779.1; 1408.1), ^{160}Tb (879.1; 1178.1), ^{169}Yb (177.0)
	28	A	^{85}Sr (514.0), ^{131}Ba (373.2; 496.3), ^{141}Ce (145.4), ^{147}Nd (531.0), ^{152}Eu (244.5; 344.2; 779.1; 1408.1), ^{153}Gd (103.2), ^{160}Tb (298.6; 879.3; 1178.1), ^{169}Yb (177.0), ^{177}Lu (208.4)
		B	^{141}Ce (145.4), ^{147}Nd (91.0), ^{152}Eu (121.8), ^{153}Gd (97.4; 103.2), ^{160}Tb (86.8), ^{170}Tm (84.3), ^{169}Yb (63.5), ^{177}Lu (208.4)

[a]See Figs. 1 and 2 for the fraction numbers. [b]A, conventional Ge(Li) detector; B, LEPD.
[c]The photopeak energies in keV [23] are given in parentheses.

the γ-ray energies of the radionuclides used. Obviously, a compromise must be made between desired and available counting time, and the optimum waiting time for the determination of the various elements in each fraction.

Data processing

The multichannel analyzers were interfaced to a PDP 11/45 computer, and the spectra were stored on magnetic tape for further processing. The elemental concentrations for conventional Ge(Li) spectra were calculated by means of the computer program OLIVE [24]. For the LEPD spectra, the LESDEP program [20] was used.

Decomposition of the irradiated samples

Dissolve the irradiated samples and the carriers in a PTFE-lined bomb, with a mixture of 20 ml of 40% HF and 1 ml of fuming HNO_3. Heat the bomb for 4 h at 240°C in an oven. Enclose a PTFE-coated stirring rod and stir the contents of the bomb every hour. Cool the bomb in a flow of compressed air before opening. Evaporate hydrofluoric acid and repeat the evaporation with another 5 ml of 40% HF. Take up the residue in 15 ml of 0.1 M HF, and leave the solution (fraction 1) to stand for one night at room temperature.

Separation of soluble and insoluble fluorides

Transfer the content of the PTFE vessel to a polyethylene tube, and centrifuge. Drain off the supernate (fraction 2) with a polyethylene pipet. Wash the precipitate (fraction 3) three times in the centrifuge tube with 2-ml portions of 0.1 M HF, centrifuging each time. Filter the original supernate and the washings through a membrane filter (5-μm pore size) mounted in a polypropylene filter holder to ensure that the solution is free of insoluble material. Add the filter to the 10 M HCl solution of the fluoride precipitate (see under Purification of the insoluble fluorides).

Cation-exchange procedure for the soluble fluorides (fraction 2)

Wash 5 g of dry Dowex 50W-X8 resin (100—200 mesh) with 6 M hydrochloric acid, and rinse with water. Prepare a resin column (1 cm × 10 cm) in a PTFE tube and condition with 50 ml of 0.1 M hydrofluoric acid.

Pass the 0.1 M HF solution (fraction 2) through the column, and elute sequentially with another 50 ml of 0.1 M HF, with 50 ml of 3 M HCl—acetone (10:90, v/v), and with 80 ml of 12 M HCl.

Separation of Zr, Sb, Hf, Ta, W and Pa. Collect the 0.1 M HF eluate in the original PTFE vessel and evaporate to about 20 ml. Add 5 mg of chromium holdback carrier (1 ml of a solution of CrO_3 in water) and oxidize all chromium to Cr(VI) by boiling with an excess of ammonium persulfate (300 mg) in presence of 3 drops of 0.1 M silver nitrate solution. Cool the solution to room temperature and neutralize to pH 1.7 (±0.2) with 6 M ammonia solution, using Merck special indicator paper (pH 0—2.5). Cool

further to about 0°C, and transfer the solution to a cooled polypropylene separatory funnel. Add 100 μl of 30% H_2O_2, and extract the chromium immediately with 25 ml of cooled ethyl acetate. Repeat the whole procedure and discard the organic phase (fraction 14). Transfer the aqueous phase (fraction 15) to a 40-ml polyethylene bottle for counting the Zr, Sb, Hf, Ta, W and Pa activities (thorium is determined via ^{233}Pa). The final volume of this solution is ca. 25 ml.

Separation of Cu, Zn and Ga. Evaporate the acetone—hydrochloric acid eluate to dryness in a beaker, and dissolve the residue in 20 ml of 8 M HCl. Reduce iron with tin(II) chloride (0.25 M in 8 M HCl). Extract gallium with 20 ml of isopropyl ether and back-extract into 25 ml of water. Re-oxidize iron with ammonium persulfate (0.25 M in 8 M HCl); extract with 25 ml of isopropyl ether and discard the organic phase (fraction 16). Combine the aqueous phase with the gallium back-extract and evaporate to dryness. Dissolve in a few ml of fuming nitric acid, and take to dryness to destroy any organic residue. Add another portion of fuming nitric acid, and evaporate nearly to dryness. Take up in 5 ml of 14 M HNO_3 and a few drops of 12 M HCl. Transfer to a 10-ml volumetric flask, and dilute to 10 ml with 14 M HNO_3. Immediately take a 100-μl aliquot for the yield determination (see below). Count the Cu, Zn and Ga activities in the volumetric flask (fraction 17).

Separation of the first Rb—Cs fraction. Collect the 12 M HCl eluate in a beaker. Evaporate to ca. 10 ml and add 5 ml of an aqueous solution of 20% citric acid and 1 ml of 30% H_2O_2. Adjust to pH 3 with 5 M LiOH or 8 M NaOH. Add disodium ethylenediaminetetraacetate (10 ml of a 6% solution in water) and neutralize further to pH 4. (Measure the pH potentiometrically with a glass electrode.) Precipitate K, Rb and Cs with a freshly prepared solution of sodium tetraphenylboron (3% in water), wait for 5 min, filter the precipitate under suction through a filter paper (2.2-μm pore size), and wash 5 times with 5-ml portions of water. Discard the supernatant liquid (fraction 7).

Purification of the insoluble fluorides (fraction 3)

Removal of scandium and iron. Dissolve the insoluble fluorides in a mixture of 20 ml of 12 M HCl, 3 ml of water and 1 ml of 30% H_2O_2. Extract Sc and Fe with 25 ml 100% tri-n-butyl phosphate, pre-equilibrated with 10 M HCl. Wash the organic phase 3 times with 25 ml of 10 M HCl and discard (fraction 9).

Removal of cobalt. Evaporate the aqueous phase to ca. 10 ml and add 10 ml of aqueous 20% citric acid solution and 1 ml of 30% H_2O_2. Adjust the pH to 3.5—4 with 5 M LiOH, and add 3 ml of a 1% (w/v) solution of 1-nitroso-2-naphthol in glacial acetic acid. (LiOH is used to neutralize; perchloric acid is added to the aqueous phase at a later stage, and $LiClO_4$ is more soluble in water than $NaClO_4$.) Allow to stand for at least 30 min at room temperature. Extract the cobalt complex once with 30 ml and once with 20 ml of chloroform. Wash the organic phase (fraction 18) twice with 30-ml portions of 5 M HCl and discard.

Separation of the second Rb—Cs fraction. Combine the aqueous phase and the washings in a beaker (fraction 19), and evaporate to ca. 10 ml. Isolate K, Rb and Cs as described above (see fraction 6 under Cation-exchange procedure for the soluble fluorides). Use LiOH to neutralize. Filter the residue on the same paper as the fraction 6 precipitate. Wrap the residues and the filter in another 10-cm diameter filter paper, and press to a pellet (12-mm diameter, 7.5-mm height) to obtain reproducible counting geometry. Count the pellet on a large Ge(Li) detector after the decay of ^{42}K.

Removal of chromium. Evaporate the supernate (fraction 12) and add 15 ml of 70% $HClO_4$. Heat the perchloric acid solution carefully to oxidize all organic material present. Continue heating to $HClO_4$ fumes until a clear solution is obtained. Transfer this solution to a round-bottomed distillation flask and distil off the rinsing water. Add 5 mg of CrO_3 and pass hydrogen chloride gas through the boiling perchloric acid solution to distil chromium as CrO_2Cl_2. Discard the distillate (fraction 21). (The distillation unit has been described [18].)

Isolation of Ca, Sr, Ba and REE. Quantitatively transfer the residue to a polyethylene bottle with water, and dilute until all perchlorates have dissolved (ca. 80 ml). Count the solution for the determination of Ca, Sr, Ba and REE.

Abridged separation scheme

When the ^{51}Cr, ^{59}Fe and ^{60}Co activities do not cause interference problems, several purification steps can be omitted (Fig. 2). Evaporate fractions 4 and 5, and transfer them respectively to a polyethylene bottle and a volumetric flask for counting of Zr, Sb, Hf, Ta, W, Pa activities and Cu, Zn, Ga activities. Use the aqueous phase of the tri-n-butyl phosphate extraction (fraction 10) as such for the precipitation of Rb and Cs. Evaporate the supernate (fraction 12) and oxidize the organic material with perchloric acid as described under Purification of the insoluble fluorides. Transfer the solution (fraction 12) to a polyethylene bottle for counting of Ca, Sr, Ba and REE.

Yield determination

Zr, Sb, Hf, Ta and W. After completion of the countings, quantitatively transfer solution 15 to a 100-ml polyethylene volumetric flask and dilute to the mark with 0.1 M HF. Pipet 1 ml of this solution with a polyethylene pipet into a 3.5-ml polyethylene bottle and wash the pipet once with 1 ml and twice with 0.5 ml of water. Evaporate this solution under an i.r. lamp. Place a filter paper on the bottom of the bottle before pipetting, to obtain a uniform distribution of the residue. Cut off the polyethylene bottle at 0.8 cm. Prepare a reference solution by pipetting 1 ml of carrier solution 2 and 100 μl of carrier solution 4 into a 100-ml polyethylene volumetric flask, and dilute with water. Transfer 1 ml to a 3.5-ml polyethylene bottle and treat further as above. Irradiate samples and reference together for an appropriate time (ca. 7 h at a thermal flux of 1.5×10^{12} n cm^{-2} s^{-1}, for the amounts given above) and correct for flux gradients, e.g. by using tiny

technical grade copper wires. Count on a large Ge(Li) detector after 1 day and after 1 month. The samples need not be transferred to another vial, because the blank values for polyethylene and filter paper are negligible.

Cu, Zn and Ga. Pipet a 100-μl aliquot of the counting solution (see under Cation-exchange procedure for the soluble fluorides) into a polyethylene bottle (2-cm diameter, 0.8-cm tall) with a filter paper at the bottom. Evaporate the solution. Prepare a reference sample in the same way from 10 ml of solution containing 100 μl of the original carrier solution. Irradiate samples and reference together for ca. 7 h at 1.5×10^{12} n cm^{-2} s^{-2}. Correct for flux gradients (use Fe wires, because recoil of Cu in the polyethylene sample vials might cause erroneous Cu-yields).

Rb and Cs. Re-activate the entire combined precipitate (fraction 13). Prepare a reference pellet by spotting 100 μl of the Rb—Cs carrier solution on a 10-cm diameter filter paper. Add an amount of K-tetraphenylboron equal to the mean weight of the Rb—Cs precipitates, to compensate for neutron absorption by boron. Pack the pellets in a polyethylene bottle, provide with a Cu flux monitor, and irradiate for 2 h at a thermal neutron flux of 2.5×10^{11} n cm^{-2} s^{-1}. Correct for the remaining Rb—Cs activities.

RESULTS AND DISCUSSION

The group separation scheme

The systematic surveys of Ito [7] and Langmyhr and Sveen [8] showed that up to 300 mg of the common rock-forming minerals decompose in mixtures of hydrofluoric and sulfuric or perchloric acid. Actually, most of the minerals dissolved after treatment for only 20 min at 95°C in a beaker. Some less common minerals such as beryl, kyanite and staurolite resisted this treatment but dissolved completely in a high-pressure bomb after 60 min at 250°C. Only topaz resisted this treatment. In the present procedure, the bombs were heated for about 4 h at 240°C, by way of precaution.

It is far from certain whether a second mineral acid is really required for decomposition in a bomb. From the scarce data available, it could be concluded that hydrofluoric acid alone is just as effective, if not more effective than mixtures with perchloric or sulfuric acid [7, 8]. Nonetheless, in the present procedure fuming nitric acid was added as an oxidant, in order to facilitate isotopic exchange for those elements that might occur in several oxidation states. For this purpose, nitric acid is a better choice than perchloric acid, because it can readily be expelled by evaporation afterwards. Moreover, the limited solubility of heavy alkali perchlorates easily develops into a nuisance.

Contrary to the findings of Ito [7], chromite was found to be rather resistant to hydrofluoric acid attack when the ultrabasic rocks DTS-1 and PCC-1 were analyzed. The undissolved chromite particles stayed together with the REE fraction, until they finally dissolved on vigorous boiling with perchloric acid during the chromium distillation.

The incomplete decomposition of chromite and concomitant lack of isotopic exchange might, in principle, lead to erroneous results, especially for those elements going into solution after sample decomposition (fraction 2). It is unlikely, however, that major fractions of the elements determined in the present procedure would partition into the minor amounts of chromite in common basaltic or ultrabasic rocks. Possible exceptions are Cu and Zn; Morgan et al. [25] found that zinc was appreciably enhanced in chromitite rocks as compared to other related rocks. Nevertheless, the analysis of DTS-1 and PCC-1 did not yield conclusive evidence for Cu and Zn retention in undissolved chromite. Therefore, it was felt that the overall advantages of the hydrofluoric acid decomposition far outweighed this minor flaw of the technique. It is also clear, of course, that the method is not the best choice for decomposition of samples in which chromite is a major mineral phase.

After sample decomposition, the interfering elements (Na, Sc, Cr, Fe and Co) are distributed between precipitate and solution in various proportions. Some selected data are shown in Table 2. Na, Cr, Fe and Co would be expected to stay quantitatively in solution. According to Langmyhr and Kringstad [26], the precipitation of these elements is probably due to the formation of insoluble complex fluorides. These authors found considerable amounts of Na, Al and Fe in the precipitate after the decomposition of a granite in hydrofluoric acid, while Na_2CO_3, Al_2O_3 or Fe_2O_3 did not yield precipitates.

A significant fraction of scandium ended up in solution, presumably because of soluble ScF_6^{3-} complexes [27]. The fluoride concentration cannot be reduced, as this might influence the stability of the other fluoride complexes. Addition of scandium carrier prior to sample decomposition did not considerably change the distribution of scandium, and was undesirable because it significantly reduced the yield of the tri-n-butyl phosphate extraction of scandium from fraction 3.

The soluble scandium fraction is eluted from the ion-exchange column, together with Zr, Sb, Hf, Ta, W and Pa. Occasionally, high scandium activity in this fraction may present a real interference problem, e.g. when Sc-rich pyroxene phenocrysts are irradiated at a high neutron dose. Unfortunately,

TABLE 2

Fraction of interfering elements (%) found in the 0.1 M HF solution (fraction 2) for various types of rocks

	Granite G-2	Basalt BCR-1	Dunite DTS-1
Na	15	45	?
Sc	10	25	3
Cr	10	80	60
Fe	85	80	50
Co	50	99	70

the rather short half-life of ^{187}W leaves little room for additional time-consuming purification procedures, for the necessary perchromic acid extraction of interfering ^{51}Cr activity requires a couple of hours. Even if there were no time restrictions, removal of scandium would not be simple. Extraction with tri-n-butyl phosphate is unsuitable because Zr, Sb, Hf, Ta, W and Pa are also extracted. Precipitation of radioactive scandium by adding Sc-carrier is inefficient; moreover, soluble inactive scandium would interfere with the yield determination by reactivation. For long-lived ^{181}Hf, ^{182}Ta and ^{233}Pa, which have intense γ- or x-rays at low energies, the situation can be rectified by counting on a LEPD instead of a large Ge(Li) detector, because a small detector is rather insensitive to the 889-keV and 1120-keV ^{46}Sc γ-rays.

The removal of the interfering ^{46}Sc, ^{51}Cr, ^{59}Fe and ^{60}Co activities from the other fractions is selective and quite effective. The perchromic acid extraction removes ca. 90% of the chromium from fraction 4. Decontamination of fraction 12 through the CrO_2Cl_2 distillation is even better, and more than 99% of the chromium is removed by a double distillation. The isopropyl ether extraction of iron from fraction 5 is selective and virtually quantitative, as is the cobalt extraction from fraction 9. More than 98% of both iron and scandium is eliminated from fraction 3 by the tri-n-butyl phosphate extraction.

The carrier-free behaviour of chromium is rather unpredictable. The fraction of total chromium eluted from the ion-exchange column with 0.1 M HF (fraction 4) seems to increase with increasing chromium content of the sample. About 30% of the chromium was eluted for BCR-1 (38 ppm Cr) but this amount increased to 70% for DTS-1 (4000 ppm Cr). It is therefore advisable to check the ^{51}Cr-activity levels in this fraction to decide whether the perchromic acid extraction is required. No chromium carrier was added prior to decomposition of the sample, to avoid the need for Cr extraction for all samples, even those with moderate Cr activities. Without extraction the Cr carrier would interfere with the yield determination of the other elements in fraction 4.

Difficulties might occur if the aliquot for the yield determination of the Cu, Zn, Ga fraction were taken after completion of the counting, particularly when the isopropyl ether extraction for iron has been used. Occasionally, a precipitate was observed after a few days and the counting solution had to be processed chemically again. There is no apparent guarantee that all elements are recovered quantitatively in this treatment. Probably the anomalously low results for gallium, and to a lesser extent Cu and Zn, in one of the DTS-1 analyses (Table 5) were caused by these difficulties in the yield determination. Therefore, it is recommended that the aliquot for re-activation be taken as soon as possible, even prior to the counting of the Cu, Zn and Ga fraction.

The radiochemical yields varied from 90 to 100% for Cu, Zr, Sb, Hf, Ta and W, from 60 to 80% for Ga and from 40 to 95% for Zn. The distribution

of Rb and Cs between soluble and insoluble fluoride fractions 2 and 3 was rather erratic. It is wise to isolate the two elements from both phases, and to combine the two tetraphenylborate precipitates to achieve greater sensitivity. The total yield of Rb and Cs was generally better than 90%.

Protactinium usually ends up quantitatively in the 0.1 M HF eluate from the ion-exchange column (fraction 15 or 4). Occasionally, ^{233}Pa was found to be distributed over the 0.1 M HF eluate, the tri-n-butyl phosphate phase (fraction 9) and the REE phase (fraction 20 or 12). In an unfavourable case, 51%, 48% and 1% of the ^{233}Pa activity were found in these three fractions, respectively. Obviously, the Pa yield cannot be determined by re-activation. Unfortunately, long-lived radioactive ^{231}Pa-tracer [28] cannot be used in γ-spectrometry, because the γ-rays of ^{231}Pa overlap with the useful γ- and x-rays from ^{233}Pa itself. Thus the distribution of ^{233}Pa over the three phases must be checked and, if necessary, a correction made by measuring these fractions under identical conditions of counting geometry. Admittedly, for ultrabasic rocks, the ^{233}Pa in the tri-n-butyl phosphate fraction might be swamped by the ^{46}Sc and ^{59}Fe, and hence might go unnoticed. The use of an LEPD, however, is very useful for counting the tri-n-butyl phosphate phase, given its low detection efficiency at higher energies.

The quantitative recovery of Ca, Sr, Ba and all the REE was extensively checked by tracer experiments. Normally, no yield determination is required for this group of elements; if necessary, the yield can be determined by re-activation for La, Sm or Yb, the three REE for which carrier is added.

Neutron-induced fission of U and Th interferes with the analysis for zirconium via ^{95}Zr and ^{97}Zr. Although uranium is not determined in the present procedure, an approximate, but acceptable, correction for the fission contribution can be calculated from the thorium abundances, for the Th/U ratio in igneous rocks is seldom far removed from the average crustal values of 4 [29]. For the irradiation conditions in the Thetis reactor, the estimated ^{95}Zr fission interference amounts to 9%, 7%, 8%, and the ^{97}Zr fission interference to 18%, 13% and 16%, for BCR-1, G-2 and AGV-1, respectively.

Interpretation of the γ-ray spectra

Justification for the selection of the γ-ray energies used for the determination of the various elements (Table 1) is already available [22, 30]. After a chemical separation several elements can be analyzed more accurately or can be determined in addition to i.n.a.a., although not all problems are solved for some elements. Some aspects of the γ-ray spectrometry deserve comment.

Copper. This element is determined via the 511-keV β^+-annihilation radiation of ^{64}Cu. This peak contains a contribution from the pair production of the highly energetic ^{72}Ga and ^{59}Fe γ-rays. Soon after the irradiation, however, the copper activity dominates, so that the interference is negligible. The 1345.5-keV peak of ^{64}Cu is unaffected, but the precision is very poor.

Zinc. Shortly after the irradiation, zinc can be determined via the ^{69m}Zn 438.7-keV peak, together with the long-lived ^{65}Zn 1115.5-keV γ-ray. For very low zinc concentrations, ^{65}Zn can be measured again after a waiting period of a few weeks.

Gallium. Determinations of gallium are straightforward, because the two most prominent γ-rays at 834.1 keV and 630.1 keV are free from interferences.

Zirconium. Soon after the irradiation, zirconium can be determined by means of the 743.2-keV ^{97}Zr γ-ray. This peak is well separated from the ^{99}Mo 739.3-keV peak. After 4 weeks, the long-lived ^{95}Zr is used: the 756.9-keV γ-ray is free from interference, whereas the 724.2-keV peak is subject to interference from the 722.7-keV peak of ^{124}Sb.

Antimony. A few days after the irradiation, the ^{122}Sb 564.0-keV peak can be used, provided that it is more intense than the neighbouring ^{76}As 559.1-keV line; otherwise, peak integration tends to be faulty. The 692.5-keV γ-ray of ^{122}Sb is well separated from the ^{187}W 685.7-keV γ-ray and from the 698.3-keV peak of ^{82}Br. The 602.7-keV and the 1691.0-keV γ-rays of ^{124}Sb are also useful. ^{97}Zr has a γ-ray at 602.5 keV, but except for high zirconium contents, this interference can be neglected.

Gadolinium. The gadolinium determinations via ^{153}Gd are always relatively insensitive, because of the low isotopic abundance of ^{152}Gd (0.2%). Yet, in principle, determinations of gadolinium by r.n.a.a. are more accurate than i.n.a.a., because the ^{233}Pa 103.8-keV peak no longer interferes with the 103.2-keV peak of ^{153}Gd.

Terbium. In addition to the 86.8-keV and 298.6-keV peaks of ^{160}Tb, the 879.3-keV and 1178.1-keV γ-ray energies can normally be used, thanks to the lowering of the Compton background by the removal of the ^{59}Fe, ^{46}Sc and ^{60}Co activities in the REE fraction.

Thulium. The 84.3-keV peak of ^{170}Tm is always affected in i.n.a.a. by the ^{182}Ta 84.7-keV peak, even in LEPD spectra. This interference is now eliminated.

Ytterbium. In i.n.a.a., ytterbium can be determined in LEPD spectra, via the ^{169}Yb 63.5-keV peak, provided that the Hf/Yb ratio is not too high; there is possible interference from the 62.95-keV Lu-$K_{\beta'2}$ x-ray of ^{175}Hf. After radiochemical separation, the 63.5-keV γ-ray can always be used, together with the ^{169}Yb 177.0-keV, ^{175}Yb 282.6-keV and 396.1-keV peaks in large Ge(Li) spectra.

Hafnium. This element can be determined via the ^{181}Hf 133.0-keV and 482.0-keV γ-energies. Shortly after the irradiation, however, these peaks may be affected by ^{187}W, which has γ-energies of 134.2 keV and 479.5 keV. The ^{181}Hf 136.25-keV and 136.86-keV peaks overlap the ^{181}Hf 133.0-keV peak; these are not true interferences, and a suitable peak-integration method can be applied.

Tungsten. Only the most prominent ^{187}W γ-energy at 685.7 keV is free of interference.

Accuracy and precision of the method

The accuracy and precision of the method were tested by repeated analyses of the U.S. Geological Survey standard rocks granite G-2, andesite AGV-1 and dunite DTS-1. Tables 3—5 list the results obtained, together with the estimates of Flanagan [31]. I.n.a.a. results for G-2 and AGV-1 [20] are given for comparison.

For G-2 and AGV-1, U.S.G.S. basalt BCR-1 was used as a multi-element reference standard for both i.n.a.a. and r.n.a.a. In the first analysis of DTS-1, BCR-1 was used as a standard, in the second one AGV-1, and in the third one the in-house standard FU-128. The concentrations used for BCR-1 and AGV-1 are listed in Tables 3 and 5, respectively. These values are based on the estimates of Flanagan [31], on the results of i.n.a.a. [20] and on recent literature values.

G-2 and AGV-1 were analyzed by means of the abridged separation scheme (Fig. 2), whereas the complete procedure (Fig. 1) was used for DTS-1. However, not every element was determined in all the runs, because the separation scheme was continuously modified and expanded.

TABLE 3

Results for granite G-2[a]

Element	Concentrations used for BCR-1 (comparator)	Experimental r.n.a.a. results	Weighted mean ± 95% confidence limit[b]	I.n.a.a. [20] ± 95% confidence limit[b,c]	Flanagan[d] [31]
Ca	4.95	1.46, 1.37	1.38 ± 0.11		1.39
Cu	18.4	9.99, 10.6	10.3 ± 0.5		11.7
Zn	120	83.3, 77.4	79.5 ± 4.0		85
Ga	20	21.7, 20.6	21.1 ± 1.1		22.9
Rb	46.6	188	188 ± 6	158 ± 20	168
Sr	330	439, 514, 477	468 ± 23		479
Zr	190	323, 314	316 ± 15		300
Sb	0.69	0.054, 0.052	0.054 ± 0.003		(0.1)
Cs	0.95	1.42	1.42 ± 0.04	1.30 ± 0.14	(1.4)
Ba	675	1842, 1840, 1902	1860 ± 93	1939 ± 70	1870
La	25	89.7, 82.2, 86.9	86.0 ± 4.3	87.4 ± 1.7	96
Ce	53.9	156.8, 157.2, 165.0	160 ± 8	161 ± 3	(150)
Nd	30	51.7, 52.3, 54.5	52.6 ± 2.6	54.6 ± 1.1	60
Sm	6.5	7.00, 6.70, 6.96	6.88 ± 0.34	6.98 ± 0.14	7.3
Eu	1.97	1.31, 1.31, 1.37	1.33 ± 0.07	1.63 ± 0.03	1.5
Gd	6.5	2.1, 4.3, 3.7	3.0 ± 0.3	3.9 ± 1.1	(5)
Tb	1.1	0.43, 0.46, 0.45	0.45 ± 0.02	0.47 ± 0.03	0.54
Ho	1.34	0.52, 0.33	0.37 ± 0.07	0.39 ± 0.09	(0.4)
Tm	0.52	0.18, 0.12, 0.19	0.14 ± 0.03	0.15 ± 0.02	(0.3)
Yb	3.36	0.72, 0.72, 0.71	0.72 ± 0.04	0.79 ± 0.02	0.88
Lu	0.55	0.110, 0.116, 0.132	0.114 ± 0.006	0.108 ± 0.007	0.11
Hf	4.8	7.83, 7.30	7.55 ± 0.38	8.13 ± 0.16	7.35
Ta	0.85	0.87, 0.85	0.86 ± 0.04	0.96 ± 0.04	0.91
W	0.40	0.12, 0.10	0.11 ± 0.01		(0.1)
Th	6.0	24.8, 23.8	24.2 ± 1.2	24.5 ± 0.5	24.2

[a]All values are given in ppm, except for Ca, where the % value is given. [b]Minimum 95% confidence limits are set at 2% and 5% for i.n.a.a. and r.n.a.a., respectively. [c]Weighted mean of 2 separate analyses. [d]The values given are recommended or average values, except for those in parentheses, which are indications of magnitude.

TABLE 4

Results for andesite AGV-1[a]

Element	Experimental r.n.a.a. results[e]	Weighted mean ±95% confidence limit[b]	I.n.a.a. [20] ±95% confidence limit[b,c]	Flanagan[d] [31]
Ca	3.54, 3.37, 3.22	3.39 ± 0.23		3.50
Cu	60.6, 57.8	59.1 ± 3.0		59.7
Zn	85.5, 77.4	82.2 ± 4.0		84
Ga	19.2, 16.1	17.4 ± 0.9		20.5
Rb	71.5	71.5 ± 1.9	57.7 ± 8.9	67
Sr	661, 630, 636	645 ± 32		657
Zr	240, 223	226 ± 11		225
Sb	4.77, 4.41	4.44 ± 0.22		4.5
Cs	1.27	1.27 ± 0.03	1.26 ± 0.11	(1.4)
Ba	1234, 1165, 1228	1207 ± 60	1236 ± 31	1208
La	39.1, 36.2, 38.5	37.8 ± 1.9	37.2 ± 0.8	(35)
Ce	70.3, 66.0, 72.5	69.4 ± 3.5	68.7 ± 1.4	63
Nd	30.8, 31.5, 33.6	31.6 ± 1.6	32.3 ± 0.6	39
Sm	5.89, 5.41, 5.83	5.69 ± 0.28	5.62 ± 0.11	5.9
Eu	1.66, 1.55, 1.66	1.62 ± 0.08	1.61 ± 0.03	1.7
Gd	4.5, 4.6, 4.2	4.6 ± 0.3	4.7 ± 0.4	(5.5)
Tb	0.68, 0.66, 0.71	0.68 ± 0.03	0.67 ± 0.02	0.70
Ho	0.77, 0.57, 0.80	0.72 ± 0.08	0.82 ± 0.06	(0.6)
Tm	0.31, 0.28, 0.39	0.31 ± 0.05	0.26 ± 0.02	(0.4)
Yb	1.71, 1.56, 1.66	1.64 ± 0.08	1.65 ± 0.03	1.7
Lu	0.275, 0.263, 0.252	0.27 ± 0.01	0.26 ± 0.01	0.28
Hf	5.04, 4.86	4.95 ± 0.25	5.06 ± 0.10	5.2
Ta	0.92, 0.93	0.93 ± 0.05	0.97 ± 0.03	0.9
W	0.53, 0.52	0.52 ± 0.03		(0.55)
Th	6.55, 6.25	6.40 ± 0.32	6.32 ± 0.13	6.41

[a]For footnotes (a)–(d), see Table 3. [e]The concentrations for the comparator (BCR-1) are given in Table 3.

It is evident that r.n.a.a. yields less reproducible results than i.n.a.a. Additional errors originate from the chemical processing and yield determinations; generally, the difference between the extreme values is less than 10%, except for some elements which are difficult to determine precisely by n.a.a. (Gd, Ho, Tm).

The standard deviations of the r.n.a.a. results based on counting statistics are similar or smaller than those of i.n.a.a. The main reasons are that smaller peaks can be determined more precisely because of the lower Compton background, and that more γ-peaks are interference-free. However, other sources of error, e.g. sub-sampling, weighing, differences in counting geometry and chemical manipulations also determine the precision and become relatively more important as the counting statistics improve. Therefore, a minimum standard deviation of 1% was set for i.n.a.a. and 2.5% for r.n.a.a., not only for individual results but for weighted means.

TABLE 5

Results for dunite DTS-1[a]

Element	Concentrations used for AGV-1 (comparator)	Experimental r.n.a.a. results	Weighted mean ± 95% confidence limit[b]	Flanagan[c] [31]
Ca	3.50	0.071, 0.079	0.074 ± 0.004	—
Cu	59.7	6.7, 5.1		7.0
Zn	84	49.5, 39.5		45
Ga	20.5	0.52, 0.17		(0.2)
Rb	58	0.051	0.051 ± 0.007	0.053
Sb	4.5	0.45	0.45 ± 0.02	(0.46)
Cs	1.4	0.0053	0.0053 ± 0.0003	0.006
La	37.2	0.023, 0.023, 0.021	0.022 ± 0.001	(0.04)
Ce	68.5	0.056, 0.066, 0.056	0.059 ± 0.008	(0.06)
Nd	32.3	0.026, 0.030, 0.026	0.028 ± 0.004	<0.02
Sm	5.62	0.0042, 0.0038	0.0041 ± 0.0002	(0.004)
Eu	1.61	0.0009, 0.0011, 0.0008	0.00093 ± 0.00006	0.0009
Ho	0.82	0.0001, 0.0008		(0.003)
Tm	0.27	0.0026, 0.0010	0.0012 ± 0.0006	(0.001)
Yb	1.65	0.010, 0.011, 0.010	0.0108 ± 0.0005	(0.01)
Lu	0.26	0.0022, 0.0025, 0.0020	0.0022 ± 0.0001	(0.002)
Hf	5.06	0.0036	0.0036 ± 0.0004	(0.01)

[a] All values are given in ppm, except for Ca, where the % value is given. [b] Weighted means for Ho, Cu, Zn and Ga are not given, because the two results differed far more than would be expected from counting statistics. Minimum 95% confidence limits are set at 5%. [c] Values shown in parentheses are estimates.

The results for granite G-2 and andesite AGV-1 can be readily compared with other literature data [32]. In general, agreement between the r.n.a.a. and i.n.a.a. results are excellent, and the results are quite close to the preferred literature values. A detailed evaluation of the results for dunite DTS-1 has been published elsewhere [33]. Such a comparison is more complicated than in the case of G-2 and AGV-1, because the literature values are far less abundant and can vary by orders of magnitude. On average, the agreement with the values proposed by Flanagan [31] is quite satisfactory, especially considering the very low contents of many trace elements in this type of rock.

We are grateful to J. Dewaele for technical assistance. The financial support of the N.F.W.O. and the I.I.K.W. is acknowledged.

REFERENCES

1 G. E. Gordon, K. Randle, G. G. Goles, J. B. Corliss, M. H. Beeson and S. S. Oxley, Geochim. Cosmochim. Acta, 32 (1968) 369.
2 G. H. Morrison, J. T. Gerard, A. Travesi, R. L. Currie, S. F. Peterson and N. M. Potter, Anal. Chem., 41 (1969) 1633.

3 J. C. Laul, D. R. Case, M. Wechter, F. Schmidt-Bleek and M. E. Lipschutz, J. Radioanal. Chem., 4 (1970) 241.
4 R. O. Allen, L. A. Haskin, M. R. Anderson and O. Muller, J. Radioanal. Chem., 6 (1970) 115.
5 A. O. Brunfelt and E. Steinnes, Talanta, 18 (1971) 1197.
6 A. O. Brunfelt, I. Roelandts and E. Steinnes, Analyst, 99 (1974) 277.
7 J. Ito, Bull. Chem. Soc., Jpn., 35 (1962) 225.
8 F. J. Langmyhr and S. Sveen, Anal. Chim. Acta, 32 (1965) 1.
9 B. Bernas, Anal. Chem., 40 (1968) 1682.
10 J. S. Fritz, B. B. Garralda and S. K. Karraker, Anal. Chem., 33 (1961) 882.
11 M. D. Foster, U.S. Geol, Survey, Bull., 950 (1946) 15.
12 W. H. Hartford, in I. M. Kolthoff and P. J. Elving (Eds.), Treatise on Analytical Chemistry, Part 2, Vol. 8, Interscience, New York, 1962, p. 314.
13 J. Korkisch and S. S. Ahuwalia, Talanta, 14 (1967) 155.
14 R. W. Dodson, G. J. Forney and E. H. Swift, J. Am. Chem. Soc., 58 (1936) 2573.
15 N. H. Nachtrieb and R. E. Fryxell, J. Am. Chem. Soc., 71 (1949) 4035.
16 T. Ishimori, K. Watanabe and E. Nakamura, Bull. Chem. Soc., Jpn., 33 (1960) 636.
17 E. Cogan, Anal. Chem., 32 (1960) 973.
18 D. De Soete, J. Hoste and G. Leliaert, Int. J. Appl. Radiat. Isotop., 8 (1960) 134.
19 P. De Paepe, Laboratorium voor Aardkunde, Rijksuniversiteit Gent.
20 J. Hertogen, Ph.D. Thesis, Rijksuniversiteit Gent, November 1974.
21 T. Smet, Ph.D. Thesis, Rijksuniversiteit Gent, in preparation.
22 J. Hertogen and R. Gijbels, Anal. Chim. Acta, 56 (1971) 61.
23 M. H. Pagden, G. J. Pearson and J. M. Bewers, J. Radioanal. Chem., 8 (1971) 127.
24 J. Op de Beeck and J. De Donder, Rijksuniversiteit Gent, private communication.
25 J. W. Morgan, R. Ganapathy, H. Higuchi and U. Krähenbühl, Geochim. Cosmochim. Acta, 40 (1976) 861.
26 F. J. Langmyhr and K. Kringstad, Anal. Chim. Acta, 35 (1966) 131.
27 G. Jantsch, in W. Fresenius and G. Jander (Eds.), Handbuch der Analytischen Chemie, Vol. II, Band III, Springer Verlag, Berlin, 1944, p. 147.
28 J. W. Morgan and J. F. Lovering, Anal. Chim. Acta, 28 (1963) 405.
29 D. H. Green, J. W. Morgan and K. S. Heier, Earth Planet. Sci. Lett., 4 (1968) 155.
30 R. Cornelis, J. Hoste, A. Speecke, C. Vandecasteele, J. Versieck and R. Gijbels, in T. S. West (Ed.), Int. Review of Science, Phys. Chem., Series Two, Vol. 12—Anal. Chem. Part 1, Butterworths, London, 1976, p. 84.
31 F. J. Flanagan, Geol. Survey Prof. Paper, 840 (1976) 131.
32 K. Govindaraju and I. Roelandts, Geostand. Newsl., 1 (1977) 163.
33 T. Smet and I. Roelandts, Geostand. Newsl., 2 (1978) 61.

Analytica Chimica Acta, 101 (1978) 63—70

HELIUM-4 AND NEUTRON ACTIVATION ANALYSIS FOR PHOSPHORUS IN ALUMINIUM—SILICON ALLOYS

P. GOETHALS, C. VANDECASTEELE and J. HOSTE*

Institute for Nuclear Sciences, Rijksuniversiteit Gent, Proeftuinstraat 86 B-9000 Gent (Belgium)

(Received 30th March 1978)

SUMMARY

An instrumental determination of phosphorus in aluminium—silicon alloys by activation with 20-MeV helium-4 particles can be based on the $^{31}P(\alpha, n)^{34m}Cl$ reaction. A mixture of aluminium powder and disodium hydrogenphosphate is used as a standard. For concentrations ranging from 1.7 to 25 $\mu g\ g^{-1}$, the experimental standard deviation ranges from 1 to 24% with an average of 8%. The method was compared with thermal neutron activation analysis based on the $^{31}P(n, \gamma)^{32}P$ reaction. ^{32}P was chemically separated by precipitation as ammonium molybdophosphate. This technique yielded results with a standard deviation between 0.3 and 7.5% with an average of 2%. The agreement between the two methods was satisfactory. The results were also compared with photometry and atomic absorption spectrometry.

Phosphorus is known to affect the mechanical properties of cast aluminium—silicon alloys, particularly of the eutectic (about 12% Si) type. When the alloy contains less than about 3 $\mu g\ P\ g^{-1}$ a laminar structure is obtained; at higher concentrations a globular structure is formed. This last form can be refined with sodium to obtain optimal mechanical properties [1].

The phosphorus concentration is usually determined spectrophotometrically with the molybdenum blue method [2]. Other possibilities are indirect atomic absorption spectrometry where the phosphorus is extracted as ammonium molybdophosphate and the absorption signal of the molybdenum is measured [3, 4], and neutron activation analysis [5].

Among the activities of BCR of the Commission of European Communities, the possibilities for the preparation and analysis of a certified reference material for phosphorus in aluminium—silicon alloy are being investigated. As different independent and absolute analytical techniques are required, a method based on the $^{31}P(\alpha, n)^{34m}Cl$ reaction was developed. It allows the instrumental determination of phosphorus by irradiation with 25-MeV helium-4 particles followed by Ge(Li) γ-ray spectrometry. Standardization is greatly simplified by utilizing aluminium powder mixed with a known amount of disodium hydrogenphosphate as a standard, so that no correction for the different stopping powers of the standard and the sample is required.

As an alternative method, neutron activation with separation of ^{32}P as ammonium molybdophosphate and measurement with a G-M detector was applied. The method was similar to that described by De Corte et al. [6] for phosphorus in high-purity silicon. The results of the two analytical methods were compared for samples from various origins with different concentrations of phosphorus.

Table 1 summarizes some pertinent nuclear data on the nuclear reactions used, on the interfering reactions and on the nuclear reactions used for beam intensity and flux monitoring. Copper and iron foils were used as monitors for helium-4 and neutron activation analysis, respectively.

TABLE 1

Nuclear reactions for the determination of phosphorus (I, V). Interfering reactions (II, III) and reactions used for beam intensity or flux monitoring (IV, VI)

Reaction	Threshold (MeV)	$T_{1/2}$	Particle or γ-ray energies (keV)
Helium-4 activation			
I. $^{31}P(\alpha, n)^{34m}Cl$	5.8	32.2 min	γ:2128
II. $^{35}Cl(\alpha, \alpha n)^{34m}Cl$	14.5		
III. $^{32}S(\alpha, d)^{34m}Cl$	13.0		
IV. $^{63}Cu(\alpha, n)^{66}Ga$	6.3	9.45 h	γ:1039
Neutron activation			
V. $^{31}P(n, \gamma)^{32}P$	—	14.3 d	β^-:1710
VI. $^{58}Fe(n, \gamma)^{59}Fe$	—	45.3 d	γ:1099; 1292

EXPERIMENTAL

Helium-4 activation analysis

Samples and standards. The samples were cylindrical discs (15 or 20-mm diameter, 1 mm thick). The standard was pure aluminium powder (Erba, p.a.) mixed with disodium hydrogenphosphate (Mallinckrodt, p.a.). Disodium hydrogenphosphate was dried for 2 h at 150°C and finely ground in a mortar. The mixture was shaken for 3 d and contained 1.9% of phosphorus. From this mixture pellets with the same dimensions as the samples were pressed at 840 kg cm^{-2}.

Irradiation. The samples and standards were irradiated with a 12 or 15-mm diameter beam of 25-MeV helium-4. The external beam of the isochronous cyclotron of the Université Catholique de Louvain was used.

A copper foil (25-μm thick) was placed before the samples and the standards, serving as a beam intensity monitor. For the standards and for the samples that were not etched after irradiation, aluminium foil (20-μm thick) was placed between the copper foil and the standard or the sample. This foil stopped recoil nuclei from reaching the monitor foil. The copper foil and the aluminium foil degraded the energy to 20 MeV. The samples that were etched after irradiation were placed directly behind the copper foil. The irradiation conditions are summarized in Table 2.

TABLE 2

Irradiation conditions for activation analysis with helium-4 particles

	Sample	Standard
Beam energy (MeV)	25	25
Energy corresponding to the depth of etching (MeV)	20	
Irradiation time (min)	20—30	1
Beam intensity (μA)	2—3	2—3

Chemical etching after irradiation. To remove possible surface contamination, some samples were chemically etched after irradiation for 2—5 min depending on the silicon concentration in a (1 + 1) mixture of 14 M nitric acid and 50% hydrofluoric acid at room temperature. A 20-μm surface layer was removed. The thickness before and after etching was measured precisely with a micrometer to a precision of a few μm. The copper monitor foil and the removed surface layer degraded the energy to 20 MeV.

Measurements. The samples were measured with a Ge(Li) detector (5% relative detection efficiency) coupled to a 4000-channel analyser, for 30 min after a 30-min cooling time. The cooling time allows for the decay of ^{30}P ($T_{1/2}$ = 2.5 min) formed by the ^{27}Al(α, n)^{30}P reaction. The standards were measured for 5 min in the same geometrical conditions as the samples, 90 min after irradiation. The beam intensity monitors were measured 1 d after irradiation.

The 2128-keV peak of ^{34m}Cl was integrated and a linear background was subtracted. Figure 1 shows a γ-ray spectrum for a sample (LMG) containing 5 μg P g^{-1}.

Standardization. Since the method was developed mainly for the analysis of proposed certified reference materials, it was important that it be standardized absolutely. A standardization method was developed that does not, during the calculations, make use of approximations based on theoretical

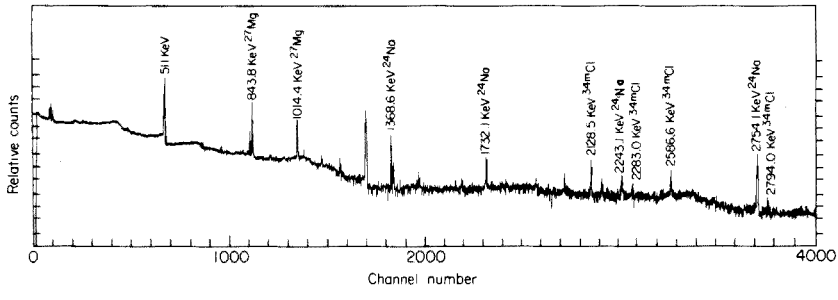

Fig. 1. Ge(Li) spectrum for a sample (LMG) containing 5 μg P g^{-1}. Irradiation time, 30 min; counting time, 30 min.

principles. As the standard, pure aluminium powder mixed with disodium hydrogenphosphate, containing 1.9% of phosphorus was utilized. Theoretical calculations based on the Tables of Williamson et al. [7] show that the stopping power (MeV g^{-1} cm^2) for 20-MeV helium-4 particles of this mixture differs by only 0.95% from that of pure aluminium and by 0.77% from that of aluminium—silicon alloy with 13% of silicon. At 5.8 MeV (threshold of the reaction) these figures are 1.3 and 1.3%. From the basic relation of charged-particle activation analysis, it follows that if no corrections for different stopping powers are applied, the systematic error is at most 1.3%, provided that the standard mixture is perfectly homogeneous (see below). Moreover, the energy of the helium-4 particles after traversing the beam intensity monitor, the aluminium foil or the etched surface layer is the same for the sample and the standard. The results can therefore be calculated from the simplified equation

$$C_x = C_s \frac{A_x}{A_s} \frac{I_s}{I_x} \frac{S_s}{S_x} \qquad (1)$$

where C is the phosphorus concentration ($\mu g\ g^{-1}$); A is the measured ^{34m}Cl activity, corrected for decay during the measurement and during the cooling time; I is the beam intensity, obtained from the area of the 1039-keV peak of ^{66}Ga in the spectrum of the beam intensity monitor, corrected for decay and saturation; and S is the saturation factor for ^{34m}Cl production.

The subscripts x and s refer to the sample and the standard, respectively.

Control of purity and homogeneity of the standard mixture

The purity of the disodium hydrogenphosphate after drying was verified gravimetrically by precipitation as ammonium molybdophosphate. It contained 99.5 ± 0.3% of the expected phosphorus content.

The homogeneity of the standard mixture was also carefully checked. In helium-4 activation, the activated mass corresponds to about 150 mg, and the standard must at least be homogeneous at this level. Five 150-mg samples of the mixture were irradiated in the nuclear reactor. The ^{24}Na activity from the sodium in the disodium hydrogenphosphate was measured and showed a standard deviation of 2.7%. Furthermore, 5 standards were analyzed by charged-particle activation. The induced ^{34m}Cl activities, corrected for decay and normalized to the same beam intensity, showed a standard deviation of 5.5%, whilst counting statistics alone accounted for 3%.

Neutron activation analysis

Samples and standards. The samples and the standards had the same dimensions as for helium-4 activation, except the "BCR" samples that were cylinders (8-mm diameter, 8-mm thick). The standard mixture had the same composition as for helium-4 activation.

Irradiation. The samples were irradiated for 5—6 h in the Thetis reactor of Ghent University at a thermal neutron flux of 1.7×10^{12} n cm^{-2} s^{-1}. Five samples,

each sandwiched between 2 iron flux monitors, were placed on top of each other in the same polyethylene container and irradiated simultaneously. Afterwards, 5 standards, also sandwiched between 2 flux monitors, were irradiated in the same irradiation position, but only for 5 min.

Chemical separation. After addition of 10 mg of disodium hydrogenphosphate (p.a. Mallinckrodt), dissolve the sample in a Teflon beaker in 10 ml of a 1:1:1 (v/v) mixture of 14 M nitric acid, 50% hydrofluoric acid and water with slight heating. Remove the silicon by evaporating with 5 × 5 ml of 50% hydrofluoric acid. Add 10 ml of fuming nitric acid and 10 ml of 14 M nitric acid and fume down until nearly dry. Repeat 5 times, adjust the volume to 20 ml with 14 M nitric acid and heat to 50°C. If a precipitate of aluminates is formed, filter and wash with 20 ml of hot 14 M nitric acid and with 20 ml of hot water. Add 15 ml of a saturated boric acid solution to the filtrate.

To the solution add 7 g of ammonium nitrate. Add dropwise 20 ml of a 10% ammonium molybdate solution with constant stirring. After digesting for 1 h, filter the precipitate on a dismountable circular glass filter and wash with 5 × 10 ml of washing liquid (50 g of ammonium nitrate and 40 ml of 14 M nitric acid per l of water). Dry the precipitate for 2 h at 250°C. Weigh the precipitate as soon as possible after cooling. On average, the chemical yield was 98%. This corresponds to 130 mg of ammonium molybdophosphate. Treat the standards similarly.

Measurements. The circular glass filter was mounted on a plexiglass holder and covered with mylar foil (8 μm). The measurements were carried out with a halogen-quenched end-window G-M tube. Measurement time was 2 h.

Identity check of the ^{32}P activities. The radionuclidic purity of the precipitate for β-counting, being essential, was checked by three methods. The Ge(Li) spectra of the precipitate did not show any activity except that of the bremsstrahlung of the ^{32}P 1710-keV β^--radiation, 511-keV annihilation radiation and the 1460-keV radiation of ^{40}K both from the natural background. A γ-spectrum is shown in Fig. 2.

The absorption curves of the β^--radiation from the precipitates for the samples and the standards were measured by interposing aluminium discs with increasing thickness between the precipitate and the G-M detector. As

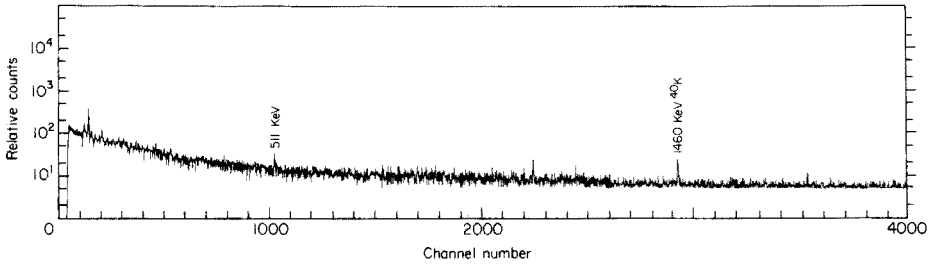

Fig. 2. Ge(Li) spectrum of an ammonium molybdophosphate precipitate (LMG sample). Counting time, 5 h.

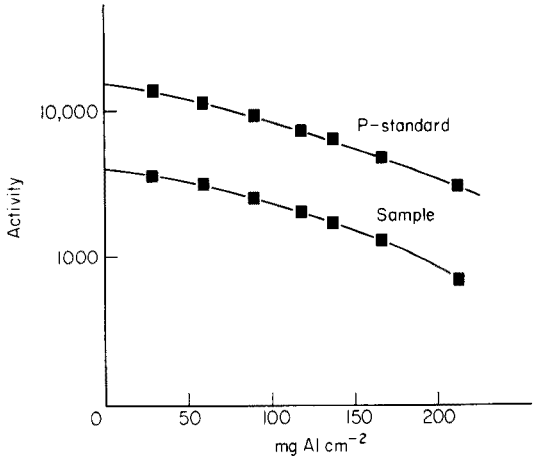

Fig. 3. β-Radiation absorption curves from the precipitates for a sample (LMG) and a standard.

shown in Fig. 3, the curves for sample and standard were parallel, indicating that in both cases a radionuclide with the same β^--energy was detected.

The half-life of the detected radionuclide was determined for five of the precipitates by repeated measurements over a 1-month period, corrections for detector fluctuations being carried out with a ^{137}Cs reference source. A value of 14.4 ± 0.2 d was obtained.

RESULTS AND DISCUSSION

The influence of the interfering reactions for α-activation given in Table 1 was studied experimentally. Pellets of aluminium powder mixed with sodium sulphate (p.a., U.C.B.) and polyvinyl chloride discs were irradiated and the ^{34m}Cl-activities produced from sulfur and chlorine, respectively, were compared to that of a phosphorus standard. From these experiments, one can deduce that for an incident energy of 20 MeV and for the same matrix, 290 and 360 μg g^{-1}, respectively, of chlorine and sulfur correspond to the same activity as 1 μg g^{-1} of phosphorus. The interference of both elements can thus be neglected in practice.

Table 3 summarizes the results for phosphorus in aluminium–silicon alloys of different origins with different silicon concentrations. The results of helium-4 activation with and without etching after irradiation do not differ significantly. The phosphorus concentration ranges from 1.7 to 25 μg g^{-1}. For helium-4 activation, the standard deviation ranges from 1 to 24% with an average value of 6%, and for neutron activation from 0.3 to 7.5% with an average of 2%.

Only for LMG do the mean values of the two methods differ significantly at the 95% confidence level. The good agreement between helium-4 activation,

TABLE 3

Phosphorus concentration in aluminium—silicon alloys ($\mu g\ g^{-1}$)

Alloy	% Si	^{4}He-activation			Neutron activation
		No etching	With etching	Mean	
AS3	3		1.72 ± 0.09[a] (n=2)[b]		1.79 ± 0.03 (n=2)
AS7	7		3.90 ± 0.93 (n=2)		3.52 ± 0.01 (n=2)
LMG	9.5	5.03 ± 0.40 (n=6)	4.22 ± 0.48 (n=5)	4.66 ± 0.32 (n=11)	5.09 ± 0.04 (n=5)
AS 13	13		5.85 ± 0.06 (n=2)		5.64 ± 0.03 (n=2)
VAW	—	8.33 ± 0.31 (n=6)	8.50 ± 0.44 (n=4)	8.41 ± 0.25 (n=10)	8.28 ± 0.07 (n=5)
BCR	12	24.4 ± 1.9 (n=5)	25.6 ± 1.2 (n=4)	25.0 ± 1.7 (n=9)	23.9 ± 1.8 (n=5)

[a]Standard deviation. [b]Number of analyses.

TABLE 4

Comparison of different methods for the determination of phosphorus in aluminium—silicon alloy

Method	Laboratory	Results
Helium-4 activation	This work	25.0 ± 1.7 (n=9)
Neutron activation	This work	23.9 ± 1.8 (n=5)
	Lab 1	23.8 ± 1.7 (n=5)
Photometry	Lab 2	24.9 ± 1.8 (n=15)
	Lab 3	32.2 ± 2.5 (n=10)
	Lab 4	35.5 ± 2.4 (n=16)
Indirect a.a.s.	Lab 5	20.0 ± 2.0 (n=5)

where only a 0.044-g cm^{-2} thick layer beneath the surface is analyzed, and neutron activation, where massive samples of about 0.4 g (1.0 g for BCR) are analyzed, proves that this layer is representative of the sample. Moreover, it is a good indication that during the dissolution of the samples activated with neutrons, no phosphorus is lost.

The BCR sample was analysed by various laboratories which used different analytical methods. Table 4 shows the results of a first intercomparison. The agreement with Lab 1 where neutron activation was used followed by extraction of ammonium molybdophosphate with isobutanol, and with Lab 2 where photometry was used, is excellent. The results of Labs 3, 4 and 5 differ significantly from these results. The reason for these discrepancies is not yet understood but will be studied in further intercomparisons. It is worthwhile mentioning that helium-4 activation is the only method applied that allows a purely instrumental determination. It appears from the intercomparison that this instrumental and rapid method gives a precision similar to those of the other methods.

Grateful acknowledgement is made to R. Kieffer for technical assistance, to the "Comité de gestion du cyclotron" at Louvain-La-Neuve for the use of the cyclotron and to the I.I.K.W. for financial support. Thanks are also due to B.C.R. of the European Communities for the organization of the round-robin and to G. Kraft (Metalgesellschaft A.G.) for providing part of the samples.

REFERENCES

1 G. Kraft, personal communication.
2 M. Davey, Metallurgia, 65 (1962) 151.
3 W. S. Zaugg and R. J. Knox, Anal. Chem., 38 (1966) 1759.
4 R. V. Ramakrishna, J. W. Robinson and P. W. West, Anal. Chim. Acta, 45 (1969) 43.
5 Ph. Albert, J. Blouri, Ch. Cleyrergue and N. Deschamp, J. Radioanal. Chem., 1 (1968) 297.
6 F. De Corte, A. Speecke and J. Hoste, J. Radioanal. Chem., 8 (1971) 277.
7 C. Williamson, J. Boujot and J. Picard, Tables of Range and Stopping Power of Chemical Elements for Charged Particles of Energy 0.05 to 500 MeV; Report CEA-R3042, 1966.

Analytica Chimica Acta, 101 (1978) 71—77

THE SEPARATION OF SELENIUM FROM SEA WATER BY ADSORPTION COLLOID FLOTATION†

JAU-HWAN TZENG and HARRY ZEITLIN*

Department of Chemistry and Hawaii Institute of Geophysics, University of Hawaii, Honolulu, Hawaii 96822 (U.S.A.)

(Received 20th March 1978)

SUMMARY

Adsorption colloid flotation can be applied successfully to the separation of selenium as SeO_3^{2-} from sea water. Separation is achieved in 5 min. The modified catalytic method of West and Ramakrishna is used to determine the selenium. The recovery of selenium based on spiked sea-water samples is 100 ± 10%. Standard addition analysis of near-shore Oahu sea water showed a value of 0.40 ± 0.12 $\mu g\ l^{-1}$.

In recent years, the physiological role of selenium as a trace element has created considerable speculation and some controversy. Selenium has been reported as having carcinogenic as well as toxic properties; other authorities have presented evidence that selenium is highly beneficial as an essential nutrient [1, 2]. Its significance and involvement in the marine biosphere is not known. A review of the marine literature indicates that selenium occurs in sea water as selenite ions (SeO_3^{2-}) with a reported average of 0.2 $\mu g\ l^{-1}$ [3]. Extensive earlier work on the separation and preconcentration of trace anionic and cationic species in sea water by adsorption colloid flotation [4—9] suggested the feasibility of applying this technique to the separation of selenium as selenite. The major advantages of this method of preconcentration are rapidity of flotation (about 5 min), simple equipment, and excellent recoveries based on spiked sea-water samples. The separation procedure makes use of a surfactant—collector—inert gas system, in which a charged surface-inactive species is adsorbed on a hydrophobic colloid collector of opposite charge. The colloid enriched with the adsorbed trace species is floated to the surface with a suitable cationic or anionic surfactant and inert gas. The foam layer is removed manually and analyzed by any appropriate method.

Separation and determination of selenium in sea water

The procedure which has been applied most commonly for the determination of selenium involves coprecipitation followed by spectrophotometry [10—13]. The neutron activation methods employed [14, 15] are highly sensitive but are expensive and not widely available. A direct gas chromatographic

†Hawaii Institute of Geophysics contribution no. 904.

determination of selenium in sea water without preconcentration has been reported [16], but its applicability is uncertain. Coprecipitation by iron(III) hydroxide, most frequently cited for the separation of selenium, is lengthy, two days being needed for complete coprecipitation. This paper is concerned with the application of adsorption colloid flotation to the separation of selenium followed by a spectrophotometric determination based on a modification of the catalytic method of West and Ramakrishna [17].

EXPERIMENTAL

Apparatus and reagents

A Corning Digital pH meter and a Beckman Spectrophotometer ACTA CIII were used. The flotation unit was that devised by Kim and Zeitlin [4]. All glassware, including the 500-ml flotation cell, was cleaned scrupulously by soaking overnight in nitric acid, and washed thoroughly with doubly-distilled deionized water.

All chemicals were of analytical grade. Aqueous solutions were prepared in doubly-distilled deionized water. A standard selenium solution (0.127 μg ml^{-1}) was prepared by dilution of a commercial selenious acid standard (5066 μg Se ml^{-1}; Spex). An alkaline sodium sulfide solution (ca. 0.1 M) was prepared by dissolving 2.40 g of sodium sulfide, 2.40 g of sodium sulfite and 4 g of sodium hydroxide in 100 ml of water; this solution remains stable for two days. A surfactant solution was prepared by dissolving 0.05 g of sodium dodecylsulfate in 100 ml of 50% ethanol—water. The collector was 0.1 M iron(III) chloride. The conditioner solution consisted of 25 g of EDTA (disodium salt), 0.4 g of iron(III) chloride, and 50 ml of triethanolamine dissolved in water and diluted to 1 l.

An ion-exchange column, prepared in a 100-ml buret (diameter 1.5 cm), was packed with 10 ml of Zeo-Karb 225 resin (H-form, 8% cross-linked, 52—100 mesh) pretreated with 0.2 M nitric acid. After use, the resin may be regenerated by washing with 2 M hydrochloric acid until free of iron and then with water until free of acid.

Clear uncontaminated near-shore sea water filtered through 0.45-μm Millipore filters was used in all subsequent work.

Procedure

To a 500-ml sample of sea water, previously acidified to pH 1—2 with 1 ml of 18 M sulfuric acid per litre, was added 5.00 ml of standard selenium solution (for preliminary tests) together with 3 ml of 0.1 M iron(III) chloride. The solution was adjusted with ammonia and hydrochloric acid to pH 3.5—5.3. The sample, now containing colloidal hydrated iron oxide, was transferred to the flotation cell and nitrogen was passed through the unit at a flow rate of 10 ml/35 ± 1 s. Sodium dodecylsulfate solution (4 ml) was injected gradually and the nitrogen was allowed to flow for 5 min. At this point, the nitrogen pressure was increased to 5 psi if necessary, to push

up the foam. The foam was collected manually and deposited in a small beaker. A cell completely clear of the colloidal collector, and the formation of a thick yellow-brown stable foam layer on the surface of the sample, signified completion of the separation. The precipitate formed in the beaker after collapse of the foam was transferred quantitatively to a centrifuge tube and washed with 7—8 ml of 0.5% (w/v) ammonium nitrate solution. The washed mixture was centrifuged and the supernatant solution decanted. The washing procedure was repeated three additional times with 7—8 ml portions of the ammonium nitrate. The washed precipitate was dissolved in 1 ml of concentrated nitric acid, and the solution was diluted to 80 ml (ca. 0.2 M). This solution was passed through the ion-exchange column and the column was eluted with 270 ml of 0.2 M nitric acid at a flow rate of 2 ml min^{-1}. Sodium hydroxide (1 ml of 2 M) was added to the eluate (350 ml) which was placed in a 1-l beaker and evaporated to dryness on a water bath. Water (10 ml) was added to the residue and the solution adjusted to near neutrality with 1 drop of 2 M ammonia. Conditioner solution (5 ml), 5 ml of formaldehyde solution (37.7%) and 1 ml of alkaline sodium sulfide were then added, mixing well after each addition. Aqueous 0.05% (w/v) methylene blue solution (0.10 ml) was added, the solution was mixed thoroughly and the time required for the decolorization of the solution commencing with the addition of the methylene blue was measured carefully with a stop watch. The absorbance was measured vs. water at 560 nm. This was most conveniently done by recording absorbance vs. time and using the intersection of the slope as the end-point of the color change (Fig. 1). The concentration of selenium in the sea water ($\mu g\ l^{-1}$) was obtained from a rectilinear calibration curve when reciprocal time (min^{-1}) is plotted against μg of selenium.

The method of standard addition was used to determine the natural levels of selenium in sea water.

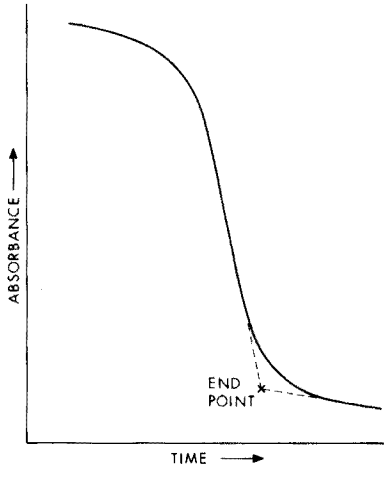

Fig. 1. The decolorization of methylene blue.

Preliminary tests

The reproducibility of the four separate steps incorporated in the analysis was checked systematically; (1) methylene blue decolorization, (2) evaporation, (3) ion exchange, (4) washing and flotation.

First, a series of solutions was prepared composed of selenium stock solution (2.00, 3.00, 5.00, 10.00 ml) and sufficient water to make a final volume of 10 ml. To each sample solution were added 5 ml of conditioner solution, 5 ml of the formaldehyde solution, and 1 ml of the alkaline sulfide solution, with thorough mixing. The above procedure was then followed. Triplicate results showed good reproducibility with the reciprocal time varying from 0.106 ± 0.001 min^{-1} for 0.254 μg Se to 0.259 ± 0.003 min^{-1} for 1.27 μg Se.

The procedure used and the results obtained in the other reproducibility tests are outlined in Table 1.

Parameters studied to determine the optimum conditions of flotation included pH, volume of collector, and volume of surfactant. Replicate 500-ml sea-water samples were treated with 5.00 ml of standard selenium solution and 3 ml of iron(III) chloride solution, and were adjusted to a pH value in the range 3.5—6.8; the analyses were then completed as in the given procedure. The pH range 3.5—5.3 was found to be effective; flotation was incomplete at pH 6.8. In a second series of similar tests, the pH was adjusted to 5.0 and the volume of iron(III) chloride solution was varied from 1.5 ml to 4 ml; 2.5—3 ml of iron(III) solution was found to be effective. With more iron(III) solution, flotation was incomplete, and with less the final results were low. In a third series of tests, at pH 5.0 with 2.5 ml of iron(III) solution, the

TABLE 1

Reproducibility for the determination of selenium (0.635 μg Se) after different procedural steps

Treatment	Reciprocal time (min^{-1})			
A	0.158	0.158	0.158	—
B	0.158	0.158	0.160	0.156
C	0.155	0.149	0.153	0.157
D	0.130 (pH 5.3)	0.130 (pH 5.3)	0.129 (pH 4.0)	0.135 (pH 4.0)

(A) The Procedure was followed from the addition of conditioner solution, etc.

(B) Selenium standard (5 ml) and 350 ml of 0.2 M HNO_3 were mixed with 1 ml of 2 M NaOH. The Procedure was then followed from the evaporation to dryness and addition of 10 ml of water to the residue.

(C) Samples were prepared containing 2 ml of iron(III) chloride solution, 5 ml of selenium standard and 80 ml of 0.2 M HNO_3. These solutions were passed through ion-exchange columns and selenium was eluted as described in the Procedure. The subsequent steps were carried out as before.

(D) Sea-water samples (500 ml), to which 5 ml of selenium standard was added, were taken through the entire procedure; two samples were adjusted to pH 5.3 and two to pH 4.0.

volume of surfactant was varied from 3 to 5 ml; the reciprocal times decreased as the amount of surfactant increased (0.135, 0.129 and 0.126 min^{-1} for 3, 4 and 5 ml of surfactant, respectively), so that a volume of 3—4 ml seemed optimal.

RESULTS AND DISCUSSION

Chau and Riley [13] coprecipitated the selenium with iron(III) hydroxide. The coprecipitate was dissolved and passed through the ion-exchange column to remove interfering iron(III) ion. The solution was then evaporated and the selenium in the residue was determined spectrophotometrically with 3,3′-diaminobenzidine. Their procedure was followed but flotation was substituted for precipitation to conserve time and the determination was completed by the sensitive catalytic methylene blue method [17]. The separation by flotation is very rapid but unfortunately the determination of the selenium after separation either by coprecipitations or flotation is time-consuming and requires a number of separate steps each of which may be subject to experimental error. To insure reliability of data a careful check was carried out on the reproducibility of the entire separation and analytical sequence.

Table 1 provides data on the precision of the methylene blue decolorization procedure, the evaporation, ion-exchange, and the washing and flotation. With some practice, it was not difficult to obtain reproducible end-points for the decolorization. The results in all cases were found to be satisfactory. Care should be exercised, however, in all manipulations. It was essential to pass all samples through the ion-exchange column, to remove the relatively high concentration of iron(III) ion used as collector plus other trace metals coprecipitated, because iron(III) interferes in the catalytic determination.

The efficiency of the flotation procedure was studied by preparing two sets of sea-water samples. To one set (A) was added 5.00 ml of standard selenium solution, the flotation procedure was carried out, and the concentration of selenium determined. Set B was treated identically except that the standard selenium solution was added to the foams after flotation of the unspiked sea-water samples; the spiked foams were then analyzed for selenium as described.

The results of these tests are summarized in Table 2. The recovery of the selenium was found to be 100 ± 10% (at the 95% confidence level). The separation of selenium from sea water by adsorption colloid flotation appears to be virtually quantitative. Any losses encountered are believed to be due to difficulties in transferring the foam completely from the sea-water surface.

Natural levels of selenium in sea water

The standard addition method was used to determine the natural level of selenium in sea water. The data obtained from the analysis of eight

TABLE 2

Flotation recovery

Set A			Set B		
Sample	Min^{-1}	pH	Sample	Min^{-1}	pH
1	0.130	5.3	1	0.130	5.3
2	0.130	5.3	2	0.132	5.3
3	0.129	4.0	3	0.124	4.0
4	0.135	4.0	4	0.126	4.0

TABLE 3

Determination of selenium in sea water
(Conditions as specified in the Procedure.)

Se added (ml)	pH	Min^{-1}	Temp. (°C)
2.00	4.5	0.087	25.5—29.8
3.00	5.0	0.105	26.8
3.00	4.3	0.099	26.1—26.3
5.00	5.0	0.125	25.8
5.00	4.7	0.122	25.8—26.1
5.00	4.5	0.125	26.8
6.00	5.0	0.135	26.5—26.8
6.00	4.8	0.133	26.8

replicates containing varying quantities of added selenium are given in Table 3. The concentration of selenium was found to be 0.40 ± 0.12 $\mu g\ l^{-1}$. It is to be noted that all the tests described were carried out in the 25.5—26.8°C temperature range. The catalytic method of West and Ramakrishna used to determine the selenium is temperature-sensitive and contributes some uncertainty to the results.

The average of the five blank replicates determined with 10-ml portions of deionized water was found to be 0.049 ± 0.005 min^{-1} (standard deviation at the 95% confidence level). In the calculation of the concentration of selenium, the blank was subtracted from the reciprocal time values obtained from analyzed samples.

REFERENCES

1 Committee on Medical and Biologic Effects of Environmental Pollutants, Selenium, National Academy of Sciences, Washington, D.C. 1976.
2 T. D. Luckey and B. Venugopal, Chem. Eng. News., 54, No. 29 (1976) 2.
3 J. P. Riley and G. Skirrow, Chemical Oceanography, 2nd edn., Vol. 1, Academic Press, New York, 1975, p. 418.
4 Y. S. Kim and H. Zeitlin, Sep. Sci., 6 (1971) 505.
5 Y. S. Kim and H. Zeitlin, Sep. Sci., 7 (1972) 1; Anal. Chem., 43 (1971) 1390; J. Chem. Soc. D, 13 (1971) 672.

6 G. Leung, Y. S. Kim and H. Zeitlin, Anal. Chim. Acta, 60 (1972) 229.
7 D. Voyce and H. Zeitlin, Anal. Chim. Acta, 69 (1974) 27.
8 F. E. Chaine and H. Zeitlin, Sep. Sci., 9 (1974) 1.
9 M. Hagadone and H. Zeitlin, Anal. Chim. Acta, 86 (1976) 289.
10 V. M. Goldschmidt and L. W. Strock, Nachr. Akad. Wiss. Goettingen, Math-Physik, Kl. IV, N.F., 1 (1935) 123.
11 H. Wattenberg, Z. Anorg. Chem., 236 (1938) 339.
12 M. Ishibashi, T. Shigematsu and Y. Nakagawa, Rec. Oceanogr. Works Jpn., Spec. Number, 1 (1953) 44.
13 Y. K. Chau and J. P. Riley, Anal. Chim. Acta, 33 (1965) 36.
14 D. F. Schutz and K. K. Turekian, Abstr. of Papers XIII, Gen. Assembly I.U.G.G. Berkeley, Paper 23, 1963.
15 D. F. Schutz, Ph.D. Thesis, Dept. of Geology, Yale University, 1964.
16 Y. Shimoishi, Anal. Chim. Acta, 64 (1973) 465.
17 P. W. West and T. V. Ramakrishna, Anal. Chem., 40 (1968) 965.

Analytica Chimica Acta, 101 (1978) 79—88

ANODIC STRIPPING VOLTAMMETRY AT A MERCURY FILM ELECTRODE: BASELINE CONCENTRATIONS OF CADMIUM, LEAD, AND COPPER IN SELECTED NATURAL WATERS

J. E. POLDOSKI* and G. E. GLASS

U.S. Environmental Protection Agency, Environmental Research Laboratory-Duluth, 6201 Congdon Boulevard, Duluth, Minnesota 55804 (U.S.A.)

(Received 30th January 1978)

SUMMARY

A simple, rapid, and inexpensive anodic stripping voltammetric method with a mercury thin film electrode is reported for the establishment of baseline concentrations of cadmium, lead, and copper in natural waters. The procedure for routine surface preparation of wax-impregnated graphite mercury film electrodes requires about 30 min. Concentrations in the 0.006—6 $\mu g\, l^{-1}$ range are determined by linear d.c. voltage sweeps; the total time for a plating and stripping cycle is 6 min or less. The need for pressure-digesting samples for copper determinations is demonstrated. The a.s.v. results correlate well with corresponding analyses performed by graphite-furnace atomic absorption spectrometry.

Characterizing trace elements in aquatic environments has become increasingly important, especially with reference to natural or relatively unpolluted conditions, such as those generally found in Lake Superior [1]. However, few analytical procedures are capable of measuring these characteristically low concentrations, and those which can are sometimes cumbersome and require a sample preconcentration step. Cadmium, lead, and copper are heavy metals which are often of concern because of their high toxicity, especially to aquatic life [2—5]. Fortunately, these three metals are amenable to determination by several electrochemical techniques, particularly anodic stripping voltammetry (a.s.v.). Although there are many published methods [6—13], few deal specifically with the accuracy attainable for these elements in waters where concentrations are very low. The objective of this paper is to describe the utility of a simple and inexpensive a.s.v. method and to explore various aspects of trace analyses for copper, lead, and cadmium in some natural waters.

EXPERIMENTAL

Electrode construction and preparation

The working electrode was a wax-impregnated graphite mercury film electrode (Fig. 1). Spectroscopic-grade graphite rods (6.4-mm diameter; National Carbon) were impregnated for 4 h by immersion in hot ceresin wax

(Fisher) under vacuum. Previous work [14] suggested relatively low residual currents for this wax type in addition to other desirable properties [15]. Graphite electrode components were machined with a small lathe (Unimat, American Edelstaal Corp.). A thin layer of graphite was removed with a microtome blade to produce a homogeneous surface of approximately 300 mm^2. Components were force fitted into Teflon (FEP) tubing. The electrode was used indefinitely with the aid of the surface-conditioning process described below.

Each time the electrode was prepared for mercury plating, a final surface preparation was made by first wiping the surface clean with a soft tissue, immersing the machined graphite surface in hot ceresin wax (5 min), and then allowing a uniform coating to harden completely on it. While the electrode was rotated in the lathe at moderate speed, several clean surfaces of a relatively hard bond typing paper were used to rub off the wax by applying firm finger pressure. This process also removed a thin layer of graphite to form a new surface onto which the mercury was plated.

To form the mercury film, the electrode was rinsed with deionized distilled water and placed in the a.s.v. cell containing 10 ml of previously degassed mercury(II) nitrate solution (200 mg l^{-1}) which was 0.1 M in nitric acid. The solution was degassed for an additional 1 min, and allowed to become quiescent before −0.8 V (vs. Ag/AgCl, 0.1 M (NaCl)) was applied to the working electrode for 3 min. The electrode was immediately removed from the solution and rinsed. The total amount of mercury which could be electrochemically stripped from the electrode was approximately 0.1—0.3 μg mm^2 (calculated area) as determined by a standard cold-vapor mercury atomic absorption procedure [16]. A solution containing 10 μg Cd l^{-1}, 10 μg Pb l^{-1}, 10 μg Cu l^{-1}, 5 mg Hg l^{-1} and 0.2% (v/v) nitric acid was then analyzed repeatedly with a 1-min plating time at −1.2 V and a linear sweep of 5 V min^{-1} to test whether acceptable response was obtained. A properly prepared electrode gave reproducible (±2%) sharp peaks with half-peak widths of about 0.04 V and peak currents in the range of 10 μA. The background current was approximately 1—2 μA and the hydrogen overvoltage was −1.2 V. The time required from the wax surface conditioning step to this point was about 30 min.

Apparatus

Data were recorded on a Hewlett-Packard Model 2D-2 X-Y recorder. A modified [17] polarographic module (Heathkit, Model EUA-19-2) was used for applying plating potentials and linear d.c. voltage sweeps. Control functions on the module were particularly suited for nulling out the background current from the electrode so that a high current sensitivity could be achieved. The design of the cell assembly was similar to one described previously [11] with a few exceptions. Main component parts were a 78 × 22-mm diameter (i.d.) flat-bottom fused quartz cell (General Electric, Willoughby, Ohio) convenient for 10-ml samples, a machined Teflon cell

head, an auxiliary electrode, and a Ag/AgCl (0.1 M NaCl) reference electrode. The auxiliary electrode consisted of a platinum wire (6 cm long by 0.5 mm in diameter) in a 3-mm i.d. FEP tube filled with 0.1 M NaCl and stoppered at the bottom with a leached porous quartz plug (Corning Glass Works, Danville, Virginia). The reference electrode was a silver chloride-coated wire, which was also immersed in 0.1 M NaCl contained in a Teflon tube with a porous quartz stopper. FEP capillary tubing (0.5-mm i.d.), with a platinum wire placed inside for stiffening, was used for dispersing water-saturated, prepurified-grade nitrogen through the cell solution to expel oxygen. A 3 × 14-mm Teflon-encapsulated magnetic stirring bar (1000 rpm) was also used to stir the solution during the plating step.

Reagents

All chemicals were of analytical-reagent grade, but ultrapure nitric acid (Baker Ultrex) was generally used for lead determinations. Ultrapure water was prepared by passing distilled water through a deionizer (Millipore Super Q). Standards were prepared by weighing and dissolving the required amount of pure metal in nitric acid and making appropriate dilutions with 0.2% (v/v) nitric acid.

Procedure

Quartz cells were cleaned and kept separate for the analysis of samples of low concentration. The cleaned cell was immediately checked for contamination by analyzing a 10-ml aliquot of acidified deionized distilled water. The acidified (0.2% v/v HNO_3) sample or blank was degassed for 2 min and stirred, after which a plating potential of −1.2 V for cadmium and lead, or −1.0 V for lead and copper, was applied for 1—5 min. Stirring was then ceased and the solution was allowed to become quiescent for 30 s, thus allowing time for the background current to decay to a minimum before balancing it to near zero. The voltage was swept from −1.0 to 0.0 V at 5—10 V min^{-1}. Application of potentials near or more positive than 0.0 V was avoided since this reduces the normal useful lifetime of the mercury film. Each sample was analyzed in duplicate; two or more different standard concentrations were then added for calibration by the method of standard additions.

Aspects of furnace atomic absorption analysis (f.a.a.s.), sampling and sample preparation have been discussed previously [18].

Samples were digested by dispensing 15-ml aliquots into a precleaned Teflon-lined pressure decomposition bomb (Parr). In addition, 0.15 ml of 10% (w/w) ammonium persulfate (Baker) was added if greater oxidizing conditions were desired. The bomb was hand-tightened and then turned an additional one-quarter turn before it was placed in an oven for 3 h at 140°C. Water samples originally high in natural color because of humic materials appeared colorless after digestion. Blanks were run and standards were

periodically added to the digestion vessel to check on recoveries. Sample cups were cleaned between digestions with ultrapure (1 + 1) nitric acid, followed by 0.2% (v/v) nitric acid, as employed in the normal digestion procedure.

RESULTS AND DISCUSSION

A.s.v. with a hanging mercury drop or mercury film electrode has been widely studied [19—22]. Although the performance of each system is a function of the type of electrode and the electronics, one limiting property of wax-impregnated graphite mercury film electrodes has been that they have finite lifetimes which are an integrated function of electrode substrate, mercury film characteristics, the chemical characteristics of the samples with which they come in contact, and the voltage ranges in which they are used. Since it is commonly necessary for the analyst routinely to prepare the surface of film electrodes, it was desirable to produce a sensitive electrode that could be prepared rapidly and reproducibly, i.e. the time involved should be several minutes rather than several hours. Such an electrode is described above. About 30 min was required for the surface-conditioning step and mercury plating. This relatively rapid procedure helped to circumvent the problems of analyzing acidified samples, since electrode lifetime was often shorter at low pH. Oxidation of active sites on the graphite

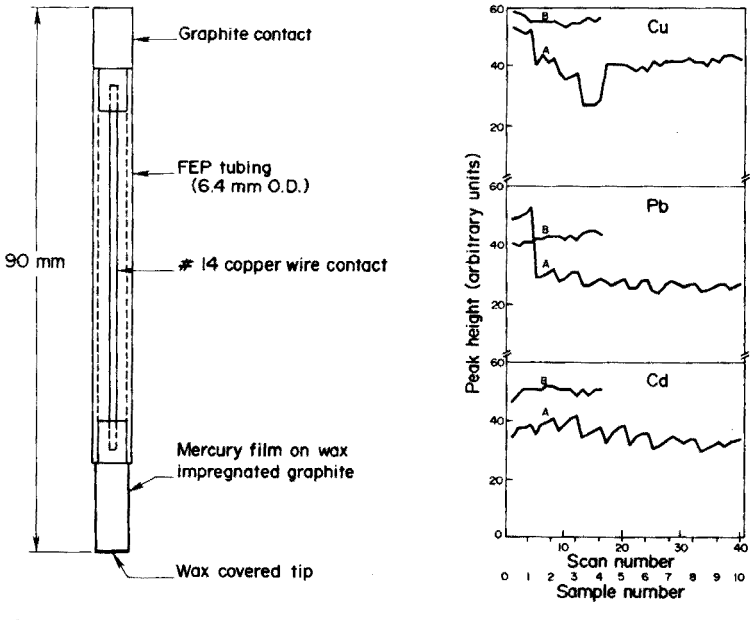

Fig. 1. Construction of wax-impregnated mercury film graphite electrode.

Fig. 2. Variations in peak height as a function of repeatedly analyzing a Lake Superior water sample containing added metal ions. Curve A represents quadruplicate scans on each of ten cell solutions; Curve B indicates several scans on the same cell solution.

surface can occur more easily as the pH decreases [23]. This condition gives rise to larger background currents and a more positive overvoltage, which can make an electrode less useful. However, this problem was offset by employing an in situ mercury plating procedure with solutions containing usually 2 mg $Hg\,l^{-1}$. The sensitivity of the electrode appeared to be relatively stable once a sufficient mercury film had been formed [6]. Peak current was a linear function of scan rate in the range 1—10 V min^{-1}.

Typical changes in electrode sensitivity were characterized as a function of electrode use by repeatedly analyzing a metal-spiked Lake Superior water sample containing 1—2 $\mu g\,l^{-1}$ each of cadmium, lead and copper (Fig. 2). The experiment was treated as routinely as possible; therefore, no special care was taken other than in normal analytical procedures. A new electrode surface was prepared just prior to each series of analyses (A and B). In curve A each sample-analysis sequence consisted of four scans on the same cell solution containing 2 mg l^{-1} mercury(II) with 2-min plating times. After each sequence the cell solution was replaced with an aliquot of the same sample for a total of 10 times, which produced 40 scans on a single acidified (0.2% v/v HNO_3) water sample. Most apparent is the relatively good reproducibility in all cases for quadruplicate scans on a single cell solution, although a noticeable upward trend of peak current with each successive scan is apparent in some groups. At the beginning of Curve A, marked differences are noted between the means of quadruplicates for copper and lead on different cell solutions of the same sample. These differences may be partly due to contamination or adsorption effects; however, past experience suggests that this is not the reason since the slope of the standard additions curve can also change between different cell solutions. For cadmium these changes are not quite so pronounced but are still apparent. Therefore, these data suggest that in sample analysis standard additions should be used to obtain the best calibration. In illustration of this point, analysis of a Lake Superior sample in triplicate for cadmium and lead at their ambient concentrations gave values of 0.023, 0.023 and 0.024 $\mu g\,l^{-1}$ for cadmium and 0.15, 0.17 and 0.18 $\mu g\,l^{-1}$ for lead. Each replicate represented separate cell solutions with duplicate scans of the cell solution and two additional scans with standard addition spikes. Curve B, representing several repeated scans on the same cell solution, shows excellent reproducibility. Figure 3 illustrates the linear nature of a typical standard addition graph for the determination of cadmium in Lake Superior water.

A display of experimental output is given in Fig. 4 with duplicate determinations of cadmium and lead in natural water giving mean concentrations of 0.055 $\mu g\,l^{-1}$ and 0.28 $\mu g\,l^{-1}$ respectively. Natural fresh-water concentrations for copper are usually in a much higher range; these determinations were done separately giving a mean copper value of 0.45 $\mu g\,l^{-1}$. Higher sensitivity can normally be obtained by increasing plating time and scan rate.

Contamination from the cell and acid was a major concern in routinely determining baseline samples. It was highly desirable to clean the cell thoroughly

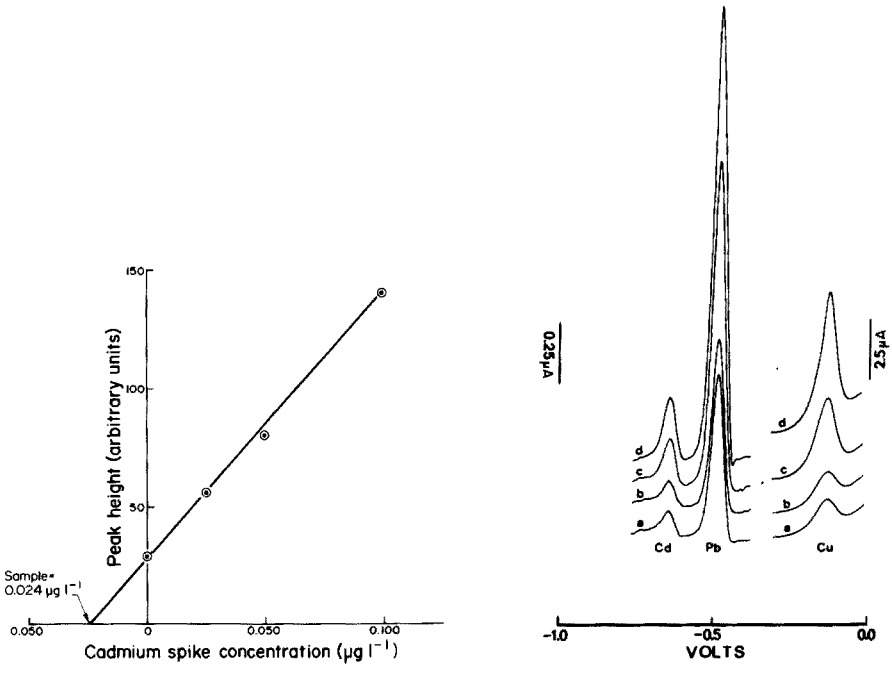

Fig. 3. Standard addition plot for cadmium in Lake Superior water.

Fig. 4. A.s.v. analysis of a natural water sample. Scan rate, 5 V min^{-1}; plating time, 90 s. Curves a and b, sample. Curve c, sample + 0.05 μg Cd l^{-1} + 0.25 μg Pb l^{-1} + 1 μg Cu l^{-1}. Curve d, sample + 0.1 μg Cd l^{-1} + 0.5 μg Pb l^{-1} + 2 μg Cu l^{-1}. Results: Cd, 0.055 μg l^{-1}; Pb, 0.28 μg l^{-1}; Cu, 0.45 μg l^{-1}.

TABLE 1

Typical analysis blanks[a]

Element	Mean concentration (μg l^{-1})	Standard deviation (μg l^{-1})	Number
Cd	<0.005	—	9
Pb	0.017	0.008	9
Cu	<0.03	—	4

[a]0.2% (v/v) nitric acid (Baker Ultrex) in deionized distilled water.

and analyze a cell blank (0.2% v/v HNO_3), particularly for cadmium and lead. Table 1 gives typical minimum blank values that could be routinely attained. Lead contamination was the most troublesome, which is reflected in a somewhat variable mean blank value of 0.017 μg l^{-1}. This concentration could easily be detected since the instrumental detection system was sensitive

TABLE 2

Typical reproducibilities and detection limits for the analysis of natural water samples

Element	Mean relative error[a] (%)	Range (%)	No. of determinations	Estimated working detection limit ($\mu g\ l^{-1}$)
Cd	11.6	2.1—32.8	24	0.005[b] (0.005)[d]
Pb	7.4	0.5—26.6	54	0.03[c] (0.005)[d]
Cu	4.3	0.2—15.1	45	0.03[b] (0.03)[d]

[a]Defined as the mean of the relative deviation from the mean for two analyses on each of several water samples. Concentration ranges: Cd, 0.005—0.28 $\mu g\ l^{-1}$; Pb, 0.06—3.2 $\mu g\ l^{-1}$; Cu, 0.5—7.7 $\mu g\ l^{-1}$.
[b]Estimated working detection limit defined as twice the mean of the deviation from the mean for two analyses on each of several water samples with very low concentrations. Cd $<$ 0.03 $\mu g\ l^{-1}$ and Cu $<$ 1.0 $\mu g\ l^{-1}$.
[c]Estimated working detection limit based on the cell blank plus twice its standard deviation.
[d]Estimated instrumental detection limit for a 5-min plating time.

to about 0.005 $\mu g\ l^{-1}$. Therefore, measurement of these baseline samples was largely dependent on maintaining the blank in this low range.

Since normal analytical procedure involved two analyses of a sample prior to spiking, their repeatability was a measure of the precision for a single analysis of a sample. Table 2 gives values for this reproducibility involving 24—45 analyses on different natural water samples. Concentrations covered a wide range for all three metals, but the mean concentrations were low (0.03 μg Cd l^{-1}, 0.03 μg Pb l^{-1}, 2 μg Cu l^{-1}). Mean relative errors ranged from 11.6% for cadmium to 4.3% for copper, which are acceptable. The estimated working detection limit for lead was calculated from the blank plus twice its standard deviation. For cadmium and copper, it was based on twice the mean of the deviation from the mean for duplicate determinations on each of several water samples containing very low concentrations. Concentrations were limited to $\leqslant$0.03 $\mu g\ l^{-1}$ for cadmium and $\leqslant$1.0 $\mu g\ l^{-1}$ for copper in this calculation. Estimated instrumental detection limits (not considering the reagent blank) were based on a concentration corresponding to a peak height deflection double the width of the baseline noise, with maximum scale expansion and a 5-min plating time. All values are acceptable for the analysis of natural waters and compare favorably with values obtained by other methods [6—13].

It is generally accepted that samples often require digestion if the total metal concentration (rather than "acid exchangeable metal") is the desired parameter. However, the digestion step introduces an additional possibility for contamination. In view of this, a relatively new digestion technique was explored: digestion at 140°C for 3 h in a Teflon-lined pressure decomposition

bomb. This method possesses the inherent advantages of a completely closed system to avoid the possibility of contamination via air during digestion and a higher digestion temperature without taking a sample to incipient dryness. Persulfate may also be added to increase oxidizing conditions. However, even without added persulfate, natural water samples, normally colored because of naturally occurring organic matter, were essentially decolorized. Ultraviolet spectrophotometric absorbance measurements on digested samples indicated a five to tenfold decrease in absorbance compared to the undigested sample, which was assumed to be due to decomposition of organic matter.

The results of a.s.v. measurements on undigested samples (samples 1—15), digested samples without added persulfate (samples (9—15) and digested samples with added persulfate (samples 9—15) are given in Table 3. All were natural water samples from wilderness streams in north-eastern Minnesota and from Lakes Superior and Huron and their tributary streams. For lead, there is a good correspondence between acid-exchangeable values and those corresponding to digested samples (total values), even with persulfate added. For copper, however, markedly lower values were obtained for acid-exchangeable metal compared to either digested or persulfate-digested samples. In some cases, the acid-exchangeable result was only one-half the total concentration. Little or no difference was observed with or without the presence of persulfate in the digestion. Filtered (0.1 μm) samples exhibited the same differences between undigested and digested samples. Therefore, it is likely that differences should be attributed not to dissolution of suspended solids, but to release of copper from electro-inactive dissolved complexes or colloidal forms which are slow to dissociate (since samples remained acidified for at least 1 week before measurement).

Because of these results, it was especially desirable to determine the possible accuracy of a.s.v. determinations by making comparative analyses with f.a.a.s. (Table 3). For the f.a.a.s. measurement, simultaneous deuterium arc background correction was always employed and calibration was by the method of standard additions. Results for copper analyses (samples 9—15) show a high degree of correlation between a.s.v. for digested samples and f.a.a.s. for either digested or undigested samples, which demonstrates the validity of the digestion step for the a.s.v. analyses. The f.a.a.s. results for lead (either undigested or digested samples) generally agree well with a.s.v. results on digested or undigested samples (acid exchangeable). Also given in Table 3 are the results of several analyses for total cadmium by f.a.a.s. and acid-exchangeable cadmium by a.s.v. The close agreement for most samples suggests that acid-exchangeable cadmium is essentially equal to the total cadmium in these cases. However, it is possible that sample digestion may be required for the determination of total cadmium for other natural waters.

Results of a.s.v. analyses for a survey of relatively unpolluted baseline natural waters of low turbidity are given in Table 4. All values correspond to acid-exchangeable metals in unfiltered samples. Over a period of several months, surface-water samples from streams in a wilderness area of north-

TABLE 3

Relationship of sample digestion to a comparison of analytical results for natural waters by a.s.v. and f.a.a.s.

Sample	Sample type[a]	Copper ($\mu g\ l^{-1}$)		Lead ($\mu g\ l^{-1}$)		Cadmium ($\mu g\ l^{-1}$)	
		F.a.a.s.[b]	A.s.v.	F.a.a.s.	A.s.v.	F.a.a.s.	A.s.v.
1[c]	UF, UD	—	—	0.2	0.20	0.031	0.013
2[c]	UF, UD	—	—	0.3	0.17	0.021	0.013
3[c]	UF, UD	—	—	0.3	0.21	0.022	0.021
4[c]	UF, UD	—	—	0.5	0.30	0.034	0.022
5	UF, UD	—	—	0.2	0.17	0.020	0.022
6	UF, UD	—	—	1.0	0.93	0.27	0.28
7	UF, UD	3.3	2.8	0.8	0.92	0.26	0.29
8	UF, UD	1.7	1.4	0.2	0.34	0.070	0.076
9	UF, UD	1.1	0.51	0.2	0.18	—	—
	UF, D	1.0	0.80	0.2	0.18	—	—
	UF, DP	—	0.99	—	0.19	—	—
10[c]	UF, UD	6.2	3.2	0.4	0.10	0.019	0.034
	UF, D	5.6	6.0	—	—	—	—
11	UF, UD	1.2	0.85	0.4	0.23	0.032	0.030
	UF, D	1.0	0.90	—	—	—	—
12[c]	F, UD	5.6	3.0	—	—	—	—
	F, D	6.3	6.5	—	—	—	—
13	F, UD	1.6	0.65	0.3	0.26	0.29	0.23
	F, D	1.4	1.5	0.3	0.23	—	—
	F, DP	—	1.3	—	0.30	—	—
14[c]	F, UD	2.4	1.3	0.4	0.39	0.13	0.16
	F, D	2.2	2.0	0.4	0.42	—	—
	F, DP	—	1.7	—	0.34	—	—
15	F, UD	1.6	0.70	0.2	0.09	0.10	0.043
	F, D	1.5	1.2	0.2	0.10	—	—

[a]UF = unfiltered acidified, F = filtered (0.1 μm) acidified, UD = undigested, D = pressure-digested, DP = pressure-digested with 0.1% (w/w) ammonium persulfate.
[b]Working f.a.a.s. detection limits: Cu = 0.2, Pb = 0.2, Cd = 0.008 $\mu g\ l^{-1}$.
[c]Indicates colored sample containing natural organic material; all other samples were low in color. All samples were of low turbidity.

TABLE 4

Analysis by a.s.v. of selected baseline natural waters[a]

Element	Mean concentration[b] ($\mu g\ l^{-1}$)	Standard deviation ($\mu g\ l^{-1}$)	Range ($\mu g\ l^{-1}$)	No. of determinations
Cd	0.019	0.008	0.006—0.034	18
Pb	0.18	0.051	0.10—0.30	27
Cu	1.25	1.09	0.46—3.35	10

[a]From western Lake Superior, at the Environmental Research Laboratory-Duluth, Duluth, Mn. and streams of Superior National Forest located in wilderness areas of north eastern Minnesota [18].
[b]Corresponds to acid-exchangeable metal for unfiltered acidified samples.

eastern Minnesota were collected directly into precleaned polyethylene or FEP containers and acidified to 0.2% (v/v) nitric acid. Lake Superior samples were also collected at the Environmental Research Laboratory in Duluth, Minnesota. Large concentration differences were not discerned with respect to time or location; concentrations were very similar at all stations (with the exception of copper for one stream in which the value was 3.4 $\mu g\ l^{-1}$). Mean values generally compared favorably with studies [10, 24] for other areas.

REFERENCES

1 U.S.—Canadian International Joint Commission, Upper Lakes Reference Group Report, The Waters of Lake Huron and Lake Superior, 1977, Vols. II, III.
2 K. E. Biesinger and G. M. Christensen, J. Fish. Res. Board Can., 29 (1972) 1691.
3 J. M. McKim and D. A. Benoit, J. Fish. Res. Board Can., 28 (1971) 655.
4 G. W. Holcombe, D. A. Benoit, E. N. Leonard and J. M. McKim, J. Fish. Res. Board Can., 33 (1976) 1731.
5 D. A. Benoit, E. N. Leonard, G. M. Christensen and J. T. Fiandt, Trans. Am. Fish. Soc., 4 (1976) 550.
6 M. Branica, L. Sipos, S. Bubic and S. Kozar, Accuracy in Trace Analysis: Sampling, Sample Handling, and Analysis, Vol. II, U.S. National Bureau of Standards Special Publication #422, Proceedings of the 7th IMR Symposium, October 1974, Gaithersburg, Md., 1976, p. 917.
7 D. Jagner and L. Kryger, Anal. Chim. Acta, 80 (1975) 255.
8 W. Lund and M. Salberg, Anal. Chim. Acta, 80 (1975) 131.
9 A. H. Miguel and C. M. Jankowski, Anal. Chem., 46 (1974) 1832.
10 H. W. Nürnberg, P. Valenta, L. Mort, B. Raspor and L. Sipos, Fresenius Z. Anal. Chem., 282 (1976) 357.
11 H. E. Allen, W. R. Matson and K. H. Mancy, J. Water Pollut. Control Fed., 42 (1970) 573.
12 T. R. Copeland, J. H. Christie, R. A. Osteryoung and R. K. Skogerboe, Anal. Chem., 45 (1973) 2171.
13 M. I. Abdullah, B. Reusch Berg and R. Klimek, Anal. Chim. Acta, 84 (1976) 307.
14 V. F. Gaylor, A. L. Conrad and J. H. Landerl, Anal. Chem., 29 (1957) 224.
15 R. G. Clem and A. F. Sciamanna, Anal. Chem., 47 (1975) 276.
16 G. F. Olson, D. I. Mount, V. M. Snarski and T. W. Thorslund, Bull. Environ. Contam. Toxicol., 14 (1975) 129.
17 R. W. Andrew, Chem. Instrum., 6 (1975) 163.
18 J. E. Poldoski and G. E. Glass, Proceedings of the International Conference on Heavy Metals in the Environment, Vol. II, October, 1975, Toronto, Ontario, Canada, 1977, p. 901.
19 R. A. Osteryoung and J. H. Christie, Anal. Chem., 46 (1974) 351.
20 W. T. DeVries and E. Van Dalen, J. Electroanal. Chem., 14 (1967) 315.
21 W. R. Matson, D. K. Roe and D. E. Carritt, Anal. Chem., 37 (1965) 1594.
22 T. M. Florence, J. Electroanal. Chem., 27 (1970) 273.
23 R. G. Clem, Anal. Chem., 47 (1975) 1778.
24 J. Kubota, E. L. Mills and R. T. Oglesby, Environ. Sci. Technol., 8 (1974) 342.

Analytica Chimica Acta, 101 (1978) 89—97

FLAME EMISSION STUDIES OF SEVERAL METAL CHLORIDES WITH VAPOR-PHASE SAMPLING

E. L. WHITE, C. A. ZIELINSKI, R. M. PORTZER, E. M. HEITHMAR and F. W. PLANKEY*

Department of Chemistry, University of Pittsburgh, Pittsburgh, Pennsylvania 15260 (U.S.A.)

(Received 22nd February 1978)

SUMMARY

A method is described for the production of spectra of aluminum chloride, iron(III) chloride, silicon tetrachloride and titanium tetrachloride vapors by flame emission spectrometry. The aluminum and iron(III) chloride vapors were prepared by heating solid samples in reaction flasks; silicon and titanium tetrachlorides have sufficient vapor pressures at ambient temperatures to produce vapor-phase samples. Techniques have been developed to introduce the sample into the flame as a vapor, and to accommodate a large concentration of sample while requiring minimum preparation. Spectra were obtained individually and as a mixture over 240—600 nm. The analytical wavelength was chosen for each element, and 10-s integrations were made by utilizing a microcomputer to slew rapidly to the line of interest, hold for 10 s on the emission line, move off wavelength, hold for a 10-s background measurement and slew rapidly to the next line of interest. The microcomputer was also used to digitize and display the number of photons counted.

Current methods for the analysis of volatile metal compounds have established that dimeric species (Fe_2Cl_6 and Al_2Cl_6) as well as monomeric species ($FeCl_3$ and $AlCl_3$) are the principal components in vapors in equilibrium with condensed phases of iron(III) chloride and aluminum(III) chloride. Monomeric and dimeric species are also characteristic of vapors in equilibrium with condensed phase silicon tetrachloride and titanium tetrachloride.

Mixtures of these four substances are of interest in certain metallurgical and chemical processes, and their analysis is therefore of some importance. Mass spectrometric analysis by Semenenko et al. [1] indicated that the mixed metal dimer $FeAlCl_6$ in the vapor phase exists in equilibrium with $FeCl_3$ and $AlCl_3$. Spectrophotometric studies by Shieh and Gregory [2] of the vapors of $FeCl_3$ and mixtures of $FeCl_3$ and $AlCl_3$ also show evidence for formation of mixed metal dimers. Formation of such species has been shown to interfere with the determination of the metal, because most absorption measurements involve molecular studies of the entire species or of some complex. It was also shown by the latter workers that the absorption maximum for a monomer appeared at a different wavelength from that of the dimer or

mixed molecule. The study also showed that substitution of an aluminum atom for one of the atoms of iron in Fe_2Cl_6 has only a minor effect on the shape of the spectrum, which suggests that in order to determine iron and aluminum in the sample, one must check for each absorbing species.

A gas chromatographic technique was described by Brazhnikov and Sakodynski [3] for the determination of volatile metal chlorides in a mixture. Retention volumes for $SiCl_4$, $TiCl_4$ and the other volatile chlorides were determined. Metal chloride vapors such as $AlCl_3$ and $FeCl_3$, however, cannot readily be chromatographed. Although gas chromatography can be used for many on-line processes, it would be very difficult to analyze a mixture of this type without changing columns during the analysis. Again, monomeric and dimeric species would give significantly different retention volumes; as a result each species would have to be separately determined. Methods based on emission spectrographic and x-ray techniques were described by Rhodes et al. [4] for determining metallic substances in air particulates by collecting the sample on a filter, but these techniques are inapplicable to the present problem.

In most methods described for atomic emission spectrometry (a.e.s.), a solution of the sample is atomized in a flame. This paper describes how the elemental content of a mixture of four chlorides in the vapor phase can be observed by measuring the emission at several pre-determined wavelengths. Each element emits radiation of a characteristic wavelength, therefore a separation procedure is not necessary for a.e.s. studies of the mixture.

EXPERIMENTAL

Apparatus

A block diagram of the instrumentation used is shown in Fig. 1. Most components described are standard with the exception of the atomization system which was modified to make it suitable for analysis of vapor samples.

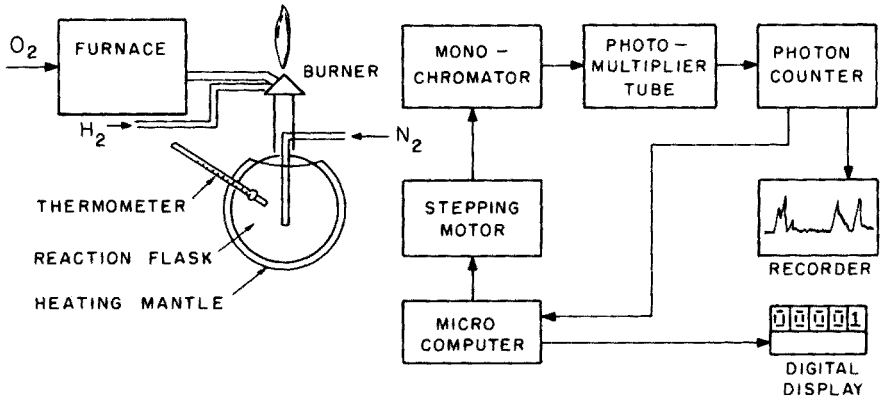

Fig. 1. Block diagram of the instrumental set-up.

A Beckman 4030 atomizer burner assembly (medium bore) was modified by changing the nebulizer capillary to 19-gauge Inconel from the base of the burner to the tip, and 1/16-in. o.d. Inconel below the burner to adapt to a Swagelok fitting. It was connected to a 1-l flask with a ground glass connection in a heating mantle, henceforth referred to as the reaction flask. The connection was made with a Kovar metal-to-glass seal and Swagelok fittings. Heating tape was used to heat from the burner tip down to the reaction flask. The system was completely insulated to maintain a constant temperature (±0.25°C).

A Burrell model H-4-9 high-temperature furnace was used to heat oxygen, used as the oxidant, to 300°C by passing the gas through stainless steel tubing (0.25-in i.d., 18-in long). Rotamers and low-pressure gauges were installed in the oxygen, hydrogen, and nitrogen lines to monitor the flows and pressures of the gases. Tubes of Dri-rite and molecular seive 5A were placed in the lines to remove moisture.

The optical system was a Jobin-Yvon model H-20 scanning monochromator with aberration-corrected concave holographic grating, and with a stepping motor controlled by a model 017-000 wavelength programmer. This programmer was operated in the external mode, controlled by a MMD-1 8080A mini-microcomputer. The detector consisted of a PAR Instruments model 1140B quantum photometer detector with a 1P28 photomultiplier tube, and model 1140A photon counting system, operated in the photon-counting mode. The data acquisition system consisted of a Sargent model SR-6 recorder and a digital system to record counts per s. The latter was prepared from TTL integrated circuits and light-emitting diode digits. Table 1 lists the sources of these items.

TABLE 1

Sources of apparatus

Item	Model	Supplier
Monochromator/Scanning System	H-20	Instruments SA, Inc., J-Y Optical Systems Div., Metuchen, N.J. 08840.
Detector/Photon Counter	1140 A/B	Princeton Applied Research Corp., Princeton, N.J. 08540.
Microcomputer	MMD-1	E & L Instruments, Inc., 61 First Street, Derby, CT 06418.
Burner	4030	Beckman Instruments, Inc., Fullerton, CA 92634
Furnace	H-4-9	Burrell Corporation, Pittsburgh, Pa. 15219.
Recorder	SR-6	Sargent-Welch Scientific Co., Stokie, IL 60076.

The wavelengths used for measurements of the various elements are given in Table 2.

Instrumental settings. A slit width of 0.05 mm and a reduced slit height of 0.5 mm were used. A range of 30,000 (30 K) to 1,000,000 (1 M) counts s^{-1} was used with a time constant of approximately 0.1 s in the photon-counting mode. A scanning rate of 10 nm min^{-1} was used during manual scans.

Reagents

Aluminum chloride and iron(III) chloride vapors were produced from powdered anhydrous aluminum chloride and anhydrous iron(III) chloride, respectively, by heating them in the reaction flask to >100°C. Silicon tetrachloride and titanium tetrachloride vapors were produced from reagent-grade liquid silicon tetrachloride and titanium tetrachloride, respectively, at room temperature in reaction flasks.

Hydrogen, oxygen, and nitrogen pressures and flow rates

The optimum pressures for hydrogen and oxygen (as a function of nitrogen flow rates) to obtain maximum intensity and stability of emission for the elements of interest were determined. Unfortunately, a compromise had to be made, as the optimum conditions for each element differ. A minimum nitrogen flow rate was used to avoid saturation of flame with sample vapor. The conditions used were 9.0 psi N_2 (50 cm^3 min^{-1}), 8 psi O_2 (2.5 l min^{-1}), 8 psi H_2 (470 cm^3 min^{-1}).

It should be mentioned that optimum conditions were not a primary concern in this work. Because of the large concentrations being analyzed, formation of aluminum oxide [5] and other oxides could occur at the tip of the burner, so it was necessary to forfeit optimum conditions by using pressures and flow rates high enough to lift the base of flame from the tip of the burner. This helped minimize or eliminate clogging problems at the tip, but did not introduce appreciable noise into the detection system. This procedure allowed the burner/sampling system to operate for several hours at a time.

TABLE 2

Wavelengths used for the various elements

Compound	Species observed	Wavelength (nm)	Background wavelength (nm)
$SiCl_4$	Si	251.6	253.7
$FeCl_3$	Fe	372.0	372.9
$AlCl_3$	Al	396.2	397.6
$TiCl_4$	TiO	516.8	523.6

Procedure for vapor production

Four 1-l flasks with a ground glass joint, modified to accommodate a ground-glass fitted thermometer (—10 to 260°C) were used as reaction flasks. Approximately 50 g of $AlCl_3$ powder was added to flask 1, 50 g of $FeCl_3$ was added to flask 2, 50 ml of $SiCl_4$ was added to flask 3 and 50 ml of $TiCl_4$ was added to flask 4. Molycote 505 paste (Dow Corning Corp.) with a temperature range of —40°C to 1093°C was applied to the joints of each flask to insure a tight seal. Each flask was stoppered immediately to avoid hydrolysis; all transfers were made in a fume hood. Flasks 1 and 2 were heated to 100°C to produce $AlCl_3$ and $FeCl_3$ vapors, respectively. Flasks 3 and 4 were kept at room temperature. The emission spectrum for each vapor was obtained individually. All flasks were then connected in series and the spectrum for the mixture obtained.

RESULTS AND DISCUSSION

Individual flame emission spectra

The flame emission spectrum of $AlCl_3$ vapor was determined over the range 240—600 nm, and is presented in Fig. 2. The characteristic lines of this spectra are almost identical to those produced by $AlCl_3$ in solution [5]. The 396.15-nm atom line was selected for analytical work, but other lines could have been selected. The background of the oxygen—hydrogen—nitrogen flame is shown in Fig. 3. Emission from fluorescent lighting Hg lines can be seen in this spectrum. The spectrum for $SiCl_4$ is shown in Fig. 4; the 251.61-nm atom line was selected for analytical work. Silicon atom lines and SiO bands can be seen in the shorter wavelength region but the number of emission lines is few, in agreement with the spectrum published by Herrmann and Alkemade [5] for silicon in aqueous solution. The spectrum for $FeCl_3$ is shown in Fig. 5. The 371.99-nm atom line was selected for analytical work. The spectrum for titanium is shown in Fig. 6. Although titanium emits no atomic lines in solution [5] it does yield a rather complex band spectrum at 500 -750 nm. This is also true for the vapor. The 516.8-nm band head was selected for analytical work although Herrmann and Alkemade [5] reported the 545.0-nm TiO band head as having greater intensity.

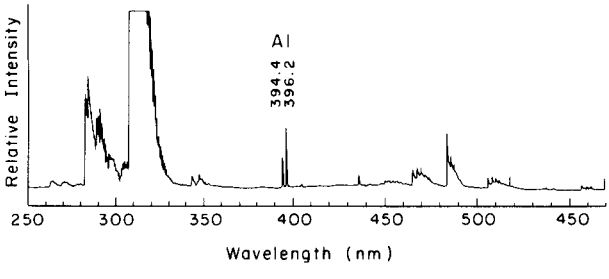

Fig. 2. H_2—O_2—N_2 flame emission spectrum of Al with $AlCl_3$ vapor sampling. Sensitivity is 3.0×10^5 cps full scale.

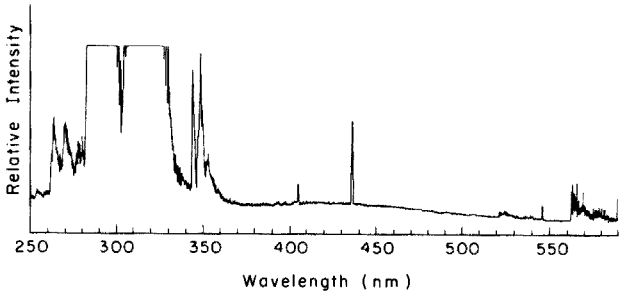

Fig. 3. Background spectrum of H_2—O_2—N_2 flame. Note the presence of mercury lines resulting from scattered fluorescent lighting at this sensitivity setting of 3.0×10^4 cps full scale.

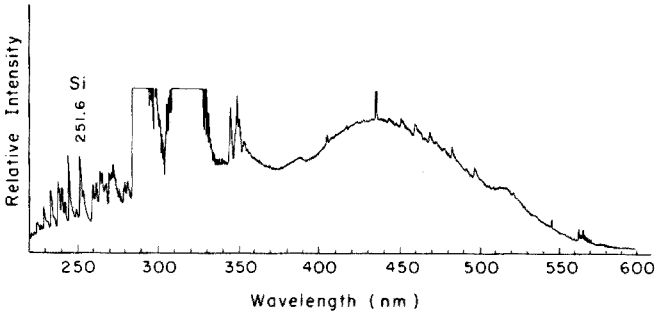

Fig. 4. H_2—O_2—N_2 flame emission spectrum of Si with $SiCl_4$ vapor sampling. Sensitivity is 3.0×10^4 cps full scale.

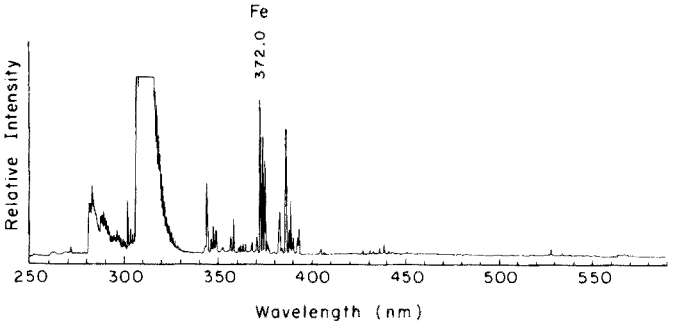

Fig. 5. H_2—O_2—N_2 flame emission spectrum of Fe with $FeCl_3$ vapor sampling. Sensitivity is 3.0×10^5 cps full scale.

In selecting the appropriate line or band for analytical studies from the individual spectrum of each vapor, the line of maximum emission (TiO band head for Ti) was chosen which had a minimum amount of interference from spectral overlap, as determined from a rigorous comparison of the spectrum of each element.

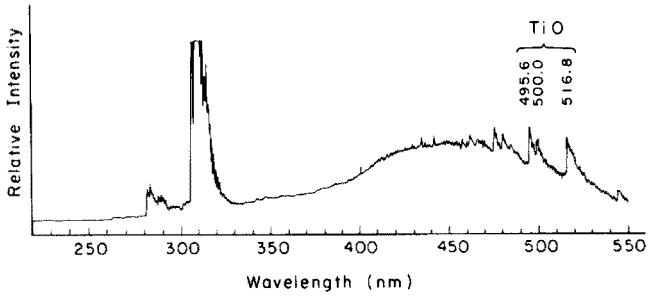

Fig. 6. H_2—O_2—N_2 flame emission spectrum of TiO with $TiCl_4$ vapor sampling. Sensitivity is 1.0×10^6 cps full scale.

The spectrum shown in Fig. 7 is that of a mixture of the four chlorides of interest. From this spectrum one can easily see there would be little difficulty in using the selected lines for either qualitative or quantitative analysis. Greatest spectral overlap is observed around 515—520 nm where AlO and TiO bands occur. There is a characteristic difference in the appearance of the Ti spectrum (Fig. 6) and that of the mixture (Fig. 7) in this region.

Additional interferences from the matrix and other chemical effects commonly observed in solution analysis are relatively small. However, the flame background (Fig. 6) is comparable. Pickett and Koirtyohann [6] reported that hotter flames provide less chemical interferences and the use of organic solvents which enhance absorption and emission intensities by improving the transport of material into the flame also enhances chemical interferences, probably because of the reduction in flame temperature. Reductions in flame temperature of this type come about from the need to reduce the fuel flow so as to avoid excessive flame richness when organic solvents are nebulized into the flame. Chemical and matrix interferences of the above type are completely eliminated in vapor analysis, as there is no solvent to burn and no matrix from sample preparations.

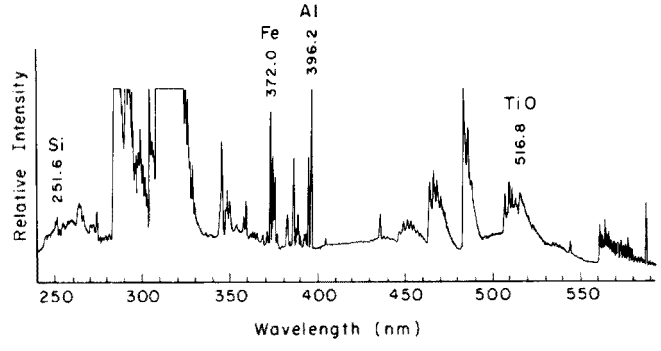

Fig. 7. H_2—O_2—N_2 flame emission spectrum for the detection of Si, Fe, Al and Ti in a combined vapor-phase sample. The most useful wavelengths for the analysis are noted. Sensitivity is 1.0×10^5 cps full scale.

Analyses were made at varying temperatures for each chloride, to determine the minimum temperature at which detectable vapors begin to form. $AlCl_3$ vapor was detected at 55—60°C and atmospheric pressure, whereas $FeCl_3$ vapors were not detected below 130—135°C. $SiCl_4$ and $TiCl_4$ samples were measured as low as 0°C in an ice bath, substantial amounts of each vapor being detected. The temperature at which a maximum amount of vapor could be produced before self-absorption became apparent was also determined for each chloride vapor (Table 3). This temperature is dependent on many factors such as flame conditions, carrier (N_2) flow rate and burner size, and the numbers quoted in Table 3 could vary considerably because of these factors.

An analysis of the mixture containing vapors of the four chlorides was made at the selected wavelengths utilizing the microcomputer to control the monochromator. The objective of this procedure was to monitor con-

TABLE 3

Vapor generation temperatures at the start of self-absorption

Sample	$SiCl_4$	$TiCl_4$	$AlCl_3$	$FeCl_3$
Temp. range (°C)	40—45	70—75	115—120	200—210

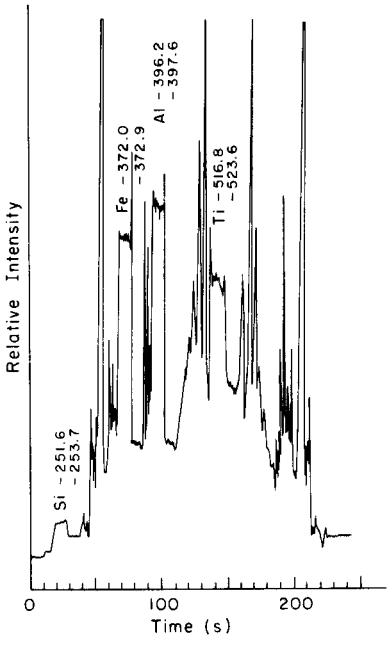

Fig. 8. Time tracing of the analog output of the photon counter as the wavelength of the monochromator is controlled by the microcomputer. The wavelength is held on the line and then off at a background measurement wavelength each for approximately 10 s, for each element. The wavelengths noted are for element and background measurement.

tinuously a stream containing a mixture of these gases. This was accomplished by measuring the emission intensity of one element and rapidly slewing to the wavelength of the next element. The program was written to adjust the monochromator from 240 nm to an initial wavelength (251.6 nm) to measure the emission intensity of silicon for 10 s. The monochromator was then rapidly slewed to a selected wavelength (253.7 nm) with a near baseline emission for a 10 s background measurement. Figure 8 shows the time-recording of measurements for the four elements. The monochromator was rapidly slewed (at 200 nm min^{-1}) to the next line of interest (372.0 nm) as controlled by the microcomputer, where the emission intensity for iron was measured for 10 s. The background measurement for iron was made at 372.9 nm for 10 s. This process was repeated for aluminum at 396.2 nm, with background measurement at 397.6 nm, and finally titanium was measured at 516.8 nm, with background measurement at 523.6 nm. To complete the cycle, the wavelength is returned to 240 nm.

The background measurements assure the analyst that the signals measured are from the elements of interest. If they are subtracted from the respective emission intensity of such elements, a quantitative procedure, now in the process of being developed, can be evolved.

The authors acknowledge the Alcoa Foundation for its generous support of this research.

REFERENCES

1 K. N. Semenenko, T. N. Naumora, L. N. Gorokhow, G. A. Semenova and A. V. Novoselova, Dokl. Akad. Nauk USSR, 154 (1964) 169.
2 C. F. Shieh and N. W. Gregory, J. Phys. Chem., 79 (1975) 828.
3 V. Brazhnikov and K. Sakodynski, J. Chromatogr., 38 (1967) 244.
4 J. R. Rhodes, A. H. Pradzynski, C. B. Hunter, J. S. Payne and J. L. Lindgren, Environ. Sci. and Technol., 6 (1972) 922.
5 R. Herrmann and C. T. J. Alkemade, Chemical Analysis by Flame Photometry, Interscience Publishers, New York, 1963, pp. 306–309; p. 555; p. 560; p. 222.
6 E. E. Pickett and S. R. Koirtyohann, Anal. Chem., 41 (1969) 28A.

Analytica Chimica Acta, 101 (1978) 99—109

INTERFACED D.C. ARGON-PLASMA EMISSION SPECTROSCOPIC DETECTION FOR HIGH-PRESSURE LIQUID CHROMATOGRAPHY OF METAL COMPOUNDS†

PETER C. UDEN*, BRUCE D. QUIMBY, RAMON M. BARNES and WILLIAM G. ELLIOTT

Department of Chemistry, GRC Tower I, University of Massachusetts, Amherst, Mass. 01003 (U.S.A.)

(Received 19th May 1978)

SUMMARY

A d.c. argon-plasma emission spectroscopic system is described for directly interfaced metal-specific detection of eluates in high-pressure liquid chromatography. Differing approaches are needed with regard to solvent systems used in normal-phase or reverse-phase chromatography. A simple nebulization system is adequate for reverse-phase applications of polar solvents. However, a novel design of an impact nebulizer-interface is required to accommodate the hydrocarbon and halocarbon solvents typically encountered in normal-phase and adsorption chromatography. The d.c. plasma detection system has been applied to the h.p.l.c. of a range of transition metal β-diketonate, β-ketoamine and diethyldithiocarbamate complexes, with good linear ranges for metal-specific detection and with detection limits in the sub ng s^{-1} range of metal eluted in the complexes.

High-pressure liquid chromatography (h.p.l.c.) is a primary method for resolution and analysis of multi-component mixtures in the liquid phase. For many complex systems, however, complete resolution of species of interest either among themselves or from other interfering constituents of the sample matrix, is not possible in a single chromatographic experiment. If the components of analytical interest share some common property not possessed by the eluent or other constituents of the sample, then the use of a detector responsive solely to that particular parameter may serve greatly to simplify both quantitative and qualitative analytical requirements. The separation parameters may then be optimized for the components of specific analytical interest.

If a particular element is found only in the species of analytical concern and not in the mobile phase or sample matrix interferences, then specific element detection simplifies chromatography. Atomic spectroscopic methods of detection are particularly attractive for determination of metals and certain hetero-atoms. Flameless atomic absorption has been employed [1, 2]

---

†Presented at the 13th International Symposium on Advances in Chromatography, St. Louis, Missouri, U.S.A., October 1978.

for the determination of organo-tin species after h.p.l.c. separation; but the necessary discontinuity of measurement introduced by fraction collecting may constitute a disadvantage. Flame atomic absorption has been utilized by Manahan and others in high-resolution ion exchange [3—8] and applications have been summarized by Fernandez [9]. Atomic fluorescence detection has been reported [10], and Freed [11] has reported flame emission h.p.l.c. detection. All the above procedures have exhibited selectivity and sensitivity for metallic species. At the present time, none of the atomic emission techniques utilizing plasma sources has been described for h.p.l.c. Since these generally exhibit sensitivities and detection limits for solution analysis comparable or superior to flame techniques, they also have promise as h.p.l.c. detectors. An inherent advantage of the emission techniques is their suitability for simultaneous multi-element analysis.

This paper describes the construction and evaluation of a metal-specific h.p.l.c. detection system based on a d.c. argon plasma emission source (d.c.p.) and a grating echelle spectrometer.

EXPERIMENTAL

Spectroscopic instrumentation

The d.c. argon plasma was of an inverted Y configuration, operated at atmospheric pressure (Spectrametrics Inc., Andover, Mass.). The plasma current was regulated at 7 A at ca. 50 V. The argon flow rates are given in Table 1. The sample aerosol generated by one of two alternative nebulization systems from the h.p.l.c. system was directed vertically into the center of the inverted Y configuration of the plasma. The region situated slightly below the intersection of the Y of the plasma and somewhat toward the cathodic side was focused by a 10-cm, f1 quartz lens on the entrance slit for optimal performance. The spectrometer used was a prototype version of that employed in the Spectraspan III instrument (Spectrametrics Inc.), incorporating a 0.75-m modified Czerney—Turner optical system having an echelle grating with an internal quartz prism cross disperser. The resolving power of the instrument is approximately 500,000 and the reciprocal linear dispersion in the wavelength region used in the work described was approximately 0.1 nm mm^{-1}. Entrance and exit slits were 100-μm wide and 300-μm high, providing resolution of approximately 0.015 nm.

TABLE 1

Argon flow rates (in $ml\,s^{-1}$) used for the d.c. argon plasma emission—h.p.l.c. interfaces

Impact nebulizer		Ceramic nebulizer	
Electrodes	31	Electrodes	27.5
Sheath	25	Sample	47.1
Sample	3.3		

Three systems were used to measure the signal from the R446 photomultiplier tube employed. The first system consisted of a photon counter of the type described by Malmstadt et al. [12], with the analog output fed to a strip-chart recorder. The second system comprised a phase-sensitive lock-in amplifier in combination with a 100-Hz chopper placed in front of the entrance slit. In the third system, the current output of the photomultiplier was measured directly with a d.c. amplifier (Keithley Model 414). The signal from the photomultiplier readout and the response from the chromatographic u.v. monitor were recorded simultaneously on a two-channel recorder (Houston Instruments, Omniscribe 5000).

Chromatographic instrumentation

The liquid chromatograph used consisted of a Tracor 3100 pumping system, a stopped-flow syringe injection system and a model 1205 single-wavelength (254 nm) u.v. monitor (Laboratory Data Control). Chromatographic columns (25 cm long) of 10-μm Partisil 10 silica with 10-μm Partisil ODS octadecyl reverse phase (Whatman, Inc.) were used as received. Spherisorb SGP 8-μm silica (Phase Separations Inc.), was slurry-packed in a stainless steel column (25 cm long, 4 mm i.d.) in the conventional manner.

Preparation of metal complexes

Based on prior chromatographic studies, typical neutral metal chelate systems were selected for evaluation to provide a representative range of metal and ligand types. Tetradentate transition metal β-ketoamine complexes investigated previously by g.c. [14] and h.p.l.c. [15, 16] were prepared by established procedures [14]. Model compounds selected were the Cu(II) and Ni(II) chelates of *N,N'*-ethylenebis(acetylacetoneimine) [Cu[en$(AA)_2$] and Ni[en$(AA)_2$] and the Cu(II) chelate of *N,N'*-ethylenebis(trifluoroacetylacetoneimine) [Cu[en$(TFA)_2$]]. Chromium β-diketonates chromatographed included the hexafluoroacetylacetonate [Cr$(HFA)_3$] and the mixed ligand system formed from the reaction of Cr(III) with a mixture of trifluoroacetylacetone and hexafluoroacetylacetone [17]. Diethyldithiocarbamate complexes of Cu(II), Ni(II), Co(III), Hg(II) and Cr(III) were also prepared [13] by the reaction of aqueous metal ion solutions with sodium diethyldithiocarbamate.

Interfacing and nebulizer systems

Reverse-phase applications. Preliminary investigations on the effect of the composition of the mobile phase on the operational characteristics of the d.c. plasma (d.c.p.) indicated that solvent systems commonly used in reverse-phase and ion-exchange chromatography may be introduced directly into the plasma by means of the standard (ceramic) nebulizer available with the commercial spectrometer. In contrast, hydrocarbon and halocarbon solvents commonly encountered in adsorption chromatography present particular difficulties, as discussed below. Various combinations and

concentrations of aqueous solutions containing ethanol, methanol, acetonitrile and potassium hydrogenphosphate buffers were successfully nebulized into the plasma at flow rates in the range 0.5—4.0 ml min^{-1}, with no apparent adverse effects on the discharge characteristics. Thus, the interfacing of the liquid chromatograph to the d.c.p. for reverse-phase applications simply involved the connection of the exit tube of the u.v. monitor to the inlet of the ceramic nebulizer by means of a short length of narrow-bore PTFE tubing (1/16 in. o.d.). In addition, the tube directing the aerosol vertically from the spray chamber into the intersection region of the plasma was replaced with borosilicate glass tubing (2.5 in. long, 3/8 in. o.d.).

Adsorption chromatography. The aspiration of hydrocarbon and halocarbon solvents with the ceramic nebulizer severely limited the d.c.p. application in the h.p.l.c. detection system. Skellysolve B (hydrocarbon solvent) was nebulized completely (i.e. no notable drain flow) under the argon flow conditions for the ceramic nebulizer (Table 1). Introduction of up to 0.6 ml min^{-1} of solvent produced large curved orange regions extending from the intersection of the inverted Y of the plasma vertically in a plane perpendicular to that of the plasma. Under these conditions, deposits of carbon black formed on the electrode sleeves within minutes, and the deposit eventually grew to extinguish the plasma. Introduction of Skellysolve B at a rate greater than 0.6 ml min^{-1} immediately extinguished the plasma. Although carbon deposition could be avoided by decreasing the diameter of the tubing directing the aerosol from the spray chamber to the intersection of the plasma, the resulting increase in the argon linear velocity extinguished the plasma. Although reduction of the volume flow rate of argon through the nebulizer would decrease the linear velocity of argon aerosol flow, this would produce detrimental effects on the nebulization characteristics, resulting in reduced sensitivity and poorer detection limits.

Therefore, a nebulization system was sought in which the generation of an aerosol was accomplished without the use of a fast stream of argon. An aerosol flow system meeting this criterion was designed and constructed (Fig. 1). The eluent from the u.v. monitor (or the h.p.l.c. column directly) is transferred to the spray chamber through PTFE tubing (0.8-mm i.d.). It enters the spray chamber through a 2-cm length of glass capillary tubing (0.8 mm i.d.), the end of which was fire-polished down to form a nozzle of about 25 μm i.d. The resulting fast stream of solvent is directed against the wall of the spray chamber directly opposite the nozzle, which is positioned such that the tip is between 1 and 1.5 cm from the point of impact on the wall. The fast stream of solvent impacting on the wall results in the generation of a fine aerosol. This is then swept from the chamber through the glass tube (2 mm i.d.) to the intersection region of the plasma by the flow of argon. Since the generation of the aerosol is not dependent on argon flow rate, the latter may be varied from zero to the rate at which the plasma is extinguished (ca. 500 ml min^{-1}). The sheath flow of argon

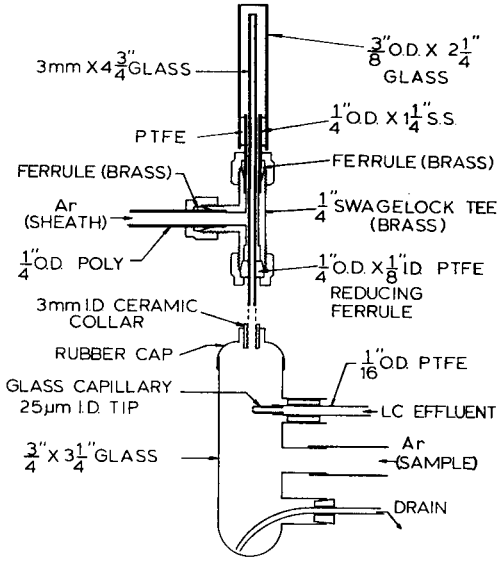

Fig. 1. Schematic diagram of aerosol—nebulizer interface for normal-phase chromatographic solvent systems.

which flows concentrically around the sample aerosol tube is provided to stabilize both the plasma and the thin stream of aerosol as it enters the plasma intersection region. Typical values of argon flow rates used with this system are listed in Table 1. As can be seen, this system consumes 20% less argon than the ceramic nebulizer system. All of the solvent systems investigated contained either hexane or Skellysolve B as the major component with various concentrations of polar modifiers such as methylene chloride, diethyl ether or acetonitrile. The eluent flow rates used were in the range 0.8—2.0 ml min^{-1}. Under these conditions, the nebulization efficiency, defined as [(Total eluent flow rate — Drain flow rate)/Total eluent flow rate] X 100, was between 20 and 25%. With this system, the plasma was sustained for periods up to 10 h of eluent introduction without evidence of carbon deposition on the electrode sleeves. Also, because of the lower efficiency of this nebulizer, no provision for splitting the eluent was required in the range of flow rates used.

RESULTS AND DISCUSSION

Reverse-phase liquid chromatography

Typical chromatograms obtained with the instrumental ceramic nebulizer system for reverse-phase systems are illustrated in Fig. 2, which shows the separation of $Cu(enAA_2)$, $Ni(enAA_2)$ and $Cu(enTFA_2)$ with sequential u.v. (254 nm) and copper-specific d.c.p. detection, and the separation of $Cu(enAA_2)$ and $Ni(enAA_2)$ with nickel-specific d.c.p. detection. Although

under the experimental conditions employed here, $Cu(enAA_2)$ and $Ni(enAA_2)$ are only partially resolved chromatographically, as is evident from the u.v. trace, the specific detection afforded by the d.c.p. system allows complete independent observation of the metal species of interest.

The chromatographic efficiency as measured by the d.c.p. detector for $Cu(enAA_2)$ was approximately 25% lower than that measured for the same peak on the preceding u.v. monitor. This band spreading may be attributed to: (a) the void volume of the u.v. detector and interconnections between it and the d.c.p. nebulizer; (b) the physical time constant of the nebulizer; (c) the time constant of the spectrometer readout; or (d) a combination of these factors. With the nebulizer argon flow rate of 50 ml s^{-1} and the nebulizer volume of 45 ml used in this experiment, the time constant for the nebulizer was ca. 1 s; the electronic time constant of the meter readout was 3 s throughout. Since W_0 (the peak width at base measured from the u.v. output) was

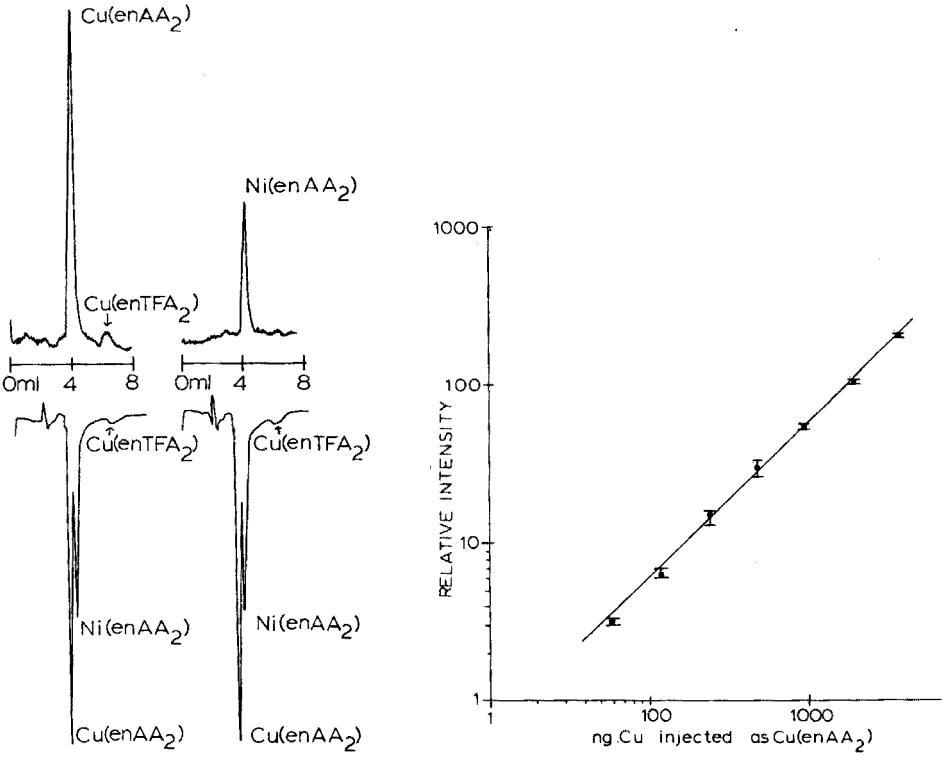

Fig. 2. Reverse-phase separation of copper and nickel chelates with copper- and nickel-specific detection at 324.7 and 341.5 nm respectively (upper traces) and u.v. detection at 254 nm (lower traces). Partisil ODS octadecyl reverse-phase column 25 cm. Eluent, 60:40 water—acetonitrile. Flow rate, 0.65 ml min^{-1}.

Fig. 3. Calibration curve (log—log) for $Cu(enAA_2)$. Copper-specific detection at 324.7 nm. Chromatographic conditions as in Fig. 2.

approximately 95 s, these two time constants contribute relatively little to the observed band spreading in the d.c.p. The void volume between the detectors thus appears to be the major factor in the noted diminution of efficiency.

A calibration curve obtained for copper as $Cu(enAA_2)$ by monitoring the 324.7-nm copper emission line is shown in Fig. 3. The limits noted on the curve indicate the range of three trials at each point. Linearity is maintained over the range 30—4,000 ng of copper. The detection limit (defined as the amount of metal required to produce a signal of twice the baseline noise, divided by the width of the peak at base) was 3.5×10^{-10} g Cu s^{-1} under the conditions noted. This value is close to that obtained for copper as the nitrilotriacetate complex by flame atomic absorption detection in ion-exchange h.p.l.c. [8].

The d.c.p. system of detection proved of great utility in providing evidence concerning the eluting integrity of metal-containing species, and in cases when either pre-column or on-column decomposition occurred, as a means of determining which decomposition peaks may contain the metal of interest. This information is especially useful when the metal-containing species decomposes on evaporation or solvent removal of the eluent during preparation for qualitative analysis. A chromatogram obtained with the u.v. monitor at 254 nm for a sample of $Cu(enAA_2)$ is given in Fig. 4 (lower trace); the complex was prepared [14] and originally recrystallized from ethanol and sublimed under vacuum. The sample analyzed was, however, about one year old, and decomposition is evident. Although the u.v. trace indicates the chelate decomposition, the chromatogram supplies no information as to whether or not the extraneous peak(s) contain metal or correspond to ligand or ligand fragments, with the metal ion perhaps being eluted in the void volume undetected by the u.v. monitor. The chromatogram obtained by monitoring the 324.7-nm copper emission with the ceramic nebulizer system is also given in Fig. 4 (upper trace). No copper is present in the void volume, but all the peak(s) that arise from decomposition do contain the metal; possibly the species observed include the tetradentate hydrated form of $Cu(enAA_2)$.

Adsorption chromatography

Chromium(III) hexafluoroacetylacetonate, $Cr(HFA)_3$, was employed as a model chelate species to evaluate the impact nebulizer in the detection system employed in adsorption chromatography. Representative chromatograms obtained with both the u.v. detector and the chromium-specific d.c.p. detector monitoring the Cr 267.7-nm emission line, are illustrated in Fig. 5. No significant loss of peak shape or efficiency was observed between the two detectors for this or any other compound examined. The calibration curve was linear between 60 ng and 2.5 μg Cr (Fig. 6). The detection limit (defined as before) was 1.25×10^{-9} g Cr s^{-1}. At present, the major drawback to quantitative application of this system is the rather large degree of imprecision indicated in Fig. 6. Although its source has not yet been fully determined,

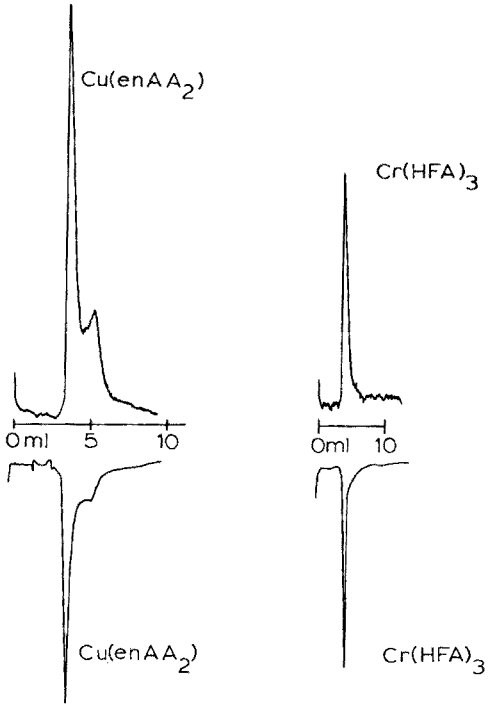

Fig. 4. Reverse-phase h.p.l.c. of partially degraded $Cu(enAA_2)$. U.v. monitoring at 254 nm (lower trace) and copper-specific detection at 324.7 nm (upper trace). Chromatographic conditions as in Fig. 2.

Fig. 5. Adsorption chromatogram of $Cr(HFA)_3$ on 10-μm Partisil. Eluent, 8% methylene chloride in Skellysolve B. U.v. monitoring (lower trace) and chromium-specific detection at 267.7 nm (upper trace).

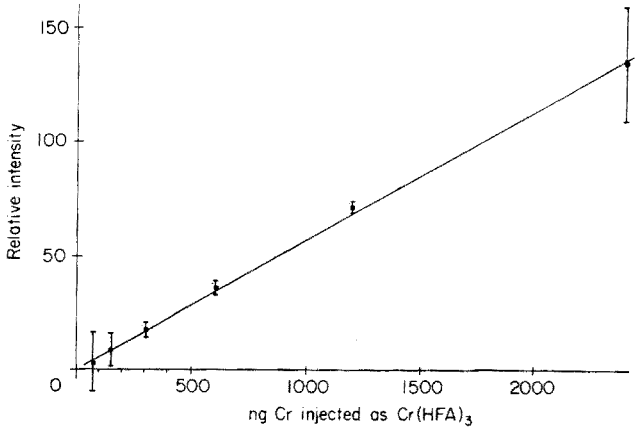

Fig. 6. Calibration curve for $Cr(HFA)_3$. Chromatographic conditions as in Fig. 5.

several factors are currently being investigated. Because the geometry of sample aerosol introduction appears to be critical for the system, further optimization of the arrangement of spray chamber, transfer tube and sheath tube may be necessary, as well as improvements to the pumping system and injection technique.

Copper(II), nickel(II) and cobalt(III) diethyldithiocarbamate complexes were recently separated on 8-μm Spherisorb columns with a 75:20:5 hexane: diethyl ether:acetonitrile eluent [13]. In substantiating the identity of the eluted species, difficulties were encountered because of decomposition of some of the chelates on evaporation of the eluent prior to mass spectral analysis. In that study, the d.c.p. system was employed as an on-line metal specific analyzer, and the impact nebulizer was used to confirm metal chelate elution with application of the Cu 324.7-nm, Co 345.3-nm and Ni 305.1-nm lines. With the same system, the elution of Hg(II) diethyldithiocarbamate was confirmed under similar conditions; the chromatograms are shown in Fig. 7.

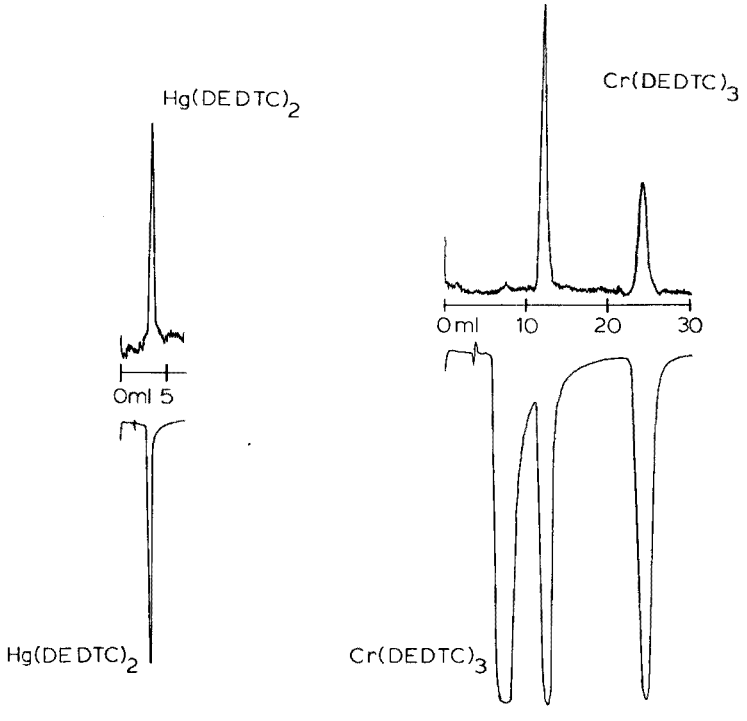

Fig. 7. Adsorption chromatogram of Hg(II) diethyldithiocarbamate on 8-μm Spherisorb. Eluent, 5:20:75 acetonitrile—diethyl ether—Skellysolve B. U.v. monitoring (lower trace) and mercury-specific detection at 253.7 nm (upper trace).

Fig. 8. Adsorption chromatogram of reaction products from the preparation of Cr(III) diethyldithiocarbamate. Chromatographic conditions as in Fig. 7. Lower trace, u.v. monitoring. Upper trace, chromium-specific detection at 267.7 nm. The u.v. trace showed non-linear response.

When Cr(III) diethyldithiocarbamate was prepared and chromatographed under these conditions, three well-shaped resolved peaks were obtained with u.v. detection at 254 nm. Decomposition of the eluate again presented difficulties during preparation for mass spectral characterization and elemental analysis of the eluted peaks; thus chromium-specific monitoring was employed at 267.7 nm (Fig. 8). As indicated in Fig. 8, the second and third peaks contain chromium. It appears that the second peak corresponds to the Cr(III) tris chelate and present evidence indicates that the third peak may be a previously unrecognised binuclear dithiocarbamate complex.

The chromium-specific mode has also been used to confirm the presence of the metal in the various mixed ligand chelates formed from the reaction of Cr(III) with trifluoroacetylacetone and hexafluoroacetylacetone mixtures. A typical isocratic chromatogram is shown in Fig. 9 with peak designations for the various chelates in the system. Comparison with the u.v. monitor shows that all major peaks eluted do correspond to chromium complexes.

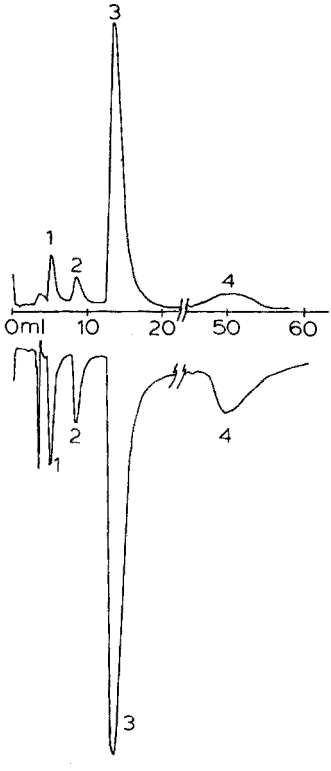

Fig. 9. Adsorption chromatogram of mixed ligand chromium trifluoroacetylacetonate—hexafluoroacetylacetonate chelates. Chromatographic conditions as in Fig. 5. Lower trace, u.v. monitoring. Upper trace, chromium-specific detection at 267.7 nm. Peak 1, $Cr(HFA)_2(TFA)$. Peak 2, $Cr(HFA)(TFA)_2$, the mer—fac isomer. Peak 3, $Cr(HFA)(TFA)_2$, a mixture of fac–fac and fac–mer isomers. Peak 4, $Cr(TFA)_3$, mer.

Conclusions

The d.c. argon plasma can be usefully applied for specific metal detection in h.p.l.c. With the reverse-phase mode, the d.c.p. system provides an ease of interfacing and detection capabilities for copper similar to those obtained by flame atomic absorption with the added advantage of simultaneous multi-element monitoring. The problems in the application of the d.c.p. emission detector in normal-phase partition and adsorption modes can be largely overcome by redesign of the nebulizer—interface system. The new system allows hydrocarbon solvents to be employed without carbon build-up on the electrodes. This system promises great utility in this important area of h.p.l.c. application, although at present it gives somewhat lower sensitivity and quantitative reproducibility than the system based on the ceramic nebulizer for polar solvents.

We acknowledge the collaboration of Imogene E. Bigley on the metal chelate h.p.l.c. This work was supported in part by the National Science Foundation through grant CHE73 05201.

REFERENCES

1 A. Y. Cantlib and D. A. Segar, Proceedings of the International Conference on Heavy Metals in the Environment, Toronto, Canada, 1976.
2 F. E. Brinkman, W. R. Blair, K. L. Jewitt and W. P. Iverson, J. Chromatogr. Sci., 15 (1977) 493.
3 S. E. Manahan and D. R. Jones IV, Anal. Lett., 6 (1973) 745.
4 M. Unebayashi and K. Kitagishi, Proc. 5th Int. Conf. on Atomic Spectroscopy, Monash University, Melbourne, Australia, 1975.
5 D. R. Jones IV and S. E. Manahan, Anal. Lett., 8 (1975) 569.
6 D. R. Jones IV, H. C. Tung and S. E. Manahan, Anal. Chem., 48 (1976) 7.
7 D. R. Jones IV and S. E. Manahan, Anal. Chem., 48 (1976) 502.
8 D. R. Jones IV and S. E. Manahan, Anal. Chem., 48 (1976) 1897.
9 F. J. Fernandez, At. Absorpt. Newsl. (Perkin Elmer Corporation), 16(2) (1977) 33.
10 J. C. Van Loon, B. Radziuk and J. Lichua, 2nd Joint Conference of the Chemical Institute of Canada and the American Chemical Society, Montreal, Canada, 1977.
11 D. J. Freed, Anal. Chem., 47 (1975) 186.
12 H. V. Malmstadt, M. L. Franklin and G. Horlick, Anal. Chem., 44 (1972) 63A.
13 P. C. Uden and I. E. Bigley, Anal. Chim. Acta, 94 (1977) 29.
14 R. Belcher, K. Blessel, T. J. Cardwell, M. Pravica, W. I. Stephen and P. C. Uden, J. Inorg. Nucl. Chem., 35 (1973) 1127.
15 P. C. Uden and F. H. Walters, Anal. Chim. Acta, 79 (1975) 175.
16 P. C. Uden, F. H. Walters and D. M. Parees, Anal. Lett., 8(11) (1975) 795.
17 R. A. Palmer, R. C. Fay and T. S. Piper, Inorg. Chem., 3 (1964) 875.

Analytica Chimica Acta, 101 (1978) 111—116

HIGH-PRESSURE LIQUID CHROMATOGRAPHIC RESOLUTION OF AMINO ACID ENANTIOMERS BY DERIVATIZATION WITH NEW CHIRAL REAGENTS

TOSHIO NAMBARA*, SHIGEO IKEGAWA, MASATOSHI HASEGAWA and JUNICHI GOTO

Pharmaceutical Institute, Tohoku University, Aobayama, Sendai 980 (Japan)

(Received 3rd April 1978)

SUMMARY

A new derivatization procedure has been developed for converting enantiomeric amino acids into diastereomers for resolution by high-pressure liquid chromatography. Two chiral derivatization reagents, (—)-1,7-dimethyl-7-norbornyl isothiocyanate and (+)-neomenthyl isothiocyanate, were synthesized from the corresponding amines. Amino acids were readily transformed with the chiral reagents into the thiourea derivatives which absorb at 243 nm (ϵ=17,000). The tert-butyldimethylsilyl esters of the diastereomeric thiourea derivatives were efficiently resolved by normal phase chromatography (μPorasil column) with cyclohexane/ethyl acetate as a mobile phase.

The application of liquid chromatography to optical resolution has developed in two ways: the direct resolution of enantiomers on a chiral stationary phase [1–5], and derivatization with a chiral reagent followed by liquid chromatography of the diastereomers on conventional columns [6–8]. A previous paper [9] reported the preparation of two chiral derivatization reagents for the resolution of amino acid enantiomers by high-pressure liquid chromatography (h.p.l.c.). However, these derivatization methods have disadvantages; the optical resolution of the racemic reagent is somewhat tedious and inefficient, and the use of *N*, *N'*-dicyclohexylcarbodiimide for coupling the reagent with amino acid results in the formation of interfering by-products. It is well known that the isothiocyanate is selectively reactive toward primary and secondary amines under mild conditions; the thiourea derivative is very sensitive for u.v. detection. The present paper deals with the preparation of two new optically active terpene derivatization reagents containing the isothiocyanato group, and their applicability to the resolution of amino acid enantiomers by h.p.l.c.

EXPERIMENTAL

Synthesis of derivatization reagents

(-)-1,7-Dimethyl-7-norbornyl isothiocyanate (I). (-)-1,7-Dimethyl-7-norbornylamine (1.81 g) obtainable from (+)-isoketopinic acid [10] was added

to water (3 ml)—carbon disulfide (2 ml) under ice-cooling and stirred at room temperature for 5 min. After the addition of KOH (1.25 g) in water (1.5 ml), the solution was heated in a sealed tube on the boiling water bath for 25 min. To the reaction mixture ethyl chloroformate (1.8 g) was added under ice-cooling, and the mixture was stirred at room temperature for 1 h. To the resulting solution was added KOH (1 g) in water (1.5 ml), and the solution was stirred at room temperature for 1 h and extracted with ether. The organic layer was washed with water, dried (Na_2SO_4), and evaporated. The crude product was distilled under reduced pressure to give (I) (1.4 g) as a colorless oil (b.p.$_5$ 94°C; $[\alpha]_D^{20}$ — 69.9°; c = 1.3, $CHCl_3$). Calcd. for $C_{10}H_{15}NS$: 66.2%C, 8.3%H, 7.7%N; found: 65.7%C, 8.1%H, 7.8%N. N.m.r. ($CDCl_3$)δ: 1.00 (3H, s, 1-CH_3), 1.32 (3H, s, 7-CH_3). I.r. ν_{max}, $CHCl_3$: 2080 cm^{-1} (SCN—).

(+)-Neomenthyl isothiocyanate (II). (+)-Neomenthylamine (1 g) obtainable from (—)-menthol [11] was added to water (1.2 ml)—carbon disulfide (0.6 ml) under ice-cooling with stirring at room temperature for 5 min. After the addition of KOH (0.5 g) in water (0.6 ml) the solution was heated in a sealed tube on the boiling water bath for 25 min. To the reaction mixture ethyl chloroformate (0.72 g) was added under ice-cooling, and the mixture was stirred at room temperature for 1 h. To the resulting solution was added KOH (0.4 g) in water (0.6 ml), and the solution was stirred at room temperature for 1 h and extracted with ether. The organic layer was washed with water, dried (Na_2SO_4), and evaporated. The crude product was distilled under reduced pressure to give (II) (0.6 g) as a colorless oil (b.p.$_5$ 55°C; $[\alpha]_D^{17}$ + 34.5°; c = 2.0, $CHCl_3$). Calcd. for $C_{11}H_{19}NS$: 67.0%C, 9.7%H, 7.1%N; found: 66.1%C, 9.5%H, 7.0%N. N.m.r. ($CDCl_3$)δ: 0.94 (6H, d, J = 6 Hz, 9- and 10-CH_3), 0.88 (3H, d, J = 6 Hz, 5-CH_3), 4.1 (1H, m, W1/2 = 6 Hz). I.r. ν_{max}, $CHCl_3$: 2160 cm^{-1} (SCN—).

Materials

Amino acids and (+)-isoketopinic acid were kindly donated by Ajinomoto Co. (Kawasaki) and Yoshitomi Pharmaceutical Industries (Yoshitomi), respectively. (—)-Menthol, tert-butyldimethylchlorosilane and imidazole were obtained from Tokyo Kasei Co. All the reagents were of analytical grade. Solvents were purified by distillation. Amino acid methyl esters were prepared by treatment with methanol and hydrogen chloride in the usual manner. The silylating agent was prepared as follows: a solution of tert-butyldimethylchlorosilane (200 mg) and imidazole (100 mg) in dimethylformamide (0.1 ml) was shaken with hexane (0.3 ml); the upper layer was used for silylation.

High-pressure liquid chromatography

A Model ALC/GPC 202 R401 high-performance liquid chromatograph (Waters Assoc., Milford, Mass., U.S.A.) with a u.v. detector (254 nm) was used. Samples were applied by a Waters Model U6K sample loop injector (effective volume, 2 ml). The μPorasil (1 ft. × 0.25 in. i.d.) and μBondapak C_{18} (1 ft. × 0.25 in. i.d.) columns (Waters Assoc.) were used under ambient conditions.

Derivatization

Methyl ester method. To a solution of amino acid methyl ester (ca. 100 μg) in acetonitrile (0.2 ml) were added (I) or (II) (ca. 2 mg) and sodium acetate (ca. 2 mg), and the resulting solution was allowed to stand at 37°C for 1 h. The reaction mixture was diluted with ethyl acetate (0.5 ml), washed successively with 5% HCl, 5% $NaHCO_3$ and water, and dried (Na_2SO_4). An aliquot was injected into the chromatograph.

tert-Butyldimethylsilyl ester method. To a solution of amino acid (ca. 100 μg) in aqueous 50% pyridine (0.2 ml) were added (I) or (II) (ca. 1 mg) and 2 M NaOH (10 μl), and the resulting solution was heated at 90°C for 1 h. The reaction mixture was diluted with water and extracted with ether to remove the excess of reagents. The aqueous layer was adjusted to pH 4 with 3% HCl and extracted with ethyl acetate. The organic layer was washed with water, dried (Na_2SO_4), and evaporated. To the residue was added the freshly prepared silylating agent (50 μl), and the resulting solution was allowed to stand at room temperature for 1 h. The reaction mixture was diluted with ethyl acetate. (0.5 ml), washed successively with 5% $NaHCO_3$ and water, and dried (Na_2SO_4). An aliquot (5 μl) was injected into the chromatograph.

RESULTS AND DISCUSSION

The design of a promising derivatization reagent for liquid chromatographic resolution of enantiomeric amines by the formation of the covalently bonded diastereomers requires the incorporation of suitable structural features, i.e. chirality leading to efficient resolution, a function highly reactive toward the amino group, and a chromophore responding with satisfactory sensitivity in the u.v. detector. These requirements prompted the preparation of new chiral derivatization reagents from naturally occurring terpenes.

Efforts were initially directed to the synthesis of (—)-1,7-dimethyl-7-norbornyl isothiocyanate (I) by the method of Spurlock and Cox [12]. (—)-1,7-Dimethyl-7-norbornylamine, obtainable from (+)-isoketopinic acid in several steps [10], was condensed with carbon disulfide in the presence of potassium hydroxide to provide the dithiocarbamate. Subsequent treatment with ethyl chloroformate afforded the desired isothiocyanate (I) in excellent yield. Similarly, (+)-neomenthyl isothiocyanate (II) was also synthesized from (+)-neomenthylamine by treatment with carbon disulfide and alkali, and then with ethyl chloroformate. The structural assignment of (I) and (II) was rationalized by elemental analysis, i.r., and n.m.r. spectra.

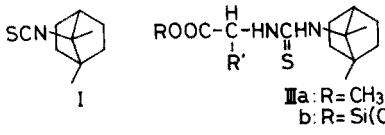

I

IIIa: R = CH_3
b: R = $Si(CH_3)_2$-t-Bu

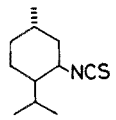

II

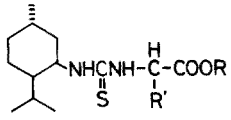

IVa: R = CH_3
b: R = $Si(CH_3)_2$-t-Bu

Reaction of an amino acid with the isothiocyanate reagent was effected under weakly basic conditions without the formation of by-products. The thiourea derivative produced from an amino acid ester showed a single, symmetrical peak, indicating excellent chromatographic properties. Excess of the derivatization reagent was eluted with the solvent front without causing any interference to the chromatogram. No racemization of the product or derivatization reagents occurred, even after a prolonged reaction period. The resulting thiourea derivative absorbed at 243 nm and responded with high sensitivity in the u.v. detector; the limit of detection for the derivatized amino acids was 10 ng.

The applicability of the two chiral derivatization reagents to the liquid chromatographic resolution of enantiomeric amino acids was investigated. It is generally accepted that diastereomers can be separated more easily by normal-phase than by reversed-phase chromatography. In practice, satisfactory separation on a μBondapak C_{18} column was not attained with either of the diastereomeric pairs formed from enantiomeric amino acids and their methyl esters.

In contrast, diastereomers derived from enantiomeric methyl esters were separated on a μPorasil column with a certain measure of success when cyclohexane/ethyl acetate was used as a mobile phase. The retention and resolution values of the diastereomeric thiourea derivatives given by the two chiral reagents are listed in Table 1. The k' and α values refer to the capacity ratio and separation factor for a pair of diastereomers, respectively. The resolution value, R, was calculated from the equation $R = 2(t_{R_2} - t_{R_1})/(W_1 + W_2)$, where t_{R_1} and t_{R_2} are retention times, and W_1 and W_2 are the bases of triangles derived from the peaks. The data show that derivatization into diastereomers (IIIa) with (I) was much more effective for optical resolution than into those (IVa) with (II). Almost all of the pairs of neutral amino acid enantiomers were satisfactorily resolved by the use of (I). With regard to acidic and hydroxyamino acids, however, each set of enantiomers could be distinguished from each other but not completely resolved.

Previous studies [6, 9] strongly implied that the degree of separation of diastereomers on a normal phase column would be dependent largely on the

TABLE 1

Separation of diastereomeric thiourea derivatives of amino acid methyl esters (t_0 = 3.0 min. Column, μPorasil. Mobile phase, cyclohexane/ethyl acetate (A) 2:1, (B) 3:1, (C) 10:1, (D) 20:1. Flow rate, 1.0 ml min^{-1}.)

	IIIa					IVa				
	k'					k'				
Amino acid	D	L	α	R	Mobile phase	D	L	α	R	Mobile phase
Alanine	4.97	4.57	1.09	1.10	C	3.49	3.04	1.15	1.73	C
Valine	8.06	7.25	1.11	1.30	D	6.07	5.71	1.06	0.75	D
Norvaline	9.13	8.00	1.14	1.48	D	6.49	6.49	1.00	0.00	D
Leucine	8.62	7.95	1.08	1.00	D	3.70	3.91	1.06	0.70	D
Norleucine	6.49	5.86	1.11	1.47	D	5.18	5.46	1.05	0.66	D
Isoleucine	7.44	6.55	1.14	1.05	D	3.70	3.91	1.06	0.63	D
Proline	5.91	6.64	1.12	1.69	C	4.13	4.72	1.14	1.79	C
Phenylglycine	9.38	8.96	1.05	0.45	D	7.30	7.53	1.03	0.36	D
Phenylalanine	8.81	7.50	1.17	1.77	D	5.23	5.47	1.05	0.62	D
Serine	4.10	4.20	1.02	0.07	A	7.00	6.46	1.08	0.59	B
Threonine	3.14	3.25	1.04	0.36	A	5.75	5.54	1.04	0.39	B
Aspartic acid	7.87	8.13	1.03	0.48	C	5.72	5.66	1.01	0.15	C
Glutamic acid	16.33	15.40	1.06	0.94	C	11.25	10.10	1.11	1.43	C

rigidity of conformation. Introduction of a bulky group into the ester moiety makes the conformation of the molecule more rigid. Of the typical protecting groups for carboxyl groups, the tert-butyldimethylsilyl residue appeared to be the most suitable because of the higher stability and hydrophobicity of the resulting silyl ester [13, 14]. Accordingly, transformation of amino acids into the thiourea derivatives followed by esterification with tert-butyldimethylchlorosilane and imidazole was carried out. Amino acid enantiomers were efficiently resolved when converted to the diastereomeric thiourea silyl esters (IIIb, IVb) by the use of (I) and (II) (see Table 2). Derivatization to the diastereomeric neomenthylthiourea silyl esters (IVb) was particularly effective for separation, and all the pairs of enantiomers were completely resolved ($R > 1$). The elution order of enantiomeric pairs was constant with the exception of proline: the D-amino acid exhibited a larger retention value than the corresponding L-enantiomer. However, any generalization is not applicable to the elution order of diastereomeric *N*-substituted amino acids [8, 9]. The rigid conformation resulting from esterification with the bulky tert-butyldimethylsilyl group is reflected in the excellent resolution of the resulting diastereomers.

The resolution and order of elution of diastereomers are influenced significantly by the α-alkyl residue of the amino acids as well as the ester moiety; hence the choice of the most suitable derivatization reagent is not always predictable. It is hoped that the discovery of new chiral reagents will increase the versatility of resolution by h.p.l.c. of enantiomeric amines obtained by diastereomeric derivatization.

TABLE 2

Separation of diastereomeric thiourea derivatives of amino acid tert-butyldimethylsilyl esters
(t_0 = 3.0 min. Column, μPorasil. Mobile phase, cyclohexane/ethyl acetate (A) 30:1, (B) 40:1, (C) 50:1, (D) 80:1. Flow rate, 1.0 ml min^{-1}.)

	IIIb					IVb				
	k'					k'				
Amino acid	D	L	α	R	Mobile phase	D	L	α	R	Mobile phase
Alanine	5.90	5.50	1.07	0.84	A	3.87	3.10	1.25	2.32	A
Valine	4.37	3.53	1.24	2.31	A	2.27	1.67	1.36	2.65	A
Norvaline	4.07	3.43	1.19	1.78	A	1.83	1.47	1.24	1.90	A
Leucine	4.03	3.37	1.20	2.00	A	1.93	1.67	1.16	1.19	A
Norleucine	3.60	2.93	1.23	2.06	A	1.37	1.10	1.25	1.51	A
Isoleucine	3.70	3.03	1.22	1.92	A	1.67	1.47	1.14	2.00	A
Proline	7.90	8.20	1.04	0.45	A	5.63	6.27	1.11	1.13	A
Phenylglycine	4.77	4.30	1.11	1.21	A	4.23	3.80	1.11	1.08	B
Phenylalanine	4.13	3.03	1.36	3.00	A	2.47	1.73	1.43	2.09	C
Serine	3.00	2.33	1.29	2.30	A	3.27	2.80	1.17	1.36	D
Threonine	6.57	5.53	1.19	1.90	A	1.60	1.07	1.50	3.33	A
Aspartic acid	3.00	2.60	1.15	1.43	A	2.03	1.63	1.25	1.82	B
Glutamic acid	6.57	6.23	1.05	0.90	A	4.83	3.87	1.25	2.38	A

The authors thank Ms. K. Mushiake and Ms. N. Obatake for technical assistance. This work was supported in part by a Grant-in-Aid for Scientific Research from the Ministry of Education, Science and Culture, Japan.

REFERENCES

1 R. E. Leitch, H. L. Rothbart and W. Rieman III, J. Chromatogr., 28 (1967) 132.
2 R. J. Baczuk, G. K. Landram, R. J. Dubois and H. C. Dehm, J. Chromatogr., 60 (1971) 351.
3 S. V. Rogozhin and V. A. Davankov, Chem. Commun., (1971) 490.
4 V. A. Davankov, S. V. Rogozhin, A. V. Semechkin, V. A. Baranov and G. S. Sannikova, J. Chromatogr., 93 (1974) 363.
5 F. Mikeš, G. Boshart and E. Gil-Av, J. Chromatogr., 122 (1976) 205.
6 C. G. Scott, M. J. Petrin and T. McCorkle, J. Chromatogr., 125 (1976) 157.
7 G. Helmchen, H. Völter and W. Schühle, Tetrahedron Lett., (1977) 1417.
8 H. Furukawa, Y. Mori, Y. Takeuchi and K. Ito, J. Chromatogr., 136 (1977) 428.
9 J. Goto, M. Hasegawa, S. Nakamura, K. Shimada and T. Nambara, J. Chromatogr., 152 (1978) 413.
10 M. Ishidate and A. Kawada, Chem. Pharm. Bull. (Tokyo), 4 (1956) 483.
11 A. K. Bose, J. F. Kistner and L. Farber, J. Org. Chem., 27 (1962) 2925.
12 L. A. Spurlock and W. G. Cox, J. Am. Chem. Soc., 91 (1969) 2961.
13 G. Phillipou, D. Bigham and R. F. Semark, Steroids, 26 (1975) 516.
14 H. Hosoda, K. Yamashita, H. Sagae and T. Nambara, Chem. Pharm. Bull. (Tokyo), 23 (1975) 2118.

Analytica Chimica Acta, 101 (1978) 117—124

THE GAS CHROMATOGRAPHY OF HIGHER SUBSTITUTED TETRADENTATE β-KETOAMINE COPPER(II) COMPLEXES**

A. KHALIQUE and W. I. STEPHEN*

Department of Chemistry, The University of Birmingham, P.O. Box 363, Birmingham, B15 2TT (Gt. Britain)

D. E. HENDERSON and P. C. UDEN

Department of Chemistry, The University of Massachusetts, Amherst, 01003, Mass., (U.S.A.)

(Received 2nd March 1978)

SUMMARY

The preparation of the Schiff's bases derived from 1,2-diaminoethane and a series of 5-alkyl substituted-1,1,1-trifluoropentan-2:4-diones is described, including the elusive compound obtained from 1,1,1-trifluoro-5,5,5-trimethylpentan-2:4-dione, and trivially denoted as $H_2[en(TPM)_2]$. Gas chromatography of the copper complexes of these ligands shows increasing retention times as the size of the alkyl substituent is increased, with the exception of $Cu[en(TPM)_2]$ which is unusually volatile and has a much reduced retention time. It is most probable that this great difference in properties occurs because of the considerable steric hindrance of the tert-butyl groups in the original β-diketone, which prevents the normal condensation reaction with 1,2-diaminoethane taking place. The properties of the metal complexes of $H_2[en(TPM)_2]$ make them ideally suited to quantitative gas chromatography.

It is now well established that in terms of thermal stability and gas chromatographic applicability, tetradentate β-ketoamine chelates have many superior features for the analysis of divalent transition metals e.g. copper, nickel, palladium [1—6] and, recently, vanadium [7].

Certain modifications to the basic ligand structure have been made in attempts to improve such factors as thermal stability, volatility and resolution between copper and nickel chelates of a given ligand. Among these modifications have been (i) the substitution of fluorinated for non-fluorinated substituent groups, notably CF_3- for CH_3- and (ii) substitution in the diamine bridge of the ligand, e.g. methyl substitution of the methylene-bridged hydrogen atoms to produce propylene- and butylene-bridged compounds [4, 8]. Both of these substitutions produce increased volatility and generally lead to an enhanced thermal stability, although usually with a decrease in the rate of chelate formation in solution. Sometimes decreased preparative efficiency and smaller yields are also noted.

** Abstracted in part from the Ph.D. dissertations of A. Khalique (University of Birmingham, 1974) and D. E. Henderson (University of Massachusetts, 1974).

Analogy with volatile metal β-diketonate chemistry suggests that replacement of the methyl substituent in the parent β-diketone by a larger, more bulky alkyl group, particularly the tertiary-butyl group, will enhance thermal stability and resolution among complexes of different metals [9, 10]. Also the increase in the size of the substituent group may lead to enhanced volatility as in the case of the bridging group substitution. A preliminary report [11] noted that the copper chelate of ethylene-bis(trifluoroacetylpivalylmethaneimine), H_2[en(TPM)$_2$], showed unexpectedly high volatility. The present paper describes the preparation of a series of terminal alkyl-substituted tetradentate β-ketoamine complexes with substituents ranging from methyl to n-amyl including both linear and branched chain species to assess substituent effects on chromatographic elution. Recently, Dilli and Patsalides [12] have reported the isolation of isomeric forms of H_2[en(TPM)$_2$] using a variety of chromatographic techniques and have confirmed the exceptionally high volatility of both ligand and complexes. They further postulate that the characteristic features of this ligand are a result of a difference in structure from other members of the series previously prepared. Specifically, bridging by the diamine moiety occurs in this case adjacent to the CF_3- group rather than the structurally hindered tert-butyl group. The present data serve to extend the overall understanding of this area of metal chelate gas chromatography.

EXPERIMENTAL

Preparation of the ligands

With the exception of H_2[en(TPM)$_2$], all the ligands were prepared by established methods. The β-diketones, except H(TPM), were obtained commercially (Eastman Organic Chemicals) and were purified by distillation before being used in the condensations with 1,2-diaminoethane. H(TPM) was prepared as described previously [10]. For the condensations, the β-diketone was added gradually to slightly less than the stoichiometric amount of the diamine, dissolved in ethanol. The mixture was heated under reflux for a short period and then cooled. White needle-shaped crystals of the respective compounds were isolated and recrystallized from ethanol. The purities of the compounds were established by elemental analysis.

When the general procedure was applied to H(TPM), a white compound gradually precipitated over a period of 10—15 min. Isolation and recrystallisation of this material from water/ethanol gave a substance melting at 98—100°C. Elemental analysis indicated that this was probably a simple adduct of the diamine and H(TPM), viz: the ethylenediammonium salt of trifluoroacetylpivalylmethane. Numerous variations in this method of preparation failed to provide the required H_2[en(TPM)$_2$]. Attempts to ease the elimination of water necessary for the condensation of the diamine and the β-diketone to occur were tried, including reflux of the adduct salt with *o*-xylene for 30 min and prolonged desiccation of the adduct in a

conventional pistol drier with phosphorus pentoxide in a boiling chloroform jacket. The yellow viscous liquids obtained in these experiments partially crystallized during 15 d, but no method of recrystallising this material was found. Elemental analysis gave an exceptionally high value for nitrogen (11.8%) compared with that calculated for $H_2[en(TPM)_2]$ (6.7%). However, by dissolving this crude product in n-hexane, and leaving the solution at 0°C for ca. 1 h, an oily layer separated out, and the clear supernatant liquid could be separated by decantation. The treatment of the oil with n-hexane was repeated 2—3 times and the combined hexane extracts were evaporated under reduced pressure to give a white crystalline substance which on recrystallization from low boiling petroleum spirit (40—60°C) gave a crop of fine needle-like crystals (m.p. 83—85°C). Complete elemental analysis gave 54.7% C; 6.7% H; 12.8% N and 25.5% F, corresponding to a molecular formula of $C_{10}H_{15}N_2F_3$. This indicated that both carbonyl oxygens of the β-diketone were eliminated in the condensation with the diamine to give compound(I) which rearranged to a dihydrodiazepin (II). This latter compound has been characterized by Dilli and Patsalides as one of the products isolated from the reaction of H(TPM) and diaminoethane [12]. It has a calculated composition of 54.5% C; 6.9% H; 12.7% N and 25.9% F, in close agreement with the values obtained above.

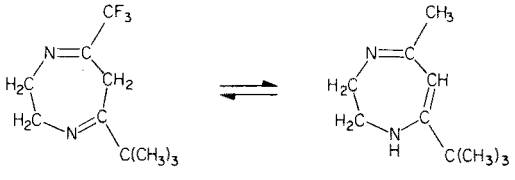

(I) (II)

Further experimentation with the adduct revealed that if it were kept in a stoppered bottle in a conventional drying oven at 55—60° C for 24 h, the solid crystalline material changed to a thick yellow liquid, not in any way amenable to crystallization, but capable of reacting with copper(II), nickel(II) and palladium(II) ions to give characteristic tetradentate metal chelates.

In favourable circumstances, it was possible to isolate about 1 g of pure metal chelate from 10 g of the crude ligand. The pure copper chelate obtained by column chromatography (see below) was decomposed in an aqueous ethanol solution with potassium cyanide and the free $H_2[en(TPM)_2]$ was extracted with diethyl ether. The ether solution was washed with water, dried with anhydrous sodium sulphate and transferred to an evaporating dish. The solvent was allowed to evaporate at room temperature to leave a white crystalline material, homogeneous by gas chromatography. Elemental analysis gave 52.0% C; 6.1% H; 6.7% N: $C_{18}H_{26}N_2O_2F_6$ requires 51.9% C; 6.2% H; 6.7% N.

The ligand structures are shown in Table 1, where nomenclature is also designated.

TABLE 1

Structures of ligands prepared and retention times of copper chelates at 220°C

	R_1	R_2	Abbreviation for ligand	Retention time (s)
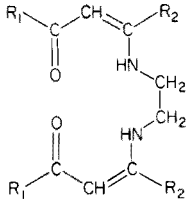	CF_3	CH_3	H_2[en(TFA)$_2$]	567
	CF_3	C_2H_5	H_2[en(TPrM)$_2$]	708
	CF_3	C_3H_7-iso	H_2[en(TiBM)$_2$]	795
	CF_3	C_4H_9-iso	H_2[en(TPnM)$_2$]	1068
	C_4H_9-tert[a]	CF_3	H_2[en(TPM)$_2$]	116[b]
	CF_3	C_5H_{11}-iso	H_2[en(TiHxM)$_2$]	1835

[a]See [12]. [b]At 170°C.

In general, yields of the ligands ranged from ca. 75% for H_2[en(TiBM)$_2$] to ca. 5% for H_2[en(TPM)$_2$], but the preparative procedures were not entirely optimized.

Preparation of the chelates

With the exception of the H_2[en(TPM)$_2$] chelates, the copper and nickel complexes of the tetradentate ligands were prepared by established methods [1, 2]. A useful general procedure was to mix a chloroform solution of the ligand with a solution of the metal tetrammine complex in water, followed by the addition of sufficient ethanol to give a single phase. After reaction (usually instantaneous) the phases were separated by the addition of sufficient water and the organic layer was evaporated to obtain the complexes.

The copper(II), nickel(II) and palladium(II) complexes of H_2[en(TPM)$_2$] were prepared from the crude ligand as follows. An excess of saturated aqueous copper(II) acetate was added dropwise with stirring to a solution of 10 g of crude H_2[en(TPM)$_2$] in 100 cm^3 of ethanol. The mixture was warmed on a boiling water-bath for 15 min, cooled, and diluted gradually with 200 cm^3 of water. The precipitated complex was filtered off, dissolved in 10 cm^3 of n-hexane, and the solution was concentrated to ca. 4—5 cm^3 by evaporation. This solution was added to a chromatographic column, containing ca. 100 g of activated alumina (100—200 mesh) and the chelate was eluted with n-hexane. During development of the column, four different bands were observed, a slow-moving green band above a blue and a yellow band, with a fast moving violet band. The violet band was eluted, and a dark violet crystalline material was obtained from the evaporated solution. This substance was exceptionally soluble in non-polar solvents, particularly n-pentane and n-hexane, and recrystallization was extremely difficult. However, by judicious slow evaporation of most of the solvent, dark violet prismatic crystals of the copper(II) complex were obtained (m.p. 114—115°C). Elemental analysis gave 45.5% C; 5.2% H; 5.7% N: $C_{18}H_{24}N_2O_2F_6Cu$ requires 45.2% C; 5.1% H; 5.9% N. The mass spectrum gave a fragmentation pattern with a top mass at *m/e* 477, which corresponded to the molecular ion.

The corresponding nickel complex was prepared from a solution of 10 g of the crude ligand in 50 cm^3 of acetone which was heated under reflux for 4 h with an excess of freshly prepared nickel(II) hydroxide. The cooled, filtered solution was diluted gradually with about 200 cm^3 of water and the precipitated complex was filtered off under suction and taken up in 10 cm^3 of n-hexane. The concentrated hexane solution was subjected to column chromatography, as for the copper complex. The leading reddish-brown band was collected by elution with n-hexane and the solid complex was isolated by evaporation of the solvent. Recrystallization from the minimal amount of n-hexane gave reddish-brown prisms (m.p. 136—137°C). The complex, dissolved in n-hexane, gave a dichroic solution, being brownish-red in reflected light and green in transmitted light. Elemental analysis gave 45.8% C; 5.2% H; 6.0% N: $C_{18}H_{24}N_2O_2F_6Ni$ requires 45.7% C; 5.1% H; 5.9% N. The mass spectrum gave a top mass of *m/e* 472, corresponding to the molecular ion.

The palladium(II) complex was obtained by refluxing a mixture of 10 g of crude $H_2[en(TPM)_2]$ in 50 cm^3 of acetone and 1.0 g of palladium(II) chloride—benzonitrile complex for ca. 4 h. The cooled reaction mixture was filtered and diluted slowly with 200 cm^3 of water. The precipitate of the palladium(II) chelate was filtered off under suction, thoroughly air-dried at room temperature and dissolved in about 10 cm^3 of n-hexane. This solution, filtered from any insoluble material, was concentrated to 2—3 cm^3 and added to a column of active alumina, as for the copper(II) and nickel(II) complexes. The yellow leading band was eluted with n-hexane and the chelate was recovered by evaporation of the solvent. It was re-crystallised from n-hexane to give yellow prismatic crystals (m.p. 122°C). Elemental analysis gave 42.0% C; 4.8% H; 5.2% N: $C_{18}H_{24}N_2O_2F_6Pd$ requires 41.5% C; 4.6% H; 5.4% N. Mass spectrometry gave a fragmentation pattern with top mass at *m/e* 520, corresponding to the molecular ion.

Similar procedures were used to prepare the copper(II), nickel(II) and palladium(II) chelates of $H_2[pn(TPM)_2]$, which was obtained in crude form by heating the 1,2-propylenediamine adduct of H(TPM) for 24 h in a sealed bottle, as for $H_2[en(TPM)_2]$. Their properties are reported elsewhere [13].

All the other complexes were purified by recrystallization and vacuum sublimation and their authenticities were confirmed by elemental analysis and direct insertion probe mass spectrometry.

Instrumentation

Gas chromatography was carried out on Pye Series 104, Perkin-Elmer 990 or Varian 2440 instruments with columns and conditions as noted, flame ionization detection being employed. Mass spectra were obtained on a Hitachi Perkin-Elmer RMU 6L or an AEI MS 9 instrument.

RESULTS AND DISCUSSION

The copper chelates were subjected to gas chromatography on a 6ft × $\frac{1}{8}$-in. o.d. stainless steel column packed with 3% QF.1 on Varaport 30, in order to assess trends in elution order as the substituent groups were increased in size. A temperature of 220°C was chosen as the most suitable for all complexes with the notable exception of Cu[en(TPM)$_2$] which had an exceptionally short retention time, even at 170°C. Retention times are given in Table 1. Increased size of the substituent groups results in increased chelate retention times, in marked contrast to the behaviour on bridge amyl substitution. This effect persists for both normal and iso-substituent groups.

A typical chromatographic separation and the peak characteristics of both the free ligand and its copper chelate are shown in Fig. 1 for H$_2$[en(TiBM)$_2$].

It can be seen that resolution of Cu[en(TiBM)$_2$] and Ni[en(TiBM)$_2$] is almost identical with that between Cu[en(TFA)$_2$] and Ni[en(TFA)$_2$] on the QF.1 column which has previously been shown to be optimal for such separations [1]. Retention times for these four complexes are 795 s, 711 s, 567 s and 510 s respectively, and thus there is no advantage for copper—nickel resolutions in using the heavier ligand. Similar or less resolution is noted for other copper—nickel pairs. All chelates appear to be eluted unchanged, even those complexes which are retained on the column for prolonged times.

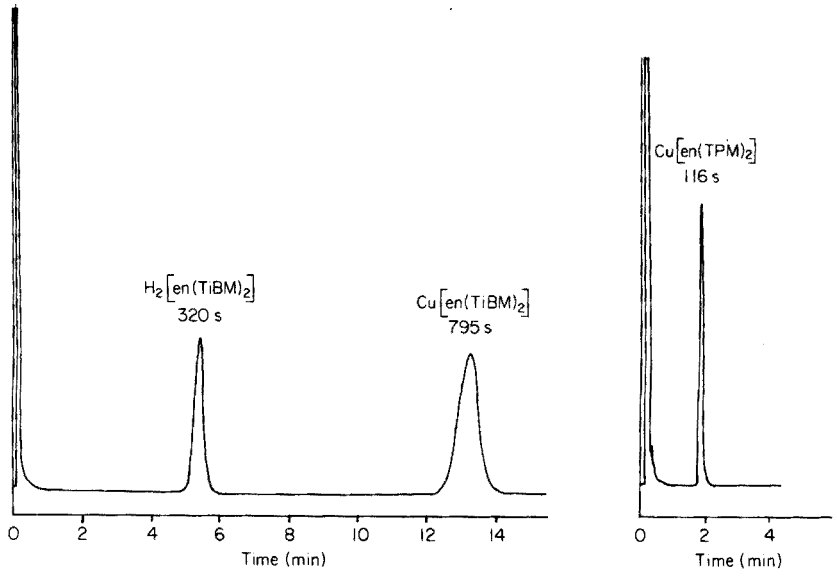

Fig. 1. Gas chromatographic separation of H$_2$[en(TiBM)$_2$]. Column 6ft × $\frac{1}{8}$ in. o.d. packed with 3% QF.1 fluorosilicone oil on Varaport 30, 80—100 mesh. Conditions: column, 220°C; injector and detector, 240°C. Helium carrier gas flow, 40 cm^3 min^{-1}.

Fig. 2. Gas chromatogram of Cu[en(TPM)$_2$]. Column as in Fig. 1. Conditions: column, 170°C; injector and detector, 200°C. Helium gas flow, 40 cm^3 min^{-1}.

The exceptional change in chromatographic retention noted for the $H_2[en(TPM)_2]$ complexes is unique in metal chelate gas chromatography. The chromatogram of $Cu[en(TPM)_2]$ at 170°C is shown in Fig. 2, in which the ligand is unresolved from the solvent. This quite unexpected finding required confirmation, particularly of the identity of the chelate by g.c.—m.s., and also by trapping of the g.c. effluent followed by solid probe m.s. analysis. The typical fragmentation pattern shown in Table 2 proves conclusively that the eluted peak is not the free ligand as might easily be suspected. Table 2 also gives the fragmentation patterns of other copper complexes for comparison.

In common with all of the series, the base peak (100) corresponds to the metal complex minus half of the tetradentate ligand, and the molecular ion is also intense. There are some mass spectral features, notably the presence of $ML—C(CH_3)_3$ which might serve to indicate a distinctive structure for $Cu[en(TPM)_2]$ since analogous ions are not present in other chelates. This tentative conclusion is fully substantiated by the data of Dilli and Patsalides [12, 14].

The only reasonable explanation for the great volatility and elution reduction exhibited by the $H_2[en(TPM)_2]$ complexes must involve a major structural difference from the other less sterically constrained members of the series investigated. As noted, the postulate of bridging adjacent to the CF_3-group rather than the tert-butyl group for either one or both of the parent β-diketone moieties now appears to be substantiated [12]. Dilli and Patsalides have established that both isomers of the ligand are formed during the reaction of H(TPM) with ethylenediamine and show good gas chromatographic resolution. There is no evidence for the existence of the third possible isomer with bridging adjacent to each of the tert-butyl groups. Although the present study has not involved the isolation of the isomers noted by Dilli and Patsalides, their findings are certainly entirely comparable with the present data. The major experimental difficulty lies in increasing the

TABLE 2

Principal features of mass spectral fragmentation patterns of tetradentate β-ketoamine copper complexes[a]

$^{63}Cu(enTFA_2)$			$^{63}Cu(enTiBM_2)$			$^{63}Cu(enTPM_2)$		
Ion	R.I.	Assignment	Ion	R.I.	Assignment	Ion	R.I.	Assignment
393	50	M.I.	449	73	M.I.	477	16	M.I.
374	2.6	M.I.—F	430	2.7	M.I.—F	458	1.1	M.I.—F
324	6.7	M.I.—CF_3	380	7.5	M.I.—CF_3	420	5.3	M.I.—$C(CH_3)_3$
228	100	M.I.—L/2	256	100	M.I.—L/2	270	100	M.I.—L/2
196.5	1.0	$(M.I.)^{2+}$	224.5	1.5	$(M.I.)^{2+}$	213	16.4	M.I.—L/2—$C(CH_3)_3$

[a]R.I. = Relative intensity; M.I. = Molecular Ion; L = Ligand—2H. Most non-copper containing ions below M.I.—L/2 are not included.

preparation yields of the Schiff's base. The procedure described above for the preparation of $H_2[en(TPM)_2]$ via the corresponding purified copper complex appears to provide a single isomeric species. Certainly, the gas chromatography of this ligand shows no evidence of inhomogeneity, yet two of the isomers of this compound isolated by t.l.c. [12] from a crude reaction mixture are quite well resolved by gas chromatography. However, both the present method and that reported by Dilli and Patsalides for the preparation of $H_2[en(TPM)_2]$ produce a complex mixture containing, amongst other things, one or more isomeric forms of the required Schiff's base and quite unsuitable for direct analytical use as a reagent. No data have as yet been reported for the copper and nickel chelates of the two isomers of $H_2[en(TPM)_2]$, so that comparison with the chelates described above is not possible. It seems likely, however, that the form of the ligand described in this report is the symmetrical one (isomer 1 of Dilli and Patsalides) in which the bridging occurs adjacent to both CH_3-groups in the two H(TPM) molecules forming the tetradentate Schiff's base. From a purely analytical standpoint, it is desirable that a single isomeric species is used as the reagent in the development of analytical procedures which exploit the extraordinary properties of the derived metal chelates. Otherwise, complications can arise through competitive chelation with a mixture of the isomeric ligands which would adversely influence quantitative gas chromatography of the metal complexes. Work is continuing in an attempt to solve this problem.

REFERENCES

1 R. Belcher, K. Blessel, T. J. Cardwell, M. Pravica, W. I. Stephen and P. C. Uden, J. Inorg. Nucl. Chem., 35 (1973) 1127.
2 R. Belcher, D. E. Henderson, A. Kamalizad, R. J. Martin, W. I. Stephen and P. C. Uden, Anal. Chem., 45 (1973) 1197.
3 P. C. Uden and D. E. Henderson, J. Chromatogr., 99 (1974) 309.
4 P. C. Uden, D. E. Henderson and A. Kamalizad, J. Chrom. Sci., 12 (1974) 591.
5 P. C. Uden and D. E. Henderson, Analyst, 102 (1977) 889.
6 R. Belcher, A. Khalique and W. I. Stephen, Anal. Chim. Acta, 100 (1978) 511.
7 S. Dilli and E. Patsalides, J. Chromatogr., 130 (1977) 251.
8 P. C. Uden and K. Blessel, Inorg. Chem., 12 (1973) 352.
9 C. S. Springer, D. W. Meek and R. E. Sievers, Inorg. Chem., 6 (1967) 1105.
10 R. Belcher, C. R. Jenkins, W. I. Stephen and P. C. Uden, Talanta, 17 (1970) 455.
11 W. I. Stephen, Proc. Soc. Anal. Chem., 9 (1972) 137.
12 S. Dilli and E. Patsalides, J. Chromatogr., 134 (1977) 477.
13 A. Khalique, Ph.D. Dissertation, University of Birmingham, 1974.
14 E. Patsalides, Ph.D. Dissertation, University of New South Wales, 1978.

Analytica Chimica Acta, 101 (1978) 125—130

BACTERIAL MEMBRANE ELECTRODE FOR L-CYSTEINE

M. A. JENSEN and G. A. RECHNITZ*

Department of Chemistry, University of Delaware, Newark, Delaware 19711 (U.S.A.)

(Received 4th April 1978)

SUMMARY

Potentiometric response to L-cysteine is obtained by coupling bacteria of the type *Proteus morganii* to a modified version of a hydrogen sulfide gas-sensing membrane electrode. The resulting electrode system shows good response to cysteine in the millimolar concentration range with moderate selectivity over related sulfur-containing amino acids. The practical applicability of the electrode is limited by the poor discrimination of the internal gas sensor between hydrogen sulfide and carbon dioxide.

Living bacterial cells can be coupled with a gas-sensing electrode to permit potentiometric determinations of several amino acids [1—3]. These bacterial electrodes offer a number of advantages over the conventional enzyme electrodes. These advantages include an increased electrode lifetime, regeneration of electrode response by storing the electrode in the appropriate growth medium, elimination of the often tedious and expensive process of enzyme purification, and the possibility of performing potentiometric determinations of compounds for which appropriate enzymes have not been isolated.

Most bacterial electrodes have utilized bacteria which have selective deaminase activity in conjunction with an ammonia-sensing electrode. However, the range of compounds which may be measured by this technique need not be restricted to those compounds which produce ammonia as metabolic products. Substrates which are metabolized to such end products as hydrogen sulfide or carbon dioxide might also be measured by coupling the appropriate bacteria and gas-sensing electrodes.

The purpose of this investigation was to demonstrate a system in which the bacterium *Proteus morganii* is coupled with a hydrogen sulfide-sensing electrode to produce a cysteine-responsive membrane electrode. Cysteine is metabolized by *Proteus morganii* to hydrogen sulfide in the reaction [4]

$$\text{Cysteine} \xrightarrow{\text{Cysteine desulfhydrase}} \text{pyruvate} + NH_3 + H_2S$$

Because the enzyme responsible for the desulfhydration of cysteine has not been isolated, it is only through the use of a bacterium with cysteine desulfhydrase activity that cysteine may be measured with a hydrogen sulfide-sensing electrode.

EXPERIMENTAL

Apparatus

A hydrogen sulfide-sensing electrode was assembled by using the body and internal pH electrode of the Orion Model 95-10 ammonia-sensing electrode, and used in the construction of the bacterial electrode. Membranes and filling solution were obtained from Lazar Research Laboratories, Los Angeles, California.

Potential measurements were made with a Corning Model 12 Research pH meter and were recorded with a Heath Schlumberger Model SR-204 strip chart recorder. All potential measurements were carried out in thermostatted cells.

Reagents

Proteus morganii (ATCC No. 8019) was obtained from the American Type Culture Collection, Rockville, Maryland. The growth medium was Bacto nutrient broth (Difco Laboratories through VWR Scientific). L-Cysteine, L-methionine, and L-cystathionine were obtained from Sigma Chemical Co., D,L-homocysteine from ICN Pharmaceuticals, and ultrapure urea from Schwarz and Mann. Buffer solutions, hydrogen sulfide and carbon dioxide standards were prepared with analytical reagent-grade chemicals.

Procedure

The internal filling solution for the electrode was prepared by diluting (1 + 9) the Lazar H_2S filling solution with 0.10 M NaCl. The Lazar H_2S membrane was used as the gas-permeable membrane.

The response of the electrode to hydrogen sulfide in 0.13 M phthalate buffer pH 5 was evaluated at 25°C. Initially, the phthalate buffer solution was degassed for 60 min with nitrogen to remove carbon dioxide. Hydrogen sulfide was produced by the addition of sodium hydrogensulfide to the buffer solution. To minimize the loss of hydrogen sulfide from solution, the cell remained sealed except during additions of sulfide.

The response of the electrode to H_2S is shown in Fig. 1. The slope of the electrode response to hydrogen sulfide increased as the hydrogen sulfide concentration was increased, reaching a Nernstian slope of 59 mV/decade at a concentration of 1 mM H_2S.

The response of the electrode to carbon dioxide in the 0.13 M phthalate buffer at 25°C was also evaluated. The electrode response to carbon dioxide (Fig. 1) was similar to that observed for hydrogen sulfide, with the potential response of the electrode reaching a near-Nernstian slope of 57 mV/decade at a concentration of 0.50 mM.

Proteus morganii was grown in nutrient broth at 37°C. After 2—3 days, the bacteria cells were collected by centrifugation and washed several times with 0.1 M phosphate buffer pH 7.45.

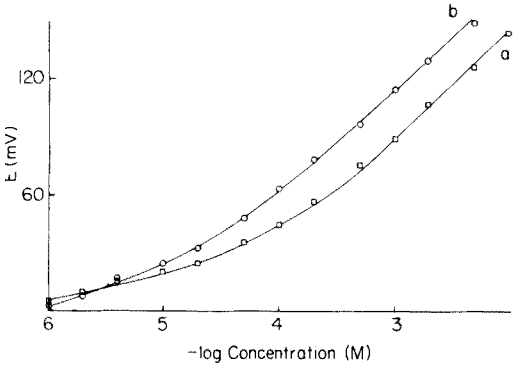

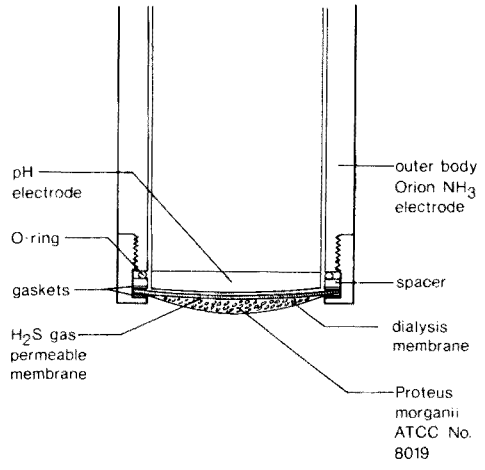

Fig. 1. Calibration curve of the response of the hydrogen sulfide-sensing electrode towards H_2S (a) and CO_2 (b) in 0.13 M phthalate buffer pH 5 at 25°C.

Fig. 2. Schematic diagram of the bacterial electrode.

Approximately 10 μl of the centrifuged bacteria was applied to the gas-permeable membrane of the hydrogen sulfide electrode, and held in place with a dialysis membrane (Fig. 2). Bacteria which were not used in the construction of the electrode were stored in autoclaved nutrient broth at 3°C.

The freshly prepared bacterial electrodes were stored for 12 h in nutrient broth at 3°C before initial use. Afterwards, the electrodes were stored in 0.1 M phosphate buffer.

Because the bacterial electrode responded to carbon dioxide, it was necessary to remove the carbon dioxide from the buffer solutions before substrate was added. Carbon dioxide was removed by aerating the buffer solutions for 1 h with a mixture of 80% nitrogen and 20% oxygen. (Solutions could not be degassed with pure nitrogen because the bacterial metabolism of cysteine was markedly decreased in the absence of oxygen.) To prevent the uptake of carbon dioxide from the atmosphere by the buffer solution during the addition of substrate, a constant pressure of 80% nitrogen and 20% oxygen was maintained above the solution.

RESULTS AND DISCUSSION

Initially, the response of the bacterial electrode towards cysteine was examined in 0.1 M phosphate buffer pH 6.75 at 37°C. At this pH, the rate of cysteine metabolism and the degree of H_2S dissociation (pK_a = 7.0) combine to give the maximum rate of undissociated H_2S production. The potentiometric response of a newly prepared bacterial electrode towards cysteine is shown in Fig. 3. Within the concentration range 5×10^{-5} to 9×10^{-4} M cysteine, the electrode showed a linear response with a slope of

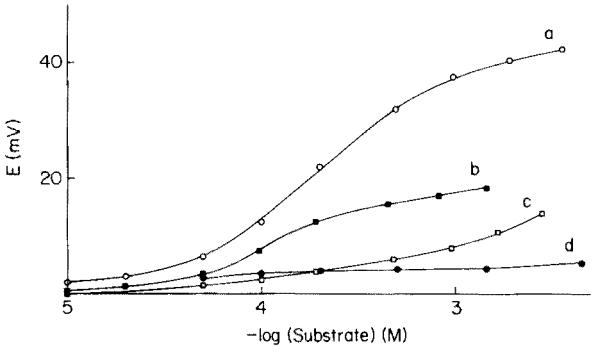

Fig. 3. Response of the bacterial electrode towards the following sulfur-containing amino acids: (a) cysteine, (b) homocysteine, (c) cystathionine, and (d) methionine. All solutions were run in 0.1 M phosphate buffer pH 6.75 at 37°C.

25 mV/decade. The electrode response time in this concentration range was typically 5—8 min.

Although the slope of the linear electrode response remained relatively constant at 23—26 mV/decade for over a week, the linear range began to decrease after six days. The initial linear range could be re-established by soaking the electrode in nutrient broth for 12—24 h. However, this procedure resulted in a significant increase in the electrode response time.

The response of the bacterial electrode toward other sulfur-containing amino acids was examined in 0.1 M phosphate buffer pH 6.75 and 37°C. The electrode gave a moderate response to homocysteine yielding a slope of 15 mV/decade in the concentration range 5×10^{-5}—2×10^{-4} M (Fig. 3); this response is not surprising, for the structures of homocysteine and cysteine differ only in that homocysteine contains an additional methylene group. The electrode showed smaller responses to cystathionine and methionine. The degree of response to these sulfur-containing amino acids can be summarized as follows: cysteine > homocysteine > cystathionine > methionine.

The response of the internal gas-sensing electrode to carbon dioxide (Fig. 1) presents an inevitable limitation for this type of electrode. While residual levels of carbon dioxide or low levels of carbonate might be removed via a pretreatment step such as solution degassing, a fundamental limitation remains, owing to the respiratory metabolism of bacterial cells to produce carbon dioxide in situ.

This difficulty is illustrated in Fig. 4 which shows the response of the cysteine electrode to urea. Here, the bacterial cells metabolize urea to yield both ammonia and carbon dioxide via the enzymatic action of urease [5]. Although the electrode does not respond to ammonia, an appreciable urea response, reaching a slope of approximately 21 mV/decade, arises from the carbon dioxide production.

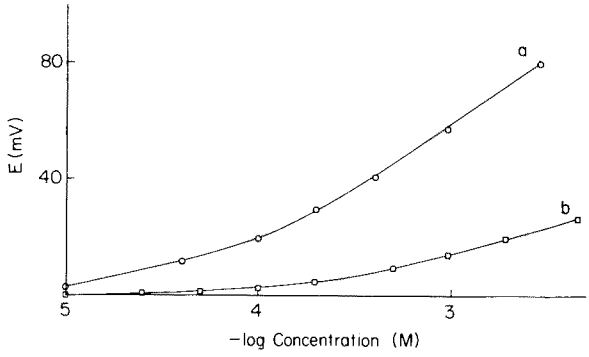

Fig. 4. Response of the bacterial electrode towards the addition of HCO_3^- (a) and urea (b) to 0.1 M phosphate buffer pH 6.75 at 37°C.

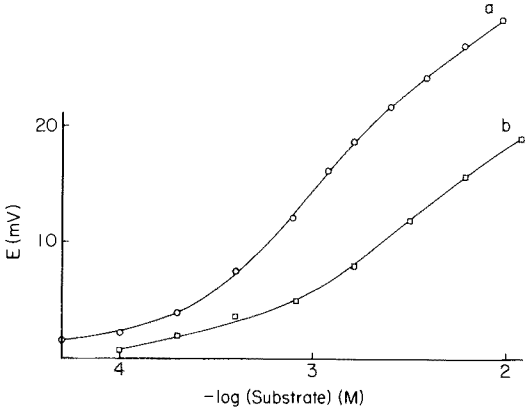

Fig. 5. Response of the bacterial electrode towards cysteine (a) and urea (b) in 0.1 M phosphate buffer at pH 7.45 at 37°C.

Since the pK_a value of H_2S (7.0) is greater than that of CO_2 (pK_a = 6.7), some improvement in selectivity for H_2S would be expected by working at higher pH values; Fig. 5 shows the response of the bacterial electrode to cysteine and urea at pH 7.45 (0.1 M phosphate buffer, 37°C). While there is some improvement in selectivity, the advantage is offset by a poorer response owing to the decrease in the levels of the undissociated gaseous species at the higher pH value.

Thus, the development of a truly practical cysteine electrode by this approach must await the availability of a hydrogen sulfide sensor with better selectivity over carbon dioxide; this might be feasible by modifications in membrane permeability. In the meantime, it has been demonstrated that bacterial cells can be effectively coupled to gas sensors other than those for ammonia, to produce substrate-sensing electrodes.

We gratefully acknowledge the support of a grant from the National Science Foundation.

REFERENCES

1 G. A. Rechnitz, T. L. Riechel, R. K. Kobos, and M. E. Meyerhoff, Science, 199 (1978) 440.
2 R. K. Kobos and G. A. Rechnitz, Anal. Lett., 10 (1977) 751.
3 G. A. Rechnitz, R. K. Kobos, S. J. Riechel, and C. R. Gebauer, Anal. Chim. Acta, 94 (1977) 357.
4 R. E. Kallio and J. R. Porter, J. Bacteriol., 60 (1950) 607.
5 B. D. Davis, R. Dulbecco, H. N. Eisen, H. S. Ginsberg, and W. B. Wood, Microbiology, Harper and Row, New York, 1970, p. 757.

Analytica Chimica Acta, 101 (1978) 131—138

APPLICATION OF SEMIDIFFERENTIAL ELECTROANALYSIS TO ANODIC STRIPPING VOLTAMMETRY

MASASHI GOTO*, KAZUHIKO IKENOYA, MASAYA KAJIHARA and DAIDO ISHII

Department of Applied Chemistry, Faculty of Engineering, Nagoya University, Chikusa-ku, Nagoya (Japan)

(Received 14th December 1977)

SUMMARY

A new voltammetric technique, semidifferential electroanalysis, in which the semiderivative, e, of the current, i, is measured as a function of electrode potential, has been applied for detection in anodic stripping voltammetry. The semiderivative of the current is defined by

$$e \equiv \frac{d^{1/2}i}{dt^{1/2}} = \frac{d}{dt}\left[\frac{1}{\pi^{1/2}} \int_0^t \frac{i(\lambda)}{(t-\lambda)^{1/2}}\, d\lambda\right]$$

Cd^{2+}, Pb^{2+}, and Tl^{+} in 0.1 M KNO_3 at different pH values were tested as samples on a hanging mercury drop working electrode. Symmetrical sharp peaks were observed for the re-dissolution processes of metal amalgams formed during pre-electrolysis at −1.0 V vs. SCE. The peak potentials of e vs. E curves for the above three amalgams agreed well with the literature values for d.c. polarographic half-wave potentials. The peak heights were proportional to the pre-electrolysis time up to about 5 min, to the potential scan rate in the range 60—160 mV s^{-1}, and to the concentrations of Cd^{2+}, Pb^{2+}, and Tl^{+} in the original solution in the range 10^{-6}–10^{-9} M. The relative standard deviation for the determination of Cd^{2+} was about ±4% at the 2×10^{-8} M level.

Recently, a new electroanalytical technique, semidifferential electroanalysis, has been developed [1—3]. The technique uses the semiderivative of the current with respect to time as the observed function against the electrode potential under the experimental conditions of linear sweep voltammetry. For reversible electrode processes, the peaks observed are symmetrical and sharp, whereas conventional current—potential peaks are asymmetrical and rather broad. The new technique provides high sensitivity and better resolution than ordinary linear-sweep voltammetry. Application of the technique for detection in anodic stripping voltammetry is described in this paper.

THEORY

Consider the electrode reaction of an amalgamated metal, Rd, which is oxidized by a reversible reaction involving n electrons to a species soluble in the supporting electrolyte: Rd − ne ⇌ Ox. If the potential E of the amalgam

electrode, initially at a value E_0 so cathodic that no reaction occurs, is changed at a constant rate v, i.e. $E = E_0 + vt$, then established theory [4] shows that

$$E = E_{1/2} + (RT/nF) \ln \{-m/(m - m_a)\} \quad (1)$$

provided that transport is solely by semi-infinite linear diffusion. Here $E_{1/2}$ is the d.c. polarographic half-wave potential, and R, T and F have their usual meanings; m is used to symbolize the semiintegral of the current

$$m \equiv d^{-1/2}i/dt^{-1/2} = 1/\pi^{1/2} \int_0^t i(\lambda)\,(t - \lambda)^{-1/2}\,d\lambda \quad (2)$$

(where λ is simply a dummy variable for the integration) and m_a is the semi-integral of the diffusion current, being given by $m_a = -nAFC'D'^{1/2}$, where A is the surface area of the amalgam electrode, and C' and D' are the concentration and the diffusion coefficient of the amalgamated metal, respectively.

Differentiation of eqn. (1) with respect to time t gives the semiderivatives of the current:

$$e \equiv \frac{d^{1/2}}{dt^{1/2}}\, i = \frac{d}{dt}\, m = \frac{nFvm_a}{4RT}\, \mathrm{sech}^2 \left\{ \frac{nF}{2RT} [E_{1/2} - E] \right\} \quad (3)$$

This equation represents the shape of curves observed in semidifferential electroanalysis with an amalgam electrode. It corresponds to a symmetrical sharp peak. The peak height is given by

$$e_p = nFvm_a/4RT = -n^2F^2Av\,D'^{1/2}\,C'/4RT \quad (4)$$

and the peak potential is simply $E_p = E_{1/2}$, i.e. the d.c. polarographic half-wave potential. The peak width (the width of the peak at half of peak height) is given by $W_p = 3.53RT/nF$. Note that the peak height is proportional to the potential scan rate and the peak width is very dependent on the electron transfer number. The re-dissolution processes of metals accumulated on a hanging mercury drop by pre-electrolysis should obey eqns. (3) et seq.

EXPERIMENTAL

Apparatus and solutions

A function generator (FN Co., model FG-121B) was employed as the applied potential sweeper. The analog semidifferentiating circuit [2] of the current is shown in Fig. 1. The current flowing through the working electrode is converted to a voltage signal by means of the current follower (OP1). The OP1 output is fed to an operational amplifier (OP2) which has a resistance in feedback loop through the semidifferential element (SDE). The output voltage of the semidifferentiator (OP2) is

$$V_{out} = R_{f_1}R_{f_2}\,(C_1/R_1)^{1/2}\,(d^{1/2}\,i/dt^{1/2}) \quad (5)$$

where R_{f_1} and R_{f_2} are, respectively, the feedback resistances of OP1 and OP2;

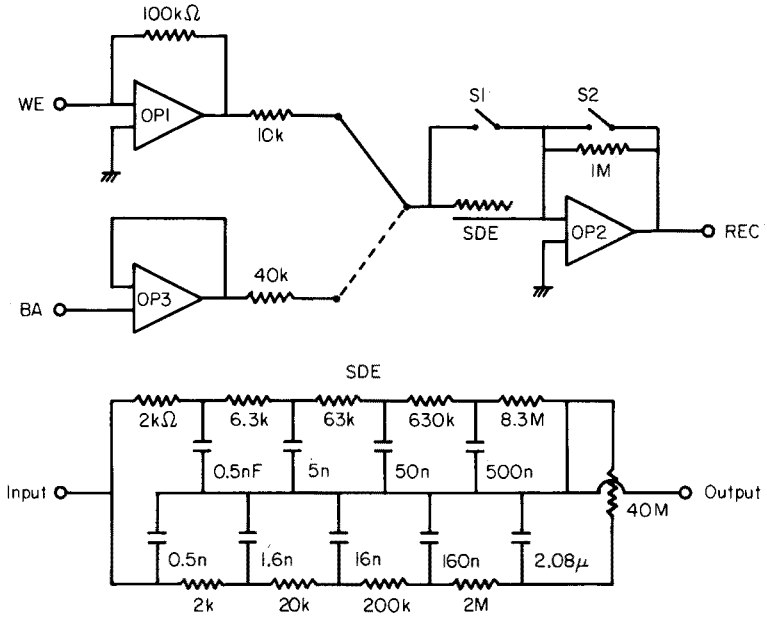

Fig. 1. Analog semidifferentiating circuit of current and semidifferential element (SDE). OP1, OP2, and OP3 are the operational amplifiers for current follower, semidifferentiator, and voltage follower, respectively; S1 and S2 are switches for circuit reset; WE is the working electrode; REC is the recorder, and BA the booster amplifier.

the $(R_1/C_1)^{1/2}$ ratio is a characteristic impedance term for the ladder network of the SDE, and i is the input current. In the present circuit, R_{f1} and R_{f2} are, respectively, 100 kΩ and 1.00 MΩ; R_1/C_1 is 1.00 MΩ μF^{-1}. Therefore

$$V_{out} = (1.00 \times 10^5)e \qquad (6)$$

The output voltage was recorded against the electrode potential on an X—Y recorder (Watanabe Co., model WA441). For trace analyses at the 10^{-9}—10^{-7} M level, a booster amplifier (Yanagimoto Co., model P8-CV) was used as the current—voltage converter and its output was fed to the voltage follower (OP3). The output of OP3 was connected with the semidifferentiator as shown by the dotted line via a 40 kΩ resistance to lower the noise level.

A hanging mercury drop electrode (Beckman model 39016) and a saturated calomel electrode with a large surface area were used as the working and counter electrodes, respectively. The latter also served as the reference electrode, and was connected with the cell through an agar salt bridge. A 50-ml glass beaker was used as the electrolytic cell; a magnetic stirrer (Toyo Co., model SS-5) with a rotating bar (8-mm diameter, 38-mm long) was used at about 100 rpm to stir the solutions.

All the solutions were prepared with reagent-grade chemicals. $Cd(NO_3)_2 \cdot 4H_2O$, $Pb(NO_3)_2$, and $TlNO_3$ were used as solutes; each stock solution was 1×10^{-3} M. The supporting electrolyte was 10^{-1} M KNO_3 at

different nitric acid concentrations. The electrolytic cell and all vessels used for sample preparation were filled with 1 M HNO_3 solution for 24 h, rinsed, and then filled with deionized water for 24 h before use.

Procedure

About 50 ml of sample solution was poured into the electrolytic cell and flushed with nitrogen for 10—15 min to remove dissolved oxygen. A hanging mercury drop of the required volume was then produced, and the required potential was applied for a defined time while the solution was stirred. After this pre-electrolysis time, the solution was left quiescent for 1 min under the applied potential; then the potential was swept anodically at a defined scan rate. During this re-dissolution process, the *e* vs. *E* curve was recorded.

RESULTS AND DISCUSSION

e *vs.* E *curves*

Figure 2 shows typical *e* vs. *E* curves of the re-dissolution processes for Cd^{2+}, Pb^{2+}, and Tl^{+}, as examples of species with 1e and 2e transfer processes.

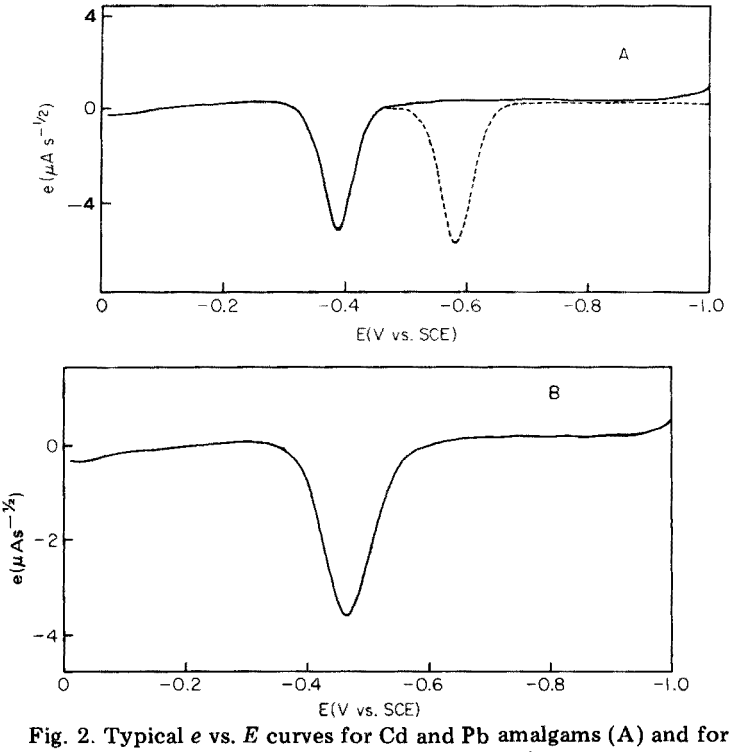

Fig. 2. Typical *e* vs. *E* curves for Cd and Pb amalgams (A) and for Tl amalgam (B). A: (——) 1.04 μM Pb^{2+} in 10^{-1} M KNO_3 plus 1.01 × 10^{-3} M HNO_3 at 29°C; (·····) 1.05 μM Cd^{2+} in 10^{-1} M KNO_3 at 28°C. B: 0.981 μM Tl^{+} in 10^{-1} M KNO_3 at 26°C. Potential scan rate, 140 mV s^{-1}; electrode area, 2.90 mm^2; pre-electrolysis potential, −1.0 V vs. SCE; pre-electrolysis time, 3 min stirring and 1 min quiescent; stirring speed, about 100 rpm.

The semiderivative of the current has the unit A $s^{-1/2}$. These curves were obtained at a scan rate of 140 mV s^{-1} after pre-electrolysis for 3 min at −1.0 V vs. SCE for about 1 μM solutions of each ion. As expected from theory, symmetrical peaks were observed for all three re-dissolution processes, although the peak for thallium was rather broader than those of Cd and Pb. The peak potentials were independent of pre-electrolysis time, electrode area, and anodic potential scan rate (Table 1); the average values were −0.585 V, −0.389 V, and −0.467 V vs. SCE for Cd, Pb, and Tl, respectively. The experimental peak potentials agree well with the literature values [5, 6] for the corresponding d.c. polarographic half-wave potentials (Table 1). The peak widths of the e vs. E curves, compared with the theoretical values predicted by the equation $W_p = 3.53RT/nF$, are also shown in Table 1. The average experimental peak width for thallium (89.6 mV) agrees well with the theoretical value, but the average peak widths for cadmium (56.8 mV) and lead (53.1 mV) are somewhat larger than the theoretical values. This seems to be due partly to the sphericity [3, 7] of the mercury drop electrode, and partly to the imperfect reversibility of the electrode reactions for the species considered.

TABLE 1

Peak potentials and peak widths of e vs. E curves for Cd, Pb, and Tl amalgams (The experimental conditions are those given in the legend for Fig. 2, except where otherwise specified below.)

Pre-electrolysis time (min)	A (mm^2)	v (mV s^{-1})	E_p (V vs. SCE)			W_p (mV)		
			Cd(Hg)	Pb(Hg)	Tl(Hg)	Cd(Hg)	Pb(Hg)	Tl(Hg)
1	2.90	100	−0.590	−0.392	−0.463	50	52	77
2	2.90	100	−0.590	−0.393	−0.466	50	45	93
3	2.90	100	−0.591	−0.393	−0.465	52	49	90
5	2.90	100	−0.591	−0.388	−0.462	57	56	90
7	2.90	100	−0.580	−0.385	−0.462	62	56	92
10	2.90	100	−0.575	−0.382	−0.468	70	61	93
3	0.89	100	−0.589	−0.380	−0.471	55	49	88
3	1.50	100	−0.585	−0.390	−0.475	55	52	87
3	2.48	100	−0.580	−0.392	−0.468	55	52	90
3	3.29	100	−0.586	−0.392	−0.470	55	52	90
3	4.02	100	−0.585	−0.388	−0.468	55	52	89
3	2.90	60	−0.582	−0.390	−0.468	55	52	87
3	2.90	80	−0.585	−0.390	−0.468	58	52	92
3	2.90	120	−0.585	−0.390	−0.468	60	55	91
3	2.90	140	−0.580	−0.389	−0.465	60	57	93
3	2.90	160	−0.583	−0.390	−0.468	60	58	92
			D.c. $E_{1/2}$ *values (V vs. SCE)*			*Theoretical values*		
			−0.578	−0.382	−0.455	46	46	92
			[5]	[5]	[5]			
			−0.59	−0.38	−0.46			
			[6]	[6]	[6]			

Dependence of peak height on pre-electrolysis time, anodic scan rate, electrode area, and pre-electrolysis potential

Figure 3(A) shows the relationship between peak height and pre-electrolysis time in stirred solutions, with all other parameters constant, for 1 μM solutions of Cd^{2+}, Pb^{2+} or Tl^{+}. In all cases, the relationship was linear for times up to about 7 min, but tended to deviate at longer times; this happens because metal deposited on the mercury surface diffuses into the mercury drop during long pre-electrolysis times. The positive intercept with the ordinate in Fig. 3(A) corresponds to pre-electrolysis for 1 min in a quiescent solution. It is clear that the peak height is proportional to the concentration of amalgamated metal, as predicted from eqn. (4). The peak heights were also proportional to the anodic potential scan rate in the range 40—200 mV s^{-1} (Fig. 3B). Figure 4(A) shows the non-linear dependences found between peak height and electrode area. As the working electrode used was a hanging mercury drop, its volume changed from 0.1 to 0.8 μl with change in surface area. It appears that a larger portion of deposited metal diffuses into the bulk mercury with increasing electrode area. For Cd^{2+}, Pb^{2+}, and Tl^{+}, almost constant peak heights were observed in the pre-electrolysis potential range of —0.7 to —1.1 V vs. SCE (Fig. 4B). Clearly, the three metal ions are quantitatively deposited on mercury by applying potentials in this range.

Analytical aspects

Figure 5 assesses how well the species is concentrated by pre-electrolysis for 2.10 μM Cd^{2+} in 10^{-1} M KNO_3 as an example. Curves (a) and (b) are the cyclic e vs. E curves obtained without and with pre-electrolysis. Comparison of peak heights between the reduction wave in curve (a) and the oxidation

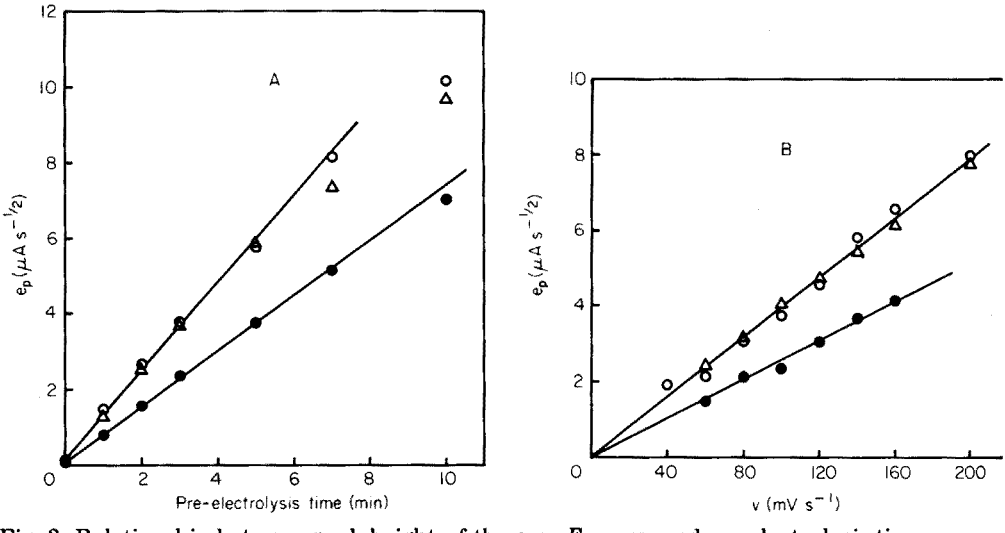

Fig. 3. Relationship between peak height of the e vs. E curves and pre-electrolysis time with stirring (A) and potential scan rate (B). Conditions except pre-electrolysis time or scan rate are the same as in Fig. 2. (○) Cd, (△) Pb, (●) Tl.

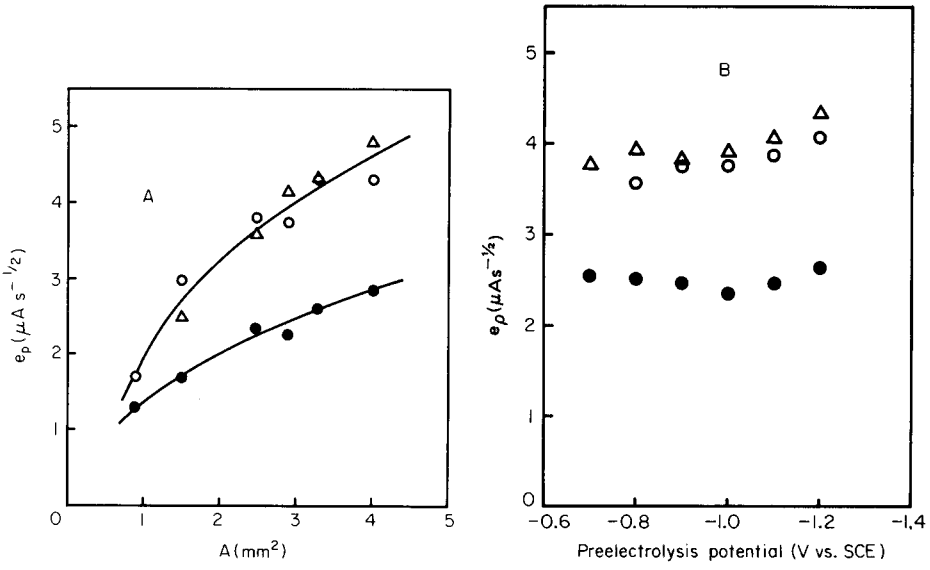

Fig. 4. Relationship between peak height of the *e* vs. *E* curves and electrode area (A) or pre-electrolysis potential (B). Conditions except electrode area or pre-electrolysis potential are the same as in Fig. 2. (○) Cd, (△) Pb, (●) Tl.

wave in curve (b) indicates that even such a short time of pre-electrolysis produces a signal about 23 times larger than the original one.

Calibration curves for Cd^{2+}, Pb^{2+}, and Tl^{+} are shown in Fig. 6. The relationships between peak height and concentration of each metal ion are linear in the range 20—100 nM. In the case of Pb^{2+}, the intercept with the ordinate corresponds to the amount of Pb^{2+} impurity in 10^{-1} M KNO_3. The relative standard deviations were about ±4%, ±7%, and ±7% for the determinations of Cd^{2+}, Pb^{2+}, and Tl^{+}, respectively, at the 20-nM level; the detection limits for Cd^{2+}, Pb^{2+}, and Tl^{+} were about 1 nM under the conditions specified.

In conclusion, anodic stripping voltammetry with semidifferential electroanalysis as the detector is a sensitive and relatively rapid method for the determination of trace species at levels of 0.1—10 ppb. The method is comparable with the well-established differential pulse stripping voltammetric method in sensitivity and precision. The stripping time is only a few seconds, but this must be weighed against the longer pre-electrolysis times necessary to achieve sensitivity comparable to that of d.p.a.s.v. It is, however, possible that this method may achieve higher sensitivity on application of faster scan rates. The instrumentation for the proposed method is simpler than that required for the differential pulse method.

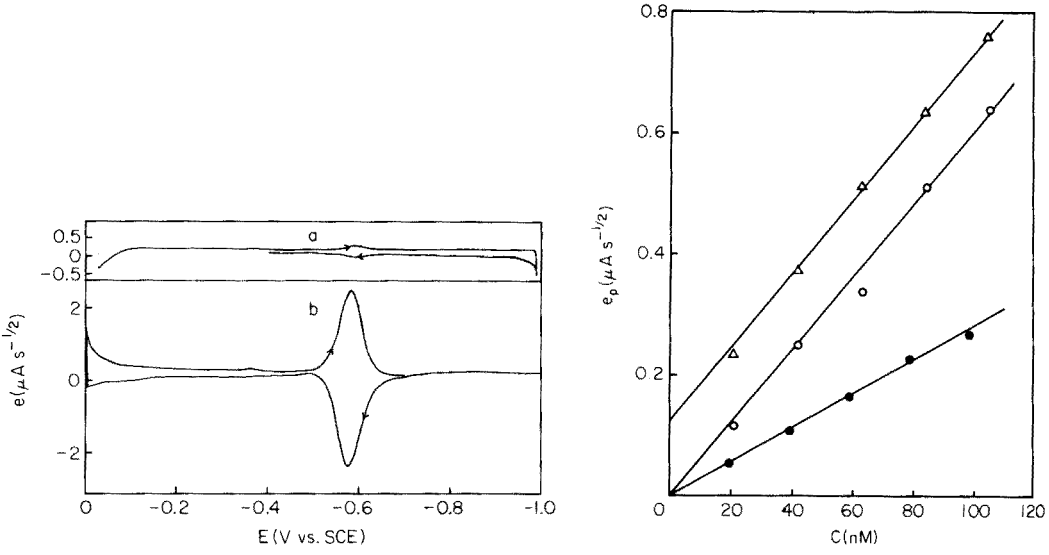

Fig. 5. Comparison between cyclic e vs. E curves with and without pre-electrolysis for 2.10 μM Cd^{2+} in 10^{-1} M KNO_3. Potential scan rate, 100 mV s^{-1}; electrode area, 4.69 mm^2; temperature, 28°C. (a) Without pre-electrolysis; (b) with pre-electrolysis for 1 min in stirred solution (ca. 100 rpm) and 1 min in quiescent solution at —1.0 V vs. SCE.

Fig. 6. Relationship between the peak height of e vs. E curves and the concentration of metal ions present in the original solution. Potential scan rate, 160 mV s^{-1}; electrode area, 1.50 mm^2; pre-electrolysis potential, —1.0 V vs. SCE; pre-electrolysis time, 10 min stirred and 1 min quiescent; stirring speed, ca. 100 rpm; supporting electrolyte, 10^{-1} M KNO_3 plus 10^{-2}M HNO_3. (○) Cd at 25°C; (△) Pb at 24°C; (●) Tl at 26°C.

REFERENCES

1 M. Goto and D. Ishii, J. Electroanal. Chem., 61 (1975) 361.
2 P. Dalrymple-Alford, M. Goto and K. B. Oldham, Anal. Chem., 49 (1977) 1390.
3 P. Dalrymple-Alford, M. Goto and K. B. Oldham, J. Electroanal. Chem., 85 (1977) 1.
4 M. Goto and K. B. Oldham, Anal. Chem., 45 (1973) 2043.
5 J. Heyrovsky and J. Kuta, Principles of Polarography, Academic Press, New York, 1965, p. 531.
6 M. Shinagawa, Polarography, Kiyoritsu Shiyupan, Tokyo, 1965, p. 295.
7 M. Goto and K. B. Oldham, Anal. Chem., 46 (1974) 1522.

Analytica Chimica Acta, 101 (1978) 139—144

ACID—BASE EQUILIBRIA IN THE MIXED SOLVENT 80% DIMETHYL SULFOXIDE—20% WATER

Part 2. Determination of pK Values and Investigation of the Conditions for Titration of some Aromatic Carboxylic Acids and their Conjugated Bases

MILKA GEORGIEVA

Institute of Chemical Technology, Darvenitza, Sofia (Bulgaria)

GEORGI VELINOV and OMORTAG BUDEVSKY*

Faculty of Pharmacy, Academy of Medicine, Ekz. Josif 15, Sofia (Bulgaria)

(Received 20th February 1978)

SUMMARY

The acid—base properties of some aromatic carboxylic acids of zero charge type HA have been investigated in the mixed solvent, 80% DMSO—20% water, by means of potentiometric measurements with a glass electrode. The pK_a values of the following aromatic carboxylic acids have been determined: benzoic, *o*-chlorobenzoic, *p*-chlorobenzoic, *m*-bromobenzoic, 2,4-dichlorobenzoic, 2,5-dichlorobenzoic, 2,6-dichlorobenzoic, 2,3,5-triiodobenzoic, 3,5-dinitrobenzoic, *p*-methylbenzoic, *m*-aminobenzoic, *o*-hydroxybenzoic 3,4-dihydroxybenzoic, 3,4,5-trihydroxybenzoic, *o*-methoxybenzoic, 2,3-dimethoxybenzoic, 5-amino-2-hydroxybenzoic, pyridine-2-carboxylic, thiophene-2-carboxylic, 1-naphthylacetic, diphenylglycolic. The mixed solvent investigated offers better titration conditions for the determination of these acids than water and some other non-aqueous solvents.

Part 1 of this series [1] showed that the mixed solvent, 80% dimethyl sulfoxide (DMSO)—water, has favourable properties which make it a suitable medium for the determination of a number of aliphatic carboxylic acids; this mixed solvent has good solvating ability, a relatively large pH region (18.40 units), high dielectric permeability (ca. 65), insignificant hygroscopicity, and the conventional glass electrode has a Nernstian pH response, so that reliable measurements can be made.

The present work reports the acid—base properties and the titration conditions for the determination of some aromatic carboxylic acids in the mixed solvent, 80% DMSO—water. The experimental titration curves coincide fairly well with the theoretical ones. These titration curves show that this mixed solvent provides better titration conditions for the determination of aromatic acids than water and some nonaqueous solvents, as was shown for aliphatic acids in Part 1.

EXPERIMENTAL

Dimethyl sulfoxide (Fluka) was purified as described previously [2]. The 80% DMSO—water mixture was prepared by weight (±0.01%) with redistilled water. Benzoic, *o*-chlorobenzoic, *p*-chlorobenzoic, *m*-bromobenzoic, 2,4-dichlorobenzoic, 2,5-dichlorobenzoic, 2,6-dichlorobenzoic, 2,3,5-triiodobenzoic, 3,5-dinitrobenzoic, *p*-methylbenzoic, *m*-aminobenzoic, *o*-hydroxybenzoic, 3,4-dihydroxybenzoic, 3,4,5-trihydroxybenzoic, *o*-methoxybenzoic, 2,3-dimethoxybenzoic, 5-amino-2-hydroxybenzoic, pyridine-2-carboxylic, thiophene-2-carboxylic, 1-naphthylacetic and diphenylglycolic acids (all reagent grade), as well as tetraethylammonium bromide (Fluka) were used without further purification. The potentiometric measurements were made, and standard solutions of hydrochloric acid and tetraethylammonium hydroxide (Et_4NOH) were prepared as described previously [1].

DISCUSSION

A solution (ca. 0.01 M) of the acid HA was titrated with ca. 0.02 M Et_4NOH. Titrations were carried out at constant ionic strength $I = 0.1$ (Et_4NBr). The cell was calibrated by means of the relationship [3]

$$pc_H = (E_{meas} - E_a^{0\prime})/0.05916$$

The specific constant of the cell, $E_a^{0\prime}$, determined in a preliminary experiment, includes the standard potential of the glass electrode, the potential of the reference electrode, activity coefficients and the liquid junction potential. This method of calibration is based on complete dissociation of the hydrochloric acid in the mixed solvent. With the electrodes used, the value $E_a^{0\prime} = 180.0 \pm 3.0$ mV was stable for many days and was used in the calculations.

The protolysis constants of the acids (pK_{HA}) were calculated from the experimental data by means of the Henderson—Hasselbach equation [4]. The value $pK_{SH}^{T} = 18.40$, determined previously [1] for the autoprotolysis constant of the mixed solvent, was used. In each calculation, the data around the buffer region in the titration of the acid with the base were used. Some characteristic titration curves are shown in Fig. 1. The curves have pronounced equivalence parts, but the equivalence points were determined by Gran's method [5], as the presence of impurities is evaluated by this method. The molarity of the tetraethylammonium hydroxide solution was checked periodically with standard hydrochloric acid in 80% DMSO—water.

Table 1 presents the pK_{HA}^{T} values for the aromatic carboxylic acids examined. The thermodynamic values of the constants were calculated from the stoichiometric values by means of the enlarged Debye—Hückel equation. The dielectric permeability of the solvent at 25°C was measured with a Radelkis Universal Dielectrometer type OH-301. The value $D = 65.2$ obtained was used in the calculation of the parameters in the Debye—Hückel equation.

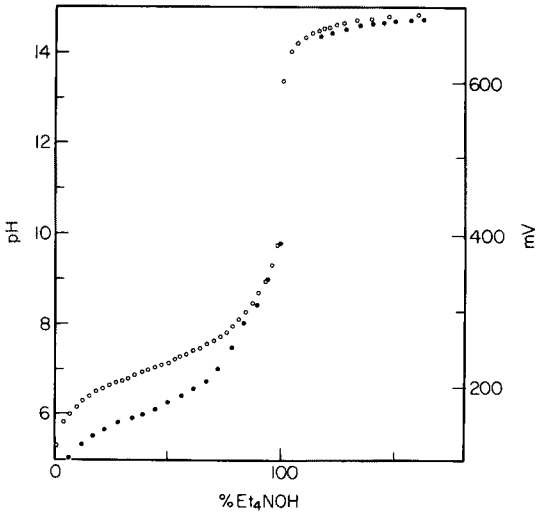

Fig. 1. Titration of benzoic (○) and *o*-chlorobenzoic (●) acids.

TABLE 1

pK values obtained for the aromatic monocarboxylic acids in the mixed solvent 80% DMSO—20% H_2O

Acid	pK^T_{HA}	pK^T_{HA} (H_2O)	ΔpK
Benzoic	7.32	4.20[a]	3.12
o-Chlorobenzoic	6.44	2.92[a]	3.52
p-Chlorobenzoic	6.48	3.98[a]	2.50
m-Bromobenzoic	6.66	3.81[a]	2.85
2,4-Dichlorobenzoic	5.66	2.68[a]	3.06
2,5-Dichlorobenzoic	5.62	2.47[a]	3.15
2,6-Dichlorobenzoic	5.60	1.59[a]	4.01
2,3,5-Triiodobenzoic	5.36		
3,5-Dinitrobenzoic	4.59	2.82[a]	1.77
p-Methylbenzoic	7.50	4.37[a]	3.13
m-Aminobenzoic	7.40	4.74[a]	2.66
o-Hydroxybenzoic	4.47	2.98[a]	1.49
3,4-Dihydroxybenzoic	7.61	4.49[a]	3.12
3,4,5-Trihydroxybenzoic	7.77	4.40[a]	3.37
o-Methoxybenzoic	7.21	4.09[a]	3.12
2,3-Dimethoxybenzoic	6.78		
5-Amino-2-hydroxybenzoic	5.69		
Pyridine-2-carboxylic	5.84	4.73[b]	1.11
Thiophene-2-carboxylic	5.92	3.53[b]	2.39
1-Naphthylacetic	7.74		
Diphenylglycolic (Benzilic)	5.25	3.04[c]	2.21

[a]Tables of Rate of Equilibrium Constants of Heterolytic Organic Reactions, Compiled by the Laboratory of Chemical Kinetics and Catalysis at Tartu State University, Editor V. A. Palm, Moscow 1975, Volume I. [b][4]. [c][8].

Column 4 of Table 1 presents the values $\Delta pK = pK^T_{HA}$ (80% DMSO—H_2O) — pK^T_{HA} (H_2O). From these values, it can be seen that the mixed solvent decreases the strength of the aromatic carboxylic acids of this zero charge type by ca. 3 pK units, and the length of the pH scale of the mixture investigated (pK^T_{SH} = 18.40) is ca. 4.4 pH units longer than that for water. Consequently, ca. 1.3—1.4 pH units are gained in the lengthening of the equivalence part of the titration curve.

Similar investigations showed that the titration of acids of zero charge type HA in various non-aqueous solvents is disadvantageous. The equivalence part of the titration curve is 2.0 pH units shorter in methanol than in water; in dimethylformamide and in acetonitrile the equivalence part is 2.9 and 3.0 pH units shorter respectively [6]. Thus the use of the DMSO—water mixture as a medium for the titration of the HA acids has an indisputable advantage.

Figure 2 shows the theoretical titration curves for 0.01 M benzoic acid in water (the dashed line) and in 80% DMSO—water (the full line); experimental data are also shown. The theoretical curves were constructed by a graphical method [7] from data obtained in the present investigation. As can be seen, there is good agreement between the theoretical curve and the experimental data; the graphical method for construction of titration curves is successful in water and in non-aqueous media. As the dilution effect was not taken into account, there is some deviation in the alkaline region. It is clear that the mixed solvent provides better titration conditions for the aromatic carboxylic acids than water, in which moreover, most of them are sparingly soluble.

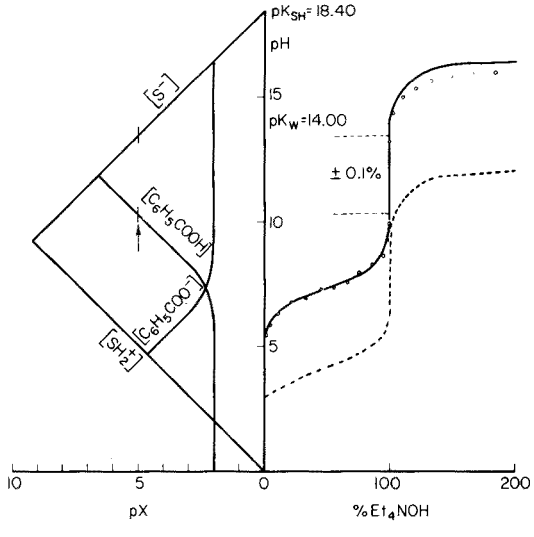

Fig. 2. Theoretical curves for titration of 0.01 M benzoic acid in 80% DMSO—water (full line) and in water (dashed line). The points show the experimental data.

The base constants of the conjugated bases, i.e. charge type A^-, can be calculated by means of the well-known relationship $pK^T_{A^-} = pK^T_{SH} - pK^T_{HA} = 18.40 - pK^T_{HA}$. Calculations showed that the strength of these bases was weakened by ca. 1.2—1.4 pK units compared with water. Consequently, the titration conditions for such bases in the mixed solvent are improved by ca. 3 pH units because of the extended equivalence part of the titration curve. Figure 3 shows the theoretical titration curves for 0.1 M sodium benzoate with hydrochloric acid in water and in 80% DMSO—water and also the experimental data for the titration in the mixed solvent. The equivalence part of the curve in water is very short (the dashed line); visual determination of the equivalence point is not possible. The titration of sodium benzoate in 80% DMSO—water can be performed visually (±0.3%), however, the equivalence part of the titration curve (the full line) is long enough to permit the use of an acid—base indicator. The DMSO—water mixture is therefore more suitable than water for the titration of aromatic bases of charge type A^-.

Comparison of the quantitative relations obtained earlier [1] with those reported here shows that the mixed solvent weakens the strength of the aliphatic and aromatic carboxylic acids in a different manner. The solvent shows some differentiating effect but it is small (of the order of 0.4 pK units) and is not of interest in analytical practice.

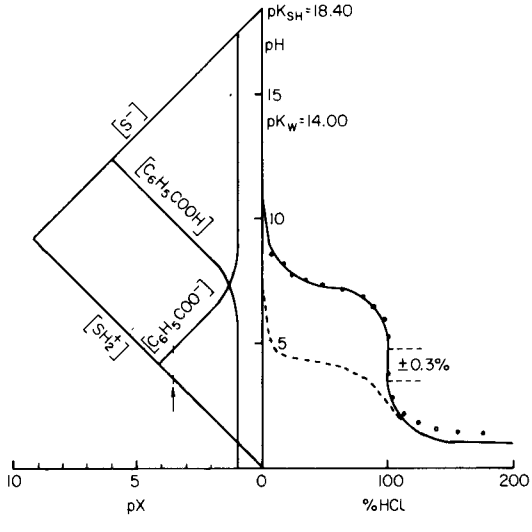

Fig. 3. Theoretical curves for titration of 0.1 M sodium benzoate in 80% DMSO—water (full line) and in water (dashed line). The points show the experimental data.

REFERENCES

1 M. Georgieva, G. Velinov and O. Budevsky, Anal. Chim. Acta, 90 (1977) 83.
2 P. Longhi, T. Mussini and M. Veleva, Anal. Quim., 71 (1975) 1043.
3 J. Tencheva, G. Velinov and O. Budevsky, J. Electroanal. Chem., 68 (1976) 65.
4 A. Albert and E. P. Serjeant, Ionization Constants of Acids and Bases, J. Wiley, New York, 1962.
5 F. J. C. Rossotti and H. Rossotti, J. Chem. Educ., 42 (1965) 377.
6 O. Budevsky, Fundamentals of Analytical Chemistry, Medicina i Fizkultura, Sofia, 1974 (in Bulgarian).
7 O. Budevsky, Graphical Method for Construction of Titration Curves, in E. Wänninen (Ed.), Analytical Chemistry, Essays in Memory of Anders Ringbom, Pergamon Press, 1977, p. 169.
8 W. Huber, Titrations in Non-aqueous Solvents, Academic Press, New York and London, 1977.

Analytica Chimica Acta, 101 (1978) 145—155

CONTROLE DE LA PURETE D'ECHANTILLONS DE NICKEL PAR SPECTROMETRIE-γ DIRECTEMENT APRES IRRADIATION AU MOYEN DE NEUTRONS THERMIQUES

P. BENABEN* et R. TARDY

Département de Métallurgie, Ecole Nationale Supérieure des Mines, 158 Cours Fauriel, 42023 Saint-Etienne Cédex (France)

N. DESCHAMPS

Laboratoire d'Analyse par Activation Pierre Sue, C.N.R.S., C.E.N. Saclay, 91190 Gif-sur-Yvette (France)

(Reçu le 29 novembre 1977)

RÉSUMÉ

Nous décrivons les possibilités d'analyses d'échantillons de nickel de haute pureté par spectromètrie-γ directe au moyen d'un détecteur Ge(Li) après activation neutronique. Les échantillons (300—600 mg) sont irradiés 65 h, dans une position où le flux de neutrons est le plus thermique. Après décroissance de la radioactivité due à la matrice, nous avons examiné les possibilités de dosage simultané de 33 éléments: pour 18, qui sont les impuretés les plus courantes dans le nickel, en prenant comme référence des étalons de ces éléments irradiés dans les mêmes conditions expérimentales; pour 15, par un calcul effectué grâce aux caractéristiques nucléaires des radioisotopes pouvant être détectés après activation neutronique. Il est possible de doser 22 éléments dans des échantillons de nickel aux concentrations inférieures à 0,1 $\mu g\ g^{-1}$. Cette méthode d'analyse simple est accessible à des laboratoires situés loin des installations d'irradiation.

SUMMARY

Purity control of high-purity nickel by direct γ-spectrometry after irradiation with thermal neutrons

The possibilities of analysing high-purity nickel samples by direct γ-spectrometry with a Ge(Li) detector after neutron activation are described. The samples (300—600 mg) are irradiated for 65 h in a thermal neutron flux of 5×10^{12} n cm^{-2} s^{-1} and the matrix radioactivity is then allowed to decay for 30 h. It is possible to determine simultaneously 18 elements (the commonest impurities in nickel) by using standards containing known quantities of these elements irradiated under the same experimental conditions. Concentration limits are calculated for 15 elements based on the nuclear characteristics of the radio-isotopes which can be detected by neutron activation. It should be possible to determine 22 elements in nickel samples, at concentrations below 0.1 $\mu g\ g^{-1}$. The method is suitable for laboratories situated far from irradiation facilities.

Poursuivant ses travaux dans le domaine de l'élaboration des métaux de haute pureté, le Département de Métallurgie (E.N.S.M.) a entrepris la fabrication de nickel en qualité et quantité semblables à celles du fer qu'il produit

actuellement [1]. Pour garantir cette production, l'analyse par activation s'impose en raison de ses performances dans le domaine du dosage des traces. Cependant il n'est pas nécessaire d'obtenir les meilleures limites de détection possibles par cette méthode; l'objectif principal est de réaliser une analyse portant sur un certain nombre d'éléments représentatifs de la pureté du métal, avec des limites de détection de l'ordre de 0,1 $\mu g\ g^{-1}$.

Nous avons étudié les possibilités de l'analyse par spectrométrie-γ, directement après irradiation en mesurant la radioactivité induite par des neutrons thermiques sur des échantillons de nickel de haute pureté au moyen d'un détecteur Ge(Li).

De nombreux auteurs ont décrit les résultats obtenus par l'analyse par spectrométrie-γ, directement après irradiation sur des échantillons de métaux de haute pureté, cependant à notre connaissance, aucune étude de ce type n'a été effectuée sur des échantillons de nickel. Les analyses qui ont été réalisées sur ce métal, l'ont été après séparations chimiques [2].

Les résultats que nous présentons portent sur 33 éléments dont 22 sont donnés, dans les cas favorables, avec des limites supérieures de concentration de 0,1 $\mu g\ g^{-1}$.

PARTIE EXPERIMENTALE

Conditions d'irradiation

Nous avons éliminé la possibilité d'utiliser les particules chargées ou les photons-γ pour une analyse multiélémentaire d'échantillons de nickel par spectrométrie-γ directement après irradiation. La période radioactive et l'énergie des photons-γ des radioisotopes issus de la matrice lors de telles irradiations empêchent ou gênent de façon importante la détection des impuretés.

TABLEAU 1

Caractéristiques des principales réactions nucléaires et des radioisotopes obtenus par action des neutrons sur les isotopes stables du nickel

Isotopes	Réaction nucléaire	Seuil (MeV)[a]	Radioisotopes obtenus	$t_{1/2}$[b]	Principaux gamma (keV)[b]
^{58}Ni	n, p	0	^{58}Co, ^{58m}Co	71,3 j; 9,15 h	511; 810,6 // 7; 24,9
	n, 2n	12,4	^{57}Ni	36 h	127,3; 511
^{60}Ni	n, p	2,07	^{60}Co; ^{60m}Co	5,263 ann.; 10,47 min	1173,2; 1332,5 // 58,6; 1332,5
^{61}Ni	n, p	0,52	^{61}Co	1,605 h	67,4
^{62}Ni	n, α	0,43	^{59}Fe	44,6 j	142,5; 192,2; 1099,3; 1291,6
	n, p	4,51	^{62}Co	13,5 min	777,8; 874,9; 1129,1; 1163,0; 1172,0; 1717,0
^{64}Ni	n, γ	0	^{65}Ni	2,544 h	366,5; 1115,45; 1481,7
	n, α	0	^{61}Fe	6,07 min	120,0; 177,1; 297,3; 4000; 1025,0; 1204,0; 1636,0
	n,p	0	^{64m}Co	28 s	95

[a]Les valeurs sont extraites de la réf. [3]. [b]Les valeurs sont extraites de la réf.[4].

Nous nous sommes intéressés aux possibilités offertes par l'activation neutronique. Nous avons rassemblé dans le Tableau 1, les caractéristiques nucléaires des principaux radioisotopes qui peuvent se créer par réaction avec les neutrons sur les isotopes stables du nickel. On constate qu'en irradiant les échantillons dans un flux de neutrons le plus thermique possible, on s'affranchit d'autant de la production de radioisotopes issus de la matrice par réaction (n, p), (n, α), et on obtiendra essentiellement le radioisotope ^{65}Ni ($t_{1/2}$ 2,52 h) par la réaction nucléaire ^{64}Ni (n, γ) ^{65}Ni. L'analyse par spectrométrie-γ directement après irradiation sera ainsi possible après attente de la décroissance de la radioactivité de ce radioisotope (30 h).

Cependant, cette attente perturbe quelque peu les analyses car elle empêche le dosage des éléments qui par activation neutronique donnent principalement des radioisotopes de courte période (Al, Ca, Ti, V, Mn $\cdots$).

Les échantillons, les étalons et les témoins d'irradiation ont été irradiés 65 h à la pile EL3 du Centre d'Etudes Nucléaires de Saclay. Le canal dans lequel ont eu lieu les irradiations permet d'obtenir un flux de neutrons thermalisés dont les caractéristiques sont approximativement: flux de neutrons thermiques, 5×10^{12} n cm^{-2} s^{-1} et flux de neutrons rapides, 10^{10} n cm^{-2} s^{-1}.

Etalonnage

Afin de réaliser une analyse quantitative, nous irradions simultanément échantillons et étalons. Ces derniers sont constitués par un dépôt sur papier filtre d'une quantité connue (généralement 20 μl) d'une solution de titre bien déterminé de l'élément à doser (Titrisol, Merck ou Standard per Assorbimento Atomico, Carlo Erba) ou des solutions étalons obtenue par mise en solution soit de l'élément soit d'un sel aussi purs que possible.

Grâce au haut pouvoir de résolution des détecteurs Ge(Li), nous pouvons utiliser des multiétalons qui évitent ainsi la contrainte fastidieuse de compter chaque étalon séparément. Nous avons réparti ces étalons en plusieurs groupes en éliminant les possibilités d'interférences de raies-γ entre les radioisotopes issus des éléments constitutifs. Par exemple, nous avons groupé les étalons Co, Au, Cr, Mo d'une part, et Cu, As, Pt, Cd d'autre part.

Le contrôle après irradiation d'un morceau de papier filtre initial nous a permis de constater que le seul élément constitutif créant une activité mesurable dans les conditions de mesure des étalons, était le sodium. Pour résoudre le problème de l'étalonnage pour le dosage de cet élément, nous irradions plusieurs étalons de Na à teneurs différentes, et connaissant la masse des papiers filtres et la contribution aux étalons Na du papier (déterminée par plusieurs mesures), il est possible de déterminer la valeur de l'activité en ^{24}Na due exclusivement au sodium déposé.

Pour des raisons de sureté d'analyse, nous irradions simultanément un échantillon (environ 300 mg) de nickel pur (Johnson-Matthey), dont nous réalisons l'analyse comme pour les échantillons à contrôler. Cela nous permet d'éviter au maximum toute possibilité de résultats erronés car l'homogénéité

de ces échantillons témoins étant pratiquement certaine, cela nous permet d'écarter les erreurs éventuelles inhérentes aux conditions de mesure (contamination du détecteur, source radioactive à proximité).

Enfin nous irradions aussi 3—10 mg d'un échantillon de fer (Bureau of Analysed Samples, spectroscopic standard) à teneur certifiée en certains éléments autre que le fer (Cr, Co, As, Sb, W ···) et dont nous réalisons à chaque fois le dosage. Ceci nous permet en confrontant les résultats obtenus à l'analyse certifiée de vérifier nos étalons.

Mesure d'activité

Les premières mesures d'activité sont réalisées sur les échantillons environ 30 h après la fin de l'irradiation, afin de permettre la décroissance de la radioactivité due au ^{65}Ni. Nous effectuons ces mesures durant 15 h et, afin de suivre la décroissance de la radioactivité des radioisotopes qui le permettent (^{24}Na, ^{64}Cu, ^{76}As ...), nous les répétons dans le temps.

La chaîne de spectrométrie-γ comprend un détecteur Ge(Li) et un analyseur 4000-canaux (DIDAC Intertechnique) avec sortie des résultats grâce à une imprimante rapide et traitement manuel. Les 6 premières analyses ont été réalisées au moyen d'un détecteur de 3 keV de résolution et de 6% d'efficacité par rapport à un NaI de 76 × 76 mm (ces valeurs étant données pour la raie à 1332,5 keV du ^{60}Co). Les deux dernières ont été réalisées au moyen d'un détecteur de 2,0 keV de résolution et de 16,1% d'efficacité (dans les mêmes conditions).

Les échantillons (300—600 mg) sont décapés avant et après irradiation dans un mélange HF—HNO_3 (1 + 1 v/v), pesés et mis en solution à chaud dans l'acide nitrique dilué. Afin d'obtenir des conditions géométriques de comptage les plus reproductibles possibles, les étalons sont eux aussi dissous dans un mélange HNO_3—H_2SO_4, volumés et placés dans des récipients identiques à ceux utilisés pour les échantillons.

RESULTATS ET DISCUSSION

Nous donnons dans le Tableau 2 les résultats obtenues lors de l'analyse de 8 échantillons de nickel. Sur les 18 éléments étudiés, il est intéressant de constater que 12 sont donnés à des teneurs ou avec des limites de détection inférieures à 0,1 $\mu g\ g^{-1}$ et que d'autre part, Fe, Co et Cu ont des teneurs voisines de quelques $\mu g\ g^{-1}$. Ceci montre que le nickel obtenu est d'une très bonne pureté en particulier pour le fer et cobalt.

On peut s'étonner de la présence bien qu'infime de métaux précieux (Au, Pt, Ir). Il semble que cela soit dû à une attaque par le chlore, de la plaque en platine irridié, utilisée comme anode dans le processus de fabrication (électrolyse du clorure de nickel).

Nous avons constaté que les réactions (n, p) sur les isotopes stables du nickel se produisent et ceci bien que l'irradiation soit effectuée dans un flux de neutrons thermalisés. C'est ainsi que l'on détecte la présence de ^{58}Co

TABLEAU 2

Résultats des analyses portant sur 8 échantillons de nickel pur
(Les valeurs sont données en $\mu g\ g^{-1}$.)

Eléments dosés	Ni 1	Ni 2	Ni 3	Ni 4	Ni 5	Ni 6	Ni 7	Ni 8
Na	<0,1	<0,1	<0,01	0,016	<0,006	<0,003	<0,001	<0,001
K	<0,15	<0,1	<0,025	<0,1	<0,05	<0,03	<0,008	<0,03
Cr	<0,25	<0,45	<0,12	<0,1	<0,04	<0,06	<0,05	<0,075
Fe	<12	<15	<5,5	<4,3	1,7	2,1	<2,0	<2,0
Co	<1,5	<1,5	$1,7 < x < 1,1$	$1,6 < x < 1,0$	<1,8	<2	$1,4 < x < 0,6$	$1,4 < x < 0,6$
Cu	0,9	0,9	1,2	1,1	2,1	1,9	1,3	1,4
Zn	<1	<1	<0,2	<0,2	<0,9	<0,5	<0,13	<0,57
Ga	<0,01	<0,01	<0,002	<0,005	<0,005	<0,003	<0,001	<0,003
As	0,12	0,10	0,04	0,04	0,02	0,03	0,029	0,029
Se	<3	<2	<0,1	<0,1	<0,04	<0,07	<0,03	<0,04
Mo	<0,15	<0,2	<0,05	<0,06	<0,02	<0,03	<0,02	<0,035
Ag	0,8	0,5	0,44	0,40	0,22	0,39	0,29	0,36
Cd	<0,15	<0,25	<0,05	<0,05	<0,03	<0,04	<0,02	<0,03
Sb	0,03	0,04	0,005	0,005	0,005	0,007	0,012	0,013
W	0,015	0,017	0,006	0,006	0,006	0,005	0,009	0,011
Ir	<0,1	<0,1	<0,1	<0,1	<0,1	<0,1	<1	<1
Pt	<0,1	<0,15	0,11	0,125	0,04	0,07	0,175	0,19
Au	0,0005	0,0004	0,0003	0,0003	0,0003	0,0005	0,009	0,008

(émetteur β^+ et de rayons-γ d'énergie 810,6 keV) et de ^{60}Co (émetteur-γ d'énergie 1173,2 keV et 1332,5 keV) qui sont obtenus par les réactions nucléaires ^{58}Ni (n, p) ^{58}Co et ^{60}Ni (n, p) ^{60}Co.

Calcul des teneurs et des limites supérieures de concentration

Pour les éléments détectés dans nos échantillons et pour lesquels nous avons irradié un étalon, la méthode de calcul de teneur est simple et bien connue, nous ne reviendrons pas sur ce type de détermination.

Dans notre cas, la nature des impuretés présentes étant reproductibles au cours des différentes fabrications; cela nous permet de prévoir la nature des étalons à irradier.

Excepté pour l'iridium, tous les éléments détectés ont été dosés. Pour plus de sécurité, nous irradions aussi certains étalons d'éléments qui pourraient éventuellement se trouver en impureté (par exemple, Zn, Ga, Mo, Cd).

Dans le cas où l'élément à doser n'a pu être détecté, nous déterminons une valeur supérieure de la concentration en utilisant un critère statistique fondé sur l'étude proposée par Currie [5] qui conduit à une limite de détection $L_D = 2{,}71 + 4{,}65\ (\mu_B)^{1/2}$ où μ_B représente l'intégrale du fond continu prise sur une bande d'énergie correspondant à celle retenue pour l'étalon. Dans ces conditions, nous pouvons calculer une limite supérieure de concentration pour l'élément correspondant, en attribuant à chacune de ses raies-γ, le nombre d'impulsions égal à la limite de détection L_D et en choisissant comme limite, la plus faible des valeurs obtenues.

Interférences nucléaires et de raies-γ

Dosage du cobalt. Dans nos conditions de mesures, le dosage du cobalt ne peut se faire que grâce aux raies-γ du ^{60}Co. Pour chiffrer l'interférence due à la matrice, on pourrait avoir recours à la double irradiation "hors cadmium et sous cadmium". Nous ne l'avons pas fait pour des raisons pratiques, mais nous avons préféré utiliser les résultats que nous avons obtenus lors de l'irradiation des échantillons témoins de nickel.

En effet, nous dosons le cobalt apparent dans ces échantillons témoins, c'est-à-dire en considérant que tout le ^{60}Co détecté est issu de la réaction (n, γ). Il est évident que cette teneur apparente est au plus égale à l'interférence due à la matrice et, chiffrée en $\mu g\ g^{-1}$, elle permet de donner une valeur supérieure, lors de l'irradiation considérée, de l'interférence due au nickel dans les échantillons analysés simultanément. Dans notre cas, cette façon de procéder est favorable car la teneur en cobalt des échantillons à analyser est plus forte que celle des échantillons témoins

Par exemple, dans le cas des échantillons de nickel 3 et 4, la teneur apparente du nickel témoin irradié dans les mêmes conditions a été trouvée égale à 0,6 $\mu g\ g^{-1}$ de Co alors que la teneur apparente des échantillons de nickel à analyser était de 1,7 et 1,6 $\mu g\ g^{-1}$. La teneur en cobalt réele de ces échantillons est donc comprise respectivement entre: 1,7 et 1,7 — 0,6 (= 1,1 $\mu g\ g^{-1}$); et 1,6 et 1,6 — 0,6 (= 1,0 $\mu g\ g^{-1}$).

Dans le cas où une meilleure précision sur le dosage du cobalt est demandée, il faut chiffrer cette interférence mais il est nécessaire, lors de chaque série de manipulation, de réaliser une double irradiation car il paraît fort probable qu'au cours du temps le rapport flux thermique sur flux rapide varie, que la répartition en énergie du flux de neutrons varie et donc que la valeur de cette interférence subisse des modifications sensibles.

Dosage du cuivre. Après une attente de 30 h, le dosage du cuivre ne peut se faire que par le radioisotope ^{64}Cu ($t_{1/2}$ = 12,74 h). A faible teneur en cuivre des échantillons, ce radioisotope n'est détectable en spectrométrie-γ que par sa raie à 511 keV due à l'annihilation du rayonnement β^+. Cependant, le ^{58}Co issu de la matrice est lui aussi émetteur β^+ et perturbe donc le dosage.

La différence entre les périodes radioactives de ces deux radioisotopes (12,74 h pour ^{64}Cu et 71,3 jours pour ^{58}Co) permet, par une étude de la décroissance de la radioactivité à cette énergie de réaliser le dosage d'autant que, dans nos conditions d'irradiation et pour la teneur en cuivre des échantillons analysés (environ 1 $\mu g\ g^{-1}$) la radioactivité due au cuivre à l'énergie considérée est 4 fois plus forte que celle due au ^{58}Co lors des premières mesures d'activité.

D'autre part, il nous est possible de vérifier nos résultats. En effet le ^{58}Co émet des rayons-γ à 810,6 keV. Après avoir déterminé la valeur du rapport de l'activité sous le pic à 810,6 keV à celle de 511 keV du ^{58}Co pur, pour le détecteur sur lequel se font les mesures, il est possible, lors des différents comptages d'en déduire la contribution à 511 keV du ^{58}Co (en connaissant l'activité à 810,6 keV) et par suite de vérifier la teneur en cuivre.

Problème du dosage du chrome en présence d'iridium. Nous avons constaté la présence d'iridium dans tous les échantillons de nickel analysés. N'ayant pas à notre disposition d'étalon iridium, nous n'avons pu doser cet élément. Nous pouvons cependant estimer, à partir des constantes radioactives, des différents radioisotopes de cet élément, que la teneur est inférieure à 0,1 $\mu g\ g^{-1}$ pour les 6 premiers échantillons et 1 $\mu g\ g^{-1}$ pour les deux derniers, cette estimation étant assez grossière. Cet élément, très sensible en analyse par activation, pose certains problèmes pour le dosage du chrome.

En effet par réaction (n, γ) sur l'un des isotopes stables de l'iridium (^{191}Ir), on obtient le radioisotope ^{192}Ir ($t_{1/2}$ = 74,2 jours) et qui émet en particulier des rayons-γ d'énergie 316,5 keV, énergie très voisine de l'énergie du rayonnement-γ, unique, émis par le ^{51}Cr (320, 1 keV) seul radioisotope utilisable ici pour effectuer le dosage du chrome. Il est nécessaire lors de chaque analyse de tracer le spectre canal par canal dans la zone d'énergie considérée (300—340 keV et d'examiner attentivement l'allure de ce spectre à l'énergie du rayonnement-γ du ^{51}Cr. Nous n'avons jamais détecté ce radioisotope; cependant la limite supérieure de concentration pour le chrome se trouve réhaussée de façon importante à cause de l'activité due au rayonnement de l'iridium qui recouvre en partie la zone d'intérêt pour le dosage du chrome.

Dosage du fer après séparations chimiques

Les premières analyses que nous avons réalisées par spectrométrie-γ, directement après irradiation ont conduit à des limites supérieures de concentration élevées pour le fer (de l'ordre de 10 $\mu g\ g^{-1}$). Cela est dû essentiellement à la faible abondance isotopique du ^{58}Fe (0,31%) sur lequel se produit la réaction (n, γ) produisant du ^{59}Fe, seul radioisotope utilisable pour effectuer ces dosages.

Pour obtenir une meilleure sensibilité, nous avons effectué une séparation radiochimique du ^{59}Fe [6]. En milieu acide chlorhydrique 12 M additionné de quelques gouttes d'eau oxygénée 110 vol., Fe(III) et Co(II) sont fixés sur résine anionique Dowex 1-X 10 (200—400 mesh forme Cl^-) alors que Ni(II) n'est pas retenu. On élue ensuite sélectivement le fer sous forme de Fe(II) par passage sur la résine d'une solution HCl 5 M—$TiCl_3$ 10% (en volume). Dans ces conditions, il nous a été possible de doser, 1,7 $\mu g\ g^{-1}$ de fer dans un échantillon de nickel. Il faut signaler que ces résultats obtenus après une durée de mesure de 15 h, grâce à un détecteur NaI de 76 × 76 mm, constituent pratiquement une limite de détection.

Avec le détecteur Ge(Li) de 16,1% d'efficacité, nous avons obtenu des limites de détection pour la même durée de mesure et sans séparations chimiques de 2 $\mu g\ g^{-1}$, ce qui est assez proche de la limite de détection obtenue grâce à un cristal NaI après séparations chimiques.

Il semblerait donc que la perte en efficacité d'un détecteur Ge(Li) par rapport à un NaI soit, dans le cas présent, largement compensée par un gain en résolution sur la mesure de la radioactivité.

Estimation de certaines limites supérieures de concentration

Il nous a semblé intéressant pour poursuivre cette étude d'examiner les possibilités que pouvait offrir ce type d'analyse pour un grand nombre d'éléments. Nous avons alors tenté de déterminer un certain nombre de limites de dosage pour des éléments dont nous n'avons pas irradié d'étalons. Pour celà, nous avons procédé en deux étapes.

(1) Nous vérifions, par l'examen du spectre-γ et la connaissance des caractéristiques nucléaires des radioisotopes [7] pouvant se former sur l'impureté envisagée par réaction (n, γ) que cet élément n'est pas détectable dans nos conditions de mesure.

(2) Connaissant les caractéristiques nucléaires de ce radioisotope et les constantes des réactions nucléaires (n, γ) pouvant lui donner naissance [8], nous calculons la radioactivité correspondante qu'aurait un étalon de cet élément, irradié dans les mêmes conditions qu'un étalon dont on a mesuré la radioactivité d'un des radioisotopes obtenu, et qui émet des photons-γ d'énergie voisine (pour minimiser l'influence de la variation du rendement du détecteur en fonction de l'énergie).

En tenant compte de la section efficace, du facteur d'irradiation, du temps de décroissance de la radioactivité, de l'abondance isotopique, du rendement d'émission des rayons-γ, il est possible de donner une valeur

approximative de l'étalon fictif pour l'élément à doser et donc, de déterminer une limite supérieure de concentration. Cette méthode n'est pas assez précise pour un calcul de teneur, mais elle permet d'obtenir une valeur indicative de la limite supérieure de concentration, compte tenu que l'irradiation se fait dans un flux de neutrons thermalisés et que l'activation dûe aux neutrons rapides peut-être, dans la plupart des cas, négligée.

Nous présentons dans le Tableau 3 les résultats que nous avons obtenus lors de ces calculs. Ces résultats ainsi que ceux obtenus avec les étalons permettent de montrer qu'il est possible de doser 33 éléments dans des échantillons de nickel dont 22 avec des limites supérieures de concentration plus petites que 0,1 $\mu g\ g^{-1}$. Nous donnons dans le Tableau 4 les limites de dosage dans des échantillons de nickel, regroupés en grande classe; on peut

TABLEAU 3

Limites théoriques ($\mu g\ g^{-1}$) calculées grâce aux constantes nucléaires des différents radio-isotopes pour 6 échantillons de nickel pur

Eléments étudiés	Ni_1	Ni_3	Ni_5	Ni_6	Ni_7	Ni_8
Sc	<0,004	<0,0008	<0,004	<0,002	<0,0005	<0,0007
Ru	<0,7	<0,3	<0,3	<0,3	<1	<0,8
Te	<0,4	<1	<2	<1,5	<0,4	<1,5
La	<0,0006	<0,0001	<0,0001	<0,0001	<0,0001	<0,0002
Ce	<0,15	<0,02	<0,015	<0,02	<0,008	<0,015
Pr	<0,001	<0,001	<0,0003	<0,0002	<0,0001	<0,00015
Nd	<7	<1	<3	<3	<1,5	<1,5
Sm	<1,5	<0,5	<0,7	<0,7	<0,3	<0,4
Gd	<0,03	<0,01	<0,004	<0,006	<0,005	<0,007
Tb	<0,005	<0,0025	<0,001	<0,001	<0,001	<0,002
Ho	<0,001	<0,002	<0,001	<0,0006	<0,0002	<0,0002
Lu	<0,01	<0,0004	<0,0001	<0,0002	<0,0002	<0,0002
Hf	<0,07	<0,02	<0,03	<0,03	<0,3	<0,3
Ta	<0,02	<0,002	<0,02	<0,1	<0,002	<0,01
Re	<0,0002	<0,005	<0,002	<0,003	<0,002	<0,003

TABLEAU 4

Limite de dosage ($\mu g\ g^{-1}$) pour les impuretés dans le nickel

$10 > x > 1$	$1 > x > 0,1$		$x < 0,1$			
Fe	Co	Ag	Na	Mo	Tb	Pt
Te	Cu	Sm	K	Cd	Ho	Au
Nd	Zn	Hf	Sc	Sb	Lu	
	Ru		Cr	La	Ta	
			Ga	Ce	W	
			As	Pr	Re	
			Se	Gd	Ir	

ainsi trouver rapidement l'ordre de grandeur de la limite de dosage pour un élément à doser dans des échantillons de ce type.

Cas du fer. La limite supérieure de concentration obtenue pour le dosage du fer est assez élevée, et il paraît souhaitable de s'intéresser à d'autres possibilités pour le dosage de cet élément. Ainsi, il semble qu'une séparation chimique identique à celle que nous avons réalisée et une mesure d'activité effectuée sur le détecteur Ge(Li) à 16,1% d'efficacité permettrait de réduire sensiblement cette limite de dosage.

D'autre part, il est possible d'envisager d'utiliser les protons de moyenne énergie (10 MeV) pour affiner le dosage du fer dans le nickel. Nous avons déjà montré tout l'intérêt que présentait de telles particules pour le dosage du fer dans le cobalt (limite théorique de 0,1 $\mu g\ g^{-1}$) [9]. En effet par irradiation dans un flux de protons de 10 MeV, le nickel ne donne naissance qu'à des radioisotopes dont la période est inférieure à 18 h [10]. Il serait donc possible, après décroissance de l'importante radioactivité due à une telle irradiation, de doser le fer par le radioisotope ^{56}Co ($t_{1/2}$ = 77,3 jours) obtenu par la réaction ^{56}Fe (p, n) ^{56}Co.

Les seules réactions avec les protons de moyenne énergie qui peuvent donner lieu à une interférence sont: ^{58}Ni (p, ^{3}He) ^{56}Co dont le seuil énergétique est à 12,02 MeV, et ^{60}Ni (p, αn) ^{56}Co dont le seuil énergétique est à 11,82 MeV.

Il a été montre qu'à 15 MeV, cette interférence n'était pas détectable et était inférieure à 0,01% [10]. A cette énergie, supérieure au seuil de production, elle est donc très faible. Avec des protons de 10 MeV, il est vraisemblable que cette interférence soit tout à fait négligeable, et il semble possible d'obtenir une limite de détection pour le fer inférieure à 0,1 $\mu g\ g^{-1}$.

CONCLUSION

La méthode décrite n'est certainement pas la plus performante dans la détermination des limites absolues de détection des éléments. En particulier une analyse par activation après séparations chimiques postérieures à l'irradiation, donnerait, certainement de meilleurs résultats pour certains éléments. Cependant la méthode proposée offre le double avantage d'être rapide et de ne demander qu'un minimum de manipulations. Les performances qu'elle permet d'obtenir eventuellement (22 éléments détectables à moins de 0,1 $\mu g\ g^{-1}$) montrent qu'elle est d'un grand intérêt pour un contrôle de pureté lors de l'élaboration de nickel pur, et qu'elle est parfaitement adaptée à la demande d'un contrôle de fabrication.

Pour des raisons de reproductibilité dans les conditions géométriques de comptage, nous avons dissous les échantillons et les étalons, mais il semble plus profitable d'essayer d'obtenir des échantillons et des étalons de forme standardisée qui permettent d'une part de s'affranchir des pertes éventuelles en éléments volatils au cours de la dissolution du nickel et d'autre part, d'apporter un gaih de temps appréciable.

L'absence de manipulation peut permettre d'automatiser cette analyse

et de lui donner ainsi la possibilité d'être utilisé comme analyse de routine dans certains cas. Son application industrielle, si elle reste limitée par l'utilisation d'un réacteur nucléaire, paraît envisageable dans la mesure où les contrôles, après envoi des navettes pour irradiation, peuvent se faire rapidement et simplement dans un laboratoire équipé et situé loin des réacteurs.

Nous sommes reconnaissants à Monsieur Levêque, Directeur du Laboratoire Pierre Sue du Centre d'Etudes Nucléaires de Saclay de nous avoir accueilli dans son laboratoire. Nous tenons à remercier tout le personnel du Laboratoire de nous avoir facilité notre travail, et en particulier, Madame Cleyrergue et Monsieur Nau.

BIBLIOGRAPHIE

1 R. Tardy, G. Cherblanc, J. Rochette, J. Y. Boos et C. Goux, Journées Métallurgiques d'Automne de la Société Française de Métallurgie, Paris (29-9-1975).
2 N. Deschamps, Thèse, Université de Paris, 1966.
3 R. J. Howerton, D. Braff, W. J. Cahill et N. Chazan, Thresholds of Nuclear Reactions, Lawrence Radiation Laboratory, Livermore, California, 1972.
4 G. Erdtmann et W. Soyka, J. Radioanal. Chem., 26 (1975) 375; 27 (1975) 137.
5 L. A. Currie, Anal. Chem., 40 (1968) 586.
6 A. Lesbats et R. Tardy, J. Radioanal. Chem., 17 (1973) 127.
7 G. Erdtmann, Kernchemie in Einzeldarstellungen, Vol. 6, Neutron Activation Tables, Verlag Chemie, Weinheim, 1976.
8 N. E. Holden et F. W. Walker, Chart of the Nuclides, Knolls Atomic Power Laboratory, 11th Edition (revised to April 1972), General Electric Company-Naval Reactors, U.S. Atomic Energy Commission.
9 P. Benaben, J. N. Barrandon et J. L. Debrun, Anal. Chim. Acta, 78 (1975) 129.
10 J. L. Debrun, J. N. Barrandon et P. Benaben, Anal. Chem., 48 (1976) 167.
11 J. N. Barrandon, J. L. Debrun, A. Kohn et R. H. Spear, Nucl. Instrum. Methods, 127 (1965) 269.

Analytica Chimica Acta, 101 (1978) 157—167

SOME NEW APPROACHES TO THE DEVIATION OF THE MOLAR ABSORPTIVITY AND FORMATION CONSTANT OF A COMPLEX FROM CONTINUOUS VARIATIONS DATA

J. S. ADSUL and P. S. RAMANATHAN*

Analytical Chemistry Division, Bhabha Atomic Research Centre, Trombay, Bombay 400085 (India)

(Received 13th January 1978)

SUMMARY

Some slope-intercept and graphical solution methods are proposed for calculation of the molar absorptivity (ϵ) and the overall formation constant (β_n) of a complex which forms exclusively in solution. The data required for applying these methods are obtained from points selected from one or more continuous variations curves. The validity and applicability of the methods proposed are demonstrated by appropriate examples.

Several procedures [1—8] have been reported for the derivation of the molar absorptivity (ϵ) and the overall formation constant (β_n) of a complex MA_n, starting from the data obtained by continuous variations experiments with equimolar solutions [9]. In the present paper, some new approaches are proposed and the validity and applicability are demonstrated.

DERIVATION OF SOME RELATIONSHIPS APPLICABLE TO SYSTEMS IN WHICH ONLY ONE COMPLEX IS FORMED

For a system in which only one complex MA is formed, the following relationships are valid:

$$\beta_1 = [MA]/[M][A] = C/[C_M - C]\ [C_A - C] \quad (1)$$

$$\beta_1 C^2 - C(\beta_1 C_0 + 1) + \beta_1 C_M C_A = 0 \quad (2)$$

where $C_0 = C_M + C_A$. Dividing throughout by C and rearrangement gives

$$(\beta_1 C_M C_A/C) = (1 + \beta_1 C_0) - \beta_1 C \quad (3)$$

Substitution of E/ϵ for C, and division throughout by β_1, gives the equation which is applicable for spectrophotometric studies:

$$C_M C_A/E = (1 + \beta_1 C_0)/\epsilon\ \beta_1 - E/\epsilon^2 \quad (4)$$

This is an alternative form of the equation proposed by Heller and Schwarzenbach [10]. Substitution for C_M and C_A in terms of C_0 and X

(the mole fraction of the ligand) gives

$$X\,(1-X)/E = [(1/C_0^2\,\epsilon\,\beta_1) + (1/C_0\,\epsilon)] - E/C_0^2\,\epsilon^2 = Y_1 - E/C_0^2\,\epsilon^2 \quad (5)$$

Equations (4) and (5) can be rearranged as follows:

$$C_M C_A = [(E/\beta_1\,\epsilon) - (E^2/\epsilon^2)] + C_0 E/\epsilon = Y_2 + C_0 E/\epsilon \quad (6)$$

$$X\,(1-X) = [(E/\epsilon\,C_0) - (E^2/\epsilon^2\,C_0^2)] + (1/C_0)\,(E/C_0\,\epsilon\,\beta_1)$$
$$= Y_3 + (1/C_0)\,(E/C_0\,\epsilon\,\beta_1) \quad (7)$$

In the case of a system in which only MA_2 is formed:

$$C/\beta_2 = C_M C_A^2 - C(4C_M C_A + C_A^2) + C^2 4C_0 - 4C^3 \quad (8)$$

$$C_M C_A^2 = [(E/\epsilon\,\beta_2) + (4E^3/\epsilon^3) - (4C_0 E^2/\epsilon^2)] + E(4C_M C_A + C_A^2)/\epsilon \quad (9)$$

$$X^2\,(1-X) = (1/C_0^3)\,[(E/\epsilon\,\beta_2) + (4E^3/\epsilon^3) - (4C_0 E^2/\epsilon^2) + (E/\epsilon\,C_0)\,(4X - 3X^2)$$
$$= Y_4 + (E/\epsilon\,C_0)\,(4X - 3X^2) \quad (10)$$

The following relationships are valid for a system in which a single complex, MA_n, forms exclusively:

$$\beta_n\,(C_A - nC)^n/C = 1/(C_0 - C_A - C) \quad (11)$$

$$(C/C_A)/\beta_n\,(1 - nC/C_A)^n = C_A^{n-1}\,(C_0 - C_A) - C_A^{n-1}\,C \quad (12)$$

$$C_A^{n-1}\,(C_0 - C_A) = [(E/C_A)/\beta_n\,\epsilon(1 - nE/\epsilon\,C_A)^n] + C_A^{n-1}\,E/\epsilon = Y_5 + C_A^{n-1}\,E/\epsilon \quad (13)$$

$$C_0/C_A = (1 + E/\epsilon\,C_A) + Y_5\,(1/C_A^n) = Y_6 + Y_5/C_A^n \quad (14)$$

$$(C_0 - C_M) = [(E/C_M)/\beta_n\,(\epsilon - E/C_M)]^{1/n} + nE/\epsilon = Y_7 + nE/\epsilon \quad (15)$$

Slope-intercept methods of obtaining β_n and ϵ

Some of the equations given above make it possible to propose a few slope-intercept procedures for obtaining the ϵ and β_n values of a complex, which is assumed to be formed exclusively in solution. The methods are summarized in Table 1.

Graphical methods of obtaining β_n and ϵ

Each of the equations referred to in Table 1 (except eqn. 14) can be rearranged to bring the constant terms Y_1, Y_2, etc. to the left-hand side and all variable terms to the right-hand side. These rearranged equations can then be made the basis of some graphical solution procedures for evaluating the two unknowns (ϵ and β_n). One case is described below to illustrate the possibilities.

Rearrangement of eqn. (5) gives

$$Y_1 = X(1-X)/E + E/C_0^2\,\epsilon^2 \quad (16)$$

TABLE 1

Summary of slope-intercept procedures

(For all these procedures, continuous variations curves must be drawn with E contributed by the complex as ordinate. The convenient abscissa functions will be: X for the first four methods, C_A for methods 5 and 6 and C_M for method 7. Each linear curve under method 4 has to be drawn with data from only two experimental points; this restriction is absent for the other cases.)

Method	Eqn.	Complex to which applicable	Conditions in selecting experimental points from c.v. curve(s)	Ordinate function	Abscissa function	Slope	Intercept
1.	5	MA	Points are chosen from one side of the maximum of a single c.v. curve	$X(1-X)/E$	E	$-1/C_0^2\epsilon^2$	Y_1
2.	6	MA	Points with the same E are chosen from a set of c.v. curves	$C_M C_A$	C_0	E/ϵ	Y_2
3.	7	MA	Points with the same E/C_0 values are chosen from a set of c.v. curves	$X(1-X)$	$1/C_0$	$E/C_0\,\epsilon\,\beta_1$	Y_3
4.	10	MA_2	Points with the same E are chosen from a single c.v. curve	$X^2(1-X)$	$(4X-3X^2)$	$E/\epsilon C_0$	Y_4
5.	13	MA_n	Points with the same E/C_A values are chosen from a set of c.v. curves	$C_A^{n-1}(C_0-C_A)$	$E\,C_A^{n-1}$	$1/\epsilon$	Y_5
6.	14	MA_n	As for method 5	C_0/C_A	$1/C_A^n$	Y_5	Y_6
7.	15	MA_n	Points with the same E/C_M values are chosen from a set of c.v. curves	C_0-C_M	E	n/ϵ	Y_7

For each point selected from the single continuous variations curve of a 1:1 complex (see method 1 in Table 1), values for the Y_1 function are calculated from: (i) the X and E values of the point chosen, (ii) the C_0 employed for the experiment, and (iii) different assumed values for ϵ. When these Y_1 values are plotted against the corresponding $1/\epsilon^2$, the straight line obtained will have a slope and intercept equal to E/C_0^2 and $X(1-X)/E$, respectively. It is obvious that one such straight line can be obtained corresponding to each point chosen on the continuous variations curve. In practice, a family of straight lines can be drawn by choosing several convenient points from the curve. As Y_1 takes up a fixed value (because of the condition stipulated in the selection of points) and $1/\epsilon^2$ is a constant for the system, all these straight lines will meet at a point. The values of Y_1 and $1/\epsilon^2$ corresponding to this point of intersection will then be the correct values representing the system. ϵ and β_1 can be calculated from the co-ordinates of this point of intersection.

Two other graphical solution procedures for a 1:1 complex can be developed along similar lines, by plotting Y_2 vs. $1/\epsilon$ or Y_3 vs. $1/\epsilon\,\beta_1$. A pair of intersecting straight lines is obtained for the 1:2 complex by plotting Y_4 vs. $1/\epsilon$. Y_5 or Y_7 plotted against $1/\epsilon$ give, in turn, their respective families of intersecting straight lines. A perusal of Table 1 shows that there is no restriction on the value of n when these two procedures involving Y_5 and Y_7 are applied.

The conditions for choosing the experimental points for the graphical solution methods are the same as those indicated in Table 1 for the corresponding slope-intercept procedures. In practice, the same data can be used in applying the slope-intercept and graphical solution procedures.

VERIFICATION OF THE APPLICABILITY OF THE PROCEDURES

Slope-intercept procedures applicable for a 1:1 complex (Methods 1, 2 and 3)

Curves a—c in Fig. 1 are the theoretical continuous variations curves of a 1:1 complex with $\beta_1 = 10^3$ and $\epsilon = 50$. Lines a—c in Fig. 2 represent, respectively, methods 1—3 in Table 1. The data for drawing these curves are given in Table 2. The ϵ and β_1 values calculated from the slopes and intercepts of these lines are shown in Table 3.

Graphical solution procedures applicable for a 1:1 complex

Typical sets of intersecting straight lines obtained by plotting (A) Y_1 vs. $1/\epsilon^2$, (B) Y_2 vs. $1/\epsilon$, and (C) Y_3 vs. $1/\epsilon\,\beta_1$ are shown in Fig. 3. The equations for drawing these lines are included in Table 4. The ϵ and β_1 values calculated from the points of intersection of each family of lines are given in Table 5.

Slope-intercept procedure applicable for a 1:2 complex (Method 4)

The continuous variations curve (E vs. X) of a 1:2 complex, is shown in Fig. 4 (A). To verify the applicability of the slope-intercept method 4, based on eqn. (10), line d in Fig. 2 was drawn, connecting $X^2(1-X)$ and $(4X-3X^2)$,

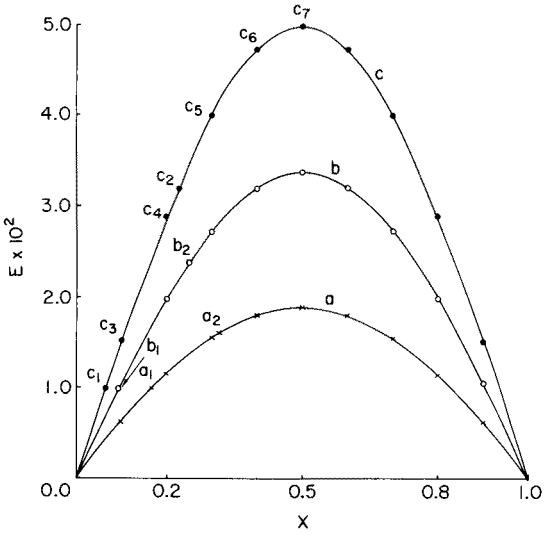

Fig. 1. Continuous variations curves (E vs. X) of a 1:1 complex with $\beta_1 = 10^3$ and $\epsilon = 50$. C_0 for curves a—c; 2.0, 3.0 and 4.0 × 10^{-3} M.

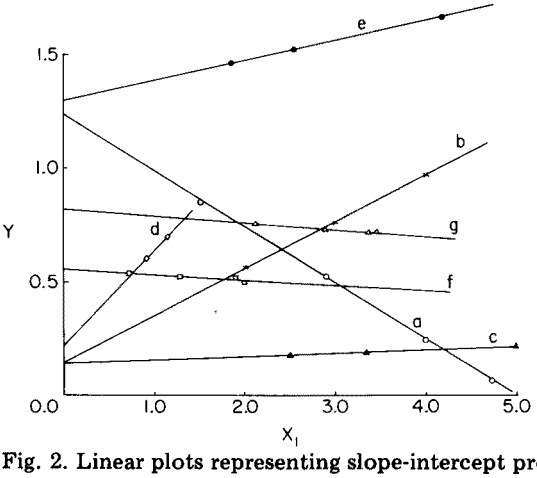

Fig. 2. Linear plots representing slope-intercept procedures. $X_1 = E \times 10^2$ for a; $C_0 \times 10^3$ for b; $1/100\ C_0$ for c; $4X - 3X^2$ for d; $1/200\ C_A^n$ for e; $E_{380} \times 10$ for f; $E_{390} \times 10$ for g. $Y = (X(1-X)/E) - 5.0$ for a; $C_M C_A \times 10^6$ for b; $X(1-X)$ for c; $X^2(1-X) \times 10$ for d; C_0/C_A for e; $(2X(1-X)/E) - 2.0$ for f; $(X(1-X)/E)$ for g. For other details of curves a—e, see Table 2. Curve f; UO_2^{2+}—SCN^- system in aqueous medium at 380 nm for $C_0 = 1.38 \times 10^{-2}$ M. Curve g; UO_2^{2+}—SCN^- system in 1:1 methanol—water medium at 390 nm for $C_0 = 1.424 \times 10^{-2}$ M.

by using data obtained from the isochromic points a_1 and a_2 with $E = 0.50$. The data needed for drawing line d in Fig. 2 are included in Table 2. As isochromic points must be chosen from a single continuous variations curve, this line must be constructed from only two experimental points. The ϵ and β_2 values calculated from the slope and intercept values are included in Table 3;

TABLE 2

Data for plotting the curves in Fig. 2 by the method outlined in Table 1

I. Curve a: $X(1-X)/E$ vs. E (Method 1)[a]

Point in curve c of Fig. 1	X	$E \times 10^2$	$X(1-X)/E$
c_3	0.1	1.535	5.86
c_4	0.2	2.895	5.53
c_5	0.3	4.00	5.25
c_6	0.4	4.735	5.07
c_7	0.5	5.00	5.00

II. Curve b: $C_M C_A$ vs. C_0 (Method 2)[b]

Curve in Fig. 1	Point chosen	$C_0 \times 10^3$	X	$C_A \times 10^3$	$C_M \times 10^3$	$C_M C_A \times 10^6$
a	a_1	2.0	0.170	0.34	1.66	0.5644
b	b_1	3.0	0.093	0.278	2.723	0.7555
c	c_1	4.0	0.065	0.260	3.740	0.9724

III. Curve c: $X(1-X)$ vs. $1/C_0$ (Method 3)[c]

Curve in Fig. 1	Point chosen	$E \times 10^2$	$C_0 \times 10^3$	X	$X(1-X)$	$1/C_0$
a	a_2	1.6	2.0	0.315	0.2158	500
b	b_2	2.4	3.0	0.250	0.1875	333
c	c_2	3.2	4.0	0.230	0.1771	250

IV. Curve d: $X^2(1-X)$ vs. $(4X-3X^2)$ (Method 4)[d]

Point in Fig. 4 A	X	$X^2(1-X)$	$4X-3X^2$
a_1	0.292	0.06036	0.912
a_2	0.917	0.06980	1.145

V. Curve e: C_0/C_A vs. $1/C_A^n$ (Method 6)[e]

Curve in Fig. 4 B	$C_0 \times 10^3$	Point chosen	$E \times 10^3$	$C_A \times 10^3$	C_0/C_A	$1/C_A^n$
a	2.0	a_1	182	1.2	1.67	833
b	3.0	b_1	298	1.96	1.53	510
c	4.0	c_1	413	2.72	1.47	368

[a] $C_0 = 4.0 \times 10^{-3}$ M for c_3—c_7. System: 1:1 complex with $\beta_1 = 10^3$ and $\epsilon = 50$.
[b] $E = 0.01$ for a_1—c_1 for the same system as in I.
[c] $E/C_0 = 8.0$ for a_2—c_2 for the same system as in I.
[d] $E = 0.50$ for a_1 and a_2. System: 1:2 complex with $\beta_2 = 10^4$ and $\epsilon = 10^3$; $C_0 = 0.012$ M.
[e] $E/C_A = 152$ for a_1—c_1. System: 1:1 complex with $\beta_1 = 10^3$ and $\epsilon = 500$.

TABLE 3

ϵ and β_n values calculated from the slopes and intercepts of the linear plots in Fig. 2

Curve in Fig. 2	Slope	Intercept	ϵ	log β_n	Remarks
a	24.8	6.24	50.2	2.995	1:1 complex. ϵ from slope and β_1 from intercept (Method 1)
b	0.2056 $\times 10^{-3}$	0.15 $\times 10^{-6}$	48.7	3.03	1:1 complex. ϵ from slope and β_1 from intercept (Method 2)
c	0.1516 $\times 10^{-3}$	0.140	47.5	3.04	1:1 complex. ϵ from intercept by solving $0.140\epsilon^2 - 8\epsilon + 64 = 0$ and rejecting the second root (9.616) as it is less than E/C_M *for* $X \geqslant 0.20$. β_1 from slope (Method 3)
d	0.042	0.022	992	3.997	1:2 complex. ϵ from slope and β_2 from intercept (Method 4)
e	4.5×10^{-4}	1.3	507	2.98	1:1 complex. ϵ from intercept and β_1 from slope (Method 6)
f	0.1175	1.275	210	1.43	UO_2^{2+}—SCN^- system. ϵ from slope and β_1 from intercept (Method 1)
g	0.30	0.815	128	2.16	UO_2^{2+}—SCN^- system. ϵ from slope and β_1 from intercept (Method 1)

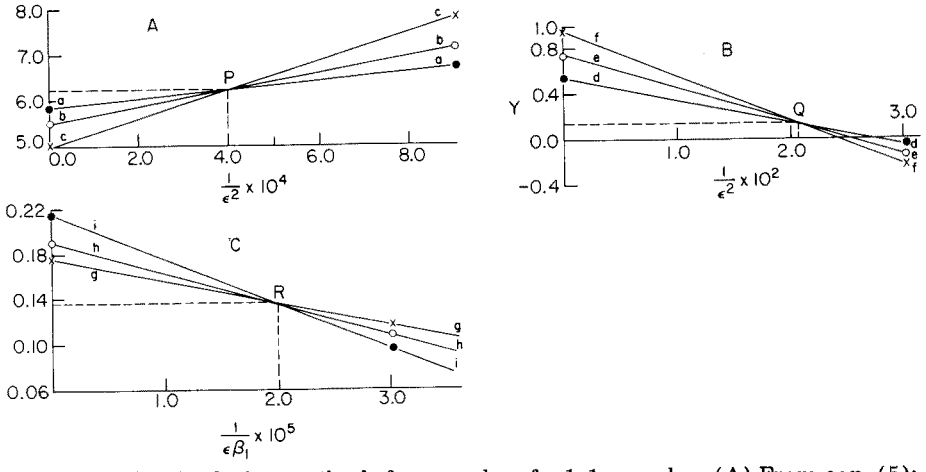

Fig. 3. Graphical solution methods for β_1 and ϵ of a 1:1 complex. (A) From eqn. (5); (B) from eqn. (6); (C) from eqn. (7). $Y = Y_1$ for a—c; $Y_2 \times 10^6$ for d—f; Y_3 for g—i. For other details of these curves, see Table 4.

TABLE 4

Data for plotting the lines in Fig. 3
(System: 1:1 complex with $\beta_1 = 10^3$ and $\epsilon = 50$)

Curve in Fig. 3	Linear equation[a]	Points and curve in Fig. 1 used for the linear eqn.
a	$Y_1 = 5.86 + 15350/16\epsilon^2$	c_3 in curve c
b	$Y_1 = 5.53 + 28950/16\epsilon^2$	c_4 in curve c
c	$Y_1 = 5.00 + 50000/16\epsilon^2$	c_7 in curve c
d	$Y_2 = 10^{-6}\,(0.5644 - 20/\epsilon)$	a_1 in curve a
e	$Y_2 = 10^{-6}\,(0.7555 - 30/\epsilon)$	b_1 in curve b
f	$Y_2 = 10^{-6}\,(0.9724 - 40/\epsilon)$	c_1 in curve c
g	$Y_3 = 0.2158 - 4000/\epsilon\,\beta_1$	a_2 in curve a
h	$Y_3 = 0.1875 - 2667/\epsilon\,\beta_1$	b_2 in curve b
i	$Y_3 = 0.1771 - 2000/\epsilon\,\beta_1$	c_2 in curve c

[a]For values of the different parameters introduced into these equations, refer to Table 2: Y_1 functions, Section I; Y_2 functions, Section II; Y_3 functions, Section III.

TABLE 5

ϵ and β_1 values calculated from the intersection point of the plots in Fig. 3
(System: 1:1 complex with $\beta_1 = 10^3$ and $\epsilon = 50$)

Curves in Fig. 3 and point of intersection	Independent variable and value at intersection point	Dependent variable ϵ calculated and value at intersection point		Log β_1 calculated
a—c, P	$1/\epsilon^2 = 4.0 \times 10^{-4}$	$Y_1 = 6.25$	50.0	3.0
d—f, Q	$1/\epsilon = 2.05 \times 10^{-2}$	$Y_2 = 0.14 \times 10^{-6}$	48.75	3.05
g—i, R	$1/\epsilon\,\beta_1 = 2.0 \times 10^{-5}$	$Y_3 = 0.136$	49.3[a]	3.01

[a]Obtained by solving the equation $0.136\epsilon^2 - 8\epsilon + 64 = 0$ and rejecting the second root (9.56), as it is less than E/C_M for $X \geqslant 0.2$.

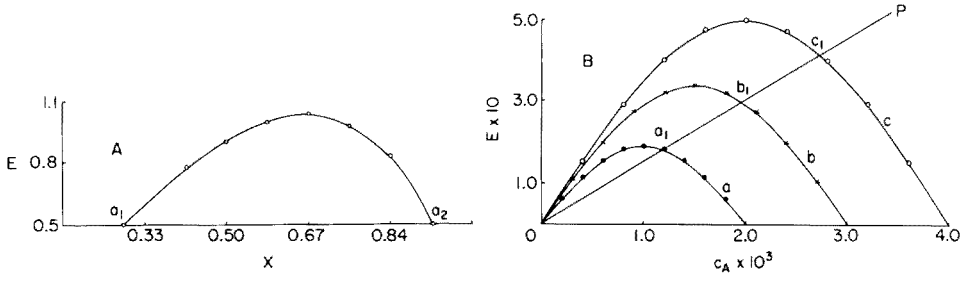

Fig. 4. Continuous variations curves for methods (4) and (6). (A) 1:2 complex (E vs. X); $\beta_2 = 10^4$; $\epsilon = 10^3$; $C_0 = 1.2 \times 10^{-2}$ M. (B) 1:1 complex (E vs. C_A); $\beta_1 = 10^3$; $\epsilon = 500$. C_0 for curves a—c; 2.0, 3.0 and 4.0×10^{-3} M.

these values can be verified by drawing other lines similar to line d based on data from other pairs of isochromic points.

General slope-intercept procedure applicable for any complex MA_n, without restriction on the value of n *(Method 6)*

Three continuous variations curves a, b and c (connecting E and C_A) for a 1:1 complex with different C_0 values are shown in Fig. 4(B). Line OP is drawn through the origin, intersecting curves a, b and c at a_1, b_1 and c_1, respectively. These points, obviously, represent one set with a constant E/C_A value (152, in this case). The experimental parameters of these three points are then used to draw the line e in Fig. 2. The data needed to draw this curve are included in Table 2. The ϵ and β_1 values calculated from the slope and intercept of this line are included in Table 3.

DISCUSSION

Of the seven possible slope-intercept methods indicated in Table 1, five (1—4 and 6) have been used above to illustrate their practical utility. The linear nature of curves a—e in Fig. 2, as well as the good agreement of the computed ϵ and β_n values (Table 3) with the expected values, attest the validity and practical utility of the methods. Method 5 is only an alternative version of method 6. Method 7 is very similar to method 6, the main difference being that one selects, from a set of continuous variations curves, a group of points with the same E/C_M ratio for method 7 and with the same E/C_A ratio for method 6. Selection of such points is simplified if the continuous variations curves are drawn with E as ordinate and C_M or C_A as the abscissa for methods 7 and 6 respectively.

The evaluation of ϵ and β_n by the slope-intercept procedures is simple and straightforward, except for method 3. In this case, the intercept Y_3 is a quadratic expression in ϵ, while the slope involves the product of ϵ and β_1; it is then necessary to solve the quadratic equation and reject the root which is inadmissible (see Table 3), to achieve the correct value of ϵ.

Of the many possible graphical solution methods, three have been chosen for illustration. Each of the three families of straight lines included in Fig. 3 converges within a narrow region, which eliminates any ambiguity in the final values of ϵ and β_1. In addition, the ϵ and β_1 values calculated (Table 5) from the coordinates of the points of intersection agree well with the expected values, confirming the validity and applicability of these procedures. As mentioned above, evaluation of the true ϵ value by graphical solution method 3 also involves the solution of a quadratic equation (see Table 5) and rejection of the inadmissible root on logical grounds.

The condition imposed for the selection of experimental points restricts the number of intersecting straight lines to a single pair in graphical solution method 4. The system, therefore, does not become over-defined.

In the slope-intercept and graphical solution methods recommended, there is the option of choosing data from more than one group of experimental points which satisfy the relevant conditions imposed. Obviously, this makes it possible to verify the values of ϵ and β_n obtained from one group of experimental points.

A critical evaluation of the different equations and the methods based on them shows that the equations derived are exact; in this vital aspect, they are superior to some approximate equations proposed earlier [11, 12]. The applicability of the methods 5—7 is not restricted by the value of n; these methods are, therefore, more attractive than that of Benesi and Hildebrand [11] which is applicable only to 1:1 complexes.

The methods are especially attractive for the evaluation of the ϵ and β_n values of a mononuclear complex which does not go to colour saturation under the experimental conditions employed. For stable complex species, simpler procedures like the colour saturation method will, obviously, be more attractive.

The applicability of the methods is restricted to systems in which the metal ion and ligand either do not absorb (in the wavelength region of interest) or exhibit very little absorption compared to the complex.

The methods presuppose a knowledge of n, the ligand number. This is not a handicap, as n can be ascertained from the X_{max} of the continuous variations curve(s) employed to generate data for drawing the linear plots. If the value of n is already known, then many of the methods require data from only a section of the curve(s).

Even in the case of a system in which the metal ion tends to hydrolyse (e.g. in solutions with low X values), all the procedures except method 4 prove useful, as data from the continuous variations curve(s) can be conveniently selected from the region of high X values.

The methods can also be used to recognize the presence of multiple equilibria, based on one or more of the following indications: (1) the plots of the slope-intercept methods will show noticeable non-linearity; (ii) in the graphical solution methods, the linear plots in a family will not intersect at a single point; (iii) the ϵ and β_n values calculated with data from different regions of the continuous variations curve(s), drawn at the same wavelength, will be inconsistent. In addition β_n values calculated from continuous variations curve(s) drawn at different wavelengths will also show remarkable deviations.

Application to a practical system

As a typical practical application, the results obtained by the slope-intercept method 1 (Table 1) for the uranyl thiocyanate system are summarized. Symmetrical continuous variations curves with X_{max} at 0.50 are obtained in this system at low C_0 values (1.50×10^{-2} M and below) [13]. With increase in C_0 value, the curves become asymmetric and the X_{max} shifts to higher values. These curves indicate that a 1:1 complex predominates

at low C_0 values. Slope-intercept method 1 was therefore applied by selecting points from the left side of the maximum of a continuous variations curve drawn for $C_0 = 1.38 \times 10^{-2}$ M with measurements at 380 nm [13]. Line f in Fig. 2 represents the corresponding linear plot. Line g in Fig. 2 was drawn by selecting points from a curve of the same system obtained in a 1:1 water—methanol medium for $C_0 = 1.424 \times 10^{-2}$ M at 390 nm [13]. The slopes and intercepts obtained, as well as the ϵ and β_1 values calculated for both these cases are shown in Table 3.

The authors are grateful to Dr. M. Sankar Das, Head of the Analytical Chemistry Division and Dr. Ch. Venkateswarlu for valuable suggestions.

REFERENCES

1 P. Hagenmuller, C.R. Acad. Sci., 230 (1950) 2190; Ann. Chim., Paris, 6 (1951) 5.
2 Y. Schaeppi and W. D. Treadwell, Helv. Chim. Acta, 31 (1948) 577.
3 J. M. Pislot and S. Combet, Anal. Chim. Acta, 85 (1976) 149.
4 Z. Slovak and J. Borak, Anal. Chim. Acta, 68 (1974) 425.
5 S. Witek and W. Ignazak Zesz. Nauk. Politech. Lodz. Inz. Chem., No. 19 (1969) 129.
6 K. S. Klausen, Anal. Chim. Acta, 44 (1969) 377.
7 H. Irving and T. B. Pierce, J. Chem. Soc., (1959) 2565.
8 M. Mandel and Cl. Depommier, Bull. Soc. Chim. Belg., 68 (1959) 139.
9 P. Job, Ann. Chim., 9 (1928) 113.
10 E. Heller and G. Schwarzenbach, Helv. Chim. Acta, 34 (1951) 1876.
11 H. A. Benesi and J. H. Hildebrand, J. Am. Chem. Soc., 71 (1949) 2703.
12 R. Foster, D. Ll. Hammick and A. A. Wardley, J. Chem. Soc., (1953) 3817.
13 H. Parasurama Iyer and Ch. Venkateswarlu, Indian J. Chem., 6 (1968) 526.

Analytica Chimica Acta, 101 (1978) 169—175

EXTRACTION—SPECTROPHOTOMETRIC DETERMINATION OF PALLADIUM(II) WITH 2-NITROSO-5-DIETHYLAMINOPHENOL

KYOJI TÔEI*, SHOJI MOTOMIZU and SHOICHI HAMADA

Department of Chemistry, Faculty of Science, Okayama University, Tsushima, Okayama-shi (Japan)

(Received 28th February 1978)

SUMMARY

An extraction—spectrophotometric determination of palladium(II) with 2-nitroso-5-diethylaminophenol is described. Complex formation and extraction of the complex with chloroform are possible with aqueous phases of about 2.5 M sulfuric acid. The molar absorptivity of the complex is 4.38×10^4 l mol^{-1} cm^{-1} at 486 nm. Few of the common ions interfere at concentrations of 10^{-4}—10^{-3} M; more than 10^{-5} M Ir(IV), 10^{-5} M W(VI), 5×10^{-6} M Au(III) and 10^{-6} M iodide cause negative errors. The method can be applied to the determination of palladium in catalysts for automobile exhaust purifiers.

Palladium(II) — the first of the Irving—Williams series — forms very stable complexes with many chelating reagents, so that many ligands have been proposed for determinations of palladium. Of these reagents, various nitroso compounds (nitrosophenols [1], nitrosonaphthols [2—4] and *p*-nitroso-dimethylaniline [5]) react with palladium in acidic solutions and provide sensitive spectrophotometric determinations of palladium.

2-Nitroso-5-diethylaminophenol (nitroso-DEAP) and 2-nitroso-5-dimethylaminophenol (nitroso-DMAP), which were first used for the sensitive extraction—spectrophotometric determination of cobalt [6] and iron [7], react with palladium in a strongly acidic solution. The complexes formed are easily extracted into chloroform and show the largest molar absorptivities in the visible region of all the nitroso compounds proposed so far, except for *p*-nitrosodimethylaniline [5] which gives a molar absorptivity of 8.6×10^4 l mol^{-1} cm^{-1} at 525 nm, but does not react at such high acidities.

This paper describes the extraction—spectrophotometric determination of palladium with nitroso-DEAP. The method has many advantages in simplicity and sensitivity, in accuracy and precision, and in an abbreviated list of interferences.

EXPERIMENTAL

Apparatus and reagents

A Hitachi Perkin-Elmer Model 139 spectrophotometer and a Hitachi Model EPS-3T recording spectrophotometer were used to measure absorbances in a quartz cell of 10-mm path length. An Iwaki Model KM shaker was used.

Standard palladium(II) solution. Weigh approximately 1.26 g of palladium nitrate into a porcelain evaporating dish, add about 20 ml of 12 M HCl, and evaporate nearly to dryness. Dissolve the residue in 100 ml of 0.5 M HCl. Standardize this solution by the gravimetric dimethylglyoxime method [8]. Pipette accurate amounts of the standardized solution into a beaker, add 2 ml each of concentrated sulfuric and nitric acids, and evaporate to white fumes. Add 0.5 ml of nitric acid and evaporate to white fumes, and repeat this process. Finally add 2—5 ml of water and evaporate to white fumes. Dilute this with 0.5 M H_2SO_4, transfer the solution to a 1-l volumetric flask and dilute to the mark with 0.5 M H_2SO_4 to give a 2×10^{-5} M palladium solution.

2-Nitroso-5-diethylaminophenol. Nitroso-DEAP was obtained by nitrosation of the parent compound (*m*-diethylaminophenol) in acidic aqueous solution with sodium nitrite [9]; the crude nitroso compound was recrystallized twice from hydrochloric acid solution. An aqueous solution (6×10^{-3} M) in 0.05 M H_2SO_4 was used.

Other reagents were of analytical-reagent grade.

Standard procedure

Pipette up to 5 ml of the solution containing palladium(II) into a stoppered test tube, and dilute to 5 ml with distilled water. Add 4.5 ml of about 5.5 M sulfuric acid and 0.5 ml of nitroso-DEAP solution and mix well. Shake the mixture with 5 ml of chloroform for 1 min. Discard the aqueous phase and wash the organic phase with 5 ml of 2.5 M sulfuric acid by shaking for about 1 min by hand, to remove the excess of reagent. Measure the absorbance of the organic phase at 486 nm.

RESULTS

Effects of experimental variables

The time necessary for complete formation of the palladium(II) complex with nitroso-DEAP is ca. 30 s at room temperature. The absorbance of the complex extracted into chloroform does not change for at least a day. The time necessary for complete extraction of the complex is 30 s by hand or mechanical shaking. When the palladium concentration is about 10^{-5} M, the addition of 0.1 ml of nitroso-DEAP solution (6×10^{-3} M) suffices for complete extraction of palladium; accordingly 0.5 ml of reagent solution should be used for safety.

The effect of acidity on the extraction of the palladium complex was examined. As shown in Fig. 1, the absorbance of the complex measured against a reagent blank was constant for concentrations of sulfuric acid from 2—3 M though the absorbance of the reagent blank varied from 0.15 to 0.04; in these experiments, the excess of reagent was not removed. To reduce the absorbance of the reagent blank, the organic phase was washed with dilute sulfuric acid after extraction of the complex; washing with 2.5—3 M sulfuric acid reduced the absorbances of the reagent blanks to about 0.004.

The effect of volume of the aqueous phase was examined for the standard procedure. When the aqueous phase was varied from 5 to 50 ml, the absorbance of the complex in the organic phase was not affected, provided that the concentration of sulfuric acid in the aqueous phase was maintained at about 2.5 M.

Chloroform was the best of the nine organic solvents tested (chloroform, carbon tetrachloride, 1,2-dichloroethane, benzene, toluene, isobutyl methyl ketone, isoamyl alcohol, ethyl acetate and ligroin). When 5 ml of chloroform was used, all the palladium was removed from the aqueous phase in the first extraction. When a second extraction was done, palladium was not detected in the organic phase.

Composition of the extracted species

The composition of the palladium complex was examined by the molar ratio methods, in which the concentration of the reagent was varied. The palladium(II):nitroso-DEAP ratio was found to be 1:2 (Fig. 2).

Calibration graph and molar absorptivity

The calibration graph with the reagent blank as reference was a straight line through the origin over the range 0—2 × 10^{-5} M Pd. The molar

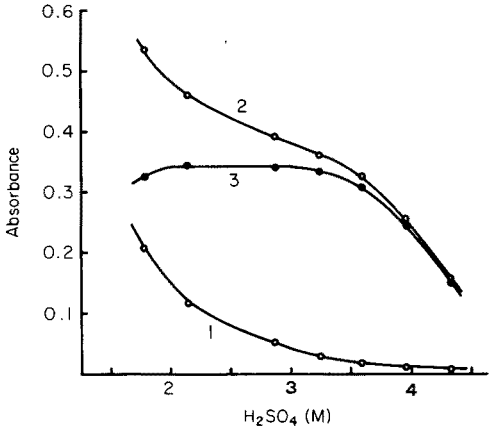

Fig. 1. Effect of acid concentration at 486 nm. (1) Reagent blank with $CHCl_3$ reference; (2) [Pd] = 8.52 × 10^{-6} M with $CHCl_3$ reference; (3) [Pd] = 8.52 × 10^{-6} M with a reagent blank reference. The organic phases were not washed with 2.5 M H_2SO_4.

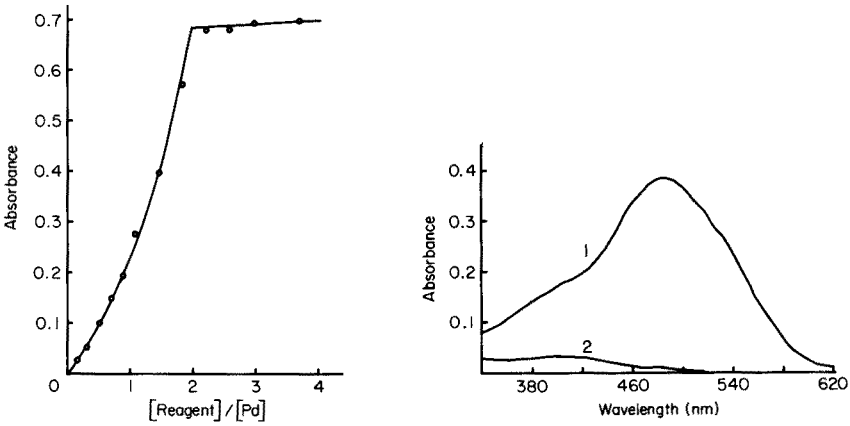

Fig. 2. Composition of palladium complex with nitroso-DEAP [Pd] = 1.60×10^{-5} M with $CHCl_3$ reference at 486 nm.

Fig. 3. Absorption spectra. (1) [Pd] = 8.52×10^{-6} M with $CHCl_3$ reference; (2) reagent blank with $CHCl_3$ reference. The organic phases were washed with 2.5 M H_2SO_4.

absorptivity calculated from the slope of the graph was 4.38×10^4 l mol^{-1} cm^{-1} at 486 nm. The absorption spectra in chloroform are shown in Fig. 3.

Effects of diverse ions

The interferences of diverse ions (Table 1) were examined by using 5 ml of sample solution containing palladium(II) (8.52×10^{-6} M) and each diverse ion. Iridium(IV) and tungsten(VI) at concentrations above 10^{-5} M and gold(III) above 5×10^{-6} M cause negative errors even when 1 ml of reagent solution is used. Iodide reacts with palladium to give negative errors.

Determination of palladium in catalysts for automobile exhaust purifiers

The palladium of the samples analysed was supported on a carrier made of silica or alumina (bead diameter, 3—5 mm). Sample A was brown, sample C was black, and sample B contained a mixture of grey and white beads. The procedure for preparation of sample solution was as follows.

Crush and grind the samples to a powder and weigh about 0.2 g into a beaker. Add 5 ml of aqueous (1 + 4) formic acid solution and heat on the water bath nearly to dryness. Add 5 ml of aqua regia and heat on the water bath until nitrogen oxides are removed. Then, add 3 ml of concentrated sulfuric acid and 2 ml of concentrated nitric acid and heat on a sand bath to white fumes. Thereafter, follow the method given for the preparation of standard palladium solutions, and finally dilute to 100 ml with distilled water.

Sample B proved to be more insoluble than other samples, and the sample solution had to be filtered before use. When the samples were not crushed and ground as described above, the palladium contents obtained were a little higher than those obtained for ground samples, but the variation of the

TABLE 1

Effect of diverse ions

Ion	Maximum tolerable concn. (M)
K^+, Na^+, NO_3^-, Cl^-	10^{-2} [a]
Mg^{2+}, Ca^{2+}, Sr^{2+}, Ba^{2+}, Pb^{2+}, Mn^{2+}, Zn^{2+}, Cd^{2+}, Co^{2+}, Ni^{2+}, Cu^{2+}, Hg^{2+}, Ag^+, Al^{3+}, Fe^{3+}, Mo(VI), U(VI)[b]	10^{-3} [a]
Os(VIII), Pt(IV), Zr(IV), Rh(III)[b], Br^-[b]	10^{-4}
Rh(III)	5×10^{-5}
Ir(IV)[b], W(VI)[b]	10^{-5}
Au(III)[b]	5×10^{-6}
I^-	10^{-6}

[a]Maximum tested. [b]1 ml of nitroso-DEAP solution (6×10^{-3} M) was used.

results obtained was almost the same (Table 2). The recovery of the palladium was examined, as shown in Table 3, by adding known amounts of palladium to a sample (without crushing) which was then treated as in the above dissolution procedure. From Tables 3 and 4, sample C did not contain palladium.

DISCUSSION

The molar absorptivities of the palladium(II) complexes of other nitroso compounds are compared with nitroso-DEAP in Table 4. The palladium complexes of the nitroso compounds were all extracted very easily with 5 ml of chloroform, and the organic phases were washed with 5 ml of

TABLE 2

Determination of palladium in catalysts
(In each case, the result given is the mean of 3 determinations; 2-ml aliquots of sample solution were taken.)

Sample	Sample soln. (mg/100 ml)	Pd found (%)	Sample	Sample soln. (mg/100 ml)	Pd found (%)
A	155.5[a]	0.163 ± 0.001	B (grey)	156.6[b]	0.176 ± 0.001
	148.9[a]	0.164 ± 0.001	(white)	146.3[b]	0.123 ± 0.001
	186.3[a]	0.176 ± 0.002	C	168.3[b]	0 ± 0
	170.3[b]	0.175 ± 0.001			
	174.2[b]	0.183 ± 0.001			
	180.4[b]	0.184 ± 0.001			
	171.4[b]	0.199 ± 0.002			

[a]About 0.5—0.7 g of sample was crushed and ground, and the ground sample was analysed.
[b]Without crushing and grinding the sample.

TABLE 3

Recovery of palladium

Sample	Sample soln.[a] (mg/100 ml)	Pd added (μg)	Pd recovery[b] (%)
A	164.7	283.2	99.1 ± 0.2
B (grey)	149.6	283.2	100.7 ± 0.5
(white)	149.8	283.2	98.0 ± 0.6
C	170.2	283.2	97.6 ± 0.3

[a]Without crushing and grinding the sample; 2-ml aliquots of sample solution were used in each case.
[b]Mean values of the three determinations.

TABLE 4

Molar absorptivities ϵ ($\times 10^4$ l mol^{-1} cm^{-1}) of palladium complexes extracted into chloroform

Reagents	nm	ϵ	Reagents	nm	ϵ
2-Nitroso-1-naphthol	309	5.0	6-Chloro-1-nitroso-2-naphthol	301	4.2
	376	2.5		434	2.5
	385	2.5		516	1.1
	564	1.0			
4-Chloro-2-nitroso-1-naphthol	316	5.1	6-Bromo-1-nitroso-2-naphthol	303	4.6
	370	2.4		434	2.7
	568	1.2		514	1.1
4-Bromo-2-nitroso-1-naphthol	316	5.4	2-Nitroso-5-methoxyphenol	400	3.3
	372	2.4		420	3.3
	570	1.2			
1-Nitroso-2-naphthol	267	2.7	2-Nitroso-5-dimethylamino-phenol (Nitroso-DMAP)	486	4.3
	282	2.8			
	441	2.7			
	505	1.1			
			2-Nitroso-5-diethylamino-phenol (Nitroso-DEAP)	486	4.4

distilled water and then with 5 ml of 1 M sodium hydroxide solution to remove the excess of reagent, before the absorption spectra of the organic phases were measured. For all these reagents, the percentage extractions of palladium were over 99%. With nitroso-DMAP and nitroso-DEAP, palladium reacts completely even in very acidic solution and the excess of reagent is soluble in acidic solution; with the other reagents, the complexes are insoluble in strongly acidic solution. Fortunately, the excess of nitroso-DMAP and nitroso-DEAP in chloroform is more easily removed with 2.5 M sulfuric acid than with sodium hydroxide solution and the absorbance of the reagent blanks was small (0.004) and constant. Though the molar absorptivity of the complex with 4-bromo-2-nitroso-1-naphthol at 316 nm is the largest of

all the reagents and wavelengths examined, the reagent blank is larger and more variable than that of nitroso-DEAP; moreover, removal of the excess of reagent is troublesome because the palladium reaction must take place in acidic solution whereas the excess of reagent must be removed with basic solution. The absorption maxima of nitroso-DMAP and nitroso-DEAP complexes lie in the visible region and their molar absorptivities are the highest in that region. The absorbance of nitroso—DMAP complex extracted into chloroform decreases gradually, so that DEAP is certainly the most useful of these nitroso compounds.

REFERENCES

1 K. Kodama, Research Reports of the Nagoya Municipal Industrial Research Institute, No. 19 (1958) 1.
2 K. D. Cheng, Anal. Chem., 26 (1954) 1894.
3 K. Kodama, Research Reports of the Nagoya Municipal Industrial Research Institute, No. 19 (1958) 4.
4 S. Komatsu and S. Kamiyama, Nippon Kagaku Zasshi, 81 (1960) 1094.
5 J. H. Yoe and J. J. Kirkland, Anal. Chem., 26 (1954) 1335.
6 K. Tôei and S. Motomizu, Analyst, 101 (1976) 497.
7 K. Tôei, S. Motomizu and T. Korenaga, Analyst, 100 (1975) 629.
8 C. L. Wilson and D. W. Wilson, Comprehensive Analytical Chemistry, Vol. 10, Elsevier, Amsterdam, 1962, p. 685.
9 R. Möhlaw, Ber., 25 (1892) 1059.

Analytica Chimica Acta, 101 (1978) 177—185

ANALYTICAL APPLICATIONS OF THIO-, SELENO- AND TELLUROETHERS.
Part 7. Spectrophotometric Determination of Successive Constants of Palladium(II) with Thioglycolic acid Derivatives**

LUIZ R. M. PITOMBO* and ELISABETH DE OLIVEIRA

Departamento de Química Fundamental, Instituto de Química, Universidade de São Paulo (Brazil)

(Received 23rd March 1978)

SUMMARY

The interaction of $[PdCl_4]^{2-}_{(aq)}$ with ethylene-bis(thioglycolic) acid (EBTGA) and β-ethylthioethylene(thioglycolic) acid (β-ETETGA), has been interpreted and evaluated quantitatively. The successive constants of palladium(II) with EBTGA and/or β-ETETGA in acid medium have been determined spectrophotometrically.

Systematic studies of the analytical potentialities [1—4] of some organic compounds containing S, Se and Te showed that ethylenebis(thioglycolic) acid (EBTGA) and β-ethylthioethylene(thioglycolic) acid (β-ETETGA) could be used in the spectrophotometric [5] or titrimetric determination of metals such as Pd(II) [6], Cu(II), Hg(II) and Ag(I) [7]. A comparative study [4] in aqueous solution with ethylthioglycolic acid ($C_2H_5SCH_2COOH$), thiodiglycolic acid ($HOOCCH_2SCH_2COOH$), β-ETETGA ($C_2H_5S(CH_2)_2SCH_2COOH$) and EBTGA ($HOOCCH_2S(CH_2)_2SCH_2COOH$) gave qualitative information regarding the selectivity of these ligands for mercury(II) and palladium(II). Spectrophotometric and conductometric studies [4] of the interaction of $[PdCl_4]^{2-}_{(aq)}$ with EBTGA and β-ETETGA showed that two complex species with 1:1 and 2:1 ratios of ligand:metal were formed. On the basis of these and other results [8, 9] it was decided to study the spectrophotometric determination of the formal constants for palladium(II) with EBTGA and β-ETETGA.

EXPERIMENTAL

Apparatus and reagents

A Zeiss spectrophotometer Model PMQII with 1.00-cm silica cells was used for absorbance measurements. For pH measurements, a Metrohm

---

**Presented at the XVIII International Conference on Coordination Chemistry (São Paulo, Brazil, July 1977).

Herisau Compensator E388 was used. Infrared spectra were taken as Nujol and Fluorolube mulls on a Perkin-Elmer spectrophotometer Model IR180.

EBTGA and β-ETETGA and their sodium salts were prepared as described previously [4]. Solutions of sodium ethylene-bis(thioglycolate) (Na_2EBTG) and sodium β-ethylthioethylene(thioglycolate) (Na-β-ETETG) were standardized by passage through resin columns in the acid form (Merck-I) and titration with standard sodium hydroxide solution. The palladium solution, prepared from palladium chloride in 0.1 M hydrochloric acid, was standardized gravimetrically with dimethylglyoxime. Sodium chloride solutions were prepared by direct weighing.

Isolation of palladium complexes

Tiberg [10] reported the preparation of palladium(II)—EBTGA complexes and Kukushkin et al. [11] reported the preparation of palladium(II) complexes with EBTGA and β-ETETGA; the 1:1 and 2:1 (ligand:metal) complexes were obtained with both ligands.

The complexes of Pd(II) with EBTGA. The procedure of Kukushkin et al. [11] was used to prepare the 1:1 complex; instead of EBTGA, Na_2EBTG was used. Yellow crystals, m.p. 194—195°C, were obtained. [Calculated for $(HOOCCH_2SC_2H_4SCH_2COOH)PdCl_2$ (m.w. = 387.5): 18.6% C, 2.6% H. Found: 18.9% C, 2.5% H.] The compound showed a maximum in aqueous solution in the same region as the 1:1 species showed previously [4].

To prepare the 2:1 species, solid NaCl was added to 125 ml of hydrochloric acid solution containing 0.885 g of $PdCl_2$ (10 mmol), to maintain the ionic strength at 3.0 M, with stirring until dissolution was complete. With continuous stirring, 120 ml of Na_2EBTG solution (2.795 g, 22 mmol) was added. After 24 h, the orange crystals were filtered off (yield 2.85 g, 90%; m.p. 148—150°C). [Calculated for $(HOOCCH_2SC_2H_4SCH_2COOH)_2PdCl_2$-$2H_2O$ (m.w. = 633.8): 22.7% C, 3.8% H, 5.7% H_2O. Found: 22.9% C, 3.8% H, 5.8% H_2O (Karl Fischer method).] The compound showed a maximum in aqueous solution in the same region as the 2:1 species previously [4]. By differential thermal analysis, Kukushkin et al. [11] showed that this species has two molecules of water of crystallization (m.p. 148°C). Table 1 presents some selected i.r. bands.

The complexes of Pd(II) and β-ETETGA. Na-β-ETETG was used in place of β-ETETGA in the procedure described by Kukushkin et al. [11] for preparation of the 1:1 species. Pale yellow crystals, m.p. 170—172°C, were obtained. [Calculated for $C_2H_5SC_2H_4SCH_2COOH)$ $PdCl_2$ (m.w. = 357.6): 20.15% C, 3.4% H. Found: 20.5% C, 3.2% H.] The compound showed a maximum in aqueous solution in the same region as the 1:1 species showed previously [4].

The 2:1 species was obtained by the procedure described by Kukushkin et al. [11] except that Na-β-ETETG was used in place of β-ETETGA. The pink-yellowish crystals melted at 128—130°C to give an oil which decomposed at 195°C. [Calculated for $(C_2H_5SC_2H_4SCH_2COOH)_2PdCl_2$ (m.w. = 537.8): 26.8% C, 4.5% H. Found: 27.05% C, 4.75% H.] The compound

TABLE 1

Selected i.r. bands (cm^{-1})

Compound	Ref.	$\nu_{(C-S)}$	$\nu_{s(COO)}$	$\nu_{a(COO)}$	δ_{H_2O}
EBTGA	present work	720 (m)	1390 (m)	1675 (vs)	
			1430 (m)	1715 (vs)	
Na_2EBTG	present work	720 (m)	1405 (m)	1570 (vs)	
			1420 (m)		
$[(EBTGA)_2Pd]Cl_2 \cdot 2H_2O$	present work	660 (s)	1375 (m)	1705 (vs)	1610 (vvw)
			1420 (m)	1725 (vs)	
				1770 (vs)	
$[Pd(EBTGA)Cl_2]$	present work	640 (m)	1370 (m)	1720 (s)	
			1410 (m)	1735 (sh)	
$[(EBTGA)_2Pd]Cl_2 \cdot 2H_2O$	[11]			1710	1620
				1730	
				1775	
$[Pd(EBTGA)Cl_2]$	[11]			1740	
				1778	

TABLE 2

Selected i.r. bands (cm^{-1})

Compound	Ref.	$\nu_{(C-S)}$	$\nu_{s(COO)}$	$\nu_{a(COO)}$
β-ETETGA	present work	720 (s)	1420 (m)	1710 (m)
Naβ-ETETG	present work	680 (m)	1390 (m)	1570 (s)
			1410 (m)	
$[(\beta\text{-ETETGA})_2Pd]Cl_2$	present work	635 (s)	1370 (m)	1715 (vs)
			1400 (m)	
$[Pd(\beta\text{-ETETGA})Cl_2]$	present work	655 (m)	1370 (m)	1715 (vs)
			1410 (m)	
$[(\beta\text{-ETETGA})_2Pd]Cl_2$	[11]			1720
$[Pd(\beta\text{-ETETGA})Cl_2]$	[11]			1730

showed a maximum in aqueous solution in the same region as the 2:1 species showed previously [4]. Table 2 presents some selected i.r. bands.

These data show that the complexes isolated are identical to those of Kukushkin et al. [11].

Determination of constants

$[PdCl_4]^{2-}$ system. Absorbance values of a solution containing 3.10 μg Pd ml^{-1} (2.91×10^{-5} M) with chloride concentration 3.0 M and pH 1.5 at 25.0°C, were measured at 260, 270 and 280 nm, against a blank containing all the reagents.

Pd—EBTG system. Absorbance values of solutions containing 3.45 μg Pd ml^{-1} (3.24×10^{-5} M) with chloride concentration 3.0 M, in which the Na_2 EBTG concentration ranged from 9.72×10^{-4} M to 2.59×10^{-2} M (10 solutions were

prepared) with pH 1.50 at 25.0°C, were measured at 260, 270 and 280 nm against a blank containing all the reagents.

Pd—β-ETETG system. Absorbance values of solutions containing 3.45 μg Pd ml^{-1} (3.24×10^{-5} M) with chloride concentration 3.0 M, in which the Naβ-ETETG concentration ranged from 3.24×10^{-5} M to 3.24×10^{-3} M (16 solutions were prepared) with pH 1.50 at 25.0°C, were measured at 260, 270 and 280 nm against a blank containing all the reagents.

RESULTS AND DISCUSSION

The following equations represent the proposed systems.

$$[PdCl_4]^{2-}_{(aq)} + H_2EBTG_{(aq)} \overset{K_1}{\rightleftarrows} [PdCl_2H_2EBTG]^{0}_{(aq)} + 2Cl^-_{(aq)}$$

$$K_1 = [PdCl_2H_2EBTG]\,[Cl^-]^2/[PdCl_4^{2-}]\,[H_2EBTG] \quad (1)$$

$$[PdCl_2H_2EBTG]^{0}_{(aq)} + H_2EBTG_{(aq)} \overset{K_2}{\rightleftarrows} [Pd(H_2EBTG)_2]^{2+}_{(aq)} + 2Cl^-_{(aq)}$$

$$K_2 = [Pd(H_2EBTG)_2^{2+}]\,[Cl^-]^2/[PdCl_2H_2EBTG]\,[H_2EBTG] \quad (2)$$

$$[PdCl_4]^{2-}_{(aq)} + HETETG_{(aq)} \overset{K_1}{\rightleftarrows} [PdCl_2HETETG]^{0}_{(aq)} + 2Cl^-_{(aq)}$$

$$K_1 = [PdCl_2HETETG]\,[Cl^-]^2/[PdCl_4^{2-}]\,[HETETG] \quad (3)$$

$$[PdCl_2HETETG]^{0}_{(aq)} + HETETG_{(aq)} \overset{K_2}{\rightleftarrows} [Pd(HETETG)_2]^{2+}_{(aq)} + 2Cl^-_{(aq)}$$

$$K_2 = [Pd(HETETG)_2^{2+}]\,[Cl^-]^2/[PdCl_2HETETG]\,[HETETG] \quad (4)$$

By spectrophotometry it was possible to determine the successive constants for the PD-EBTG and Pd-β-ETETG systems at ionic strength 3.0 M, pH 1.50 and 25.0°C.

The $[PdCl_4]^{2-}_{(aq)}$ species exists only in the pH range 1—2 and at high chloride concentration [9, 12]. In this pH range the EBTG and β-ETETG anions are practically in the protonated form. If $pK_1 = 3.28$ and $pK_2 = 4.03$ for EBTGA [13], calculation of α_0, α_1 and α_2 and plotting the relative amounts of the species at various pH values indicates that, at pH 1 and pH 2 99.5% and 95% of the ligand is present as H_2L, respectively. If $pK = 3.61$ for β-ETETGA [14], at pH 1 and pH 2 99.8% and 97.8% of the ligand is present as HL respectively.

Thus in equilibrium (1) (or 3), two chloride ions should be replaced by one H_2EBTG (or HETETG), resulting in a mixed complex (1:1 species); probably the ligand will be bound to the metal by the two sulphur atoms (bidentate ligand), forming a five-membered ring. In equilibrium (2) (or 4), the mixed complex reacts with one more ligand to give the 2:1 species.

Newman and Hume [8] presented general equations by means of which the absorbance can be used to determine successive formation constants and absorptivities for systems containing either single or mixed ligand complexes.

These equations were derived on the basis that the absorbance values of a mixture depend on the absorptivities, stepwise constants and the central atom and ligand concentrations. For the Pd—EBTG and Pd—β-ETETG systems, the following equation for 3 absorbing species similar to that of Newman and Hume [8] was obtained

$$A = \frac{1}{K_2}\left\{\left[\frac{1}{K_1}\left(A_0\frac{M_t}{M_0} - A\right)\frac{(C_{Cl^-})^2}{C_L} - A + \epsilon_1 M_t\right]\frac{(C_{Cl^-})^2}{C_L}\right\} + \epsilon_2 M_t \qquad (5)$$

or

$$\left(A_0\frac{M_t}{M_0} - A\right)\frac{(C_{Cl^-})^2}{C_L} = \frac{A\,C_L}{(C_{Cl^-})^2}K_1K_2 - M_t\frac{C_L}{(C_{Cl^-})^2}K_1K_2\epsilon_2 + AK_1 - M_t\epsilon_1K_1 \qquad (6)$$

where A is the absorbance when all three species $[PdCl_4]^{2-}_{(aq)}$, $[PdCl_2L]^{0}_{(aq)}$ and $[PdL_2]^{2+}_{(aq)}$ exist; A_0 is the absorbance when only $[PdCl_4]^{2-}_{(aq)}$ exists; M_t is the central atom concentration, when all three species exist; M_0 is the central atom concentration, when only $[PdCl_4]^{2-}_{(aq)}$ exists, C_{Cl^-} is the chloride concentration and C_L the ligand concentration (L = H_2EBTG or HETETG); the unknowns are K_1 and K_2 (stepwise constants) and ϵ_1 and ϵ_2 (molar absorptivities).

If a wavelength is selected where only two species absorb, a new equation can be used [8]

$$\left(A_0\frac{M_t}{M_0} - A\right)\frac{(C_{Cl^-})^2}{C_L} = AK_1 - M_t\,\epsilon_1\,K_1 \qquad (7)$$

where K_1 and ϵ_1 are the unknowns. If only chloride is added in great excess compared with the concentration of the central atom, then $A_0 = \epsilon_0 M_0$ and $\epsilon_0 = A_0/M_0$, where A_0 is the absorbance and M_0 the concentration of the central atom, all of which is assumed to be in the form of the highest complex $[PdCl_4]^{2-}_{(aq)}$.

Table 3 and Fig. 1, curve 11 or Fig. 2, curve 17 (spectrum of $[PdCl_4]^{2-}_{(aq)}$), show the absorbance values and molar absorptivities for the $[PdCl_4]^{2-}_{(aq)}$ system.

TABLE 3

Absorbance and molar absorptivities of $[PdCl_4]^{2-}_{(aq)}$
(I = 3.0 M, pH = 1.5, T = 25.0°C, 2.91 × 10^{-5} M $PdCl_2$ present)

$\lambda_{(nm)}$	Absorbance	ϵ (× 10^3 l mol^{-1} cm^{-1})	Ref.
260	0.083	2.78	present work
270	0.262	9.00	present work
278	—	11.2	[12]
		10.8	
280	0.334	11.5	present work
280	—	11.0	[15]

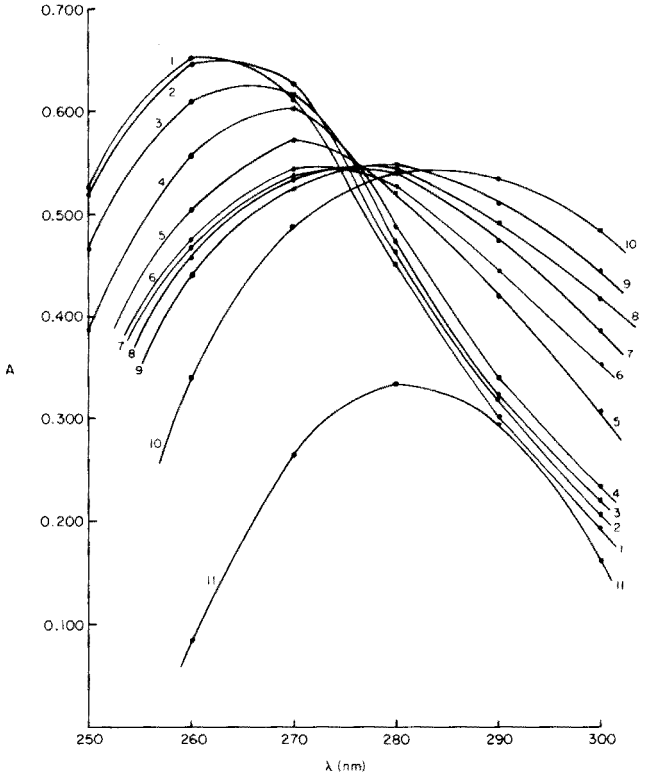

Fig. 1. Absorption spectra for the Pd—EBTG system. For solutions (1) to (10), 3.24×10^{-5} M $PdCl_2$ was present; (1) 9.72×10^{-4} M L; (2) 1.63×10^{-3} M L; (3) 2.27×10^{-3} M L; (4) 3.24×10^{-3} M L; (5) 9.72×10^{-3} M L; (6) 1.62×10^{-2} M L; (7) 1.94×10^{-2} M L; (8) 2.11×10^{-2} M L; (9) 2.27×10^{-2} M L; (10) 2.59×10^{-2} M L. For solution (11), 2.91×10^{-5} M $PdCl_2$ was present, no ligand. I = 3.0 M, pH = 1.50, T = 25.0°C. Measurements made against reagent blank.

Figure 1, curves 1—10 shows the absorbance values and spectra of the Pd—EBTG system. Figure 2, curves 1—16, shows the absorbance values and spectra of the Pd—β-ETETG system.

Taking into account the equations shown, the absorbance values and spectra of the Pd—EBTG and Pd—β-ETETG systems, and assuming that in the region from 260 to 280 nm the 1:1 species predominates and that the contribution of the absorbance values of the second species is negligible in solutions (1) to (4), K_1 and ϵ_1 were calculated by means of eqn. (7).

From solution (5) onwards in Figs. 1 and 2, the conversion of the two ligand species increases due to the increased ligand concentration, and the maxima are shifted to higher wavelengths. Thus, from solution (5) to (10) for the Pd—EBTG system and from solution (5) to (16) for the Pd—β-ETETG system, K_2 and ϵ_2 were calculated from eqn. (6) and the known values of K_1 and ϵ_1.

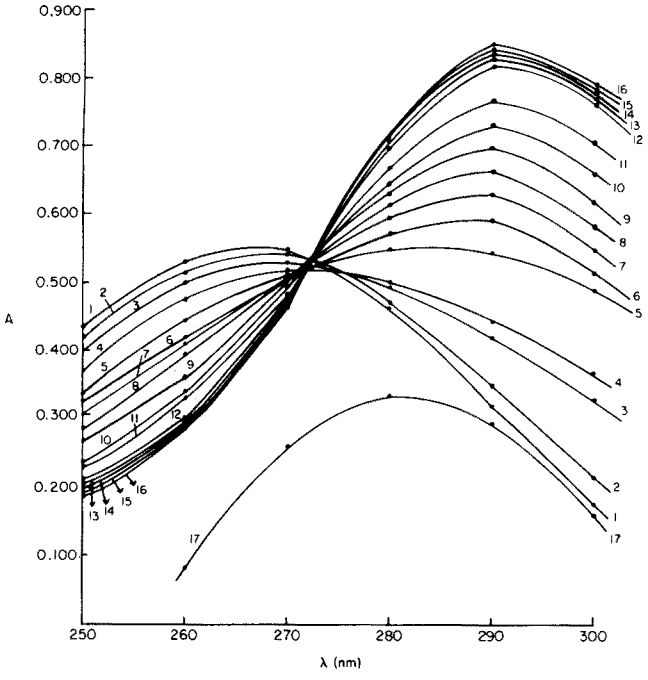

Fig. 2. Absorption spectra for the Pd—β-ETETG system. For solutions (1) to (16), 3.24×10^{-5} M $PdCl_2$ was present; (1) 3.24×10^{-5} M L; (2) 4.86×10^{-5} M L; (3) 6.48×10^{-5} M L; (4) 9.72×10^{-5} M L; (5) 1.13×10^{-4} M L; (6) 1.30×10^{-4} M L; (7) 1.62×10^{-4} M L; (8) 1.94×10^{-4} M L; (9) 2.27×10^{-4} M L; (10) 2.59×10^{-4} M L; (11) 3.24×10^{-4} M L; (12) 6.48×10^{-4} M L; (13) 1.30×10^{-3} M L; (14) 1.94×10^{-3} M L; (15) 2.59×10^{-3} M L; (16) 3.24×10^{-3} M L. For solution (17), 2.91×10^{-5} M $PdCl_2$ was present, no ligand. I = 3.0 M, pH = 1.50, T = 25.0°C. Measurements made against reagent blank.

TABLE 4

Results for the Pd—EBTG and Pd—β-ETETG systems
(I = 3.0 M, pH = 1.5, T = 25.0°C. Molar absorptivities, ϵ, are given in l mol^{-1} cm^{-1})

λ (nm)	Pd—EBTG system				Pd-β-ETETG system			
	K_1 ($\times 10^4$ M)	ϵ_1	K_2 ($\times 10^2$ M)	ϵ_2	K_1 ($\times 10^6$ M)	ϵ_1	K_2 ($\times 10^4$ M)	ϵ_2
260	2.71	2.23×10^4	2.69	1.13×10^3	2.21	1.66×10^4	4.85	7.98×10^3
270	2.72	2.10×10^4	2.61	8.44×10^3	2.13	1.72×10^4	4.75	1.42×10^4
280	2.78	1.50×10^4	2.73	1.95×10^4	2.13	1.52×10^4	4.77	2.26×10^4

Pd—EBTG system: K_1 average = $(2.74 \pm 0.04) \times 10^4$ M; K_2 average = $(2.68 \pm 0.06) \times 10^2$ M.
Pd—β-ETETG system: K_1 average = $(2.16 \pm 0.05) \times 10^6$ M; K_2 average = $(4.79 \pm 0.05) \times 10^4$ M.

The equilibrium constants were found by solving the simultaneous equations (Hewlett-Packard 25 calculator) and by linear fit of the available data. Both methods gave consistent results, which are presented in Table 4.

EBTGA and β-ETETGA form complexes with Pd(II) even for the ratios $[EBTGA]/[Cl^-] = 3.24 \times 10^{-4}$ and $[\beta\text{-ETETGA}]/[Cl^-] = 1.08 \times 10^{-5}$; ligands

with sulphur atoms (soft ligands) prefer bonding with soft cations such as Pd(II) [16].

These results confirm [17] that formation constants of complexes containing heavy halides and sulphur compounds as ligand are high when the complexes contain low spin d^8 ions, e.g. Pd(II), Pt(II), Au(III), and d^{10} ions, e.g. Cu(I), Hg(II), Ag(I) and Au(I). In consequence, such ligands, especially β-ETETGA, could be used as a masking agent for Pd(II) in acidic medium.

Some considerations can be made to explain the different values of the constants for the systems studied. The ligands EBTGA and β-ETETGA have at least one sulphur atom in a β-position with regard to —COOH and $-CH_3$ groups. As the —COOH group has a $-I$ effect (groups withdrawing electrons inductively, relative to hydrogen) [18] the adjacent carbon atom will try to accommodate its induced charge by withdrawing electrons from the atom to which it is bonded. Thus the sulphur atom will present less of the characteristics of a soft ligand than the sulphur atom in a position β with respect to a $-CH_3$ group, which has a $+I$ effect (group that donates electrons) [18]. Such a sulphur atom will show less tendency to react with Pd(II) (a soft cation); the complex between Pd(II) and EBTGA is weaker than that between Pd(II) and β-ETETGA as shown by the values of the constants for Pd(II) with EBTGA and β-ETETGA (Table 4). The determination of formal constants of the systems formed between Pd(II) and other ligands, e.g. ethylthioglycolic acid, thiodiglycolic acid and nitroso-R salt are in progress.

For the Pd—EBTG system, the C—S and symmetric and asymmetric —COO stretching frequencies (Table 1) agree with previous results [4, 19]. The palladium—sulphur coordination in the complexes is shown by the fact that the C—S stretch is shifted to a lower wavenumber compared with the free acid and its sodium salt.

A comparison of the ν_s and ν_a COO frequencies obtained for the complexes, Na_2EBTG and EBTGA, indicates that the carboxylic groups are intact in the palladium complexes; the intense, broad absorption in the range 2,300—3,600 cm^{-1}, with various maxima, is characteristic of OH-groups involved in hydrogen bond associations [4, 20].

From the i.r. spectra (Table 2) for the Pd—β-ETETG system, similar conclusions can be reached; fewer bands than for the Pd—EBTG system were observed from 2,300 to 3,600 cm^{-1}.

Kukushkin et al. [11] reported that the i.r. spectra of $[Pd(EBTGA)Cl_2]$ and $[(EBTGA)_2Pd]Cl_2.2H_2O$ show splitting of the $\nu_a(COO)$ frequencies. This is probably related to the *cis* position of the carboxylic groups. In the i.r. spectra of $[Pd(\beta\text{-}ETETGA)Cl_2]$ and $[(\beta\text{-}ETETGA)_2Pd]Cl_2$, splitting was not observed and the carboxylic groups of the complex $[(\beta\text{-}ETETGA)_2Pd]Cl_2$ were assigned to *trans* positions [11].

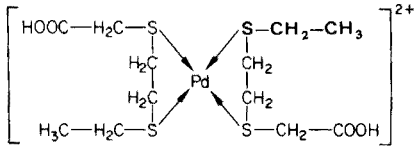

The hypothesis of Kukushkin et al. [11] is probably correct, as the large number of i.r. bands observed, related to the —OH groups involved in intramolecular hydrogen bond associations [21] probably arises when the parent —COOH groups are in the *cis* position.

REFERENCES

1 L. R. M. Pitombo, Anal. Chim. Acta, 46 (1969) 158.
2 L. R. M. Pitombo, Anal. Chim. Acta, 62 (1972) 103.
3 L. R. M. Pitombo and E. R. Cartaxo, Talanta, 21 (1974) 965.
4 L. R. M. Pitombo and G. Oliveira Neto, Anal. Chim. Acta, 75 (1975) 391.
5 L. R. M. Pitombo, G. Oliveira Neto and E. Oliveira, Mikrochim. Acta, I (1976) 121.
6 L. R. M. Pitombo and G. Oliveira Neto, Anal. Chim. Acta, 75 (1975) 401.
7 J. M. Cesário, Dissertação de Mestrado, São Paulo, Brazil, 1977.
8 L. Newman and D. N. Hume, J. Am. Chem. Soc., 79 (1957) 4571.
9 W. F. Rittner, A. Gulko and G. Schumckler, Talanta, 17 (1970) 807.
10 A. Tiberg, Thesis, Lund, Sweden, 1924.
11 Yu. N. Kukushkin, R. A. Vlasona and E. A. Kondratow, Koord. Khim., 2 (1976) 971.
12 A. Gulko and G. Schumckler, J. Inorg. Nucl. Chem., 35 (1972) 603.
13 L. R. M. Pitombo and E. Oliveira, Unpublished paper.
14 M. C. Medeiros, Dissertação de Mestrado, São Paulo, Brazil, 1977; M. P. Peters, Dissertação de Mestrado, São Paulo, Brazil, 1977.
15 L. Victori, X. Tomás and F. Malgosa, Afinidad, XXXII 303 (1975) 867.
16 R. G. Pearson, J. Am. Chem. Soc., 85 (1963) 3533.
17 S. E. Livingstone, Q. Rev. Chem. Soc., 19 (1965) 386.
18 J. A. Hirsch, Concepts in Theoretical Organic Chemistry, Allyn and Bacon, Boston, 1975, p. 91.
19 J. Podlaha and J. Podlahoná, Inorg. Chim. Acta, 5 (1971) 413.
20 L. J. Bellamy, Advances in Infrared Group Frequencies, Methuen, London, 1968, p. 270.
21 K. Nakamoto, Infrared Spectra of Inorganic and Coordination Compounds, J. Wiley, New York, 1963, p. 224.

Analytica Chimica Acta, 101 (1978) 187—191

SEMIQUANTITATIVE ANALYSIS BY COMPARING THE SPEED OF DECOLORIZATION ON FILTER PAPER

HERBERT WEISZ*, SIEGBERT PANTEL and ROLF GIESIN

Lehrstuhl für Analytische Chemie, Chemisches Laboratorium der Universität, Freiburg i.Br. (Federal Republic of Germany)

(Received 20th February 1978)

SUMMARY

An extremely simple method is described for semiquantitative determination of various substances, based on comparison of the speed of decolorization of coloured reaction products of the test substance on filter paper. Time measurements are unnecessary, because the unknown and two suitable standards are observed simultaneously on the same paper. The substances can be applied either as spots or as ring-shaped segments prepared with a ring oven. Substances such as Ni, Cu, Fe(III), iodide and resorcinol can be determined in the microgram range.

Some fifteen years ago, a semiquantitative analytical method based on measurement of bleaching time of coloured test spots was reported. A drop (about 1 μl) of the sample solution was spotted on filter paper, and a suitable reaction was applied to give a coloured stable product. The paper was then bathed in some reagent solution so that the spot was either dissolved or transformed to a colourless compound. As long as the individual chemical reaction, the filter paper used, the temperature and the concentration of the bleaching solution were kept identical, the time of decolorization depended only on the unknown concentration of the sample solution, and calibration graphs of bleaching time vs. concentration could be constructed. This method has been used to determine various metals and anions [1—3]. However, this simple chronocolorimetric technique demands precise time measurement (10—120 s) and accurate reproducibility of the above-mentioned working conditions.

The new approach discussed here is even simpler: three drops — the sample drop and two standards — are spotted on a filter paper strip to form an equilateral triangle. The substance to be estimated is converted to a sufficiently stable coloured product, the paper is rinsed well and dipped into a bleaching solution, and the bleaching speeds are compared. The spot containing the lowest concentration is obviously the first to be bleached. The order of decolorization indicates whether the sample spot has a concentration within or outside the range of standards, and further spots are compared as required. Because the spot reactions are carried out simultaneously on the

same paper and in the same bleaching solution, the working conditions are not critical; the time need not be measured, and mere comparison of the speeds of decolorization suffices.

Six standard solutions (I, II, IV, VI, VIII, X) of the test substance are necessary, with concentrations in the ratio 1:2:4:6:8:10. In the first observation, the sample drop and one drop each of solutions IV and X are compared. In further steps, the sample drop and drops of suitably chosen standards are spotted on the filter paper and the procedure is repeated. Three comparison steps normally suffice to indicate which standard is closest to the unknown. Two further estimates are then made with suitable dilutions of the sample solution, based on the information already obtained. For practical reasons, the sample solution should correspond to at least the concentration of solution IV, so that the necessary dilutions can be made. Application of more than one sample drop on one spot is not permissible because the spots become inhomogeneous.

If ring segments rather than spots are bleached, several sample drops can easily be applied. On three concentric points around the middle of a round filter paper (55 mm diameter) are placed one drop each of the sample solution and of two standard solutions (Fig. 1a). The filter is placed on the ring oven [4] and the drops are washed as usual from the center to the ring zone with a suitable solvent (Fig. 1b). The colour-producing reaction is then used, so that three sharp ring segments, 10—20 mm long become visible (Fig. 1c); this procedure is derived from the ring oven segment technique and ring colorimetry [5,6]. The segments are then decolorized. Because of the reduced area of a ring segment compared to a 1-μl spot, this technique is more sensitive than the spot method.

The determination of nickel will illustrate these variations. Some other examples are discussed only briefly.

DETERMINATION OF NICKEL

For the determination of nickel, the well known reaction with diacetyldioxime (DMG) is applied; the chelate can be decomposed by treatment with potassium cyanide, which forms tetracyanonickelate(II).

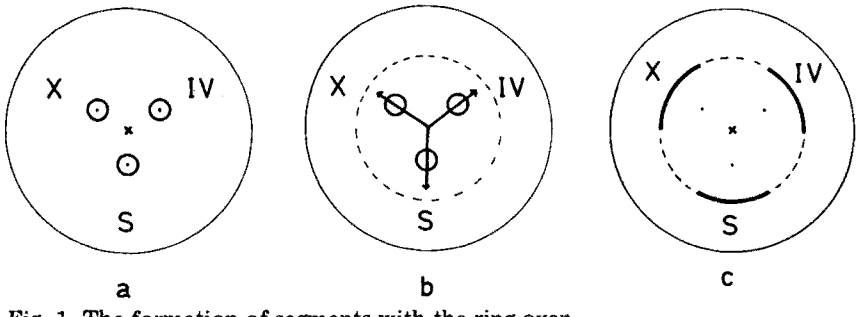

Fig. 1. The formation of segments with the ring oven.

Spots

Six standard solutions (I, II, IV, VI, VIII and X) are needed containing 1, 2, 4, 6, 8 and 10 mg Ni ml^{-1}. With a capillary pipette (about 1 μl), one drop each of the sample solution and of standards IV and X are spotted on a filter paper strip (25 × 55 mm). The filter is fumed over ammonia, bathed in an alcoholic 1% solution of DMG, rinsed well with water and pressed on filter paper. The strip is then immersed with a plastic clamp, in a 6% potassium cyanide solution in a 200-ml beaker and the order of decolorization is observed whilst the mixture is stirred magnetically.

As an example, if the speed of bleaching for the sample lies between those for standards IV and X, but nearer X, the second test then involves comparison with standards VIII and X. If the speed for the sample then lies between these two standards, this result is designated S = IX. (Only standard numbers or the arithmetic mean of two neighbouring standards are permissible.) In the next step, a diluted (1:1) sample solution is compared with more dilute standards and so on. The results of each observation step are tabulated, with the bleaching speed decreasing from left to right; for example, IV ... S ... X means that the bleaching speed for the sample lies between the speeds for standards IV and X, whereas IV/S ... VI means that standard VI is bleached more slowly than the sample, which is bleached at about the same speed as standard IV (sample nearer to IV). Thus, a full set of observations would be tabulated as follows:

Orientation:	IV ... S/X	
1st test	: VIII ... S ... X	result: S = IX
2nd test	: IV/$\frac{1}{2}$S ... VI	result: $\frac{1}{2}$S = IV
3rd test	: II/$\frac{1}{4}$S ... IV	result: $\frac{1}{4}$S = II

The concentration of the sample solution is then calculated by the "weighted average" method [4,7]:

$$\frac{7}{4}\,S = XV;\ S = \frac{15 \times 4}{7} \times 1 = 8.57 \text{ mg Ni ml}^{-1}$$

Segments

Six standard solutions (I ... X) of nickel containing 0.4—4 mg Ni ml^{-1} are needed. One drop each of the unknown solution and of two suitable standard solutions are spotted concentrically on the paper and concentrated on the ring oven in three sharply outlined segments with 0.1 M HCl as wash solution. The further procedure — colour formation, bleaching and calculation — are exactly the same as for spots.

Table 1 gives some results for the estimation of nickel by the two techniques.

OTHER EXAMPLES

Iron(III)

The estimation of iron(III) is also based on the bleaching of a coloured compound (Prussian blue) by complex formation (0.2 M EDTA). The six

standard solutions I ... X used contain 0.1—1 mg Fe(III) ml^{-1} for spots and 0.04—0.4 mg Fe(III) ml^{-1} for segments.

Copper(II)

The determination of copper(II) is based on the oxidative bleaching of copper(II) dithiooxamide (spots or segments fumed over ammonia and bathed in an alcoholic 1% solution of dithiooxamide) by a saturated solution of potassium peroxodisulfate in 1 M H_2SO_4 at room temperature. Alternatively, the coloured complex can be bleached with bromine vapour, by holding the filter paper in a wide-necked bottle over saturated bromine water.

The standard solutions required contain 1—10 mg Cu ml^{-1} for spots and 0.4—4 mg Cu ml^{-1} for segments.

Iodide

The indirect determination of iodide is based on its precipitation as silver iodide (bathing the paper in aqueous 0.1 M $AgNO_3$ in 0.01 M HNO_3). After exposure for 1 min to daylight, the spots or segments are bathed in a photographic developer (thus forming brown to black spots or segments of silver) and then bleached in a solution of potassium hexacyanoferrate(III) and potassium cyanide (100 ml of 2% KCN + 20 ml of 2% $K_3[Fe(CN)_6]$).

The standard solutions required contain 1—10 mg I ml^{-1} for spots and 0.4—4 mg I ml^{-1} for segments.

Resorcinol

This is also an indirect determination, being based on the reduction of molybdophosphoric acid to molybdenum blue by resorcinol and oxidative bleaching by hypochlorite. The spots or segments (transferred to the ring zone with water) are sprayed with aqueous 10% molybdophosphoric acid, fumed over ammonia and immersed in a sodium hypochlorite solution acidified with HCl. The standard resorcinol solutions contain 1—10 mg ml^{-1} for spots and 0.4—4 mg ml^{-1} for segments.

TABLE 1

Estimation of nickel (mg ml^{-1}) by bleaching of nickel—diacetyldioxime complex with cyanide

Spots				Segments			
Given	Found	Given	Found	Given	Found	Given	Found
5.1	4.6	17.2	16.0	0.51	0.52	2.18	2.17
8.2	8.0	24.8	24.0	0.85	0.86	2.26	2.53
12.2	12.0	33.2	32.0	1.28	1.33	2.54	2.40
16.2	16.0	36.2	34.3	1.67	1.60	2.62	3.08
16.4	14.9	40.0	41.6	2.01	2.13	3.54	3.88

For all the determinations mentioned here, the range of errors was about the same as that indicated for estimations of nickel. Accordingly, no results are given.

REFERENCES

1 H. Weisz, Analytical Chemistry 1962, Proceedings Feigl Anniversary Symposium Birmingham, Elsevier, Amsterdam, 1963, p. 93.
2 H. Weisz, Anal. Chim. Acta, 30 (1964) 163.
3 R. C. Srivastava and G. S. Deshmukh, J. Inst. Chemists (India) Vol. XLVII (1975) 200.
4 H. Weisz, Microanalysis by the Ring Oven Technique, 2nd edn., Pergamon, Oxford, 1970.
5 H. Weisz, S. Pantel and I. Vereno, Mikrochim. Acta, (1975 II) 287; (1976 I) 289.
6 H. Weisz and M. Hanif, Anal. Chim. Acta, 81 (1976) 179.
7 W. Knödel and H. Weisz, Mikrochim. Acta, (1956) 667.

Analytica Chimica Acta, 101 (1978) 193—197

Short Communication

SIMULTANEOUS EXTRACTION OF MERCURY AND ARSENIC FROM FISH TISSUES, AND AN AUTOMATED DETERMINATION OF ARSENIC BY ATOMIC ABSORPTION SPECTROMETRY

HAIG AGEMIAN* and VENGHUOT CHEAM

Canada Centre for Inland Waters, Water Quality Branch, 867 Lakeshore Road, P.O. Box 5050, Burlington, Ontario (Canada)

(Received 17th January 1978)

It is often necessary to determine several metals in fish; for routine analysis of many samples it is advantageous to have a common extraction system. This communication describes a method for the simultaneous extraction of mercury and arsenic from fish, and their subsequent automated determination.

The determination of mercury in solid environmental samples requires low-temperature preparation techniques to prevent loss of organomercury compounds. Armstrong and Uthe [1] used a sulfuric and nitric acid digestion at 58°C followed by permanganate oxidation to extract mercury from fish tissue, but nitric acid and nitrate interfere with arsine generation by borohydride reduction [2]. Automated reduction followed by quartz tube atomization reduces but does not eliminate this interference; the use of sulfuric acid is preferable [2].

The Analytical Methods Committee [3, 4] described the use of hydrogen peroxide and sulfuric acid for the destruction of organic matter, and it has been applied [5] to mercury in biological materials. This digestion system can be coupled with permanganate—persulfate oxidation to recover completely organomercury and organoarsenic compounds from fish. This sample preparation technique has been adapted to automated reduction and determination by a.a.s. The automated system reported previously [6] was used for mercury, and an automated system based on sodium borohydride reduction with atomization in a quartz tube was developed for the determination of arsenic.

Experimental

Sampling. Prior to digestion, the fish tissue samples must be homogenized. Efficient transfer of aliquots of such samples into long-necked digestion or extraction flasks requires a long delivery tube. A syringe-like device has been proposed [7] but the device shown in Fig. 1 was found to be more satisfactory. The barrel and plunger are commercially available (Part 432, Oxford pipettor Model S-A, cat. No. 13-687-75, Fisher Scientific). The ground glass

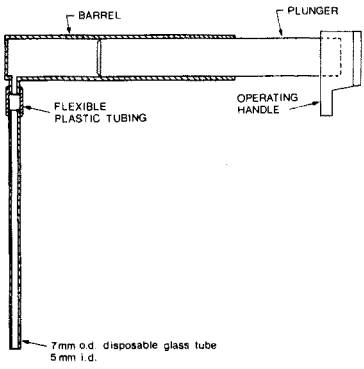

Fig. 1. Transfer device.

piston delivers a good vacuum so that thick samples can be used. The sample touches only the disposable glass tube; these are pre-cut and pre-washed suitably; a 6 in. length suits most analytical requirements. This device is economical, efficient, time-saving, free from cross-contamination and easy to construct reproducibly.

Reagents. All reagents were certified analytical grade.

Digestion. Add 1 ml of 30% H_2O_2 solution to the digestion flask containing the sample and let it stand for ca. 10 min. Add, slowly, 10 ml of 18 M H_2SO_4 while cooling the flask efficiently in an ice bath. If, after 5 min the sample has not dissolved, put the flask in a shaking water bath at 60°C for 30 min. Remove the flask, place in an ice bath and add 20 ml of 5% $KMnO_4$ solution slowly to avoid frothing. Let the solution stand for 60 min. Add 60 ml of 5% (w/v) potassium persulfate solution and leave overnight.

Clear the solution by adding 5 ml of 20% (w/v) hydroxylamine sulfate—20% (w/v) sodium chloride solution. Adjust to 100 ml.

Prepare valid standards with the same reagents. Analyse the samples with the manifold shown in Fig. 2. Use a 40—1/2 cam in the autosampler to obtain a sampling time of 30 s and a wash time of 60 s.

Optimization of manifold. Several manifolds [8—11] have been reported for the automated determination of arsenic; they use different reagents and concentrations and different designs of gas—liquid separators. It was intended to optimize these variables and provide a manifold which would recover arsenic(III) and arsenic(V) equally; the effects of sulfuric, nitric and hydrochloric acids on their recovery were investigated. The effect of the wash column was also investigated; without drying, water vapour condensed inside the line to the furnace, and both the precision and detection limit ($0.1/\mu g\ l^{-1}$) attainable with the manifold in Fig. 2 decreased.

Each of the gas—liquid separators used earlier [8—11] was tested for efficiency. Figure 3 shows the calibration curves obtained; the separator used by Goulden and Brooksbank [8] is the most efficient.

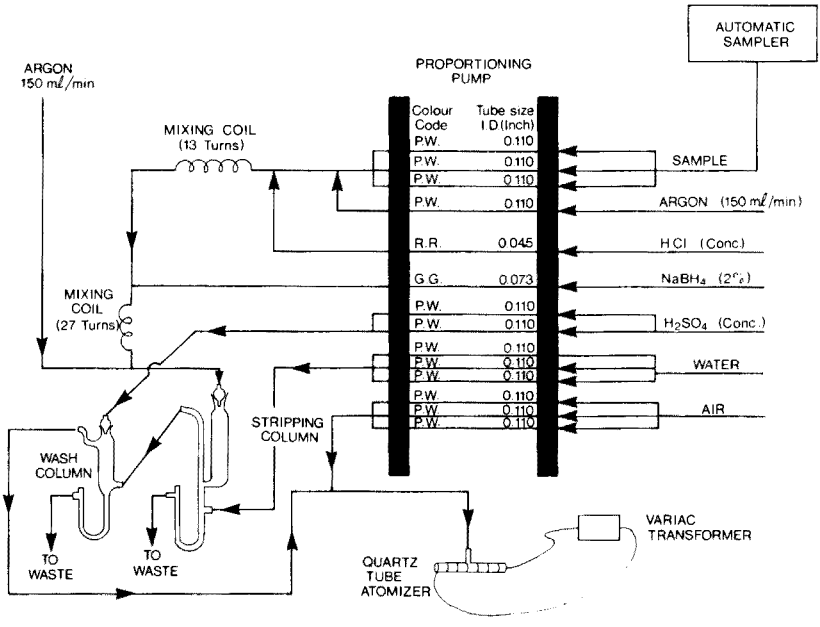

Fig. 2. Arsenic manifold.

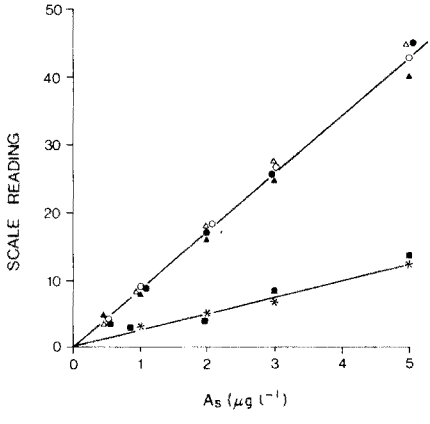

Fig. 3. The effect of the gas—liquid separator on the sensitivity of the arsenic calibration curve. (○) As(III) in distilled water [8]; (●) As(III) in reagent matrix of method [8]; (△) As(V) in distilled water [8]; (▲) As(V) in reagent matrix method [8]; (*) As(V) in distilled water [10]; (■) As(V) in distilled water [9, 11].

Apparatus. The equipment (Fig. 2) consisted of a Technicon Auto Analyzer II sampler with 40—1/2 cam; proportioning pump (Auto Analyzer II); Technicon Auto Analyzer mixing coils and tubing of specified dimensions; flowmeter for argon (150 ml min^{-1}); stripping column and wash column [8]; furnace made from silica tubing (1 cm i.d., 10 cm long). At the center of this

tube a "T" is made with silica tubing (2 mm i.d.) for the gas entry port. The furnace is wrapped with asbestos paper and chromel wire (26-gauge; resistance, 20Ω). Silica tubing mounted close to the furnace contains a pyrometer; the furnace is heated to 850°C through a variac transformer. The Perkin-Elmer Model 503 atomic absorption spectrometer used was equipped with an arsenic EDL lamp and power supply and recorder (Hewlett-Packard Model 7128A).

Discussion

The organoarsenic compounds present must be broken down to inorganic arsenic before arsine can be formed by borohydride reduction. The rate of reduction of As(III) and As(V) is different [12]. A manifold in which both arsenic species could be determined would undoubtedly be superior. Although the arsenic sensitivity by borohydride reduction is constant for 1—6 M hydrochloric acid [13], the reduction rate in solutions containing varying amounts of reagents became dependent on the hydrochloric acid concentration in the manifold, and As(III) and As(V) were not reduced at the same rate under all conditions. It was necessary to study the effect of the fish extracts and reagent matrix on the borohydride reduction of arsenic.

Concentrations from 0.5 to 1.5 M hydrochloric acid gave the highest sensitivity; both As(III) and As(V) were equivalently detected. When the HCl concentration was increased from 2 to 6 M, the sensitivity for both species decreased, particularly for As(V). Replacement of the HCl line (Fig. 2) with an H_2SO_4 line, to give a common acid in the manifold and sample digests, reduced the sensitivity for As(III) by ca. 30%, and As(V) gave a sensitivity of ca. 50% of that of As(III).

Fishman and Spencer [14] added the $NaBH_4$ (2% w/v in 1 M NaOH) prior to the HCl in the manifold. However, when HCl was added first here, the precision was better (r.s.d. 0.88% compared with 2.9%, $n = 10$) with only a slight drop in sensitivity (mean peak height 39.8 compared with 41.4 divisions for a pure As(III) solution containing 1 μg As l^{-1} , $n = 10$) but as the sample extracts in this method are highly acidic, it is essential that the borohydride be added after the HCl.

The digestion procedure used by Friend et al. [5] recovers mercury, including methylmercury, without the need for treatment with permanganate and persulfate. The oxidation potential of the hydrogen peroxide—sulfuric acid mixture is high enough to oxidize methylmercury but did not oxidize organoarsenic compounds completely; arsenic from methylarsonic acid, *p*-arsanilic acid and phenylarsine oxide was partially recovered but arsenic from dimethylarsonic acid was not recovered. Inclusion of the permanganate—persulfate oxidation step gave complete recovery from all of these compounds and from both As(III) and As(V).

Figure 4 shows a standard additions curve for As(III) and As(V) for a typical fish sample. The recoveries of As and Hg were 99% and 101%, respectively, from National Bureau of Standards SRM 1571 (Orchard Leaves),

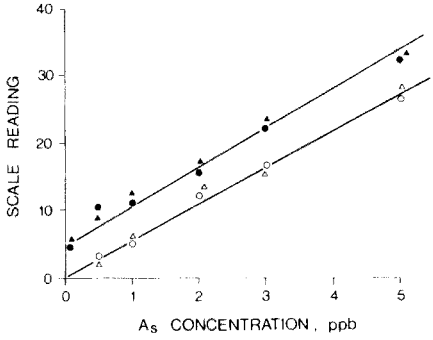

Fig. 4. (○) Calibration curve for As(III). (●) Standard additions curve for As(III) in a fish sample; (△) calibration curve for As(V); (▲) standard additions curve for As(V) in a fish sample.

which contain 10 ± 2 μg As g^{-1} and 0.155 μg Hg g^{-1}. Replicate determinations at a level of 0.10 μg As g^{-1} and 0.14 Hg g^{-1} in a typical fish sample gave relative standard deviations of 15% and 9%, respectively.

The authors thank B. G. Oliver for comments on the original manuscript and C. Pacenza for secretarial help.

REFERENCES

1 F. A. J. Armstrong and J. F. Uthe, At. Absorpt. Newsl., 10 (1971) 101.
2 F. D. Pierce and H. R. Brown, Anal. Chem., 49 (1977) 1417.
3 Analytical Methods Committee, Analyst, 92 (1967) 403.
4 Analytical Methods Committee, Analyst, 101 (1976) 62.
5 M. T. Friend, C. A. Smith and D. Wishart, At. Absorpt. Newsl., 16 (1977) 46.
6 H. Agemian and A. S. Y. Chau, Anal. Chim. Acta, 75 (1975) 297.
7 Analytical Methods Manual, Inland Water Directorate, Water Quality Branch, Ottawa, Canada 1974.
8 P. D. Goulden and P. Brooksbank, Anal. Chem., 46 (1974) 1431.
9 Kwok-Toi Kan, Anal. Lett., 6 (1973) 603.
10 P. N. Vijan and G. R. Wood, At. Absorpt. Newsl., 13 (1974) 33.
11 F. J. Schmidt, J. L. Royer and S. M. Muir, Anal. Lett., 8 (1975) 123.
12 K. G. Brodie, Am. Lab., March (1977) 73.
13 F. J. Ferdandez, At. Absorpt. Newsl., 12 (1973) 93.
14 M. Fishman and R. Spencer, Anal. Chem., 49 (1977) 1599.

Analytica Chimica Acta, 101 (1978) 199—201

Short Communication

DETERMINATION OF TIN BY NON-DISPERSIVE ATOMIC FLUORESCENCE SPECTROMETRY WITH A HYDRIDE GENERATION TECHNIQUE AND A SMALL ARGON-HYDROGEN-ENTRAINED AIR FLAME

K. TSUJII* and K. KUGA

Central Research Laboratory, Hitachi Ltd., Kokubunji, Tokyo (Japan)

(Received 20th February 1978)

A previous paper [1] reported that the small argon-hydrogen-entrained air flame improves the signal-to-noise ratio in the non-dispersive atomic fluorescence spectrometric determination of arsenic and antimony by a sodium borohydride reduction technique. This report extends the application of the small flame atomization technique to the determination of tin in steel samples.

Experimental

Apparatus and reagents. The apparatus was described previously [1]. The light source was a Perkin-Elmer electrodeless discharge lamp (Sn) operated at 7 W with a Perkin-Elmer Model 185-120 power supply.

The stock solution used was a commercially available 1000-ppm tin(IV) solution (Kanto Chemical Corp.) made from tin(IV) chloride. A 1000-ppm tin(II) standard solution was prepared from tin(II) chloride in hydrochloric acid medium. Sodium borohydride solution (1%) was prepared, just before use, by dissolving sodium borohydride pellets (98% min. pure, Alfa Inorganics) in water. All other chemicals were of analytical-reagent grade.

Procedure. Sodium borohydride solution (1%, 2 ml) was transferred to the hydride generation cell. The sample solution (500 μl) was injected by Eppendorf pipette (with plastic tip) into the cell. The reduction product was supplied continuously to the flame by a constant flow rate of argon (1.0 l min^{-1}). Peak height signals were measured.

Results and discussion

The atomic fluorescence intensity was maximal between 0.25 and 0.5 M hydrochloric acid, and then decreased with increasing acid concentration. The following measurements were made with 0.5 M hydrochloric acid.

Solutions of tin(IV), containing 0.5 M hydrochloric acid and nitric acid (0—5 M) or perchloric acid (0—4 M), were prepared. The marked depressive effects of nitric acid and perchloric acid are shown in Fig. 1.

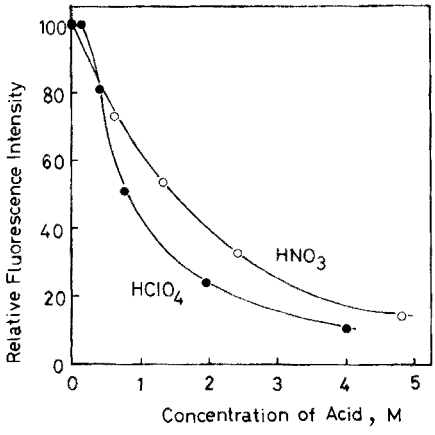

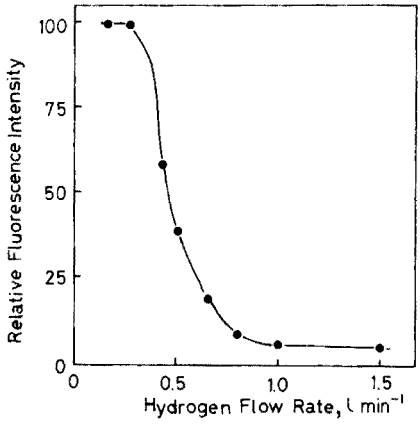

Fig. 1. Effect of nitric acid and perchloric acid concentrations on tin fluorescence intensity.

Fig. 2. Effect of hydrogen flow-rate on tin fluorescence intensity. Argon flow-rate, 1.0 l min^{-1}.

The oxidation state of the tin did not affect the fluorescence intensity; this is similar to the result reported by Nakashima [2] in a study of plasma emission spectrometry with a hydride generation technique. The following measurements were made with tin(IV) solution.

For an argon flow-rate of 1.0 l min^{-1}, the effect of the hydrogen flow rate on tin fluorescence intensity is shown in Fig. 2. The increase in signal intensity with decreasing hydrogen flow rate shows the tendency reported for arsenic and antimony [1]. The small argon-hydrogen-entrained air flame (flame height: ca. 1 cm), obtained at 0.25 l min^{-1} of hydrogen and 1.0 l min^{-1} of argon, was used in the following measurements.

Detection limit and analytical working curve. The detection limit, defined as the amount of tin for which the signal-to-noise ratio equals two, was 0.6 ng; the reagent blank value was 2 ng. This detection limit is inferior to those for arsenic and antimony [1], possibly because the solar-blind photomultiplier has poor sensitivity, even though it responds to radiation below 320 nm, for the most sensitive atomic fluorescence spectral line of tin (317.5 nm) [3].

The analytical working curve was linear up to 0.5 μg. The relative standard deviation for 0.2 μg (500 μl of 0.4-ppm solution) of tin was 2.3% (n = 8).

Effect of foreign elements. The interfering effects of 100-fold amounts (by weight) of eight elements present in steel samples were investigated. No interference was observed for chromium, manganese, and molybdenum. The elements which decreased the fluorescence intensity by more than 5% are listed in Table 1. Nickel gave a marked depressive effect.

Determination of tin in low-alloy steel samples. This technique was applied to the determination of tin in low-alloy steel samples (British Chemical Standards). The sample (ca. 0.1 g, accurately weighed) was dissolved in aqua regia

TABLE 1

Effect of foreign elements on the recovery of 200 ng of tin

Element	Cu	Fe	Ni	P	V
Sn found (ng)	160	186	61	188	167
Recovery (%)	80	93	30	94	84

TABLE 2

Determination of tin in BCS low alloy steel samples

BCS sample	Certified value (%)	This method[a] (%)
No. 253	0.007	0.0071 (±3.1)
No. 258	0.009	0.0093 (±2.5)

[a]Average of four determinations (±% relative standard deviation).

(10 ml). Perchloric acid (5 ml) was added and the solution was heated until white fumes were evolved. The solution was transferred to a 25-ml volumetric flask and diluted to the mark, and aliquots were analysed.

To eliminate interference effects, a standard addition method was employed. The results (Table 2) agree well with the certified values.

We are grateful to Dr. Kazuo Yasuda and Mr. Mitsuo Hayashi for valuable discussions.

REFERENCES

1 K. Tsujii and K. Kuga, Anal. Chim. Acta, 97 (1978) 51.
2 R. Nakashima, Bunseki Kagaku, 25 (1976) 869.
3 R. F. Browner, R. M. Dagnall and T. S. West, Anal. Chim. Acta, 46 (1969) 207.

Analytica Chimica Acta, 101 (1978) 203—206

Short Communication

A SIMPLE APPARATUS FOR THE SPECTROMETRIC DETERMINATION OF MERCURY BY THE COLD VAPOUR—ATOMIC ABSORPTION TECHNIQUE

J. F. CHAPMAN* and L. S. DALE

Chemical Technology Division, Australian Atomic Energy Commission, Research Establishment, Lucas Heights, NSW, 2232 (Australia)

(Received 6th March 1978)

The determination of mercury by atomic absorption spectrometry (a.a.s.) with the cold vapour technique is well documented [1, 2]. Poluektov et al. [3] were the first to couple the reduction of mercury(II) to mercury with atomic absorption measurements of the vapour in an absorption cell.

Many variations of the apparatus used to generate and transfer the mercury vapour to the absorption cell have been described. Generation may be carried out by aeration of the reduced solution in a reaction vessel connected directly to an absorption cell [4]. Another technique relies on partitioning of the reduced mercury between a fixed volume and the liquid phase while the liquid is vigorously stirred; the equilibrated gas phase is then transferred to the cell with a gas purge [5]. In both cases the mixture of gas and mercury vapour is exhausted from the cell. A continuous recirculation system [6] employing aeration, in which equilibrium partitioning of the gas phase is achieved in a closed system, produces steady absorption signals in contrast to the other systems which give sharp absorption peaks.

Flow-through systems require an auxiliary gas stream and suffer from a reduction in sensitivity because the mercury vapour is diluted. In addition where an aeration rather than partitioning technique is employed the use of cell windows requires the incorporation of moisture traps or bypass lines to prevent fogging. These traps however introduce variable memory effects.

To overcome these problems, a simple apparatus which uses water displacement to transfer the equilibrated mercury vapour, at a constant rate, to the absorption cell has been devised. The absorption cell has been designed so that windows are not required and the rate of introduction of the mercury vapour into the cell is similar to the rate of diffusion from it. As a result, absorption signals persist for about 10 s.

Experimental

Equipment. Measurements were made with a Varian-Techtron Model AA5 atomic absorption spectrometer. The hollow-cathode lamp was operated at

3 mA. Other conditions were: scale expansion × 1, and spectral band pass 0.2 nm. Signals were recorded on a 10-mV strip chart recorder at a chart speed of 30 mm min^{-1}.

Apparatus. The absorption cell and displacement apparatus are shown in Fig. 1. The cell was fabricated from glass tubing with dimensions 260 mm long, 12.5 mm i.d.. The diameter was reduced around the centre inlet, this section being 80 mm long, 5 mm i.d.. The displacement apparatus consists of a 100-ml Erlenmeyer flask joined to a separatory funnel by a modified B14 ground glass joint which has a side-arm with an S19 spherical glass joint to facilitate connection to the cell.

Operating conditions. The reduction is carried out by adding 1 ml of 30% tin(II) chloride solution in 10% sulphuric acid to a prepared sample in the Erlenmeyer flask. After the addition, the flask is immediately connected to the displacement apparatus and the solution is stirred vigorously with a magnetic stirrer. The separatory funnel is filled with 100 ml of water. After 2 min, the stirring is stopped, the tap is opened, and water displaces the equilibrated gas phase from the flask into the absorption cell at a rate of 7 ml s^{-1}. After recording the steady part of the absorption signal, the residual mercury is purged from the system with nitrogen.

It is necessary to calibrate the volume of the Erlenmeyer flasks and to reject those which vary by more than 2 ml.

Results

The characteristic mass (weight of mercury per 1% light absorption) was 1 ng, equivalent to 0.1 $\mu g\ l^{-1}$ per 10 ml of sample. Larger samples can be handled with a corresponding improvement in the detection limit.

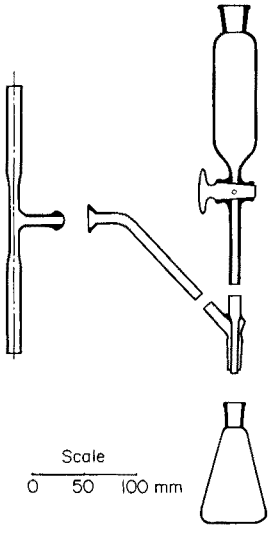

Fig. 1. Absorption cell and displacement apparatus.

In the range 10—100 ng of mercury, the relative standard deviation was 2%. Figure 2 shows the reproducibility obtained at the 100-ng level.

The absolute detection limit was determined from 10 runs on both the reagent blank and the 0.1 ng mercury standard, with high scale expansion. A signal equal to 2 σ of the blank value, related to the standard, gave a detection limit of 0.04 ng.

As well as high sensitivity and reproducibility, the calibrations had a high degree of linearity; a calibration consisting of 13 points in the range 0—100 ng of mercury gave a correlation coefficient of 0.999.

The procedure has been used to determine mercury in liquid effluent samples. Preliminary treatment of the samples was as described by Omang [7]. To a 10-ml sample in an Erlenmeyer flask, 1 ml of 3% potassium permanganate solution and 1 ml of concentrated sulphuric acid were added. The flask was stoppered immediately and left to stand overnight. The excess of potassium permanganate was then reduced by the dropwise addition of 3% hydroxylammonium chloride solution just before the determination. All reagents were A.R. grade.

For the analysis of each sample, additions of 50 ng and 100 ng of mercury were made in duplicate. Each of the additions was treated as described above. Figure 3 is a typical calibration showing the absorption signals obtained.

Discussion

In addition to simplicity, the apparatus has other noteworthy features. The use of Erlenmeyer flasks for storage of samples, chemical pretreatment, and reduction of the mercury is convenient; the flasks form a good seal with the connecting apparatus and, because only one container is used, contamination risk is minimized and analysis time is reduced. The absence of cell windows eliminates fogging problems and there is no need for moisture traps or gas bypass lines. The most important aspect is that the equilibrated gas phase is undiluted so that maximum sensitivity can be achieved.

The absorption cell dimensions are important in obtaining prolonged absorp-

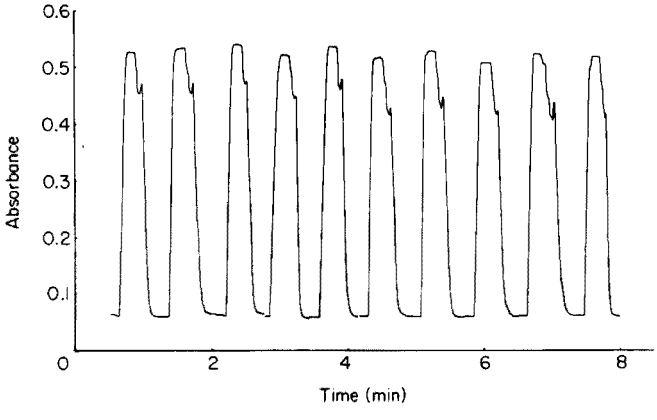

Fig. 2. Reproducibility for 100 ng of mercury.

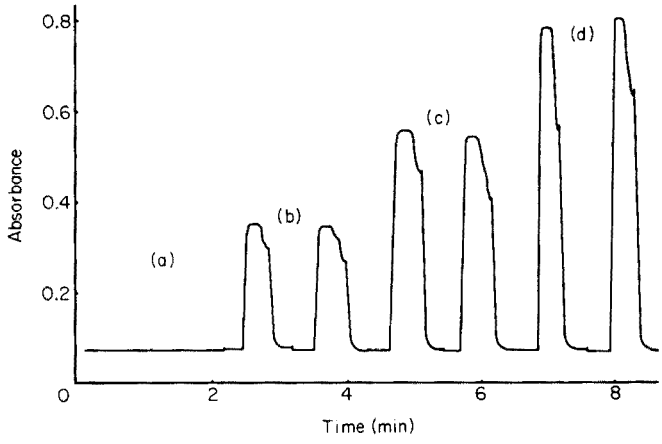

Fig. 3. Typical standard addition calibration for an effluent sample spiked with 50 ng and 100 ng mercury. (a) Blank; (b) effluent sample; (c) sample + 50 ng of Hg; (d) sample + 100 ng of Hg.

tion signals. The volume of the Erlenmeyer flask is 130 ml; the gas transfer rate is 7 ml s^{-1}. With a cell volume of ca. 84 ml, the absorption signal is maintained for 8—10 s indicating that the rate of introduction of the gas phase into the cell is equal to the rate of diffusion from the cell over this period. The long path length and minimum volume of the absorption cell provide prolonged absorption signals and high sensitivity.

REFERENCES

1 D. C. Manning, At. Absorpt. Newsl., 9 (1970) 97.
2 A. M. Ure, Anal. Chim. Acta, 76 (1975) 1.
3 N. S. Poluektov, R. A. Vitkun and Yu. V. Zelynkova, J. Anal. Chem. U.S.S.R., 19 (1964) 873.
4 R. Stux and E. Rothery, Varian Techtron Tech. Top., January 1971, p. 1.
5 A. M. Ure and C. A. Shand, Anal. Chim. Acta, 72 (1974) 63.
6 W. R. Hatch and W. L. Ott, Anal. Chem., 40 (1968) 2085.
7 S. H. Omang, Anal. Chim. Acta, 53 (1971) 415.

Analytica Chimica Acta, 101 (1978) 207—210

Short Communication

DISTRIBUTION COEFFICIENTS OF METALS ON A STRONGLY BASIC ANION-EXCHANGE RESIN IN AQUEOUS THIOCYANIC ACID

TETSUYA KIRIYAMA

Chemistry Laboratory, Faculty of Education, Kagoshima University, Gungen, Kagoshima (Japan)

ROKURO KURODA

Laboratory for Analytical Chemistry, Faculty of Engineering, University of Chiba, Yayoi-cho, Chiba (Japan)

(Received 14th March 1978)

Since the early work of Kraus and Nelson [1] systematic determinations of the distribution coefficients of elements between a strongly basic resin and mineral acid media have been made [2, 3]. Information on the distribution coefficients of metals in aqueous thiocyanic acid is lacking, although the column elution behaviour and distribution coefficients of many elements in thiocyanate salt solution and/or thiocyanate—hydrochloric acid media are available [4—6].

Systematic determinations of the distribution coefficients for many metal ions are presented in this report because they offer a better starting point in attempting separations than some methods reported in the literature.

Measurement of distribution coefficient

A strongly basic anion-exchange resin, Amberlite CG 400 type I (100-200 mesh) was used in the thiocyanate form. Weight distribution coefficients (amount of ion per g of dry resin/amount of ion per ml of the solution) were determined by the batch equilibrium method at room temperature with a loading of 0.1 mmol of metal ion on 1.00 g of resin. Thiocyanic acid concentrations ranged from 0.010 to 1.00 M. The equilibration period was 20 h.

Results and discussion

The distribution coefficients of various metal ions on Amberlite CG 400 (SCN^-) are listed in Table 1; the metals are arranged according to their distribution coefficients in 1.00 M thiocyanic acid. Of the metal ions tested, Na, K, Mg(II), Ca(II), Sr(II), Ba(II), Y(III), La(III), Sm(III), Yb(III), Al(III), Cr(III) and As(III) were not sorbed to any great extent from 1.0, 0.30, 0.10, 0.030 and 0.010 M thiocyanic acid solutions, and are not included in Table 1. Tl(I) was precipitated, probably as TlSCN, from 0.3 and 1.0 M thiocyanic acid solutions. Sb(III) forms an insoluble oxycompound at lower acid concentrations (0.30 to 0.010 M).

TABLE 1

Distribution coefficients on Amberlite CG 400 in thiocyanic acid media

Element	HSCN, M				
	1.0	0.30	0.10	0.030	0.010
Pd(II)	$> 10^5$	$> 10^5$	$> 10^5$	$> 10^5$	$> 10^5$
Mo(VI)	$> 10^5$	$> 10^5$	6.9×10^4	5.4×10^3	4.5×10^3
U(VI)	$> 10^5$	6.6×10^4	6.8×10^4	2.1×10^4	3.5×10^3
Bi(III)	6.2×10^4	$> 10^5$	5.5×10^4	ppt.	ppt.
Zn(II)	4.2×10^4	$> 10^5$	$> 10^5$	8.3×10^4	8.2×10^3
Zr(IV)	2.2×10^4	3.4×10^3	69	< 1	< 1
Sb(III)	2.1×10^4	ppt.[a]	ppt.	ppt.	ppt.
V(IV)	1.4×10^4	2.2×10^4	1.6×10^4	4.3×10^3	5.4×10^2
Fe(III)	1.4×10^4	1.1×10^4	3.2×10^3	8.4×10^2	1.8×10^2
Co(II)	1.3×10^4	8.5×10^3	3.4×10^3	6.5×10^2	1.1×10^2
Sn(IV)	9.3×10^3	1.0×10^4	2.3×10^3	ppt.	ppt.
W(VI)	8.0×10^3	4.7×10^3	4.7×10^3	9.6×10^3	2.3×10^4
Pt(IV)	5.1×10^3	$> 10^5$	$> 10^5$	$> 10^5$	$> 10^5$
Cu(II)	4.3×10^3	5.7×10^4	$> 10^5$	5.6×10^4	3.4×10^4
Sc(III)	2.0×10^3	1.7×10^2	26	2.5	< 1
Cd(II)	1.5×10^3	1.6×10^3	9.9×10^2	2.9×10^2	80
Ti(IV)	1.5×10^3	1.9×10^2	25	1.7	< 1
Mn(II)	2.1×10^2	1.0×10^2	30	6.6	1.8
Pb(II)	2.0×10^2	94	22	3.5	< 1
In(III)	1.5×10^2	5.9×10^2	1.4×10^3	2.2×10^3	2.5×10^3
Ga(III)	1.5×10^2	2.2×10^2	77	14	2.3
Th(IV)	1.4×10^2	27	2.9	< 1	< 1
Re(VII)	1.4×10^2	26	74	2.4×10^2	6.1×10^2
Ni(II)	1.1×10^2	70	28	8.0	< 1
Ge(IV)	5.4	< 1	< 1	< 1	< 1

[a]ppt.: precipitation taken place.

Table 1 shows that the sorption of most metal ions increases greatly with increasing concentration of thiocyanic acid in spite of the limited concentration range involved; this is the case for Mo(VI), U(VI), Zr(IV), Fe(III), Co(II), Sc(III), (Cd(II)), Ti(IV), Mn(II), Pb(II), Th(IV), Ni(II) and Ge(IV). The distribution coefficients of Mo(VI), U(VI), Zr(IV), Fe(III) and Co(II) reached values as high as 10^4—10^5 in 1.0 M thiocyanic acid; in hydrochloric acid media [1] these values are never reached over the concentration range up to 12 M, except for Fe(III). Although they are not sorbed, or sorbed very slightly, from hydrochloric acid solutions, Sc(III), Ti(IV), Mn(II), Th(IV) and Ni(II) gave distribution coefficients as high as 2000 for Sc(III), 1500 for Ti(IV), 140 for Th(IV), 110 for Ni(II) etc. from 1.0 M thiocyanic acid solution.

Sorption of Bi(III), Zn(II), V(IV), Sn(IV), Cu(II), (Cd(II)) and Ga(III) increases with increasing concentration of thiocyanic acid up to a maximum, and then decreases as the concentration of thiocyanic acid is increased

further. Of the metals mentioned, Zn(II), Sn(IV), Cu(II), Cd(II) and Ga(III) also exhibit maxima in hydrochloric acid media, but at much higher acid concentration. In addition, the distribution coefficients are extraordinarily high, particularly for V(IV) and Cu(II), in thiocyanic acid media; these metals are only sorbed to a slight extent over a wide concentration range of hydrochloric acid. Although not so marked as for V(IV) and Cu(II), Bi(III), Sn(IV) and Zn(II) give much higher sorption in thiocyanic acid than in hydrochloric acid media.

In hydrochloric acid solution [1, 3] the distribution coefficient of Ga(III) increases from ca. 80 in 3 M acid to ca. 10^5 in 7 M acid, after which it decreases to 10^4 in 12 M hydrochloric acid. In contrast, the distribution coefficient of Ga(III) is much less in thiocyanic acid media, reaching a maximum value of 220 in 0.3 M acid.

Of the metal ions investigated, a few metals including Pt(IV), In(III) and perhaps Pd(II), show a tendency for the distribution coefficient to increase with decreasing concentration of thiocyanic acid. In(III) is much more markedly sorbed on the anion-exchange resin from thiocyanate media rather than from hydrochloric acid media; the distribution coefficients of In(III) on resins of the quaternary ammonium type are 10, 8 and 5 in 3, 7 and 12 M hydrochloric acid, respectively [1, 3]. Stabilities of $MSCN^{2+}$ species follow the sequence In > Ga > Al in accordance with their sorption sequence in thiocyanic acid media; of these, only In(III) forms an inner-sphere complex [7].

Re(VII) exhibits a minimum on the sorption curve (K_d vs. [HSCN]) as is the case for mixed thiocyanate–hydrochloric acid (0.5 M) media [8].

Inspection of the distribution coefficients given in Table 1 provides useful data for separations that are difficult in other ion-exchange systems. Some advantages of anion exchange in thiocyanic acid, compared with hydrochloric acid media, are the sorption of Sc(III), Ni(II), Th(IV) and the enhanced sorption of Zr(IV), V(IV), Co(II), Cu(II), Mn(II), In(III), etc. from rather lower concentration. By proper choice of thiocyanic acid concentration the following quantitative separations were achieved: Al(III)–Ti(IV), Al(III)–Ni(II), Al(III)–Fe(III), Al(III)–Ga(III), As(III)–V(IV), Cr(III)–Ni(II), Cr(III)–V(IV), Cr(III)–Mn(II), Ga(III)–In(III), Ge(IV)–Sn(IV), Mn(II)–Co(II), Mn(II)–Zn(II), Mn(II)–Cd(II), Mn(II)–Re(VII), Ni(II)–Co(II), Ni(II)–Cu(II), Pb(II)–Cd(II), Re(VII)–Mo(VI), Re(VII)–Zn(II), Ti(IV)–V(IV), Tl(I)–In(III), Y(III)–Sc(III), [La(III), Sm(III) or Yb(III)]–Sc(III), [Y(III), La(III), Sm(III) or Yb(III)]–Th(IV), Th(IV)–Sc(III), Zr(IV)–U(VI), thus confirming the validity of the distribution coefficients in Table 1. Multicomponent separations are also feasible as shown in Fig. 1.

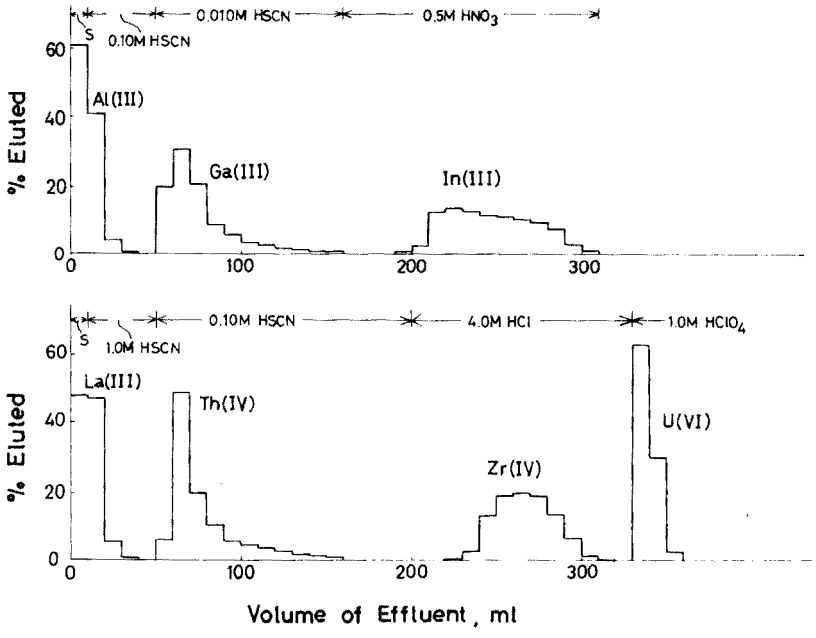

Fig. 1. Multicomponent separations. Column: 1.0 cm (i.d.) × 8 cm (3.0 g resin). Upper: Al 2.79 mg, Ga 9.49 mg and In 10.2 mg in 10 ml of 0.10 M HSCN. Lower: La 13.3 mg, Th 22.4 mg, Zr 9.93 mg and U 22.4 mg in 10 ml of 1.0 M HSCN.

REFERENCES

1 K. A. Kraus and F. Nelson, Proc. Int. Conf. Peaceful Uses At. Energy, Geneva, 7 (1956) 113.
2 W. Rieman, III and H. F. Walton, Ion Exchange in Analytical Chemistry, Pergamon Press, Oxford, 1970.
3 J. Korkisch, Modern Methods for the Separation of Rarer Metal Ions, Pergamon Press, Oxford, 1969.
4 A. K. Majumdar and B. K. Mitra, Fresenius Z. Anal. Chem., 208 (1965) 1.
5 K. Kawabuchi, H. Hamaguchi and R. Kuroda, J. Chromatogr., 17 (1965) 567.
6 J. S. Fritz and E. E. Kaminski, Talanta, 18 (1971) 541.
7 R. C. Das, A. C. Dash and J. P. Mishra, J. Inorg. Nucl. Chem., 30 (1968) 2417.
8 H. Hamaguchi, K. Kawabuchi and R. Kuroda, Anal. Chem., 36 (1964) 1654.

Analytica Chimica Acta, 101 (1978) 211—214

Short Communication

INDOPHENOL DERIVATIZATION IN DIFFERENTIAL PULSE POLAROGRAPHY: APPLICATION TO THE DETERMINATION OF AMMONIA, *p*-AMINOPHENOL AND SULPHANILAMIDE

A. G. FOGG* and Y. Z. AHMED

Chemistry Department, Loughborough University of Technology, Loughborough, Leicestershire (Gt. Britain)

(Received 1st February 1978)

Studies of the colorimetric determination of *p*-aminophenol [1, 2] and sulphanilamide [3] as indophenol derivatives have already been reported. In the presence of excess of phenol in alkaline solution, *p*-aminophenol is oxidized completely to indophenol by the molecular oxygen which exists naturally in the water: in acidic conditions hypochlorite can be used to oxidize *p*-aminophenol to *p*-quinonechlorimine which can then be coupled with phenol in alkaline solution to give indophenol [1]. The former method is clearly more convenient. To determine sulphanilamide as its indophenol derivative, oxidation is done with alkaline hypochlorite in the presence of sodium nitroprusside acting as catalyst [3]: this procedure is identical to that commonly used for the colorimetric determination of ammonia.

In this communication, the possibilities of using indophenol derivatization in the differential pulse polarographic (d.p.p.) determination of ammonia, *p*-aminophenol and sulphanilamide are described. When solutions were prepared by a procedure similar to that recommended [3] for colorimetry, well-defined d.p.p. peaks at —0.33 V were obtained at the 10^{-4}—10^{-5} M level of sulphanilamide. Further investigation showed that this procedure was also suitable for the determination of *p*-aminophenol and of ammonia. In these determinations, the catalyst, sodium nitroprusside, was present in slight excess of a 1:1 (nitroprusside:sample) ratio, and this was found to be adequate. The addition of a large excess of nitroprusside had to be avoided, as the nitroprusside caused a peak to appear at —0.27 V. However, the necessity of judging fairly closely the amount of nitroprusside to add could be avoided by adding twice the amount of sodium sulphite as the nitroprusside originally added; this effectively removed the excess of nitroprusside without affecting the indophenol. The order of addition hypochlorite—phenol—nitroprusside gave slightly better baselines than the order normally used in colorimetry, i.e. phenol—nitroprusside—hypochlorite.

Experimental

Instrumentation. Polarography was carried out with a PAR 174 polarographic analyzer (Princeton Applied Research). A large-area saturated calomel electrode served as the counter electrode in two-electrode operation. For all differential pulse polarograms reported here, a 2-s forced drop time was used with a 50-mV pulse height and a scan rate of 2 mV s^{-1}. Deoxygenation was effected with nitrogen which had been passed through a vanadium(II) scrubber.

Standard solutions, 10^{-5} M. These were prepared from more concentrated standard solutions by dilution with ammonia-free distilled water. Standard ammonia and *p*-aminophenol solutions were prepared from ammonium chloride and *p*-aminophenol hydrochloride. For sulphanilamide, a little dilute hydrochloric acid was needed for complete dissolution.

Alkaline phenol solution. Dissolve 30 g of phenol and 20 g of sodium hydroxide carefully in water and dilute to 100 ml.

Sodium hypochlorite solution. Dilute 10 ml of a commercial sodium hypochlorite solution (10—14% available chlorine) to 25 ml.

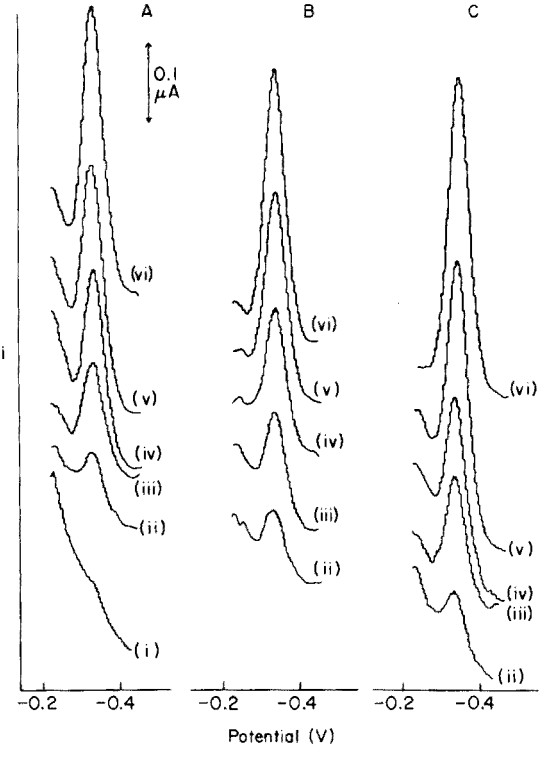

Fig. 1. Differential pulse polarograms of the indophenol dye formed from (A) ammonia, (B) *p*-aminophenol and (C) sulphanilamide. The concentrations of the sample materials in each solution were: (i) 0, (ii) 0.4, (iii) 1.2, (iv) 2.0, (v) 3.2, (vi) 4.0 × 10^{-6} M.

Procedure. Transfer an aliquot of standard or sample solution containing 0.1—15 μg of ammonia (or 0.5—100 μg of *p*-aminophenol, or 1—150 μg of sulphanilamide) to a 40-ml boiling tube and dilute to 20 ml with distilled water. Add by pipette, in turn, with swirling and at 1—2 min intervals, 0.2 ml of sodium hypochlorite solution, 0.5 ml of alkaline phenol solution, and 0.2 ml of freshly prepared sodium nitroprusside solution (1 mg ml^{-1}). Heat the solution for 20—30 min at 60—70°C in a water bath, to form the indophenol derivative. Add 0.5 ml of freshly prepared solution (1 mg ml^{-1}) of sodium sulphite heptahydrate, and continue the heating for a further 15 min. Cool the solution and dilute to 25 ml in a calibrated flask.

Deoxygenate the solution and record the differential pulse polarogram between —0.22 and —0.44 V. Measure the height of the peak at —0.33 V.

Results and discussion

Typical polarograms which were obtained for calibration over the range 1×10^{-7}—4×10^{-6} M for the determination of ammonia, *p*-aminophenol and sulphanilamide are shown in Fig. 1. The calibration graphs are rectilinear and the coefficients of variation (10 determinations) at the 4×10^{-6} M level were 3% for ammonia and 4% for *p*-aminophenol and sulphanilamide. Similar calibration graphs up to 4×10^{-5} M were also rectilinear: at these higher levels the baselines of the polarograms were flat.

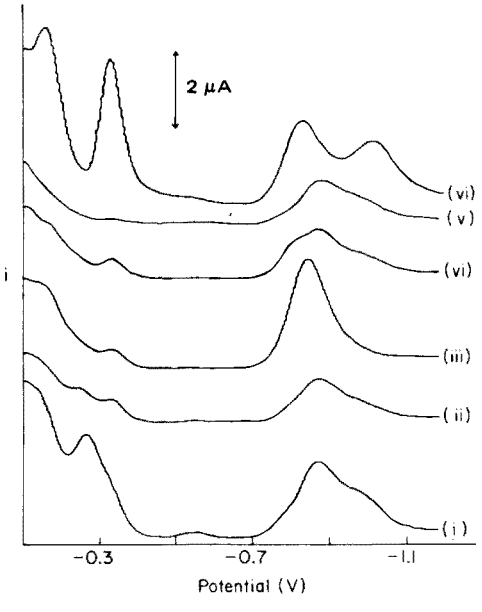

Fig. 2. Effect of sulphite on the differential pulse polarograms obtained with 5.4×10^{-5} M sodium nitroprusside in presence and absence of ammonia. For curves (i)—(v), no ammonia was added. For curve (i), no sulphite was added. The nitroprusside:sulphite mole ratios were: (ii) 2:1, (iii) 1:1, (iv) 2:3, (v) 1:2. For curve (vi) the nitroprusside:sulphite mole ratio was 1:2, and 4×10^{-5} M ammonia was present.

The effect of sulphite in improving the baseline is shown in Fig. 2. In alkaline solution, nitroprusside $[Fe(CN)_5NO]^{2-}$ is converted [4] to its conjugate base pentacyanonitroferrate(II), $[Fe(CN)_5NO_2]^{4-}$; its yellow colour disappears on addition of hypochlorite, and the true catalyst is probably pentacyanoaquoferrate(III). This unidentified species, which gives the interfering peak at −0.27 V (curve (i), Fig. 2), seems to be the oxidant in the oxidative coupling reaction as a good baseline can be obtained without addition of sulphite if the nitroprusside is present in a stoichiometric amount with the substance to be determined. The removal of excess of this species — presumably by reduction — by sulphite is shown in curve (v) of Fig. 2. Clearly, it is better to add excess of nitroprusside and then remove it with sulphite.

For most applications in which ammonia is determined in clear solutions, the present polarographic method would have no advantage over the colorimetric method. The indophenol derivatives have molar absorptivities of about 2.5×10^4 l mol^{-1} cm^{-1} at $\lambda_{max} = 625$ nm, which means that a 4×10^{-7} M solution has an absorbance of 0.01 in 1-cm cells. The polarographic method can be considered as an alternative near the limit of the colorimetric method, in the presence of coloured interferents, or in turbid solutions.

REFERENCES

1 D. R. Davis, A. G. Fogg, D. T. Burns and J. S. Wragg, Analyst, 99 (1974) 12.
2 C. T. H. Ellcock and A. G. Fogg, Analyst, 100 (1975) 16.
3 C. T. H. Ellcock and A. G. Fogg, Lab. Pract., 23 (1974) 555.
4 J. H. Swinehart, Coord. Chem. Rev., 2 (1967) 385.

Analytica Chimica Acta, 101 (1978) 215—219

Short Communication

MULTIPARAMETRIC CURVE FITTING AND THE NUMBER OF CALCULATED PARAMETERS

BRUCE H. CAMPBELL

J. T. Baker Chemical Company, Phillipsburg, NJ 00865 (U.S.A.)

(Received 22nd December 1977)

With the increased availability of computers, many curve-fitting programs have been tailored to keep computational times as short as possible. One of the approaches is to try to reduce the number of parameters whose values are to be calculated. As is demonstrated here, increasing the number of parameters to be calculated can lead to decreased computational times as well as increased accuracy.

The particular program used for this study involves multiparametric curve fitting [1]. Although the program differs in detail from others, the principle is the same in that a set of curves is generated and the one that gives the best "goodness of fit" is selected. The details of the program can be summarized. The user selects a general equation taken from the underlying theory of the experiment. Usually, this is a closed equation. Next, pairs of data sets for the two variables are entered, followed by the number of parameters for which values are to be calculated, and then by an initial estimate of the values for each of the parameters. Finally, "fixed" values are assigned to those parameters that are assumed to be known or measured accurately. The program then calculates the value of the dependent variable corresponding to each value of the independent variable. Next, the deviations of the computed values of the dependent variable from the experimental values are calculated, squared, and summed. The values of the parameters are then changed by the program, another set of values for the independent variable is generated and the sum of the squares of the deviations recalculated. If the new value of the sum of the squares is smaller than the previous one, the parameter values are refined in the same direction. This process continues until the value of the sum of the squares either reaches an acceptably low result or does not change by more than 0.01% for ten cycles.

When a "fixed" value of a parameter is entered by the user, the program uses that value as "exact" and error-free. If the "fixed" value is in error, the computed values of the other parameters will be in error. The extent of the resulting error depends not only on the magnitude of the original error but on the mathematical relationship of a computed value of the parameter to the "fixed" one. This situation is illustrated below.

Curve fitting for polarographic data

Three cases of fitting curves to polarographic data are considered in terms of computational time and accuracy. These examples focus on the results of assigning a fixed value to one parameter and not assigning values to any other parameter apart from initial estimates. The first case is a calculation utilizing "artificially" generated data; the second and third are calculations based on actual experimental data. For the first case, the data were generated from the Nernst equation for a single polarographic wave.

$$E = E_{\frac{1}{2}} + (RT/\sigma F) \ln (i_d - i/i) \quad (1)$$

where E is the potential, $E_{\frac{1}{2}}$ is the half-wave potential, i_d is the diffusion current, i is the current, $\sigma = n$ if the wave is Nernstian but $\sigma = \alpha n_a$ if it is not, and the other parameters have their usual significance. The temperature was taken to be 298.1 K.

Data sets for E—i were obtained for 19 points with equal increments of E, with $E_{\frac{1}{2}}$, i_d, and n having values of exactly one. The data sets were entered into the curve-fitting program along with eqn. (1) as well as estimates of initial values of the parameters. Calculations of $E_{\frac{1}{2}}$ and n were performed where the various values of i_d assigned differed from exactly one. The results are given in Table 1. Next, values of $E_{\frac{1}{2}}$, n, and i_d were calculated with no value assigned to i_d. It took 2.5 s for the computation when values for all three parameters were calculated. The calculated values of $E_{\frac{1}{2}}$, n, and i_d were 1.000000, 0.999888, and 0.999985, respectively. In every trial, the same initial estimates of the values of $E_{\frac{1}{2}}$ and n were used.

The next two cases involve the polarographic reduction of 2-fluoronaphthalene and the reduction of an impurity in a sodium carbonate solution (Fig. 1). The initial approach was to try the curve-fitting procedure on the data with the assumption of only one reduction wave. The resultant fits suggested that two reduction waves are involved in each case [2—4]. Therefore, the following

TABLE 1

A comparison of errors in $E_{\frac{1}{2}}$ and n as functions of known errors in the diffusion current, calculated from eqn. (1) with artificial data

Wave height i_d		Calcd. value of $E_{\frac{1}{2}}$ (True $E_{\frac{1}{2}}$ = 1.000)		Calcd. value of slope parameter, σ (True σ = 1.000)		Processing time (s)
% of true value	% Error	V	% Error	eq./mol	% Error	
110	+10	1.008	+0.8	0.84	—16	2.4
101	+1	1.001	+0.1	0.98	—2	1.7
99.9	—0.1	0.9999	—0.01	1.001	+0.1	6.8
99	—1	0.999	—0.1	1.02	+2	1.9
90	—10	0.993	—0.7	1.21	+21	2.5
70	—30	0.981	—1.9	1.68	+68	2.8

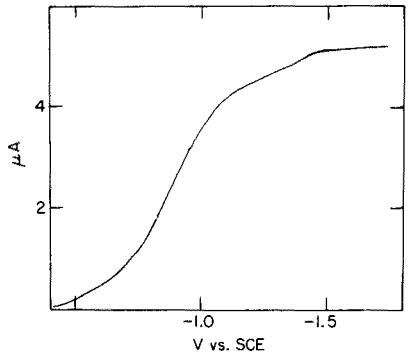

Fig. 1. Polarographic wave of an impurity in aqueous sodium carbonate solution.

two-wave equation was solved for i and substituted in the program:

$$E = (E_{\frac{1}{2}})_1 + (RT/\sigma_1 F) \ln [(i_{d1} - i)/i] + (E_{\frac{1}{2}})_2 + (RT/\sigma_2 F) \ln [(i_{d2} - i)/i] \quad (2)$$

where subscript 1 on the parameters $(E_{\frac{1}{2}})_1$, i_{d_1}, and σ_1 refers to the first wave and $(E_{\frac{1}{2}})_2$, $i_{d\,2}$ and σ_2 to the second. Then, similarly to the first case, values of the parameters were calculated and compared to the data, by entering a fixed value for the total value for $i_{d\,1}$ and $i_{d\,2}$, and next by using no fixed value for any parameter or combination of parameters. The results are shown in Tables 2 and 3.

TABLE 2

Polarographic reduction wave of 2-fluoronaphthalene in dimethylformamide. The values of the parameters are calculated by curve-fitting, with the total diffusion current fixed at 4.40 μA for the case of the five calculated parameters, and no values of parameters fixed for the six-parameter case

	$-E_{\frac{1}{2}}$ (V vs. SCE)	i_d (μA)	σ	R.m.s. deviation[a] (μA)	Processing time (s)
Five calculated parameters ($i_{d_1} + i_{d_2} = 4.40$ μA)					
Wave 1	2.292	1.908	0.760		
				0.0840	61.7
Wave 2	2.330	2.492	1.122		
		(Total $i_d = 4.40$)			
Six calculated parameters (no parameter value fixed)					
Wave 1	2.295	2.125	0.725		
				0.0738	37.3
Wave 2	2.326	2.405	1.033		
		(Total $i_d = 4.53$)			

[a] R.m.s. deviation = $(d_i^2)^{\frac{1}{2}}$, where d_i is the difference between values for data and calculated points for the ith point.

TABLE 3

Polarographic reduction wave of an impurity in aqueous solution of sodium carbonate. The values of the parameters are calculated by curve-fitting with the total diffusion current fixed at 5.2 μA for the case of the five calculated parameters, and no values of parameters fixed for the six-parameter case.

	$-E_{\frac{1}{2}}$ (V vs. SCE)	i_d (μA)	σ	R.m.s. deviation[a] (μA)	Central processing unit time (s)
Five calculated parameters ($i_{d_1} + i_{d_2} = 5.2\ \mu A$)					
Wave 1	0.795	4.768	0.359		
				0.0955	28.1
Wave 2	1.303	0.432	0.597		
		(Total = i_d 5.200)			
Six calculated parameters (no parameter value fixed)					
Wave 1	0.795	4.778	0.359		
				0.0956	11.6
Wave 2	1.366	0.415	0.597		
		(Total = i_d 5.193)			

[a]See footnote to Table 2.

Discussion

The results can be examined with respect to the accuracy of the computation and the computational time. The accuracy is best appreciated from the results in the first case. As can be seen in Table 1, as the magnitude of error in i_d increases, the errors in $E_{\frac{1}{2}}$ increase, but not as much as the increase in the magnitude of σ values. This is expected because for the data points close to $E_{\frac{1}{2}}$, the term containing i_d is small, and these data points have a large influence on the computed value of $E_{\frac{1}{2}}$. Thus, errors in the value of i_d have little influence on $E_{\frac{1}{2}}$ errors. Because the parameter σ is in the same term as i_d, the influence of errors in i_d values is greater for σ. When the calculation was done with no fixed value of i_d, the results agreed very well, within truncation error, with the true values of $E_{\frac{1}{2}}$, σ, and i_d. These results show that fixing a value of a parameter is unnecessary and can lead to an incorrect answer.

The accuracy of the values obtained for the parameters of the second and third cases is difficult to assess, except by comparing deviations of the calculated data pairs for E—i with the experimental pairs. When the program was used to calculate values of all parameters (none fixed), the deviations were smaller for the second case than when a value of i_d (total) was fixed.

The reduction in computational time for non-fixed values compared to entering a fixed value is very evident in the second and third cases. In the first case, it can be seen that increasing the error in the value of the fixed parameter, i_d, causes increased computational times. (The one case in Table 1, that of the 6.8-s time, is attributed to the inability of the program to distinguish quickly between a situation that is almost correct, and the true one.) As it is usually impossible to measure i_d values with a high degree of accuracy,

some error will always exist and computational times will be longer than in the situation when no fixed value of i_d is used. It appears that the advantage of fixing the value(s) of one (or more) parameter(s) may not be as large as it has been thought to be and that it may even be disadvantageous to do so in some cases.

In conclusion, it has been shown that by fixing a value to one of the parameters, computational times are increased and accuracy may be reduced.

REFERENCES

1 L. Meites, The General Multiparametric Curve-fitting Program CFT3, March 1973, revised June, 1974, Computing Laboratory, Chemistry Dept., Clarkson College of Technology, Potsdam, NY 13676.
2 L. Meites, personal communication.
3 B. H. Campbell, Anal. Chem., 44 (1973) 133.
4 L. Lampugnani and L. Meites, Anal. Chem., 45 (1973) 1317.

Analytica Chimica Acta, 101 (1978) 221—224

Short Communication

DETERMINATION OF CHLORINE IN ORGANIC MATERIALS BY POTENTIOMETRIC TITRATION AFTER DECOMPOSITION WITH SODIUM BIPHENYL

GEORGE W. HEUNISCH

Conoco Coal Development Company, Research Division, Library, PA 15129 (U.S.A.)

(Received 11th November 1977)

A quick, accurate method that can be adapted to routine analysis has been developed for the determination of chlorine in coal-derived synthetic fuels. While the method has been used primarily for the analysis of coal-derived products, it should also be applicable to the analysis of petroleum products. The chlorine-containing organic compound is decomposed with sodium biphenyl [1] to produce NaCl in a cloudy, aqueous mixture with a small concentration of residual organic material; addition of acetone finally produces a clear solution that can be titrated by the potentiometric method developed by Clark [2]. A modification of the Clark method is discussed by Shiner and Smith [3] and involves the use of a non-ionic detergent to stabilize the potential near the end-point.

Clark, as well as Shiner and Smith, used silver/calomel electrode systems. LaCroix et al. [4], however, showed that a chloride-selective electrode can be used as the indicator electrode, and a selective electrode was used in this investigation. The combination of the selective electrode with the non-aqueous solution lowers the limit of determination of chlorine by an order of magnitude.

Experimental

Apparatus and reagents. An Orion Model 801A pH/mV meter equipped with an Orion Model 94-17 chloride-selective electrode and an Orion Model 90-02 double-junction reference electrode were used. Sodium biphenyl solution was obtained commercially (Southwestern Analytical Chemicals, Austin, Texas).

Standardization of titrant. Aliquots of a standard NaCl solution, prepared from certified sodium chloride dried at 120°C, were titrated in a 60% acetonic medium with the $AgNO_3$ solution (about 0.01 M). The relative standard deviation for three titrations was 0.5%.

Procedure. Place 20 ml of chlorine-free iso-octane in a dry, 250-ml separatory funnel and accurately weigh 1—50 g of organic sample into the funnel. Water and hydroxyl interfere with the sodium biphenyl decomposition.

Add one bottle (15 ml) of sodium biphenyl solution, mix, and allow to stand for 30 s. Destroy the green color by swirling 2 ml of 2-propanol into the mixture, and extract the colorless mixture with three 10-ml aliquots of water, collecting the extracts in a beaker. Neutralize the aqueous solution with 6 M HNO_3 to the phenolphthalein end-point, and add 0.5 ml of HNO_3 solution in excess. Dilute the solution to approximately 80 ml with acetone. Place the electrodes into the solution, and titrate the chloride potentiometrically with 0.01 M $AgNO_3$. Use 0.001 M $AgNO_3$ if less than 200 μg of chloride is expected.

Blank determinations done by the above procedure showed no measurable chloride concentration.

Results and discussion

Silver chloride has a finite solubility in water (ca. 10^{-5} M); as a result, chloride concentrations below about 10^{-3} M (3500 μg/100 ml) cannot be titrated accurately in aqueous solution because precipitation is incomplete and no distinct end-point is observed. When solutions containing 215 μg and 189 μg of chlorine abstracted with sodium biphenyl from trichloroethylene and chlorobenzene, respectively, were titrated with 0.001 M $AgNO_3$ solution in aqueous solution, no end-point deflections were observed. Similar titrations done in a 60% acetonic solution gave titration curves such as those shown in Fig. 1. All of the end-points were easily measurable; unexpectedly, the potential jump at the end-point was steeper at the lower chloride concentrations.

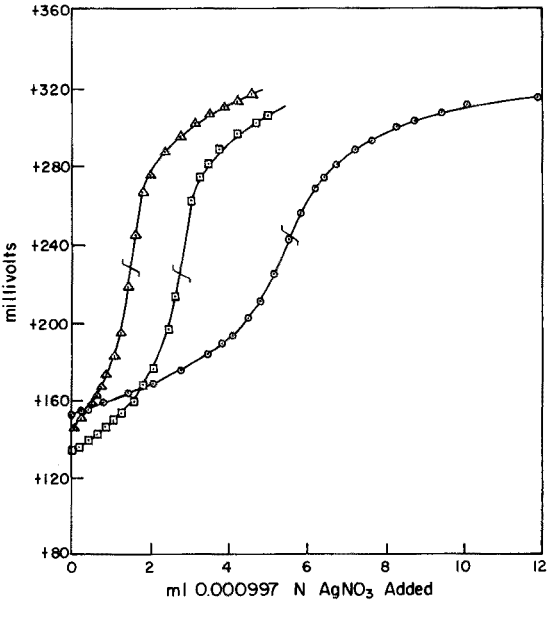

Fig. 1. Typical titration curves. ○ 189 μg Cl, □ 76 μg Cl, △ 38 μg Cl.

TABLE 1

Chlorine recovery data

Compound	Taken (μg)	Found (μg)	ppm[a]	Recovery (%)	Compound	Taken (μg)	Found (μg)	ppm[a]	Recovery (%)
Chloro-	38	52	0.7	137	Trichloro-	43	54	0.7	126
benzene	76	97	1	128	ethylene	86	93	1	108
	189	197	2	104		215	219	3	102
	378	380	5	102		429	440	5	103
	756	750	9	98		858	850	11	99
	1890	1880	23	100		2146	2120	26	99

[a]Ppm chloride in the solution titrated.

Recovery data are given in Table 1. In the lower concentration range, the results are consistently high because AgCl is still slightly soluble in the acetonic medium. This behavior is analogous to the aqueous titration except that the acetone has reduced the K_{so} value to a lower level. The titration of 40 μg of chloride represents the limit of the method. While the curve and the end-point are discernible, the accuracy deteriorates significantly, although it could, of course, be improved by appropriate empirical calibration. Because of the extraction step, the volume titrated does not necessarily depend on sample size; the lowest sample concentration that can be determined is limited primarily by the amount of sample available.

The higher concentrations (200 to 2100 μg Cl^-) given in Table 1 indicate the wide range that can be determined. Distinct, classical potentiometric curves were obtained with 0.01 $AgNO_3$ titrant, and the recovery data suggest quantitative titration.

Two distillate samples from a coal-to-gasoline conversion process were analyzed for chlorine to demonstrate the applicability of the method to a complex sample system. The samples were analyzed by the described method, spiked with aliquots of trichloroethylene and chlorobenzene, and re-analyzed to determine the recovery. Trichloroethylene (TCE) and chlorobenzene(CB) are considered representative chlorinated species found in coal and in products from the coal conversion process. The recoveries (Table 2) are good, indicating that complex samples can be analyzed satisfactorily.

The reproducibility of the method was measured for coal-derived samples. Fraction IBP—200°C gave chlorine contents of 55, 55 and 58 ppm in triplicate analyses; fraction 325—475°C gave contents of 51 and 54 ppm in duplicate analyses.

It should be mentioned that the electrode system has not been significantly degraded by the non-aqueous medium; the system has been in use for approximately six months. The only regular maintenance has been changing the filling solutions in the reference electrode.

TABLE 2

Recovery data for complex process samples

Distillate fraction	Spike	μg Cl			Recovery (%)
		Spike	Distillate	Total found	
IBP—200°C	TCE	2146	534	2664	99
	CB	1892	535	2415	100
325—475°C	TCE	2146	628	2768	100
	CB	1892	468	2418	102

REFERENCES

1 L. M. Liggett, Anal. Chem., 26 (1954) 748.
2 W. Clark, J. Chem. Soc., (1926) 749.
3 V. J. Shiner and M. L. Smith, Anal. Chem., 28 (1956) 1043.
4 R. L. LaCroix, D. R. Keeney and L M. Walsh, Soil Sci. Plant Anal., 1 (1970) 1.

Analytica Chimica Acta, 101 (1978) 225—228

Short Communication

MICRODETERMINATION OF LEAD WITH SODIUM RHODIZONATE BY THE RING-OVEN TECHNIQUE IN AIR POLLUTION STUDIES

YASH PAUL GROVER

Med. Institut für Lufthygiene und Silikoseforschung an der Universität Düsseldorf, 4 Düsseldorf (Federal Republic of Germany)

(Received 10th January 1978)

Traces of toxic metals, e.g. cadmium, lead, chromium and nickel, are frequently determined routinely in air pollution studies. Lead is usually determined spectrophotometrically (dithizone extraction) [1], by atomic absorption [2] or spectrographically [3]. However, less expensive methods can be useful in pollution studies. This communication reports the sensitive detection and quantitative evaluation of lead by a ring-oven technique [4, 5] coupled with a micro-photometric system [6].

The Weisz ring-oven technique has been used for the semiquantitative estimation of various air pollutants [5]. The accuracy of the results at the nanogram level is often similar to that obtained spectrophotometrically. Jungreis and West [7] estimated lead (0.05—2.0 μg) in air by using the ring-oven with diphenylcarbazide and sodium molybdate reagents, by visual comparison of the rings with standard rings. Shendrikar and West [8] have reported a similar technique with dithizone as reagent. Fugas and Paukovic [9] estimated the lead as chromate and applied their ring-oven method to smoke samples [10].

This communication describes the use of sodium rhodizonate as the reagent in a ring-oven technique for estimating atmospheric lead. Neutral or weakly acidic lead solutions produce coloured basic lead rhodizonate when treated with freshly prepared sodium rhodizonate [11]. The test spot is washed with tartaric acid to transport lead ions to the ring zone. The lead is then estimated by measuring the intensities of the rings at 500 nm with a microphotometer system [6].

Experimental

Choice of filter paper. Various qualities of filter papers were examined as reported earlier [6]. Schleicher and Schüll No. 589[2] white-band cellulose filter paper was selected because of its strength and uniformity and because rings appeared on both sides of the filter. The selected filter was free of lead and other impurities. If necessary, impurities can be removed by pre-washing with twice-distilled water.

Treatment of test spot. To concentrate the minimum amount of lead tested

in a suitable ring, a ring-oven with a 14-mm diameter borehole was used. The ring-oven was maintained at 80°C, which was checked by measuring with a surface thermometer. The filter with the test spot in the centre was placed on the ring-oven; for standard lead rings on the filter, appropriate volumes of standard solution were placed in the centre of filters with a calibrated micropipette. The lead spot was washed to the ring zone with a buffer solution pH 2.79 (sodium hydrogentartrate and tartaric acid). The scarlet-red lead rhodizonate ring was developed by spraying with freshly prepared aqueous 0.2% (w/v) sodium rhodizonate solution.

Microphotometric evaluations. The lead rhodizonate rings on the dried filters were evaluated with a microphotometer (MPE, Leitz). The filter was placed in a filter holder, which was screwed tightly to achieve a uniform stretched surface. The holder was then fixed in a stand positioned under the objective of the microphotometer. The diffuse reflected light passed through the interference filter to the photomultiplier, and the intensity at 500 nm was recorded on a Servogor strip-chart recorder (Metrawatt, Krefeld). The filter holder was rotated by a small asynchronous motor (AMY 5). The measuring beam aperture was such that it did not exceed double the width of the ring (0.1—0.3 mm). The mechanical rotation of the filter holder was observed microscopically and centering of the lead ring under the measuring objective was maintained by adjusting the coaxial knob.

Results

Calibration curve. Microphotometric evaluation of standard lead rhodizonate rings on the filter was carried out at 500 nm (maximum transmission). The lower limit of determination for lead with this system is 0.25 μg; the colour intensities of rings containing less than 0.2 μg of lead is too difficult to evaluate. The upper limit of determination is 1.5 μg of lead. Lead oxide, bromide and nitrate solutions were used for calibration over the range 250—1000 ng (Fig. 1).

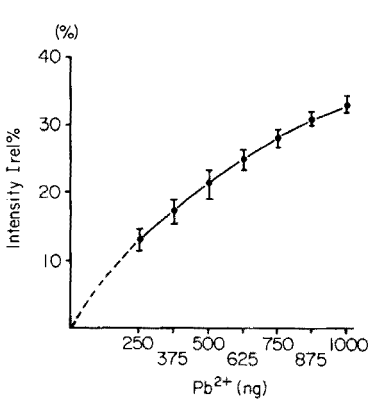

Fig. 1. Calibration curve for lead at 500 nm. Each point is the mean of six determinations with lead oxide, bromide or nitrate.

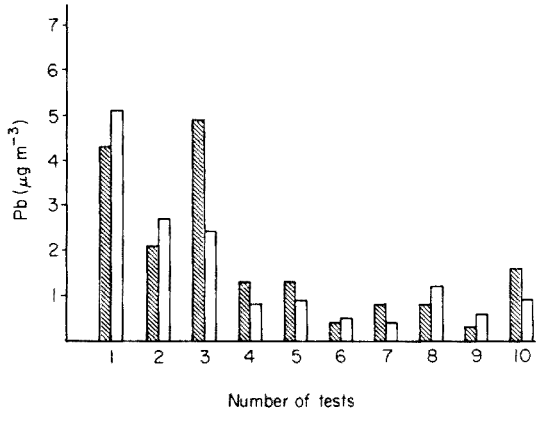

Fig. 2. Comparison of values obtained simultaneously by the ring oven—microphotometric system (shaded columns) and by atomic absorption spectrometry (open columns).

Interferences. Special consideration was given to metal ions that are most likely to be present in air. Sodium rhodizonate forms coloured complexes with Tl^+, Ag^+, Cd^{2+}, Ba^{2+} and Sr^{2+} at pH 3 [11]. According to the National Air Sampling Network [12], Ba^{2+}, Cd^{2+} and Sr^{2+} are present in ambient air at average concentrations of 25×10^{-3} $\mu g\ m^{-3}$, 5×10^{-3} $\mu g\ m^{-3}$ and 8×10^{-2} $\mu g\ m^{-3}$, respectively. To determine the effects of these metals, rings were prepared from 0.25 μg of lead with and without 0.25 μg of the possible interferent. The ion was established as non-interfering when the ring of the possible interferent was blank and the intensity of the lead-containing ring agreed with the calibration curve within normal experimental error.

Analysis for particulate lead. Ten 24-h dust samples, collected by BAT I [13] on membrane filters (SM 11305, 120-mm diameter), were analysed simultaneously by the proposed method and by atomic absorption spectrometry with electrothermal atomization (Perkin-Elmer Model 303 with HGA 70). For a.a.s., a quarter of each filter was washed with 6 μl of concentrated sulphuric acid and 1 ml of hydrogen peroxide (30% solution) at 250°C, and the residue was dissolved in 50 ml of distilled water for analysis. For the ring-oven method, a 3-mm diameter circle was cut from each of the filters with a punch, and fixed in the centre of the filter-paper on the ring-oven for analysis by the procedure described above. The total lead concentration of each sample was then calculated. The data obtained by these two methods are shown in Fig. 2.

Conclusions

The combination of the ring-oven with the microphotometer system offers a simple, fast, sensitive and inexpensive method for the determination of lead in the range usually found in ambient air. The reasonably close agreement found between the results obtained by this method and by a.a.s. (Fig. 2) confirms the accuracy of the microphotometer system. Digestion and separation of interfering elements are not required.

With the sodium rhodizonate reagent, the lower detection limit is 0.25 μg, which is more sensitive than the dithizone or chromate methods [8, 9]. Moreover, overlapping or masking effects are easily detected by the microphotometric system, and sample dissolution is not necessary. Standard rings with the sodium rhodizonate reagent are stable for some days, and the calibration curve once obtained is a permanent reference. In the methods based on visual comparison of rings [7—9], fresh standard rings are always necessary for matching the unknown concentration, so that there is a greater possibility of variation and error, as well as greater time consumption. With the microphotometer system, the intensities of the standard and unknown rings are recorded, and there is less opportunity for personal error.

REFERENCES

1 Community Air Quality Guides, Am. Ind. Hyg. Assoc. J., 30 (1969) 95.
2 Analytical Guides, Am. Ind. Hyg. Assoc. J., 30 (1969) 102.

3 R. G. Keenan, D. H. Byers, B. E. Saltzman and F. L. Hystop. Am. Ind. Hyg. Assoc. J., 24 (1963) 481.
4 H. Weisz, Mikrochim. Acta, (1954) 140.
5 H. Weisz, Microanalysis by the Ring Oven Technique, 2nd edn., Pergamon Press, Oxford, 1970.
6 K. H. Friedrichs and Y. P. Grover, Staub-Reinhalt. Luft, 32 (1972) 23.
7 E. Jungreis and P. W. West, Isr. J. Chem., 7 (1969) 413.
8 A. D. Shendrikar and P. W. West, Anal. Chim. Acta, 61 (1972) 43.
9 M. Fugas and R. Paukovic, Anal. Chim. Acta., 49 (1970) 356.
10 M. Fugas, R. Paukovic, V. Vadic and J. Hrsak, Anal. Chim. Acta, 49 (1970) 359.
11 F. Feigl, Spot Tests in Inorganic Analysis, 3rd edn., Elsevier, Amsterdam, 1956.
12 National Air Sampling Network, Staub, 19 (1959) Nr. 9, 338.
13 H. Breuer, Staub, 22 (1962) Nr. 11, 444—451.

Analytica Chimica Acta, 101 (1978) 229—230

Short Communication

THE SELECTIVE DETECTION OF TRACES OF CADMIUM WITH A BENZOTHIAZOLE DERIVATIVE (PYRUVYLIDINE-2-HYDRAZINO-BENZOTHIAZOLE)

ESTHER K. LIBERGOTT*, CARMEN L. S. ROQUETTE PINTO and POMPEU L. A. AGUIAR NETO

Ministério da Indústria e do Comércio, Instituto Nacional de Tecnológia, Avenida Venezuela, 82 Rio de Janeiro (Brasil)

(Received 24th February 1978)

Despite the existence of several reagents for the identification of traces of cadmium, few are selective enough to be applied without previous separation of interfering elements [1]. The new reagent described here is sensitive and highly selective for cadmium, and does not react with zinc. By addition of appropriate masking agents, the reaction can be made specific for cadmium.

The reagent is a yellow compound obtained by the condensation of 2-hydrazinobenzothiazole and pyruvic aldehyde:

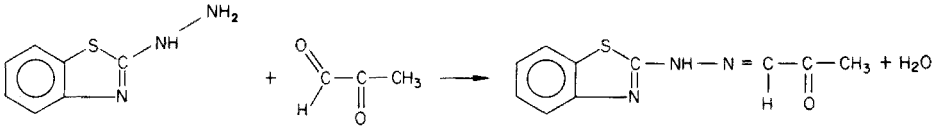

With cadmium ions in an alkaline medium it forms an orange precipitate which can be dissolved in benzene. The following elements do not interfere: Al, Sb, As, Ba, Be, Bi, Ca, Cr, Ga, Ge, In, Mg, Mo, Os, Rh, Ag, Na, Sr, Sn, Ti, W, U, V, Zn and Zr. Colored compounds are produced with Cu, Ni, Co, Pb, Au, Mn, Tl, Ce, Hg and Fe but these metals can be masked as described below.

Experimental

Preparation of the reagent. Heat together for 30 min equimolar solutions of 2-hydrazinobenzothiazole and pyruvic aldehyde in dilute acetic acid. Filter off the yellow precipitate and wash with distilled water until acetic acid is completely eliminated.

Test for cadmium. Treat a drop of alkaline test solution in a small test tube with 5 drops of the reagent solution (0.05% w/v in benzene). An orange colour in the upper, benzene layer indicates the presence of cadmium.

Identification limit, 0.5 μg. Dilution limit, $1:10^5$.

If interfering ions are present, use the following procedure. Mix 1 drop of the alkaline test solution in a small test tube with 2 drops of 10% (w/v) sodium tartrate solution, 2 drops of 1% (w/v) sodium hydroxide solution, 1 drop of 20% (w/v) potassium cyanide solution, 1 drop of concentrated formaldehyde solution and 5 drops of the reagent solution.

In this way 5 μg of cadmium can be detected in the presence of 0.5 mg Pb, 1 mg Co, 2 mg Ni, 5 mg Cu, and 0.5 mg of Fe, Au, Ce, Hg, Mn or Tl.

Identification of cadmium in alloys. Place 20—30 mg of alloy in a small test tube and add 5 drops of concentrated nitric acid. Heat the solution obtained to expel the nitrous vapors and test as described above.

With this test 1 μg of cadmium was identified in a sample containing 99.8% of zinc.

The Conselho Nacional de Pesquisas Científicas e Tecnológicas is thanked for financial support.

REFERENCE

1 F. Feigl and V. Anger, Spot Tests in Inorganic Analysis, 6th edn., Elsevier, Amsterdam, 1972.

(continued from outside of cover)

Short Communications

Printed in The Netherlands

VOL. 101 No. 1 ANALYTICA CHIMICA ACTA OCTOBER 1, 1978

CONTENTS

(continued on inside page of cover)